A PARAMETRIC INVESTIGATION OF THE EFFECT OF SURFACE TENSION AND RHEOLOGICAL PROPERTIES OF THE LUBRICANT ON THIN FILM BEHAVIOR IN TRIBOLOGY

By

JOON HYUN KIM

A DISSERTATION PRESENTED TO THE GRADUATE SCHOOL
OF THE UNIVERSITY OF FLORIDA IN PARTIAL FULFILLMENT
OF THE REQUIRMENTS FOR THE DEGREE OF
DOCTOR OF PHILOSOPHY

UNIVERSITY OF FLORIDA

1998

To my Parents
and
To my Family

ACKNOWLEDGEMENTS

I would like to express my deepest gratitude to my advisor and the chairman of my advisory committee, Dr. Ali A. Seireg, for his continuous guidance and encouragement throughout my study.

I wish to extend my thanks and appreciate to my committee members, Dr. James F. Klausner and Dr. William E. Lear, Dr. Jill E. Peterson, and Dr. Li C. Shen for their advice, comments and patience in reviewing this dissertation.

Gratitude is due to Dr. Gerald Micklow of the University of Alabama and Dr. Insoo Cho for their technical assistance in dealing with computer facilities in the beginning of the Ph.D. program. The CFD technique helped directly or indirectly in the completion of this study. My appreciation goes to my group fellows Dr. Yong Hoon Chang of Sam Sung Aerospace Inc. and Jong Ho Lee for assistance and useful discussion.

Certainly, I am so much grateful to my family members, those who are still in this world and those who live in my heart only. Especially, I would like to express my deepest appreciation to my wife, Young Hee, for her valuable love and continuous spiritual support during my long study abroad.

I am greatly indebted to my lovely son, Hyun Chul, and daughter, So Hyun, who grew up during my study abroad, for their lovely smiles that make my family life so beautiful. Finally, this work is dedicated to my parents Do Kyung and Bun Do Choi for their love and financial support through my life.

TABLE OF CONTENTS

Page

ACKNOWLEDGEMENTS iii

ABSTRACTS vi

CHAPTERS

1 INTRODUCTION 1

- 1.1 Outline of the Problems 2
- 1.2 Objective 5

2 LUBRICATION FLUID MECHANICS (HYDRODYNAMICS) 7

- 2.1 Introduction 7
- 2.2 Lubrication Approximation 8
- 2.3 Reynolds Equation 11
- 2.4 Energy Equation 13
- 2.5 Summary and Conclusion 15

3 FREE SURFACE FILM FLOWS 17

- 3.1 Introduction 17
- 3.2 Landau-Levich Solution 19
- 3.3 Extension to the Landau-Levich Model 22
- 3.4 Application to the Cylindrical Coordinate 27
- 3.5 Mathematical Solution and Discussion 28
- 3.6 Summary and Conclusion 30

4 FREE SURFACE FILM FLOWS IN THE PRESENCE OF A STATIONARY CONSTRAINT 42

- 4.1 Introduction 42
- 4.2 Literature Review 43
- 4.3 Mathematical Formulation 44
- 4.4 Coyne and Elrod Boundary Condition 47
- 4.5 Boundary Conditions 49
  - 4.5.1 Partially Flooded Inlet Boundary Condition 49
  - 4.5.2 Swift-Stieber Outlet Boundary Condition 50
  - 4.5.3 Separation Outlet Boundary Condition 51
- 4.6 Mathematical Solution and Discussion 53
- 4.7 Summary and Conclusion 55

5. THERMOHYDRODYNAMIC ANALYSIS 61

5.1 Introduction 61
5.2 Literature Review 62
5.3 Design Parameters 64
5.4 Dependence of Viscosity on Temperature and Pressure 65
5.5 Simplified Reynolds Equation 66
5.6 Energy Equation 68
5.7 Dimensionless Analysis for the Governing Equations 70
5.8 Performance Parameter of the Lubricating System 74

6 NUMERICAL TECHNIQUE 76

6.1 Introduction 76
6.2 Finite Difference Form of the Reynolds Equation 77
6.3 Finite Difference Form of the Energy Equation 79
6.4 Grid System 82
6.5 Consistency and Stability 83
6.6 Computational Procedure 84
6.7 Numerical Calculation and Comparison 85
6.8 Model with Full Film Shear Zone in the lubricating Zone 87
6.9 Summary and Conclusion 90

7 RHEOLOGICAL MODEL WITH NON-NEWTONIAN EFFECTS 105

7.1 Introduction 105
7.2 Non-Newtonian Behavior 107
7.3 Rheological Model Description 109
7.4 Non-Dimensionalization of Governing Equations 115
7.5 Numerical Scheme 120
7.6 Computational Procedure 122
7.7 Empirical Evaluation of the Thin High Shear Zone and Experimental Data 124
7.8 A Parametric Investigation of the Effect of Rheological Properties 127
    7.8.1 Journal Bearing 127
    7.8.2 Slider bearing 130
7.9 Summary and Conclusion 132

8 SUMMARY, CONCLUSIONS AND RECOMMENDATIONS 174

8.1 Summary and Conclusions 174
8.2 Recommendations 177

REFERENCES 179

BIOGRAPHIC SKETCH 184

Abstract of Dissertation Presented to the Graduate School
of the University of Florida in Partial Fulfillment of the
Requirements for the Degree of Doctor of Philosophy

A PARAMETRIC INVESTIGATION OF THE EFFECT OF SURFACE TENSION AND RHEOLOGICAL PROPERTIES OF THE LUBRICANT ON THIN FILM BEHAVIOR IN TRIBOLOGY

By

Joon Hyun Kim

May 1998

Chairperson: Dr. Ali A. Seireg
Major Department: Mechanical Engineering

The study reported in this dissertation investigates the effect of surface tension on film flows on rollers in the presence of stationary objects due to its relevance in hydrodynamic and elastohydrodynamic lubrication. An analysis is introduced to predict the film layer thickness in the free surface as an extension of the Landau and Levich theory and is utilized in the study. Parameters of liquid entrainment are considered to solve the numerical problem and to examine the effect of the boundary conditions characterizing the formation of the liquid film. It is shown in the analysis that surface tension, gravity and inertia effects have considerable influence in determining the film thickness and its associated boundary conditions.

A mathematical model is also developed for parametric investigation of the influence of the rheological properties of the lubricant in the thermohydrodynamic film conditions which occur in slider and journal bearings. It is shown in the analysis that yield in shear have considerable influence on the flow velocity distribution and the pressure developed in thin film lubrication. A parametric investigation is performed for predicting the thickness of the shear zone where heat generation occurs in fluid films with fixed geometry between the stationary and moving surfaces. The investigation shows

that the shear zone thickness is significantly smaller than the fluid film thickness in the lubrication zone. The results of this procedure also show the same trend as the experimentally determined square root relationship between the pressure and sliding velocity in journal and slider bearings.

CHAPTER 1
INTRODUCTION

Many applications in engineering practice involve the entrainment of liquid films on solid objects. To identify some of these systems, these applications may be classified as problems in withdrawal, removal, and drainage [1, 2].

In withdrawal the motion of an object from a liquid container causes entrainment of the wetting liquid. Withdrawal is limited to the case where a part of the solid support remains in contact with the liquid container. In removal, an object of finite length is entirely removed from a liquid container so that the entrained film is separated from the container. In drainage, when the solid support is stationary the liquid flows downward by gravity. These three problems are closely related.

In these problems, the mass flow rate or flux of the liquid is unknown. Thus the class of problems considered here is quite different from that of liquid film situations where the flux is known, such as in flow down wetted wall. The flux is closely related to the entrainment, the film distribution, and the total amount of liquid removed.

To the engineer, the most important parameter is probably the flux of the liquid. Other parameters of interest are the thickness of the film and the velocity distribution in the film. The engineer would like to predict of these quantities as functions of position, time, and the physical properties of the liquid. Knowledge of the dynamics of these films is useful in many practical fields such as coating, cleaning, draining, and lubrication. The problems as indicated above are liquid flows and show important roles of fluid dynamics.

The phenomenon of fluid film has been of considerable interest in areas such as polymer engineering. In the tribological problems it also has been an active subject for research. There is a wide range of applications where these problems arise as indicated in Table 1.

Table 1: General Application

Application	Specific application	Classification
Coating	film and wire photographic film	withdrawal
Cleaning	electroplating rinsing	removal
Draining	drainage	drainage
Lubrication	gears bearings disk	withdrawal

1.1 Outline of the Problem

The objective of this study is to develop a mathematical model for thin film lubrication problems which occur in practice. The first consideration is to model the hydrodynamic phenomenon between a rotating disc and a fixed surface in Newtonian fluids. The second consideration is the thermohydrodynamic phenomenon of lubricating films between rotating (or sliding) solids and any adjacent constraint. This also includes the fluid film lubrication that is associated with elements in relative motion.

The first part deals with the flow of a viscous fluid on the surface of a partially submerged, rotating bearing (disk) which is one of the basic coating (free surface) problem as shown in part A of Figure 1-1-(a) and (b). The main features of this type of flow for a Newtonian fluid are described by the Landau-Levich theory [3]. The problem is treated using a nonlinear approach without the inertia effects. In the free surface flow the formation of the liquid films is characterized by a meniscus thickness decreasing with distance above the container and eventually approaching a constant thickness. The resultant constant thickness is a function of the velocity of withdrawal, gravity, and the physical properties of liquid (density, viscosity, and surface tension). The meniscus region is characterized at the interface by a stagnation point [4]. The film maybe divided about this point into thin and thick menisci. Here such parameters of liquid entrainment occurring from a container will be considered. Thus, the main point for solving this problem is the boundary conditions characterized by the formation of the liquid film [3, 5, 6, 7]. This can make two different flow regions match at a common boundary. Without the use of asymptotic techniques or numerical methods such as the finite element method it will be possible to solve the full Navier-Stokes equations based on this key point. The model gives a relationship between the dimensionless film thickness, T, and the Capillary number, Ca. To develop valid viscous free surface flows at relatively low Reynolds numbers, a boundary-layer type of approximation is introduced [8-15].

When a journal or a disk rotates about its axis while partially submerged in a liquid, a layer of the liquid is entrained and withdrawn from the liquid container. In the absence of a constraining boundary the film thickness is found to exhibit a strong dependence on disk speed, fluid viscosity and surface tension. In the free surface flows with stationary constraint the formation of these liquid films is characteristically the hydrodynamic lubrication problem as shown in part B of Figure 1-1-(b). For lightly loaded situations wide ranging numerical approaches are carried out to predict the film rupture location and pressure distributions using the cavitation boundary conditions of Coyne and Elrod and two additional Swift-Stieber (Reynolds) and separation boundary models [16–21]. For over a century the Reynolds equation has been used to analyze this problem. When the lubrication film thickness profile is known and under idealized conditions of isothermal, highly viscous Newtonian flows the basic theory of lubrication is generally expressed by the Reynolds equation [22]. Classical lubrication mechanics constitutes the solutions to Reynolds equation with various boundary conditions simulating various system configurations. However, much of the modern lubrication literature deals with departures which are due to thermal effects, inertial effects, and undetermined film thickness profiles. Consequently, this problem will be dealt with as an extension of the first procedure with the boundary conditions and parameters of liquid entrainment occurring from a layer of the liquid on the rotating system entrained and withdrawn from the container. While the film thickness in the absence of a constraining boundary seems to have a strong dependence on the rotating speeds, as well as fluid viscosity and interfacial tension, the effects of an adjacent constraining boundary requires a mathematical model based on lubrication theory. This study will be concerned with the hydrodynamic behavior for the critical conditions at the onset of film formation

The last procedure deals with the development of a thermohydrodynamic computational procedure for evaluating the pressure, temperature and velocity distributions in thin fluid films with fixed geometry between the stationary and moving bearing (disk) surfaces as shown in part C of Figure 1-1-(b). When temperature rise across the system such as bearing is small, the classical isothermal theory with an effective viscosity may be applied. However, in practical cases, thermal effects may be significant, thus, the classical theory is no longer adequate [23]. The thermohydrodynamic (THD) theory of lubrication is applied to evaluate local viscosity. Further, in most industrial applications where the rotating speed is high, the systems are often operated in a special regime. In practical applications, when the lubricant is subjected to high shear force which act for only a relatively short period of time, the assumption that the entire film behaves as a Newtonian fluid may not be valid. A primary hypothesis of this study is that in fluid film lubrication there exists a small shear zone at the middle thickness of the film where the lubricant undergoes a high shear rate [24-27]. This shear zone thickness inside the lubricant film is controlled by the surface tension at the solid boundaries and the rheological behavior of the lubricant under different pressure, temperature, and speed conditions. The velocity variations and the heat generation are assumed to occur intensively in a central zone having rapidly changing high shear rate with the same length (or length of the lubrication zone obtained from the second procedure) and width as the bearing (disk) but with a significantly smaller thickness than the fluid film thickness. A transient thermohydrodynamic model with a rectangular computational domain is utilized which generalizes the analysis for any given film geometry. The developed procedure also gives an analytical basis for explaining the "Fogg effect" (thermal wedge) where significant pressures can be generated in bearings as a result of the thermal expansion of the film in the direction of the thickness [28].

A numerical solution to the thermohydrodynamic lubrication with consideration of both the thermal and non-Newtonian effects have been obtained. The computational technique requires the simultaneous solution of the Newtonian hydrodynamic, the load, the viscosity, and the energy equations. Most information for computation of this part come from the two previous procedures. Some parameters are involved in determining the rotating system performance, such as bearing, disk. The analysis on a case-by-case basis is performed for the design of such as journal bearings, finite slider bearings and rotating cylinder (disc) – plate systems.

1.2 Objective

The main objective of the present study is to investigate the role of surface tension in forming adhered films for tribology and attempt to theoretically predict the dimension of the shear zone in thermohydrodynamic lubrication by using a rheological model for the lubricant which is expected to behave rheologically under pressure. The present study searches for functions that approximate the cavitation point and the distribution of film pressure, temperature, and velocity.

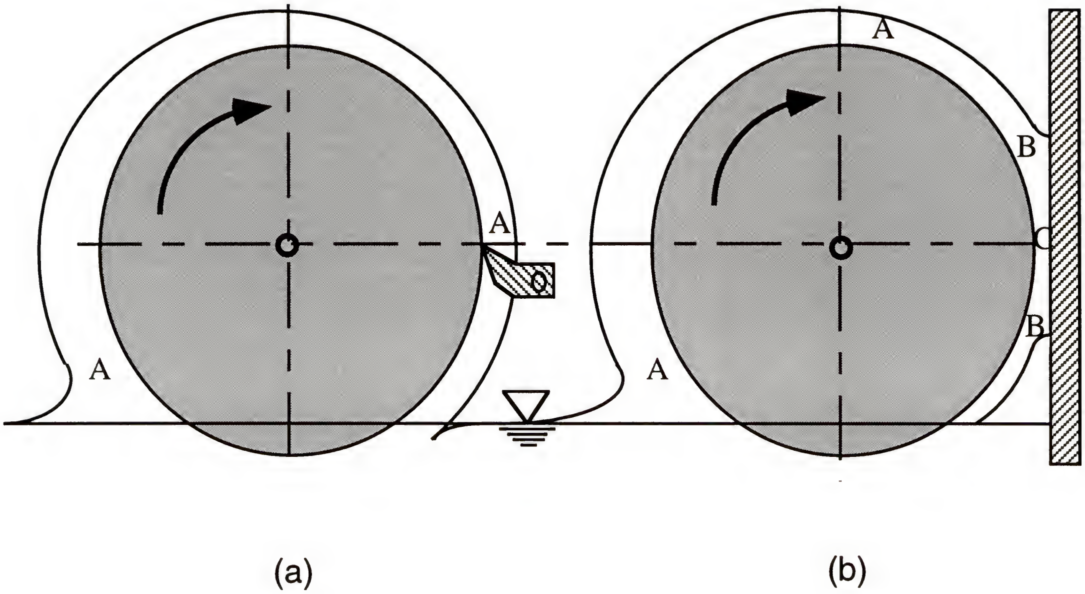

Figure 1.1 Geometry of simple rotating systems:
(a) Freely confined withdrawal
(b) Partially confined withdrawal

CHAPTER 2
LUBRICATION FLUID MECHANICS

2.1 Introduction

The subject of hydrodynamics is concerned with the motion of fluids. There are various types of fluids. Essentially the study of hydrodynamics is the study of rates of flow of fluid in conjunction with momentum of the fluid and its action under the forces placed upon it.

The study of the motion of fluids is very important to lubrication, hence hydrodynamics is a basic element of lubrication theory. However, hydrodynamics alone is insufficient to describe the full characteristics of lubrication because the lubricant properties are temperature dependent [29-32]. For example, the viscosity of a lubricant is a dissipative factor turning mechanical energy into heat. Thus many applications in lubrication must consider the thermal effects which are connected with the viscosity in the hydrodynamics of the system. Another important element of lubrication theory is the relationship between hydrodynamics and the flow passage [29]. The geometry of the flow passage can change with pressure. This greatly couples hydrodynamics with deformation mechanics in some cases such as the elastohydrodynamic lubrication. This phenomenon becomes a very important design factor in systems where the pressure in the lubricating film is high enough to deform the solids.

The basic equations for a viscous fluid are the Navier-Stokes equations. They are derived by applying to a fluid the principle of conservation of momentum. Although the general Navier-Stokes equations are rather complicated, approximations can be made for the study of thin film of fluids. The thin film approximation is the classic approximation for boundary layer theory. However, in addition to the thin film approximation, in most situations the motion of fluids in thin film is so viscous that the momentum convected by the fluids is insignificant. Consequently, inertial terms can be discarded in the Navier-Stokes equations which results in the Reynolds equation, which is the nucleus of the hydrodynamic theory of lubrication.

In steady state and two dimensional flow, the Navier-Stokes equations reduces to a pair of elliptic partial differential equations as follows,

$$\rho\left(u\frac{\partial u}{\partial x}+w\frac{\partial u}{\partial z}\right)=-\frac{\partial p}{\partial x}+\mu\left(\frac{\partial^2 u}{\partial x^2}+\frac{\partial^2 u}{\partial z^2}\right)+\rho g \qquad (2.1)$$

$$\rho\left(u\frac{\partial w}{\partial x}+w\frac{\partial w}{\partial z}\right)=-\frac{\partial p}{\partial z}+\mu\left(\frac{\partial^2 w}{\partial x^2}+\frac{\partial^2 w}{\partial z^2}\right) \qquad (2.2)$$

$$\frac{\partial u}{\partial x}+\frac{\partial w}{\partial z}=0 \qquad (2.3)$$

2.2 Lubrication Approximation (Boundary Layer Theory)

Considering a thin liquid film on a flat substrate, as shown in Figure 2.1, the flow is two-dimensional with *B*, a characteristic length in the *x* direction and *h*, a characteristic length in the z direction [33]. Now using the following dimensionless variables to scale the Equations (2.1), (2.2), and (2.3),

$$u=u_o u^* \ , \ x=Bx^* \ , \ z=h z^*$$

$$w=\frac{h}{B}u_o w^* \ , \ p=\frac{\mu u_o B}{h^2}p^* \ , \ g=\frac{\mu u_o^2}{\rho h^2}g^* \qquad (2.4)$$

Then Equation (2.3) becomes

$$\frac{\partial u^*}{\partial x^*}+\frac{\partial w^*}{\partial z^*}=0 \qquad (2.5)$$

Equation (2.1) becomes

$$\rho\left(\frac{u_o^{2}}{B}u^{*}\frac{\partial u^{*}}{\partial x^{*}}+\frac{u_o^{2}}{B}w^{*}\frac{\partial u^{*}}{\partial z^{*}}\right)=-\frac{\mu u_o}{h^2}\frac{\partial p^{*}}{\partial x^{*}}+\mu\frac{u_o}{h^2}\left[\frac{\partial^2 u^{*}}{\partial z^{*2}}+\left(\frac{h}{B}\right)^2\frac{\partial^2 u^{*}}{\partial x^{*2}}\right]+\frac{\mu u_o}{h^2}g^{*} \tag{2.6}$$

Then, introducing the assumption for thin film, $h/B<<1$, and the Reynolds number, $Re=\rho u_0 B/\mu$, the above Equation (2.6) becomes

$$\mathrm{Re}\left(\frac{h}{B}\right)^2\left(u^{*}\frac{\partial u^{*}}{\partial x^{*}}+w^{*}\frac{\partial u^{*}}{\partial z^{*}}\right)=-\frac{\partial p^{*}}{\partial x^{*}}+\frac{\partial^2 u^{*}}{\partial z^{*2}}+g^{*} \tag{2.7}$$

Now applying similarly Equation (2.2) becomes

$$\mathrm{Re}\left(\frac{h}{B}\right)^4\left(u^{*}\frac{\partial w^{*}}{\partial x^{*}}+w^{*}\frac{\partial w^{*}}{\partial z^{*}}\right)=-\frac{\partial p^{*}}{\partial z^{*}}+\left(\frac{h}{B}\right)^2\frac{\partial^2 w^{*}}{\partial z^{*2}} \tag{2.8}$$

In general, for many lubrication problems $Re(h/B)^2<<1$, and consequently the inertia force terms of the left hand side of Equation (2.7) can be neglected. However, when Reynolds number is large $Re(h/B)^2<<1$ must be retained in Equation (2.7). However, $Re(h/B)^4<<1$ is negligible, so that the left hand side of Equation (2.8) is essentially zero. Since $(h/B)^2<<1$, Equation (2.8) simply becomes

$$\frac{\partial p^{*}}{\partial z^{*}}=0 \tag{2.9}$$

Applying this to the three dimensions case, the dimensional form of the equations for this problem becomes as follows,

$$\frac{\partial p}{\partial x}=\mu\left(\frac{\partial^2 u}{\partial z^2}\right)+\rho g \tag{2.10}$$

$$\frac{\partial p}{\partial y}=\mu\left(\frac{\partial^2 v}{\partial z^2}\right) \tag{2.11}$$

$$\frac{\partial p}{\partial z}=0 \tag{2.12}$$

$$\frac{\partial u}{\partial x}+\frac{\partial v}{\partial y}+\frac{\partial w}{\partial z}=0 \tag{2.13}$$

Neglecting the inertia and gravity terms in Equation (2.10) throughout Equation (2.13) are the basic equations for the lubrication approximation. Because of their very simple structure they can be solved directly and expressed in alternative, more useful forms. The following form is for the x-component of velocity, Equation (2.10), for any point in the lubricant film

$$u = \frac{1}{2}\frac{1}{\mu}\frac{dp}{dx}z^2 + C_1 z + C_2 \tag{2.14}$$

$$v = \frac{1}{2}\frac{1}{\mu}\frac{dp}{dy}z^2 + D_1 z + D_2 \tag{2.15}$$

where C_1, C_2, D_1, and D_2 are constants. The physical significance of equation (2.14) is that it consists of two flow components of velocity, which represent the hydraulic flow and the shear flow, within the film.

Equation (2.14) is simply the equation describing the velocity distribution between two surfaces with an imposed pressure gradient. This is a typical situation to be considered in applications to coating problems as shown in part A of Figure 1-1-(a) and part B of Figure 1-1-(b). Now the viscosity of the lubricant may change considerably across the thin film as a result of temperature variations that arise in some rotating systems such as the constraint withdrawal problem. And, the pressure also changes along the thin film due to convergent or convergent-divergent geometry as shown in part C of Figure 1-1-(b). Using Equation (2.14) is satisfactory in majority of fluid film applications but is not sufficient for usage in the case of severe operational condition, and complicated boundary conditions. Considering the core zones which may be attached to both surfaces in the system, this approach is not useful. This study will be dealt with Chapter 7. With these expressions, Equations (2.14) and (2.15), for the velocity gradients and the velocity components, can be now derived as expressions for the volume rate.

The volume rates per unit width in the x and y directions are defined as

$$q_x = \int_0^h u dz \quad \text{and} \quad q_y = \int_0^h v dz \tag{2.16}$$

Substituting Equations (2.14) and (2.15) into Equation (2.16) gives

$$q_x = \int_0^h \left[\frac{1}{2}\frac{1}{\mu}\frac{dp}{dx} z^2 + C_1 z + C_2 \right] dz \text{ and } q_y = \int_0^h \left[\frac{1}{2}\frac{1}{\mu}\frac{dp}{dy} z^2 + C_1 z + C_2 \right] dz \tag{2.17}$$

The component of these equations represents the well known Poiselle (or pressure) flow, and the Coutte (or velocity) flow.

2.3 Reynolds Equation

The introduction of a fluid film between moving surfaces provides a lubricating effect which substantially reduces the coefficient of friction between them. As previously discussed, such films are usually sufficiently thin that viscous forces are large in comparison with inertia forces, so that the latter may be neglected. The Navier-Stokes equation in fluid dynamics can be shown to reduce to the Reynolds equation in lubrication theory when inertia effects are negligible [22].

Using the preceding Equations (2.10) and (2.11) as a start and integrating them with respect to z with the boundary conditions that $u(h) = v(h) = 0$ and $u(0) = U, v(0) = V$ gives

$$u = \frac{1}{2\mu}\frac{\partial p}{\partial x} z(z-h) + U\frac{(h-z)}{h}$$

$$v = \frac{1}{2\mu}\frac{\partial p}{\partial y} z(z-h) + V\frac{(h-z)}{h} \tag{2.18}$$

Now assuming $\rho \neq \rho(z)$ and integrating the continuity equation (compressible, unsteady state flow) with respect to z across the passage.

$$\int_0^h \frac{\partial \rho u}{\partial x} dz + \int_0^h \frac{\partial \rho v}{\partial y} dz + \rho w(h) + \frac{\partial \rho}{\partial t} h = 0 \tag{2.19}$$

where $w(h) = \frac{\partial h}{\partial t}$, Equation(2.19) can then be rewritten as:

$$\int_0^h \frac{\partial \rho u}{\partial x} dz + \int_0^h \frac{\partial \rho v}{\partial y} dz + \frac{\partial \rho h}{\partial t} = 0 \qquad (2.20)$$

Now applying Leibnitz's rule for differentiating an integral gives:

$$\frac{\partial}{\partial t} \int_{a(t)}^{b(t)} f(x,t) dx = f[b(t),t]\frac{db}{dt} - f[a(t),t]\frac{da}{dt} + \int_{a(t)}^{b(t)} \frac{\partial f(x,t)}{\partial t} dx \qquad (2.21)$$

The result of this operation gives

$$\frac{\partial}{\partial x} \int_0^h \rho u dz + \frac{\partial}{\partial y} \int_0^h \rho v dz + \frac{\partial \rho h}{\partial t} = 0 \qquad (2.22)$$

Since $\rho \neq \rho(z)$ is assumed, it can be removed from the integral, and from Equation (2.18)

$$\int_0^h u dz = -\frac{1}{12\mu}\frac{\partial p}{\partial x} h^3 + \frac{Uh}{2} \text{ and } \int_0^h v dz = -\frac{1}{12\mu}\frac{\partial p}{\partial y} h^3 + \frac{Vh}{2} \qquad (2.23)$$

Substituting (2.23) into (2.22) the result is as follows [34],

$$\frac{\partial}{\partial x}\left(\frac{\rho h^3}{\mu}\right)\frac{\partial p}{\partial x} + \frac{\partial}{\partial y}\left(\frac{\rho h^3}{\mu}\right)\frac{\partial p}{\partial y} = 6\left[\frac{\partial}{\partial x}(\rho U h) + \frac{\partial}{\partial y}(\rho V h)\right] + 12\frac{\partial \rho h}{\partial t} \qquad (2.24)$$

The physical significance of equation (2.24) is that the generation of hydrodynamic pressure within the film is a function of three terms which have been called the wedge, stretch, squeeze contributions to load and local expansion. The wedge term appears to be the most important of the three terms in common application such as bearing design. Most lubrication examples assume smooth and rigid bounding surfaces for the lubricant, and in such cases the stretch term has no significance. The squeeze contribution is due to normal approach of the surfaces, whether or not sliding motion occurs between them. This effect can be caused by slow speed squeezing action, or by relative normal vibration between the surfaces.

2.4 Energy Equation

During the lubrication process energy is dissipated in the two ways, the action of viscous friction and compression (smaller effect) [35, 36]. Both of these sources release heat which changes the fluid temperature. Energy dissipation is highly dependent on the viscosity of the fluid which changes the dissipation as well as the flow and pressure. The energy equation results from a balance between the heat generated by mechanical dissipation and the heat transported. The mechanisms of heat transport are conduction and convection. The effects of heat conduction are described by means of Fourier's Law.

A fundamental equation of hydrodynamics is the law expressing the conservation of energy at a point in the lubricant film. In the unsteady-state form, with no external sources of film heating and constant pressure across the film thickness it may be expressed in the Cartesian coordinates as [35, 37]:

$$\rho\left[\frac{\partial E}{\partial t}u\frac{\partial E}{\partial x}+v\frac{\partial E}{\partial y}+w\frac{\partial E}{\partial z}\right]+\rho p\left[u\frac{\partial}{\partial x}\left(\frac{1}{\rho}\right)+v\frac{\partial}{\partial y}\left(\frac{1}{\rho}\right)+w\frac{\partial}{\partial z}\left(\frac{1}{\rho}\right)\right]=$$

$$\left[\frac{\partial}{\partial x}\left(k\frac{\partial T}{\partial x}\right)+\frac{\partial}{\partial y}\left(k\frac{\partial T}{\partial y}\right)+\frac{\partial}{\partial z}\left(k\frac{\partial T}{\partial z}\right)\right]-\lambda\left[\frac{\partial u}{\partial x}+\frac{\partial v}{\partial y}+\frac{\partial w}{\partial z}\right]+\Phi \qquad (2.25)$$

The first term is the change in the internal energy and internal energy, E, which can be expressed in terms of known quantities of lubricant. Enthalpy per unit mass, V, is defined as

$$I = E + V = E + \frac{1}{\rho}$$

and, differentiating, $\partial E = \partial I - p\partial V - V\partial p$

Also $\partial E = c_p T - T\left(\frac{\partial V}{\partial T}\right)\partial p - p\partial V$

Define the coefficient of thermal expansion α as

$$\alpha = \frac{1}{V}\left(\frac{\partial V}{\partial T}\right)$$

Therefore:

$$\partial E = c_p T - \alpha T V \partial p - p \partial V$$

also $$\partial E = c_p T - \alpha T\, \partial p / \rho - p \partial (1/\rho) \tag{2.26}$$

Substituting for ∂E in Equation (2.25),

$$\rho c_p\left[\frac{\partial T}{\partial t} + u\frac{\partial T}{\partial x} + v\frac{\partial T}{\partial y} + w\frac{\partial T}{\partial z}\right] - \alpha T\left[u\frac{\partial p}{\partial x} + v\frac{\partial p}{\partial y} + w\frac{\partial p}{\partial z}\right] =$$

$$\left[\frac{\partial}{\partial x}\left(k\frac{\partial T}{\partial x}\right) + \frac{\partial}{\partial y}\left(k\frac{\partial T}{\partial y}\right) + \frac{\partial}{\partial z}\left(k\frac{\partial T}{\partial z}\right)\right] - \lambda\left[\frac{\partial u}{\partial x} + \frac{\partial v}{\partial y} + \frac{\partial w}{\partial z}\right] + \Phi \tag{2.27}$$

where the last two terms are the dissipation function. This is given as the rate at which the viscous forces do work. λ is volume viscosity and

$$\Phi = \mu\left[2\left(\frac{\partial u}{\partial x}\right)^2 + 2\left(\frac{\partial v}{\partial y}\right)^2 + 2\left(\frac{\partial w}{\partial z}\right)^2 - \frac{2}{3}\left(\frac{\partial u}{\partial x} + \frac{\partial v}{\partial y} + \frac{\partial w}{\partial z}\right)^2\right] +$$

$$\mu\left[\left(\frac{\partial u}{\partial y} + \frac{\partial v}{\partial x}\right)^2 + \left(\frac{\partial v}{\partial z} + \frac{\partial w}{\partial y}\right)^2 + \left(\frac{\partial w}{\partial x} + \frac{\partial u}{\partial z}\right)^2\right]$$

The physical significance of equation (2.27) is that the generation of temperature within the film is a function of four parts which are the compression, viscous, convection, and conduction. The first term in the left hand side of Equation (2.27) expresses the convection of the internal energy of the fluid. The convection cooling term is generally not considered to be significant in such a lubrication problem with very narrow passage. Cameron justified its principal cooling term with an order of magnitude analysis by comparing it in application to a hydrodynamic type bearing [34]. Accordingly, the conduction cooling term in the first term of the right hand side is more important. The relative importance of the heating terms may provide a useful tool to avoid some difficulty in solving the equation. Results estimated with the viscous heating term alone as the heating source are found in many references [35-37]. However, in this study all terms are considered.

2.5 Summary and Conclusion

This chapter has dealt with the basic lubrication equations used in the study of thermohydrodynamic problem. The Navier-Stokes equations have been derived in general form for lubricating films. The Reynolds equation was then derived from the coupling of the reduced general form with the continuity equation. The Reynolds equation contains viscosity and density as parameters. These properties are depend on the pressure, film thickness, and time. The energy equation governs the temperature distribution within the lubricant. The coupling of the Reynolds equation and energy equation will be dealt with in Chapter 5, where the full theory of thermohydrodynamic lubrication is developed. Velocity expression derived from the reduced general form is used for determining the shear zone using Newtonian behavior. This will be classified with two different approaches considered to determine the shear zone in the thermohydrodynamic problem.

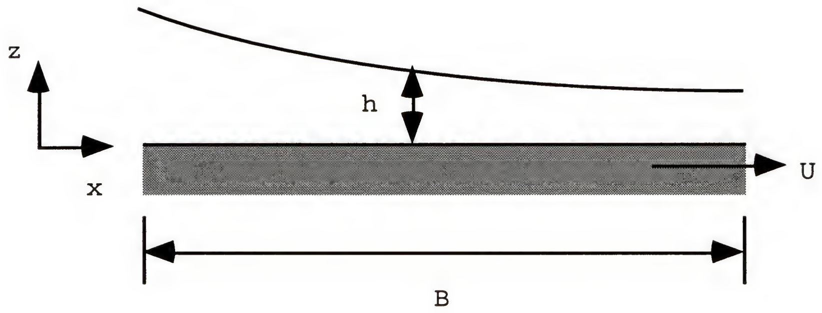

Figure 2.1 Schmatic of free surface flow

CHAPTER 3
FREE SURFACE FILM FLOWS

3.1 Introduction

The first theoretical treatment of the withdrawal processes was presented by Jeffreys [6]. Since he neglected the effect of surface tension, his results predict the maximum film thickness for a given set of conditions. Surface tension forces tend to squeeze out liquid from the film thus decreasing film thickness.

A more accurate description of the withdrawal process was presented by Landau and Levich [3]. The initial work of Landau and Levich regarded the problem as one-dimensional, neglecting the velocities in the meniscus region normal to the moving sheet. Furthermore, the gravity forces were also. They introduced the static meniscus condition, considering equilibrium between gravitational and capillary forces in the thick meniscus region. Therefore, their work considered the effect of surface tension and made the assumption that the convective momentum terms were negligible. The curvature match method used by Landau-Levich and others to derive withdrawal theories is based on matching surface curvatures in the meniscus region [3]. Later, White and Tallmadge included gravitational forces, while retaining the one-dimensional assumption [5, 8]. However, in order to apply the static meniscus condition derived by Landau and Levich and obtain an analytical but approximate expression for the relationship between the parameters of the problem. Soroka and Tallmadge presented the solution including the nonlinear inertia effects for a Newtonian fluid [38]. They assumed that the non-linear inertial terms in momentum equations can be linearized by considering the treatment of Oseen [33]. It is found that the inertia effects become very important for capillary number in the case of $Ca > 1.0$ [13-15].

The previous predictions for the film thickness in the case of angular withdrawal of flat plate from liquid container were based on a one-dimensional linear approach introduced by Deryagin and Levi and developed by Tallmadge [7, 8]. Deryagin and Levi obtained a solution by assuming constant surface tension, a one-dimensional flow in the thin meniscus, and a negligible value of the thin thickness gradient $dh/dx \ll 1$ [9, 10].

There have been many studies of the film thickness on a rotating cylinder. Tharmalingam and Wilkinson applied the theory of flat plate withdrawal to that of the cylinder. They also analyzed the thickness of the liquid adhering to cylinder although their predicts are too large [10].

When a partially submerged cylinder rotates in an oil bath as in Figure 1.1-(a) a thin film of liquid is withdrawn from the container. This simple system provides a model both physically and mathematically. It is considered the phenomenon of fluid dynamics under relatively idealized conditions. It is desired to predict the flow rate, q, which is constant around the periphery, and the film thickness, h, which depends on the angle of measure, θ_m, as functions of the fluid properties, μ, ρ, and σ the angle of contact θ_C, the cylinder radius, R, and the rotating speed, U. The withdrawal problem of Newtonian liquids onto a rotating cylinder reduces to the drag-out problem due to a plate inclined at an appropriate angle θ_C to the horizontal liquid surface. The problem for the inclined flat plate is sketched in Figure (3.2).

The study described in this proposal deals with the dynamics of liquid films on flat plate and extends the case to the cylindrical geometry,

1. The fluid is incompressible and isotropic
2. The flow is laminar and stable
3. Gravity is the only body force

4. The solid support is completely wetted by the fluid
5. The fluid is Newtonian

With contact angles other than zero, and using the assumptions stated above the steady state momentum Equations (2.11), (2.12), and continuity equation (2.13) referred in Chapter 2 becomes,

$$u\frac{\partial u}{\partial x}+w\frac{\partial u}{\partial z}=-\frac{1}{\rho}\frac{\partial p}{\partial x}-\frac{1}{\rho}\frac{\partial \tau_{xz}}{\partial z}-g\sin\theta_c \tag{3.1}$$

$$\frac{\partial p}{\partial z}=\rho g\cos\theta_c \tag{3.2}$$

$$\frac{\partial u}{\partial x}+\frac{\partial v}{\partial z}=0 \tag{3.3}$$

It is assumed that the interfacial shear stresses are negligible and that the only pressure existing at the interface besides atmospheric is that due to surface tension:

$$\vec{\tau}\cdot\vec{s}=\tau_{xz}=0 \text{ and } p=p_\sigma \qquad \text{at } z=h \tag{3.4}$$

The free surface can be described by the *h(x),* and the radius of curvature of the surface is given by $\frac{1}{R}=-\frac{d^2h/dx^2}{\left[1+(dh/dx)^2\right]^{3/2}}$ [3]. Since the curvature is assumed to be small, Laplace's capillary statics equation can be used to approximate the pressure [3, 4].

$$p_\sigma=-\sigma\frac{d^2h}{dx^2} \tag{3.5}$$

For another condition at the free surface it is also assumed that the interfacial shear stresses exists and that the pressure existing at the interface besides atmospheric is that due to surface tension and normal stress:

$$\vec{\tau}\cdot\vec{n}=\tau_{zz}=-\tau_{xx} \text{ and } p+\tau_{zz}=p_\sigma \qquad \text{at } z=h \tag{3.6}$$

where $\vec{\tau}\cdot s$ and $\vec{\tau}\cdot n$ are the shear and normal components of stress, respectively.

At the wall of the moving plate the non-slip condition is involved:

$$u=U \text{ and } w=0 \qquad \text{at } z=0 \tag{3.7}$$

The Newtonian relationship between shear stress and rate of deformation:

$$\tau_{xz} = -\mu \frac{\partial u}{\partial z} \tag{3.8}$$

Combining Equations (3.4), (3.5), (3.6), (3.8) and substituting into Equation (3.1) gives:

$$u\frac{\partial u}{\partial x} + w\frac{\partial u}{\partial z} = \frac{\sigma}{\rho}\frac{d^3 h}{dx^3} + \frac{\mu}{\rho}\frac{\partial^2 u}{\partial z^2} - g\sin\theta_c \tag{3.9}$$

3.2 Landau-Levich Solution

In the theoretical development, the withdrawal process is divided into three regions as described by Gutfinger and Tallmadge, Landau-Levich [2, 3]. These three regions describe different phenomena of flow dynamics as follows:

Region 1. This is the region above the liquid level where the film thickness is a constant (h_O). Surface tension effects are not effective. The resulting flow equation is:

$$\frac{\mu}{\rho}\frac{\partial^2 u}{\partial z^2} - g\sin\theta_c = 0 \tag{3.10}$$

Region 2. This is the "dynamic meniscus" region. Here viscous, surface tension, and gravitational forces are present:

$$\frac{\mu}{\rho}\frac{\partial^2 u}{\partial z^2} + \frac{\sigma}{\rho}\frac{d^3 h}{dx^3} - g\sin\theta_c = 0 \tag{3.11}$$

Region 3. This is the "static meniscus" region near the liquid surface. Only surface tension forces are considered. The process is described by Laplace's equation of capillary statics:

$$-\frac{p}{\sigma} = \frac{\dfrac{d^2 h}{dx^2}}{\left[1+\left(\dfrac{dh}{dx}\right)^2\right]^{3/2}} = \frac{\rho g x}{\sigma}(1-\cos\theta_c) \tag{3.12}$$

An approximate solution to the continuous withdrawal process results from a combined solution of the three regions. Boundary conditions for the moving film are given as

$$\tau_{xz} = 0 \qquad \text{at } z = h$$

$$u = U \qquad \text{at } z = 0 \tag{3.13}$$

Equation (3.10) using the boundary conditions gives the velocity profile for region 1 and the flow rate can be obtained by integrating Equation (3.9).

In similar manner Equation (3.11) gives the flow rate for region. These solutions to regions 1 and 2 are matched by using the steady state condition of equal flow rates in both regions,

$$Uh_0 - \frac{\rho g \sin\theta_c}{\mu}\left(\frac{h_0^3}{3}\right) = Uh - \left(-\frac{\sigma}{\mu}\frac{d^3h}{dx^3} + \frac{\rho g \sin\theta_c}{\mu}\right)\left(\frac{h^3}{3}\right) \tag{3.14}$$

Equation (3.14) is a third order non-linear differential equation in h with the boundary conditions,

$$h = h_0, \qquad dh/dx = 0, \qquad d^2h/dx^2 = 0 \qquad \text{at } x = 0 \tag{3.15}$$

This equation is put into dimensionless form by considering the treatment of White with the substitutions [5],

$$\varsigma = \frac{h}{h_0},\ T_o = h_o\left(\frac{\rho g \sin\theta_c}{\mu U}\right)^{1/2},\ C_a = \frac{\mu U}{\sigma},\ \lambda = -\frac{x}{h_o}(3Ca)^{1/3} \tag{3.16}$$

With the substitutions, Equation (3.14) becomes in dimensionless form,

$$\varsigma^3\frac{d^3\varsigma}{d\lambda^3} = \varsigma - 1 - \frac{T_0^2}{3}\left(\varsigma^3 - 1\right) \tag{3.17}$$

with the boundary conditions,

$$\varsigma = 1, \qquad \frac{d\varsigma}{d\lambda} = 0, \qquad \frac{d^2\varsigma}{d\lambda^2} = 0, \qquad \text{at } \lambda = 0 \tag{3.18}$$

To match the solution for the static meniscus, region 3, with that of the dynamic meniscus, region 2, the condition must be needed that, the curvature computed from the dynamic meniscus Equation (3.11) is identical to that computed from the static meniscus Equation (3.12). It is approached from the dynamic meniscus side or from that of the static meniscus.

The curvature match condition is stated in dimensionless form as [3, 5, 8],

$$\left(\frac{d^2\varsigma}{d\lambda^2}\right)_{\varsigma_2\to\infty} = \left(\frac{d^2\varsigma}{d\lambda^2}\right)_{\varsigma_3\to 1} \tag{3.19}$$

Integration of the Equation (3.12) for the region 3 with the boundary condition $h = \infty$ at the horizontal liquid surface gives [39],

$$\frac{\dfrac{dh}{dx}}{\left[1+\left(\dfrac{dh}{dx}\right)^2\right]^{1/2}} = \frac{\rho g x^2}{2\sigma}(1-\cos\theta_c)-1 \tag{3.20}$$

From the condition that $dh/dx \to 0$ as $h \to h_0$, the solution of Equation (3.20) is $x \to \sqrt{2}\left(\dfrac{\sigma}{\rho g(1-\cos\theta_c)}\right)^{1/2}$. Substituting this solution into Equation (3.12), the curvature is obtained as follows,

$$\left(\frac{d^2 h}{dx^2}\right)_{h\to h_0} \to \sqrt{2}\left(\frac{\rho g(1-\cos\theta_c)}{\sigma}\right)^{1/2} \tag{3.21}$$

which becomes in dimensionless form,

$$\left(\frac{d^2\varsigma}{d\lambda^2}\right)_{\varsigma\to 1} \to \frac{\sqrt{2}}{h_0}\left(\frac{\rho g(1-\cos\theta_c)}{\sigma}\right)^{1/2}\left(\frac{\sigma h_0^{3}}{3\mu U}\right)^{2/3} \tag{3.22}$$

In the Equation (3.17) with $T_0^{\,2} << 1$ it takes the form as follows,

$$\varsigma^3\frac{d^3\varsigma}{d\lambda^3} = \varsigma - 1 \tag{3.23}$$

From a numerical integration of Equation (3.23) results are shown in Figure (3.3) as follows [3, 5, 9],

$$\left(\frac{d^2\varsigma}{d\lambda^2}\right)_{\varsigma\to\infty} \to 0.643 = S \tag{3.24}$$

Substitution of Equations (3.22) and (3.24) into Equation (3.19) gives,

$$S = 0.643 = \frac{\sqrt{2}}{h_0}\left(\frac{\rho g(1-\cos\theta_c)}{\sigma}\right)^{1/2}\left(\frac{\sigma h_0{}^3}{3\mu U}\right)^{2/3} \tag{3.25}$$

Introducing the dimensionless variables, the Landau-Levich' result is,

$$T_0 = \frac{3^{2/3}}{\sqrt{2}} Ca^{1/6} S\left(\frac{\sin\theta_c}{1-\cos\theta_c}\right)^{1/2} \tag{3.26}$$

3.3 Extension to the Landau-Levich Model

In deriving Equation (3.17), Landau and Levich neglected the drainage down the plate due to gravitational force [3]. When gravity is taken into account, the governing equation and boundary conditions are already obtained in Equations (3.17) and (3.18) in dimensionless form.

To match boundary conditions of Equation (3.17) when $\frac{d^3\varsigma}{d\lambda^3} \to \frac{1}{3}T_0{}^2$ as $\varsigma \to \infty$, Equation (3.17) can be linearized by substituting $\varsigma = 1+\varepsilon$ and neglecting terms of the order ε^2 [5]. Therefore,

$$\varsigma^3\frac{d^3\varsigma}{d\lambda^3} = \left(1 - T_o{}^2\right)\varepsilon \tag{3.27}$$

After making a change of variables to $\chi = \left(1 - T_o{}^2\right)^{1/3}\lambda$, Equation (3.27) transforms to

$$\varsigma^3\frac{d^3\varsigma}{d\chi^3} = \varepsilon \text{ or } \varsigma^3\frac{d^3\varsigma}{d\chi^3} = \varsigma - 1 \tag{3.28}$$

which is similar to the Landau and Levich equation. In same manner used in Equation (3.23),

$$\left(\frac{d^2\varsigma}{d\chi^2}\right)_{\varsigma_2\to\infty} = 0.643 = S \tag{3.29}$$

where S is constant and independent on Ca and T_O.

Equation (3.29) also can be written by a change of variable used above as,

$$\frac{d^2\varsigma}{d\lambda^2} = \left(1 - T_0{}^2\right)^{2/3} \frac{d^2\varsigma}{d\chi^2} = \left(1 - T_0{}^2\right)^{2/3} S \tag{3.30}$$

Proceeding using the same method as Landau and Levich, an equation that related the dimensionless film thickness to the capillary number can be obtained. Substituting Equations (3.29) and (3.30) into Equation (3.19),

$$\frac{T_0}{\left(1 - T_o{}^2\right)^{2/3}} = \frac{3^{2/3}}{\sqrt{2}} Ca^{1/6} S \left(\frac{\sin\theta_C}{1 - \cos\theta_C}\right)^{1/2} \tag{3.31}$$

The modified treatment is presented to give a more realistic boundary condition [11, 12]. The tangential stress at the free surface becomes,

$$\frac{1}{2}\left(\tau_{xx} - \tau_{zz}\right)\sin 2\theta + \tau_{xz}\cos 2\theta = 0 \tag{3.32}$$

and the normal stress at the free surface becomes,

$$p + \tau_{xx}\sin^2\theta + \tau_{zz}\cos^2\theta + \tau_{xz}\sin 2\theta = p_0 - \frac{\sigma}{R} \tag{3.33}$$

The boundary conditions apply in the case of $\theta = 0^o$ due to the free wave, thus Equations (3.32) and (3.33) become as follows,

$$\tau_{xz} = -\mu\frac{\partial u}{\partial z} = 0 \tag{3.34}$$

$$\frac{p}{\sigma} + 2\frac{\mu}{\sigma}\frac{\partial u}{\partial x} = -\frac{d^2 h}{dx^2} \qquad \text{at } z = h \tag{3.35}$$

To give the velocity profile from equation (3.11) as,

$$u = U + \frac{\rho g \sin\theta_c + \dfrac{dp}{dx}}{\mu}\left(\frac{z^2}{2} - hz\right) \tag{3.36}$$

Differentiating Equation (3.35) and substituting Equation (3.35) into Equation (3.36), the result is given by

$$\sigma\frac{d^3h}{dx^3}-3\mu q\sin\theta_c\frac{d}{dx}\left(\frac{1}{h^2}\frac{dh}{dx}\right)+\frac{3\mu}{h^3}\left(Uh-q-\frac{\rho g\sin\theta_c h^3}{3\mu}\right)=0 \qquad (3.37)$$

or

$$\frac{d^3\varsigma}{d\lambda^3}+(3Ca)^{2/3}\left(1-\frac{T_0^{\,2}}{3}\right)\frac{d}{d\lambda}\left(\frac{1}{\varsigma^2}\frac{d\varsigma}{d\lambda}\right)-\frac{1}{\varsigma^3}\left[(\varsigma-1)+\frac{1}{3}T_0^{\,2}\left(1-\varsigma^3\right)\right]=0 \qquad (3.38)$$

Equation (3.38) can be linearized by substituting $\varsigma=1+\varepsilon$ where ε is small and neglecting terms of the order ε^2 [5]. Introducing the change of variable again, Equation (3.38) becomes,

$$\frac{d^3\varsigma}{d\chi^3}+(3Ca)^{2/3}\left(1-\frac{T_0^{\,2}}{3}\right)\left(1-T_0^{\,2}\right)^{-1/3}\left(-2\frac{\left(\frac{\partial\varsigma}{\partial\chi}\right)^2}{\varsigma^3}+\frac{\frac{\partial^2\varsigma}{\partial\chi^2}}{\varsigma^2}\right)-\frac{\varsigma-1}{\varsigma^3}=0$$

(3.39)

Upon numerical solution of Equation (3.39) the curvature at $\chi\rightarrow 0$ has a finite value.

$$\left(\frac{d^2\varsigma}{d\chi^2}\right)_{\chi\rightarrow 0}=S(Ca,T_0) \qquad (3.40)$$

The numerical integration of Equation (3.40) can be carried out using Euler predictor-corrector method with the starting value procedure introduced by Landau and Levich [5]. Values of *S(Ca, T* are plotted in Figure (3.2) with T_O and Ca. Here, at the high Capillary numbers, the results show that film thickness are relatively larger as the values of the curvature coefficient S rapidly increase.

Substituting Equation (3.40) into Equation (3.22), therefore,

$$\left(\frac{d^2\varsigma}{d\lambda^2}\right)_{\varsigma\rightarrow 1}\frac{1}{\left(1-T_0^{\,2}\right)^{1/3}}\rightarrow\frac{\sqrt{2}}{h_0}\left(\frac{\rho g(1-\cos\theta_c)}{\sigma}\right)^{1/2}\left(\frac{\sigma h_0^{\,3}}{3\mu U}\right)^{2/3} \qquad (3.41)$$

or

$$\frac{T_o}{\left(1-T_0{}^2\right)^{2/3}} = \frac{3^{2/3}}{\sqrt{2}} S(Ca,T_0)Ca^{1/6}\left(\frac{\sin\theta_c}{1-\cos\theta_c}\right)^{1/2} \qquad (3.42)$$

The above Equations (3.42) have been tested over a range speed and viscosity indicated by a range of Capillary Number from 0.001 to 10 as given in Table 2. There is no reason to doubt its applicability at value of Ca lower than 0.01. Calculated data obtained from three theories are considered to be good when 0.01 < Ca < 0.05 as shown in Figure (3.5). The small differences may not be significant since they are not affected by any surface tension and gravity force in this region. For high Ca, from 0.05 to 0.5 the results of Equation (3.42) with realistic boundary conditions seems to have more accurate values compared with the other two results from Equations (3.26) and (3.31). However, for higher Capillary Number, Ca > 0.5, the results of Equation (3.36) seem to have stable values compared with other two results from Equations (3.31) and (3.42). Significant differences in this region are due to the assumption of negligible gravitational forces in Equation (3.26) with respect to viscous forces, and inertia forces in all theories. Thus, when Ca > 0.5 it is necessary that the theoretical development include inertia forces to obtain results much better than that given by previous theories. Some assumptions may be limited above much high Capillary Number by the occurrence of waves or turbulence even though inertia forces are considered.

Table 2: Constant Values Dependent on Ca and To

Ca	T_O $^{(3)}$	S(Ca,To) $^{(3)}$	Ca	T_O $^{(3)}$	S(Ca,T_O) $^{(3}$
0.001	0.1954	0.6446	0.6	0.5638	0.8054
0.003	0.2330	0.6473	1.0	0.6177	0.8651
0.006	0.2602	0.6503	2.0	0.6956	0.9791
0.01	0.2823	0.6536	3.0	0.7417	1.0694
0.03	0.3369	0.6660	4.0	0.7736	1.1469
0.06	0.3775	0.6797	6.0	0.8163	1.2798
0.1	0.4113	0.6945	8.0	0.8443	1.3944
0.2	0.4635	0.7240	10.0	0.8644	1.4971
0.3	0.4979	0.7481			

Note : (3) Equation (3.42)

3.4 Application to the Cylindrical Coordinates

Equations (3.26), (3.31), and (3.42) have the non-dimensional uniform thickness, T_O, to be calculated as a function of the Capillary number, Ca, and the angle of contact θ_C. By using the final uniform film thickness, h_O, the liquid flow rate, q, and the steady state condition of equal flow rates can be calculated as follows,

$$q = Uh_0 - \frac{\rho g\, h_0^3 \sin\theta_c}{3\mu} \tag{3.43}$$

Knowing the predicted flow rate based on the uniform film thickness it is possible to apply it to the rotating cylinder for the corresponding contact angle. The analysis which is applicable to the flat plate of Equations (3.26), (3.31), and (3.42) can be modified to determine the positions and the variation of film thickness around the cylinder as follows [9],

$$q = Uh - \frac{\rho g\, h^3 \sin\theta_m}{3\mu} \tag{3.44}$$

where h is the film thickness at any point, θ_m and $R >> h$.

At the top of the rotating cylinder, $\theta_m = 0$, Equation (3.44) gives,

$$q = U\tilde{h} \tag{3.45}$$

where $\tilde{h}$ is the film thickness on the top of the rotating cylinder.

Using Equation (3.43) throughout Equation (3.45), it gets

$$\tilde{h} = h_o - \frac{\rho g h_o^3 \sin\theta_c}{3\mu U} = h - \frac{\rho g h^3 \sin\theta_m}{3\mu U} \tag{3.46}$$

Multiplying Equation (3.46) by $(\rho g \sin\theta_c/\mu)^{1/2}U$, an alternative form is as follows,

$$\tilde{T} = T_o - \frac{1}{3}T_o^3 \tag{3.47}$$

where $\tilde{T} = \tilde{h}\left(\frac{\rho g \sin\theta_c}{\mu U}\right)^{1/2}$

Similarly, multiplying Equation (3.47) by $(\rho g \sin\theta_c/\mu)^{1/2}U$, the form is,

$$\tilde{T} = T - \frac{1}{3}T^3\left(\frac{\sin\theta_m}{\sin\theta_c}\right) \tag{3.48}$$

where $T=h(\rho g \sin\theta_c/\mu U)^{1/2}$ is the film thickness at the position on the rotating cylinder. The dimensionless film thickness, T, can be calculated by using the Newton-Raphson method.

3.5 Mathematical Solution and Discussion

There is experimental data with which the final results of the Equation (3.48) given by Equations (3.26), (3.31), and (3.42) can be compared. That is the direct measurement of steady state thickness of a film withdrawn on a rotating cylinder as carried out at the University of Wisconsin-Madison. The oil used, its properties, and the measured thickness are given in Table 3. This is accomplished by scraping fluid off a continuously rotating cylinder as shown in Figure (3.1). This experimental device consists of scraper and rotating steel disc. Oil attached to the surface of rotating disk is collected by scraper located at the side of the disk. Theoretical values of dimensionless thickness, *T*, for various Capillary numbers, *Ca*, are changed to the dimensional form for comparison with the experimental results.

Table 3: Experimental Data and Lubricant Properties

Motor Oil (23.9°C)	rpm	h (cm) (θ_m= -90°)	g (m/s^2)	μ (N-s/m^2)	ρ (kg/m^3)	σ (N/m)
SAE 10W	40	0.08382	9.807	0.08	878.24	3.6×10^{-2}
	90	0.13462				
	180	0.17780				

Source: (personal communication, A. A. Seireg, 1996)

The calculated results by three different theories are presented graphically in Figures (3.6) to (3.8) by plotting the thickness, h, against rotating speed, rpm. As expected the results show that the film thickness becomes thinner as the position angle, θ_m decreases. It is considered that the results are more reliable for values of θ_c of 90^o due to the characteristics of the assumed model. Hence, the numerical solution is not stable beyond θ_m=30^o for equations (3.26) and (3.42). As rotating speed, N (rpm), increases, the film thickness also increases in the low speed range. The dimensionless film thickness depends on one dimensionless physical parameter Ca. When the surface tension of the lubricant is given, the value of Ca is related to the value of the product μU. As the velocity increases or decreases Ca corresponds to a variation of meniscus shape at low speed. The meniscus shape for various speeds changes the film thickness attached on the rotating cylinder surface.

Figure (3.9) shows a comparison of these theories with the experimental data given in Table 3 over the range of the experimental data and the theoretical results listed in Table 2. It is seen that the results of Equation (3.31) agree very closely experimental data up to a value of about 100 rpm (Ca=1.7733 in dimensionless value). The differences between the theories and experimental data at high speed (or Ca) is to be expected due to the assumption of one-dimensional flow and negligible inertia terms in the meniscus region. For higher values of Ca such assumption is no longer valid and capillary statics are no longer adequately describe the shape of the film near the liquid container. Accordingly in this study the theoretical prediction of Tallmadge and White, Equation (3.36), will be mainly considered to analysis the effect of surface tension in the phenomenon of the lubrication problem between two surfaces system which will be discussed later.

Figures (3.10) and (3.11) show the film thickness, h, at different circumferential positions on the rotating cylinder, θ_m, for the SAE 10W motor oil. It can be seen in Figure (3.10) that the larger rotating speed of the cylinder, U, the larger the film thickness, h, is. Figure (3.10) also shows that the film thickness, h, decreases with decreasing θ_m for contact angle, $\theta_c = 120^{\circ}$. This can be attributed to the increase in the velocity of the film in the circumferential direction due to gravity forces. The contact angles, $\theta_c = 60^{\circ}$, 90°, and 120°, which correspond to the situations of the cylinder submerged to three different levels are considered. Figure (3.11) shows the variations of film thickness, h, against θ_m for these contact angles. The film thickness, h, can be seen to approach a constant value with respect to θ_m near the top of the cylinder.

3.6 Summary and Conclusion

A general solution of the continuous withdrawal process from the liquid container can be made using marching technique for integrating the Navier-Stokes equations (one continuity and two momentum equations). Some approximations and simplification of the two momentum equations are introduced based on physical considerations. A withdrawal analysis on a rotating cylinder is introduced as an extension of the flat plate theory of Landau-Levich without the effect of inertia forces. The results will be useful in determining lubricating zone in the hydrodynamic analysis.

The withdrawal theory is not entirely satisfactory for predicting the film thickness at high speed (N>100 rpm). Numerical analysis by the Landau-Levich method is restricted to Ca<10 for its application. It is apparent that this is due to the reduced Navier-Stokes equations under the assumption of inertia free and one-dimensional flow. A more detailed study of the two-dimensional flow with the effect of inertia forces and interfacial boundary conditions is necessary to improve the solution for much higher speeds.

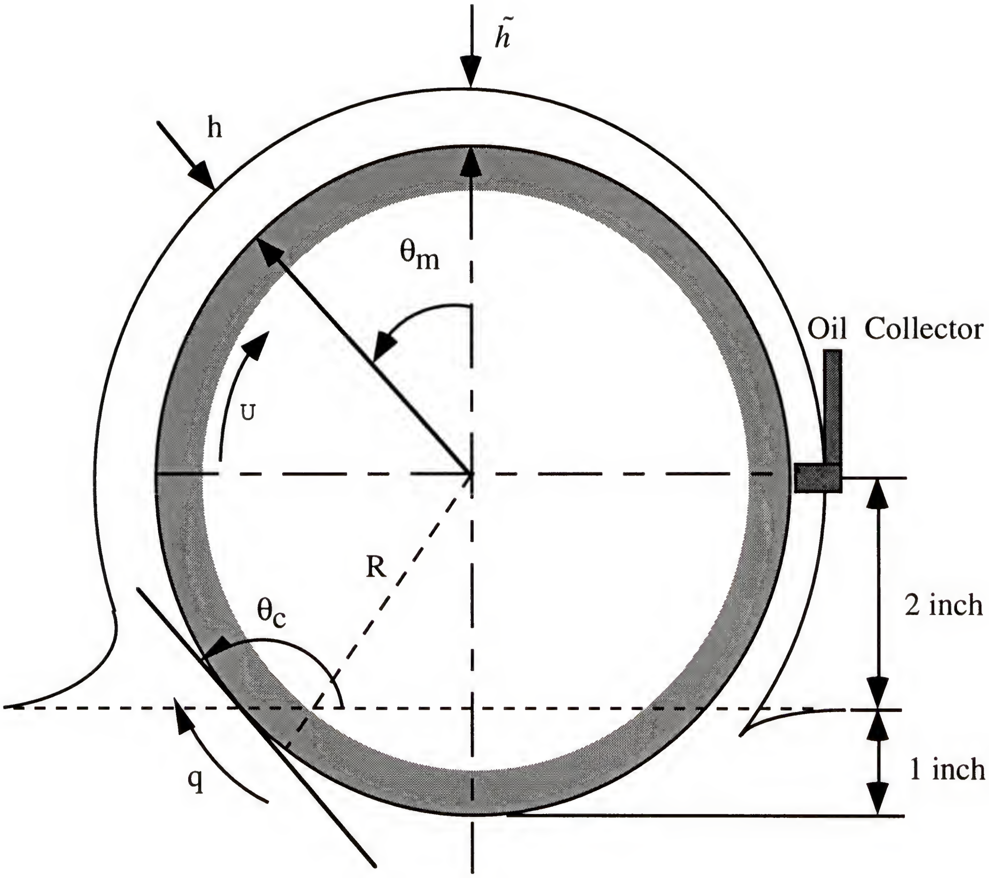

Figure 3.1 Diagram of a partially submerged rotating cylinder (disk) in an oil batrh

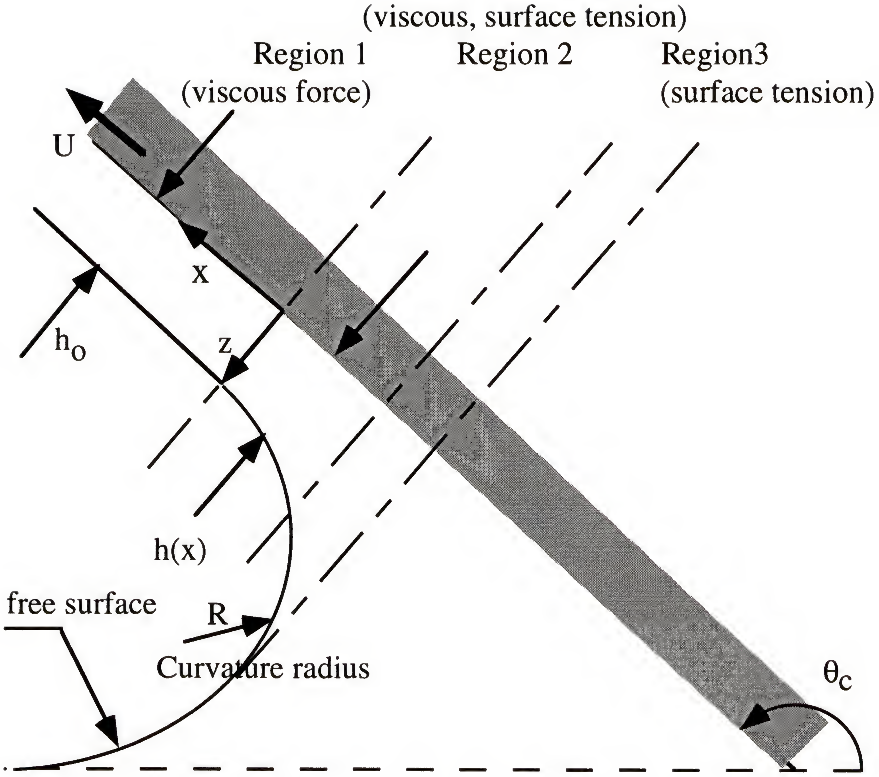

Figure 3.2 The analogy for flat plate with contact angle θ_c

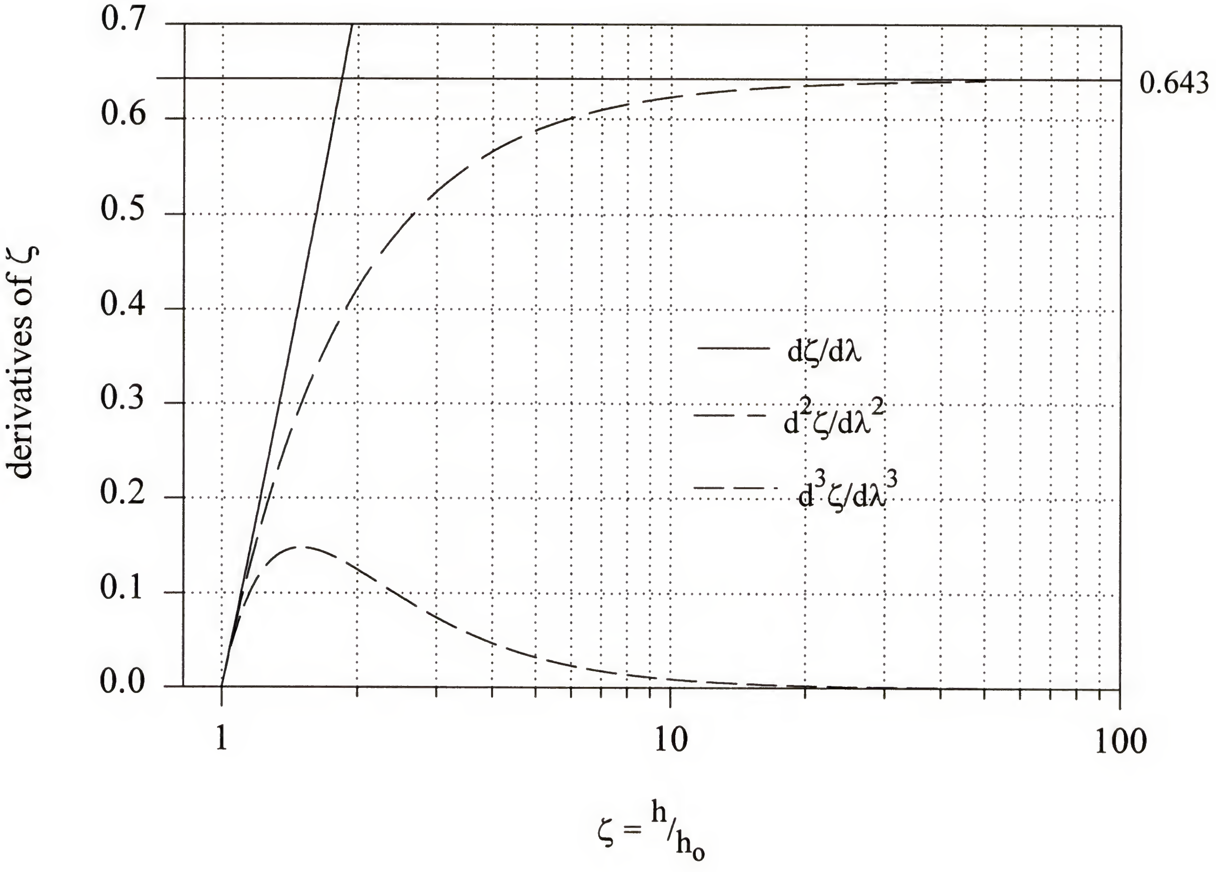

Figure 3.3 Computed solution to Equation (3.23)

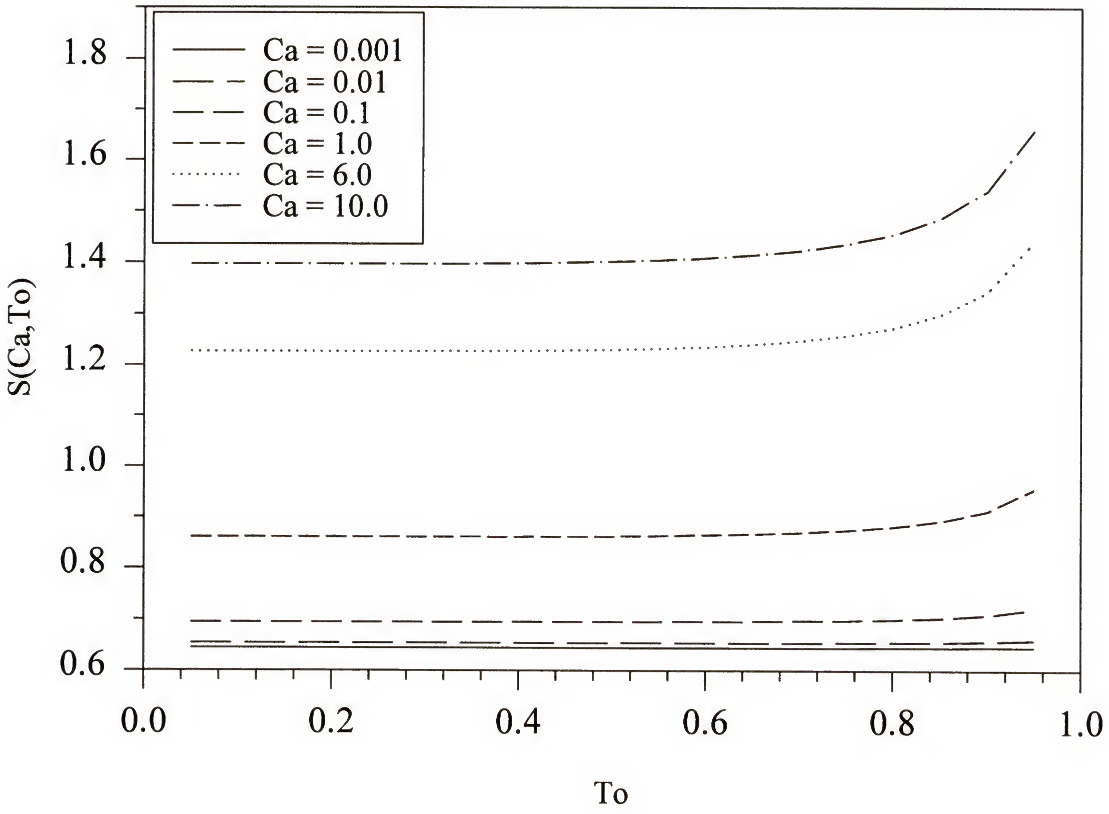

Figure 3.4 The curvature coefficient
S is Equation (3.40) as function of T_o and Ca

$T_o = h_o(^{\rho g \sin\theta c}/_{\mu U})^{0.5}$

$Ca = {}^{\mu U}/_{\sigma}$

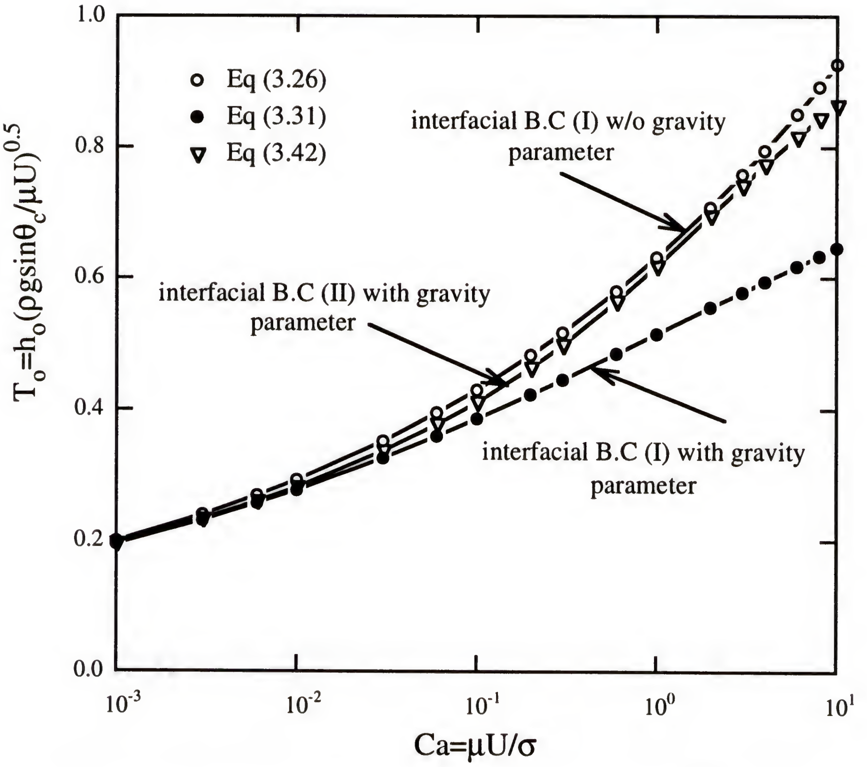

Figure 3.5 Comparison of theoretical predictions (constant film thickness in the case of a inclined flat plate)

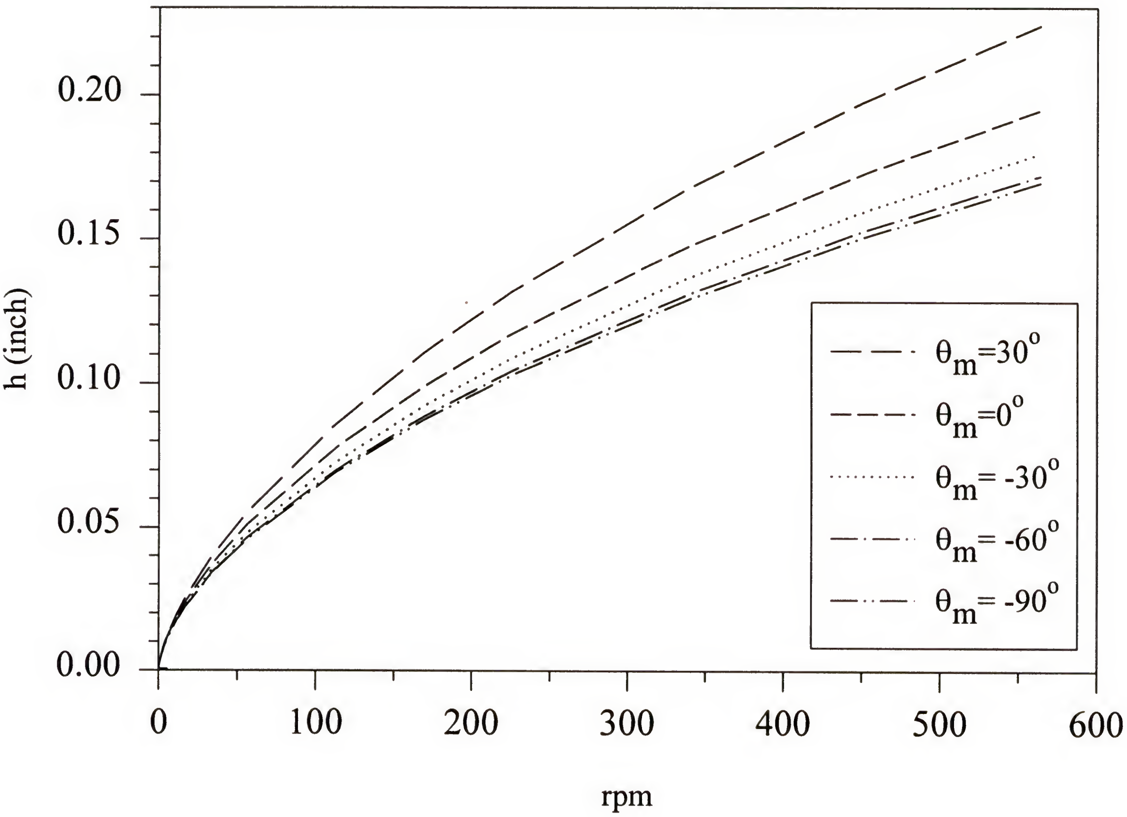

Figure 3.6 Film thickness for Landau-Levich solution to Equations (3.26) and (3.48) $\theta_c = 131.81°$

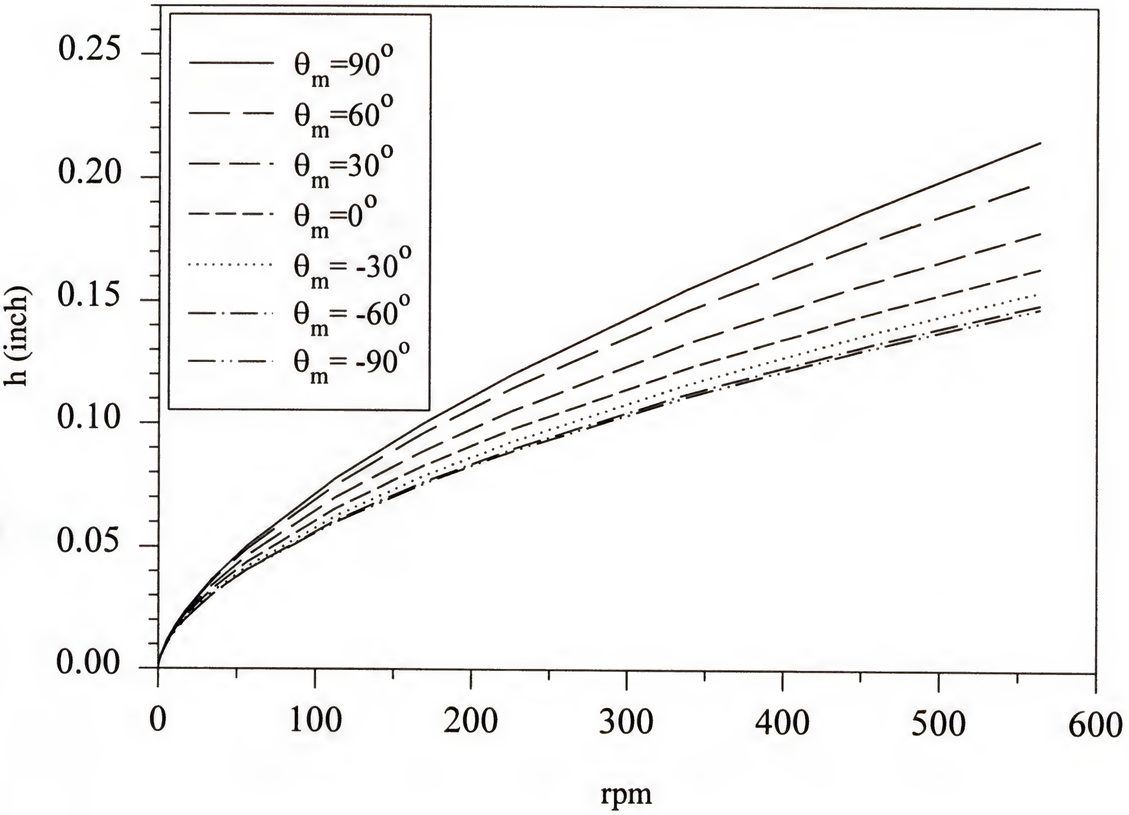

Figure 3.7 Film thickness for Equations (3.31) and (3.48)

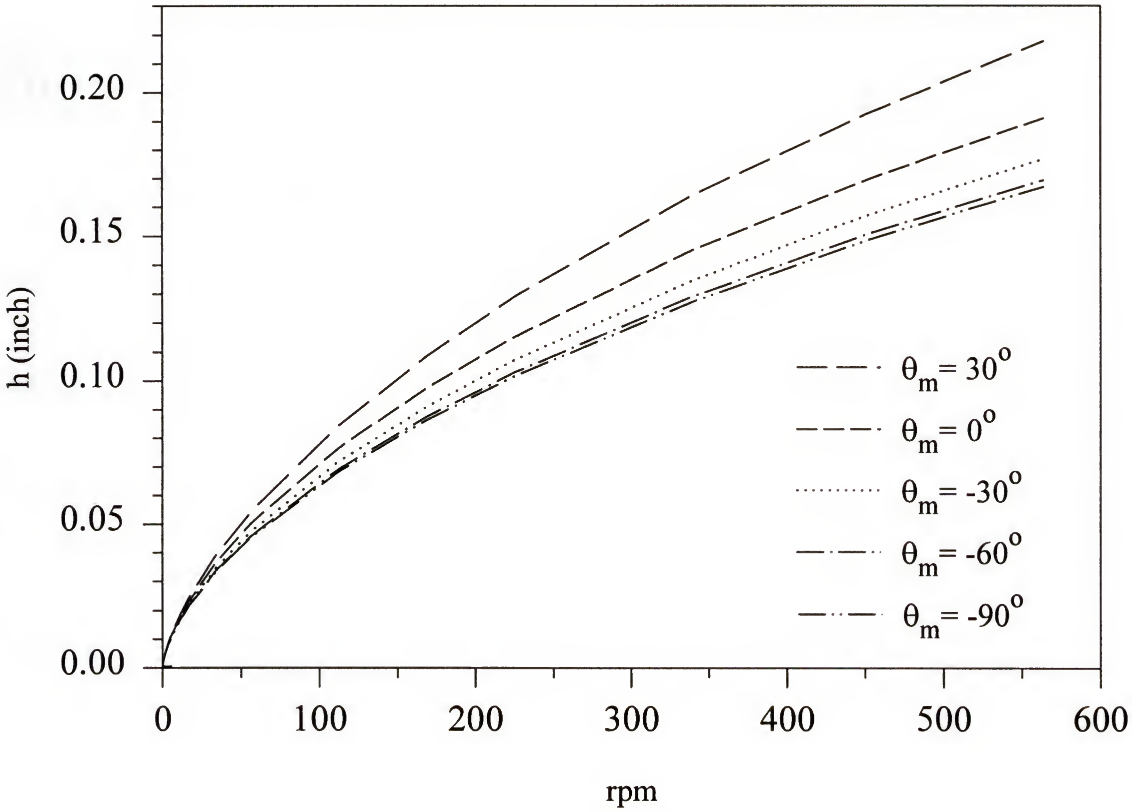

Figure 3.8 Film thickness for Equations (3.42) and (3.48)

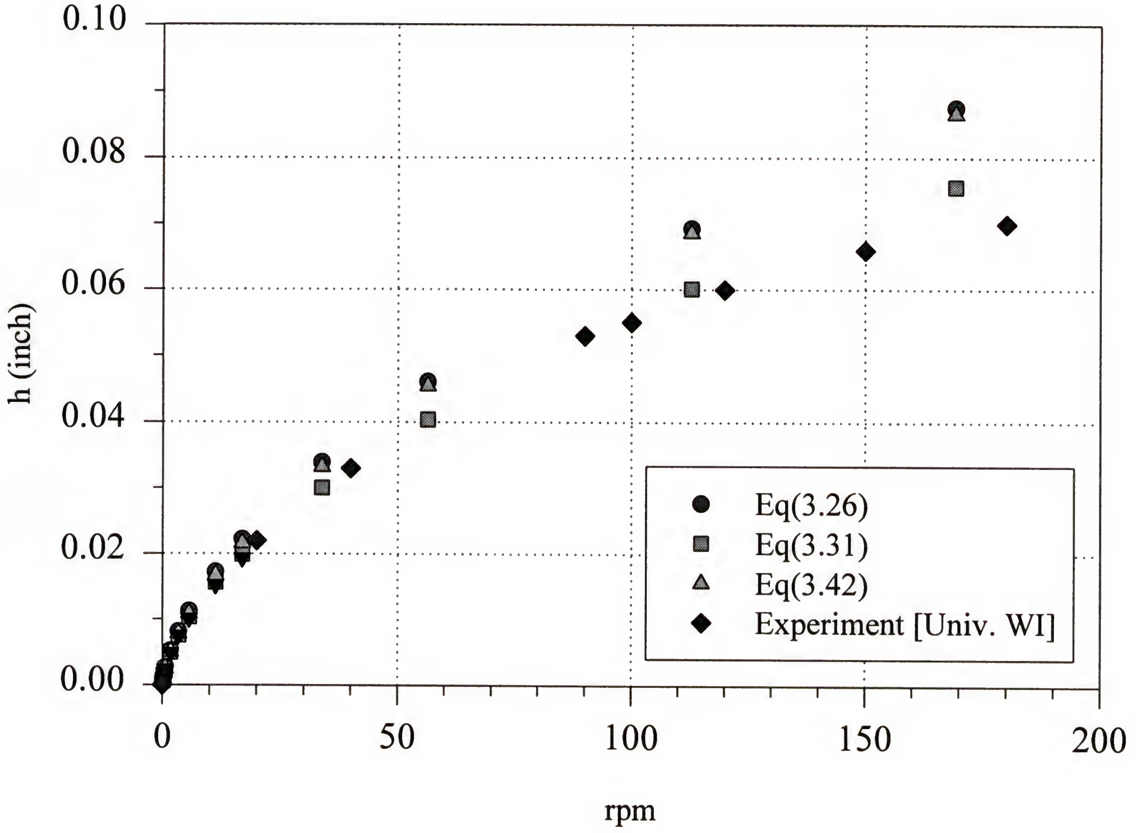

Figure 3.9 Film thickness at $\theta_m = -90^{o}$, $\theta_c = 131.81^{o}$
Comparison between analytical results of the 3 different methods, and experimental data

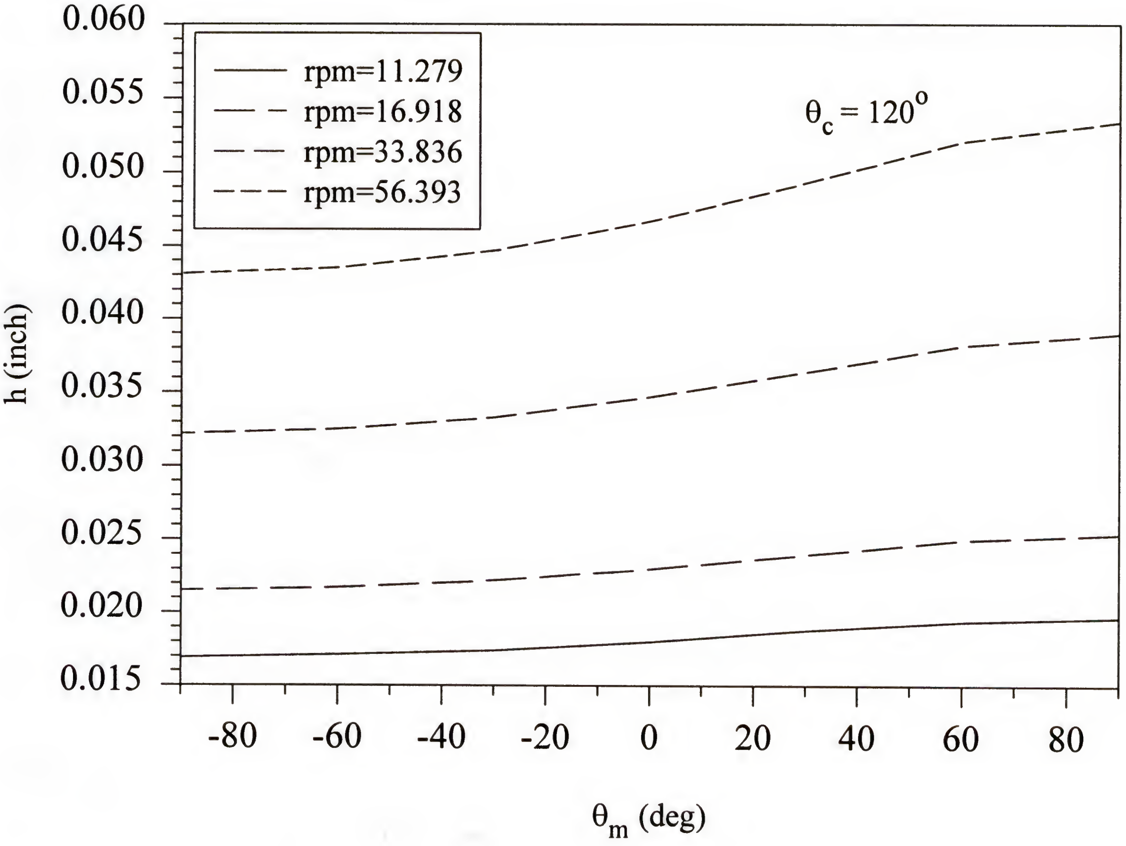

Figure 3.10 Film thickness for Equation (3.31)
(Effects of rotating speed of cylinder)

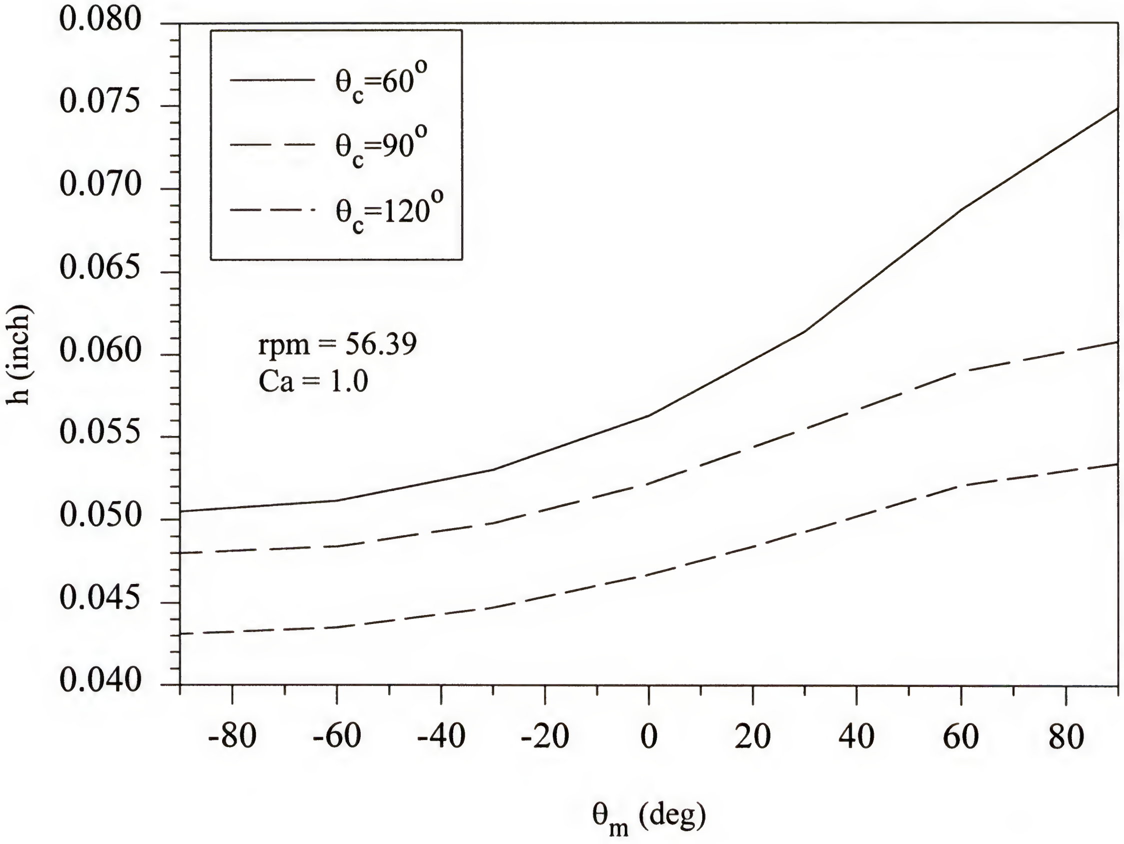

Figure 3.11 Film thickness for Equation (3.31)
(Effects of contact angle)

CHAPTER 4
FREE SURFACE FILM FLOWS IN THE PRESENCE OF A STATIONARY CONSTRAINT

4.1 Introduction

There are several basic problems in the study of slow, and two-dimensional flow of a Newtonian viscous fluid in which a single stream separates when constrained. An example is shown in Figure (4.1). Here, a rotating disc (or cylinder) and a stationary flat plate are partially immersed in a large container of viscous fluid. As the cylinder turns, fluid is drawn on the outside of rotating cylinder and enters the narrow gap between the two bodies. After flowing through the section of the closed area between the cylinder and flat plate the fluid separates under a surface tension membrane into two films.

The system in the above case has a convergent-divergent geometry in the direction of motion and the film adhering to the moving surface will be dragged into the narrowing clearance space, thus building-up a pressure which is sufficient to carry load. This is the principle of hydrodynamic lubrication, a mechanism which is essential to the efficient functioning of many systems in industry.

The problem is to how analyze the phenomenon of the flow under the surface tension membrane at the inlet and outlet regions. The shape of the membrane is not known, but must be found as part of the solution. The mathematical formulation must consider the cylinder rotation speed, the viscosity and surface tension of the fluid, cylinder radius, and clearance between two surfaces.

4.2 Literature Review

The withdrawal process by two surfaces of viscous fluid has received much attention over a period of half a century. The reason for this is partly due to the difficulty of defining suitable criteria for finding the position of the line of separation or rupture in an adhered layer between diverging surfaces. Current interest in this type of separation or rupture appears to have started with an investigation concerning the hydrodynamic behavior of lightly loaded surface in a fluid-filled capillary container [40-44]. A similar two-dimensional separating flow at the exit from the nip of an eccentric journal bearing was experimentally investigated by Taylor [43]. Approximate theoretical treatment of separation flows were undertaken by Pearson [18], and Pitts and Greiller [40]. In both investigations, gravitational effects were not included as their influence was found to be small. Some analysis for these flows such as the forward rolling process where the liquid flowing into a narrow gap between two rotating cylinders have dealt with the problem from three perspective (i) classical lubrication theory [21, 34, 40, 41], (ii) asymtotic expansion [45], and (iii) solution of the Navier-Stokes system in relevant flow domain by Galerkin/finite element method [42]. For fluid film systems in a convergent-divergent geometry some realistic cavitation boundary condition at the line of seperation or rupture have been suggested by Swift and Stieber, Floberg, and Coyne and Elrod [19, 46, 47]. They are applied to systems such as the rolling system in viscous flow by Taylor, Middleman, and Savage [21, 41, 44]. In this chapter the withdrawal process of the viscous flow in the cylinder-plane geometry is modeled using lubrication theory with known boundary conditions. The principal objective is to extend the work of Middleman and Savage to the general lubrication situation which involves flow rupture which occurs at the exit in plane-cylinder geometry as influenced by the rotating speed and surface tension [21, 44].

4.3 Mathematical Formulation

The flow pattern in the region of the meniscus is complicated and exact theoretical treatment of the problem is extremely difficult. The motion of the liquid in the region where the gap is narrow is predominantly determined by the drag due to the rotating cylinder and the variation in the width of the gap. It can be shown that inertia terms in the hydrodynamic equations can be neglected without serious error except at very high speed as illustrated in results of previous chapter. Terms representing the effect of gravity are included in the original treatment but can be also omitted for simplicity, since their influence is small except for the lowest speeds of rotation and for the larger gap widths.

To calculate the flow in the narrow part of the channel, it will be convenient to use the coordinate system in Figure (4.1). Introducing the dimensionless variables to lubrication with the gravity term for Newtonian liquid [16-18, 21],

$$\xi = \frac{x}{(RH_o)^{1/2}} \ , \ \eta = \frac{y}{H_o} \ , \ \delta = \frac{h(x)}{R}$$

$$\phi = \frac{u}{U} \ , \ \varphi = \frac{v}{U} \tag{4.1}$$

$$\mathrm{P} = \frac{pH_o^{3/2}}{\mu U R^{1/2}} \ , \ \Gamma = \frac{\rho g H_o^{2}}{\mu U} \ .$$

Equations (2.11) and (2.14) of the two-dimensional case can be transformed to the following forms,

$$\frac{\partial^2 \phi}{\partial \eta^2} = \frac{\partial P}{\partial \xi} - \Gamma \tag{4.2}$$

$$\frac{\partial \phi}{\partial \xi} + \frac{\partial \varphi}{\partial \eta} = 0 \tag{4.3}$$

Equation (4.2) may then be integrated twice with respect to η to give u in the form

$$\phi(\eta) = \frac{1}{2}\frac{\partial P}{\partial \xi}\left[\eta^2 - \tilde{H}(\xi)\eta\right] - \frac{1}{2}\Gamma\left[\eta^2 - \tilde{H}(\xi)\eta\right] + \frac{\eta}{\tilde{H}(\xi)} \tag{4.4}$$

where $\tilde{H}(\xi) = h(x) / H_o$ is the dimensionless separation between the two surface. In Equation (4.4), the boundary conditions are used as follows;

$$\phi = 0 \text{ at } \eta = 0$$

$$\phi = 1 \text{ at } \eta = \tilde{H}(\xi) \tag{4.5}$$

It is necessary to introduce an additional equation for the conservation of mass. This is given in the form

$$q = U\,H_L = \int_0^{\tilde{H}(\xi)H_o} u\,dy \tag{4.6}$$

Also, a dimensionless film thickness can be written as

$$\Theta = \frac{H_L}{H_o} = \frac{q}{UH_o} = \int_0^{\tilde{H}(\xi)} \phi\,d\eta \tag{4.7}$$

where H_L is a constant film thickness after rupture at outlet zone and then

$$\Theta = \frac{\partial P}{\partial \xi}\left[\frac{1}{6}\tilde{H}^3(\xi) - \frac{1}{4}\tilde{H}^3(\xi)\right] - \Gamma\left[\frac{1}{6}\tilde{H}^3(\xi) - \frac{1}{4}\tilde{H}^3(\xi)\right] + \frac{1}{2}\tilde{H}(\xi) \tag{4.8}$$

H_L is the film thickness which becomes uniform on a region of the cylinder surface far removed from the meniscus region where q is the flow-rate entrained by the cylinder. After performing the integration implied by Equation (4.7) and rearranging Equation (4.8) it can be solved for $dP/d\xi$ to give:

$$\frac{dP}{d\xi} = 12\frac{\frac{1}{2}\tilde{H}(\xi) - \Theta}{\tilde{H}^3(\xi)} + \Gamma \tag{4.9}$$

$$\frac{dP}{d\eta} = O(\delta) \tag{4.10}$$

It follows then, that

$$P(\xi_a) - P(\xi) - \Gamma\,\xi_a + \Gamma\,\xi = 12\int_{\xi}^{\xi_a} \frac{\frac{1}{2}\tilde{H}(\xi) - \Theta}{\tilde{H}^3(\xi)}\,d\xi \tag{4.11}$$

Choosing an assumed position ξ_a that has the external atmospheric pressure and no gravity force at the outlet region, it follows then that

$$P(\xi_a)-\Gamma\xi_a=0 \tag{4.12}$$

and then Equation (4.11) is reduced to,

$$-P(\xi)+\Gamma\xi=12\int_{\xi}^{\xi_a}\frac{\frac{1}{2}\tilde{H}(\xi)-\Theta}{\tilde{H}^3(\xi)}d\xi \tag{4.13}$$

where $\tilde{H}(\xi)=1+\frac{1}{2}\xi^2$. This expresses 'no slip' on the cylinder surface, defined by the function $\tilde{H}(\xi)$. $\tilde{H}(\xi)$ is the circular arc

$$\tilde{H}(\xi)=1+\frac{R}{H_o}-\left[1-\frac{H_o}{R}\xi^2\right]^{1/2} \tag{4.14}$$

This expression introduces algebraic complications and a common approximation for $\tilde{H}(\xi)$, taking note of the fact that $H_o/R<<1$ in any lubrication problem is obtained by expanding the bracketed term.

Equation (4.13) may then be integrated, and the result is

$$-P(\xi)+\Gamma\xi=12\left[\frac{-\Theta\xi}{\left(2+\xi^2\right)^2}-\frac{3}{4}\frac{\Theta\xi}{2+\xi^2}-\frac{3}{8}\Theta\sqrt{2}\tan^{-1}\left(\frac{1}{2}\xi\sqrt{2}\right)\right.$$

$$\left.+\frac{1}{2}\frac{\xi}{2+\xi^2}+\frac{1}{4}\sqrt{2}\tan^{-1}\left(\frac{1}{2}\xi\sqrt{2}\right)\right]_{\xi}^{\xi_a} \tag{4.15}$$

Θ is still an undetermined parameter. To obtain a relationship between ξ_a and ξ_b, a boundary condition must be imposed on the pressure. From Figure (4.1) it can be expressed as $P(-\xi_b)=0$ by considering a partially flooded inlet boundary condition and calculated from:

$$0=12\left[\frac{-\Theta\xi_a}{\left(2+\xi_a{}^2\right)^2}-\frac{3}{4}\frac{\Theta\xi_a}{2+\xi_a{}^2}-\frac{3}{8}\Theta\sqrt{2}\tan^{-1}\left(\frac{1}{2}\xi_a\sqrt{2}\right)\right.$$

$$+\frac{1}{2}\frac{\xi_a}{2+\xi_a{}^2}+\frac{1}{4}\sqrt{2}\tan^{-1}\left(\frac{1}{2}\xi_a\sqrt{2}\right)\Bigg]$$

$$-\left[\frac{+\Theta\xi_b}{\left(2+\xi_b{}^2\right)^2}+\frac{3}{4}\frac{\Theta\xi_b}{2+\xi_b{}^2}-\frac{3}{8}\Theta\sqrt{2}\tan^{-1}\left(-\frac{1}{2}\xi_b\sqrt{2}\right)\right.$$

$$\left.-\frac{1}{2}\frac{\xi_b}{2+\xi_b{}^2}+\frac{1}{4}\sqrt{2}\tan^{-1}\left(-\frac{1}{2}\xi_b\sqrt{2}\right)-\Gamma\xi_b\right] \tag{4.16}$$

Symbolically,

$$0=f(\Theta,\xi_a,\xi_b,\Gamma) \tag{4.17}$$

Equation (4.17) expresses the relation between the entry position and the rupture position by using Swift-Stieber boundary condition and partially flooded condition explained as one of the boundary models considered in the next section (4.5).

4.4 Coyne and Elrod Boundary Condition

The Swift-Stieber or Reynolds boundary condition for cavitation applies a zero pressure gradient between the full film and the cavitating regions [47]. It is known to result in reasonably precise predictions of bearing performance for moderately or heavily loaded lubricated contacts. This does not necessarily imply that the physical assumptions of the condition are correct. For lightly loaded situations, however, the boundary condition proves inadequate.

The occurrence of a reserve flow adjacent to a stationary surface causes separation of the flow. Coyne and Elrod have performed a sophisticated analysis to determine the location of such an interface and interpreted their results in terms of boundary conditions on the full film. Their analysis makes the following assumptions [46],

(1) The cavity region is two-dimensional and corrugations do not exist at the leading edge. All the lubricant is therefore carried away by the surface that is moving

and separation of the flow occurs from the opposite stationary surface. The analysis is not directly applicable to the situation in which both surfaces are in motion.

(2) A balance of forces, including surface tension, exists across the interface.

(3) The interface is a free surface.

The boundary condition for Reynolds equation considering pressure continuity is expressed as

$$p = -\frac{\sigma}{r} + \Delta p \tag{4.18}$$

where r is the radius of curvature of the free film at the separation point. The first term of Equation (4.18) represents the pressure-drop across the interface due to surface tension.

Introducing the dimensionless variables into Equation (4.18) the boundary condition represents a force or pressure balance at the separation point, x_a, and equates the pressure, p, to the pressure associated with surface tension, σ,

$$p = -\frac{\sigma}{r} \qquad \text{at } x = x_a \tag{4.19}$$

otherwise

$$P = -\frac{H_o}{r}\beta\ \sigma \text{ at } \xi = \xi_a \tag{4.20}$$

where the additional parameter is a modified capillary number as follows [16-18],

$$\beta = \frac{\sigma}{\mu U}\left(\frac{H_o}{R}\right)^{1/2} = \frac{1}{Ca}\left(\frac{H_o}{R}\right)^{1/2} \tag{4.21}$$

The curvature of the surface, r, is unknown a priori. Since the surface tension contribution is a small one, a simple approximation to r proves to be useful. The free surface is taken to be semicircular, then a good approximation is

$$r = h(x_a) - H_L \tag{4.22}$$

or

$$\frac{r}{H_o} = \frac{h(x_a)}{H_o} - \frac{H_L}{H_o} = \frac{h(x_a)}{H_o} - \Theta \tag{4.23}$$

Substituting Equation (4.23) into Equation (4.22), we obtain:

$$P = \left[\frac{1}{\tilde{h}(\xi_a) - \Theta}\right]\beta \qquad \text{at } \xi = \xi_a \qquad (4.24)$$

4.5 Boundary Conditions

4.5.1 Partially flooded inlet boundary

The fully flooded or downward inlet boundary for large-sized cylinder (p = 0 at $x_b = -\infty$) in Figure (4.1) cannot occur in a real system. It is just a convenient assumption for simplifying the analytical solution of the Reynolds equation. Most of these cases are presented as fully flooded for known positions of the inlet boundary. In the hydrodynamic problems this assumption has widely been used [18, 21, 42].

If the inlet region is adequately filled with the lubricant on the circumferential surface entrained by the rotating cylinder from the liquid container the inlet pressure buildup will act on the free surface of lubricant beyond a certain point such that the inlet pressure is insensitive to further increase in the lubricant supply entrained by the rotating cylinder.

For practical cases, the extent of the pressure zone is small compared with the dimensions of the cylinder's radius. It is also expected that the pressure does not contribute much to load capacity until the closest zone between cylinder and the flat plate. For a given load, speed and viscosity, only part of the lubricant injected into the nip and carried on the cylinder's entraining surfaces may pass through to outlet. Such a state arises when there is a surplus of lubricant in entry zone. In order to predict the position where the pressure starts to develop the surface tension effects are considered to be negligible. Accordingly the contact point where the free surface contacts the stationary flat plate becomes the starting point of pressure development,

$$p_{in} = p_{atm} \qquad \text{at } x = -x_b \qquad (4.25)$$

4.5.2 Swift-Stieber outlet boundary condition

The Swift-Stieber (Reynolds) outlet boundary condition has already been used to solve the Reynolds equation. It is appropriate here to discuss it in more detail as it is the most frequently employed method when solving this problem. In the experimental observations that prompted its formulation for relatively high speeds and thin films, there was no noticeable negative pressure [16, 17]. The outlet was marked by lines of shaped air cavities separated by liquid streams. The cavities are considered to occupy most of the clearance space depth except for liquid layers on the moving. Each of the moving cylinder's surface leaves with a residue of evenly spaced circumferential liquid streamer of lubricant. The appropriate condition at the film rapture can be formulated by flow continuity considerations. In the region of the air cavities, the pressure is taken to be zero with only Couette flow (flow caused by surface velocities only). As there is flow continuity, a suitable boundary condition for the general case is,

$$p = \frac{\partial p}{\partial x} = \frac{\partial p}{\partial y} = 0 \qquad \text{at } x = x_a \tag{4.26}$$

A boundary condition involving surface tension would have to be introduced for more detailed dynamic analysis. First of all, it is not necessary to formulate a complex model in order to yield results for the general features of this system. For the undetermined parameter, Θ, it can be evaluated from the additional boundary condition on pressure, imposed at $\xi = \xi_a$:

$$\frac{dP}{d\xi}(\xi_a) = 0 \tag{4.27}$$

Accordingly,

$$0 = 12\frac{\frac{1}{2}\left(1 + \frac{1}{2}\xi_a^{\ 2}\right) - \Theta}{\left(1 + \frac{1}{2}\xi_a^{\ 2}\right)^3} \tag{4.28}$$

Arranging Equation (4.28) for Θ,

$$\Theta = \frac{1}{2}\tilde{H}(\xi_a) \tag{4.29}$$

Substituting Equation (4.29) into Equation (4.13), a relationship is obtained for ξ, ξ_a, and ξ_b. In the absence of gravity, the values of ξ_a, and ξ_b can be calculated by using a simple numerical technique.

4.5.3 Separation outlet boundary condition

The separation type outlet boundary condition is appropriate at low speeds and thick films. It was formulated following experimental observations of a distinct sub-cavity pressure loop prior to the film end that occurred under certain conditions [16, 17]. Thus, it was considered that flow separation might be contributing to the film rupture. Separation first occurs at the location x_a of the outlet film, where its velocity profile has a value

$$u = \frac{\partial u}{\partial y} = 0 \tag{4.30}$$

This implies that the position is both a stagnation point and a point of separation. Such a position may be located either on the interface or at the onset of the reverse flow region. The pressure gradient is positive just upstream of x_a with the pressure having a slight negative value. This is analogous to the zero reverse flow inlet condition, where the reverse flow upstream is eliminated. Here, reverse flow downstream in the expanding exit causes suspended gas in the lubricant to form a cavity pattern of closely spaced air fingers more rounded at their ends than the Swift-Stieber type cavities. In this case, the majority of the lubricant flow is believed to be carried in layers adjacent to the entraining surfaces.

For simplicity, $\Pi = dP/d\xi - \Gamma$, Equation (4.2) can be transformed to the following form;

$$\frac{\partial^2 \phi}{\partial \eta^2} = \frac{\partial \Pi}{\partial \xi} \tag{4.31}$$

If gravity is accounted for a trivial modification to this condition subsequent work will be done in same manner used in section 4.3. The velocity is given as follows,

$$\phi(\eta) = \frac{1}{2}\frac{\partial \Pi}{\partial \xi}\left[\eta^2 - \tilde{H}(\xi)\eta\right] + \frac{\eta}{\tilde{H}(\xi)} \tag{4.32}$$

To find the pressure, it is necessary to satisfy the conservation of mass of Equation (4.6).

$$\Theta = \frac{\partial \Pi}{\partial \xi}\left[\frac{1}{6}\tilde{H}^3(\xi) - \frac{1}{4}\tilde{H}^3(\xi)\right] + \frac{1}{2}\tilde{H}(\xi) \tag{4.33}$$

Changing to an integration form the pressure gradient is found to be

$$\frac{d\Pi}{d\xi} = 12\frac{\frac{1}{2}\tilde{H}(\xi) - \Theta}{\tilde{H}^3(\xi)} \tag{4.34}$$

The boundary conditions on pressure asserts that the pressure including gravity effects at inlet region, Π, is ambient as $x \rightarrow -x_b$. A boundary condition at the outlet region is

$$\Pi(\xi) = 12\int_{\xi_b}^{\xi} \frac{\frac{1}{2}\tilde{H}(\xi) - \Theta}{\tilde{H}^3(\xi)} d\xi \tag{4.35}$$

The boundary condition represents a force or pressure balance at the point ξ_a, and equates the pressure Π to the associated surface tension σ as shown in Equation (4.20).

When the boundary condition in the Equation (4.20) is considered, the pressure balance becomes as follows,

$$\Pi(\xi_a) = \left[\frac{1}{\tilde{H}(\xi) - \Theta}\right]\beta \cdot 12\int_{\xi_b}^{\xi_a} \frac{\frac{1}{2}\tilde{H}(\xi) - \Theta}{\tilde{H}^3(\xi)} d\xi \tag{4.36}$$

The final boundary condition expressing stagnation point of ϕ about the $\eta = 0$ and $\xi = \xi_a$, and expressing a wetting angle of 90^o is

$$\frac{\partial \phi}{\partial \eta} = 0 \qquad \text{at } \eta = 0 \text{ and } \xi = \xi_a \tag{4.37}$$

When boundary condition Equation (4.37) is imposed, the results of Equation (4.34) is found to give

$$\Theta = \frac{1}{3}\widetilde{H}(\xi_a) \tag{4.38}$$

To obtain a relationship between ξ_a and ξ_b, Coyne and Elrod boundary condition, Equation (4.24), must be imposed on the pressure. From Figure (4.1) it can be expressed as $P(-\xi_b) = 0$ for inlet zone.

4.6 Mathematical Solution and Discussion

A surplus of lubricant in the entry zone makes the previous model difficult for predicting the exact position of the inlet boundary due to the fluid mechanism in the convergent geometry. However, if there exists some means of establishing the outlet boundary distance, ξ_a, and inlet boundary distance, ξ_b, from the closest nip in the lubricating zone then Equation (4.16) would give a solution for $\Theta(\Gamma)$. For fluid film plane flat-cylinder which have a convergent clearance space geometry, two realistic cavitation boundary conditions have been suggested. In the Swift-Stieber condition, the cavity pressure usually taken to be atmospheric and surface tension effects are usually of secondary importance. The use of this boundary condition in analysis predicts pressure profiles with relative ease. Although separation boundary condition has often been suggested for lightly loaded fluid film bearings, not a great deal of numerical design information appears in the bearing situation to be discussed in the next chapter.

Figure (4.2) shows the solution for $\Theta(\Gamma)$ of Equation (4.16) obtained by using the Swift-Stieber cavitation boundary condition. As expected the effect of gravity is an increase in the distance of the inlet boundary with increasing $\Gamma = \frac{\rho g H_O^2}{\mu U}$. The positions of the outlet boundary are not greatly affected by those of the inlet boundary except for the effect of gravity in the case of $\Gamma > 0.3$. For instance, from the known experimental data used in Chapter 3, Γ is approximately 0.02 (when H_O=0.01inch, and U=56 $^{m}/_{sec}$).

In practice, the effect of gravity has some significance in the relationship between the outlet boundary distance, ξ_a, and inlet boundary distance, ξ_b. A more detailed dynamic analysis would be needed to yield the relationship between ξ_a, and ξ_b as affected by boundary conditions involving surface tension. However, as done in the previous section the partially flooded inlet boundary and the Swift-Stieber outlet boundary condition are introduced to yield results for the general features. The results are obtained from the Reynolds equation with different inlet boundary distances and Swift-Stieber outlet conditions.

Equations (4.29) and (4.39) show that the dimensionless film thickness, Θ, only depends on the outlet boundary distance, ξ_a. Surface tension is not accounted for in the model by Swift-Stieber (Reynolds) boundary condition. However, surface tension is accounted for the model by the separation boundary condition connected with Coyne and Elrod boundary condition. Both cases in Figure (4.3) uggests that the dimensionless film thickness, Θ, after rupture at the outlet zone should depend only on the distance of the outlet boundary, ξ_a as shown in Figures (4.4) and (4.5). The dimensionless film thickness, Θ, as function of the distance of outlet boundary, ξ_a, can be used to determine the distance of the outlet boundary, ξ_b, depending on the Capillary Number. The film thickness after rupture show that the case of Reynolds boundary condition is much thicker than that of separation boundary condition. This relationship will provide some help in modeling the flow with high shear rate in the lubricating zone to be discussed layer.

It is apparent that the model based on the lubrication approximations is not adequate possibly at small value of ξ_a due to numerical instability. The relationship between $\xi_a$and ξ_b is developed for explaining starved inlet and outlet boundary. From this phenomenon and analytical solution the results show the model has limits on the size of the rotation system. This needs a reasonable disc size to give starved boundary condition and to avoid numerical difficulty in small size. It seems likely that one source of error arises from the phenomenon in the case of having surface tension acting on the free surface where entry zone, ξ_a, and exit zone, ξ_b, exist around the minimum gap.

At higher speed and moderately loaded operation condition it is already recognized that Swift-Stieber (Reynolds) boundary condition is more suitable to use in the above case. Up to high value of speed, the film thickness by withdrawal increases in the free surface with increasing speed. Hence, high speed affects the surplus at inlet. It also causes pressure rise in the fluid with a constraint.

4.7 Summary and Conclusion

A simple mathematical formulation based on the lubrication model can predict the dimensionless film thickness to be formed after the outlet zone for both Swift-Stieber boundary condition and separation boundary condition. It is a function of outlet zone position and dimensionless film thickness. The position of the outlet boundary is governed by the inlet boundary position. The position of the inlet boundary is mainly determined by the geometrical parameter H_0/R, rotating speed, and Ca.

The difficulty in the analysis lies in the complexity of the flow in the neighborhood of the regions of the inlet and outlet boundary zones. Some research points out that a recirculation pattern exists at outlet zone near stationary surface [16, 17]. It would not explain the conditions required for the validity of a lubrication model, in which it is assumed that the streamlines are nearly parallel throughout the flow region. Actually, it needs appropriate boundary conditions at the separation point. The major point is that the Swift-Stieber condition is not suitable to deal with the existence of a negative pressure before the separation and recirculating flow.

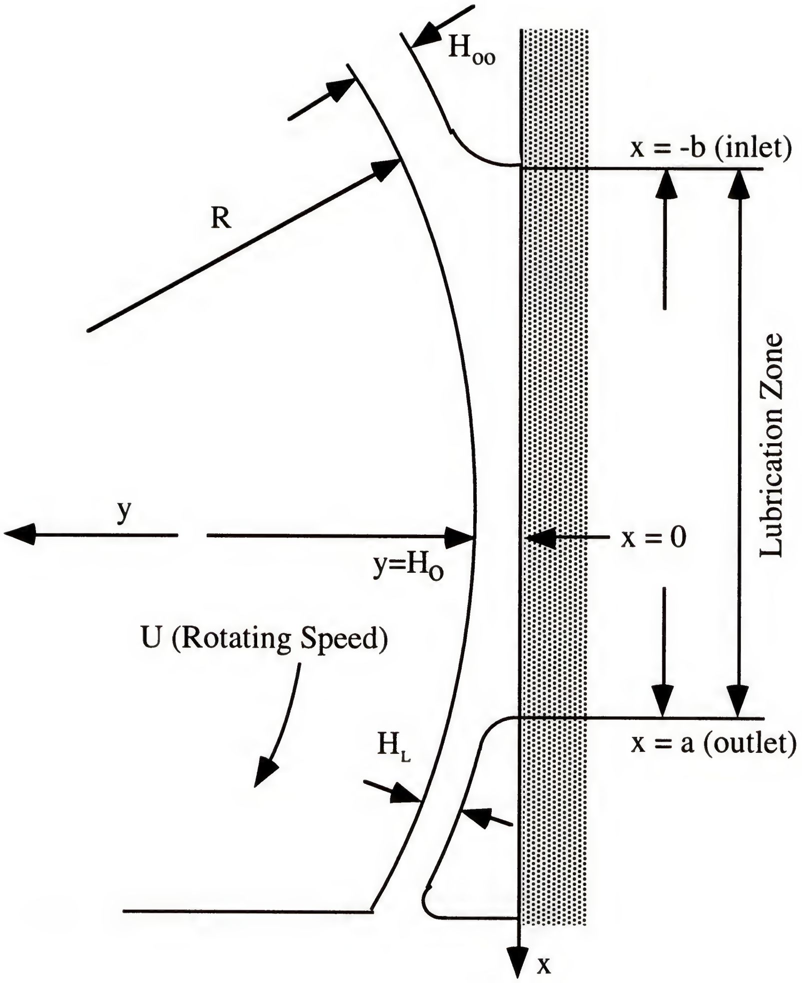

Figure 4.1 Cylinder-flat plate geometry and nomenclature

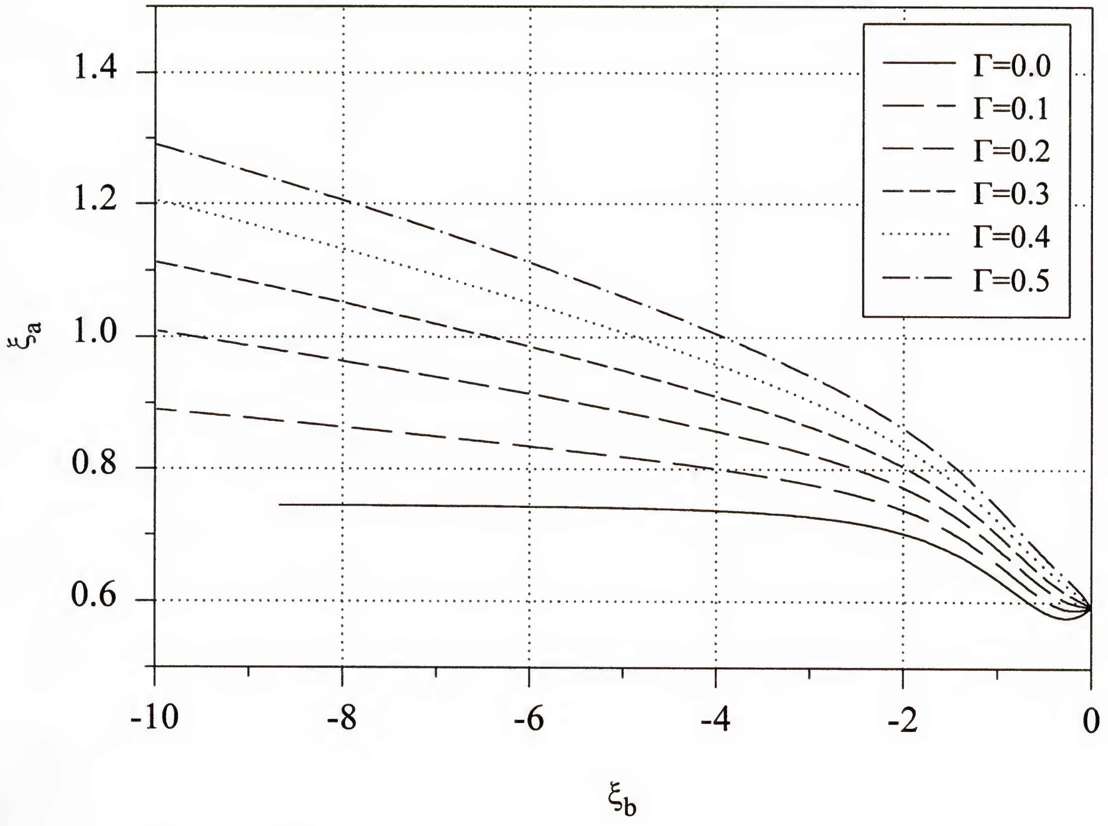

Figure 4.2 Relationship between inlet (ξ_b) and outlet (ξ_a) position for various values of Γ (gravity parameter) by using Swift-Stieber boundary condition.

$$\Gamma = {}^{\rho g h^2}/_{\mu U}$$

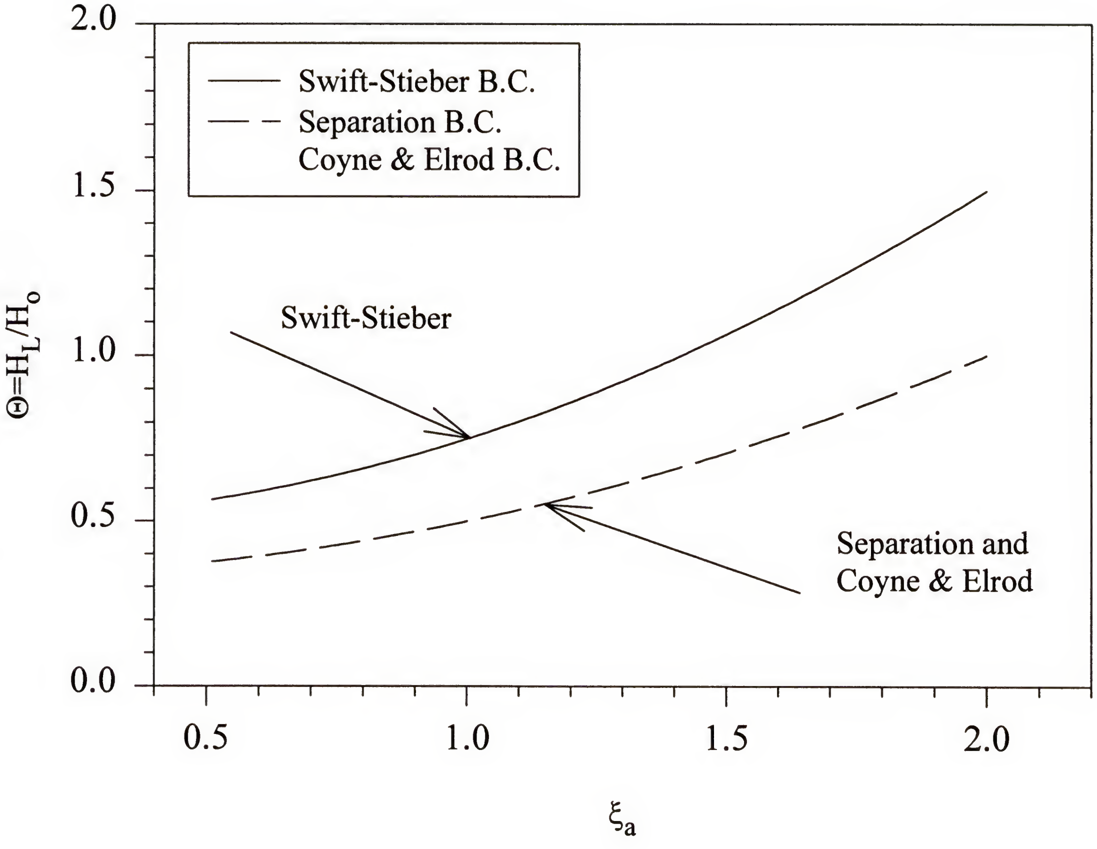

Figure 4.3 Dimensionless film thickness occurred from rupture region as function of exit zone, ξ_a (Comparison of Swift-Stieber B.C. and Coyne & Elrod and Separation B.C.)

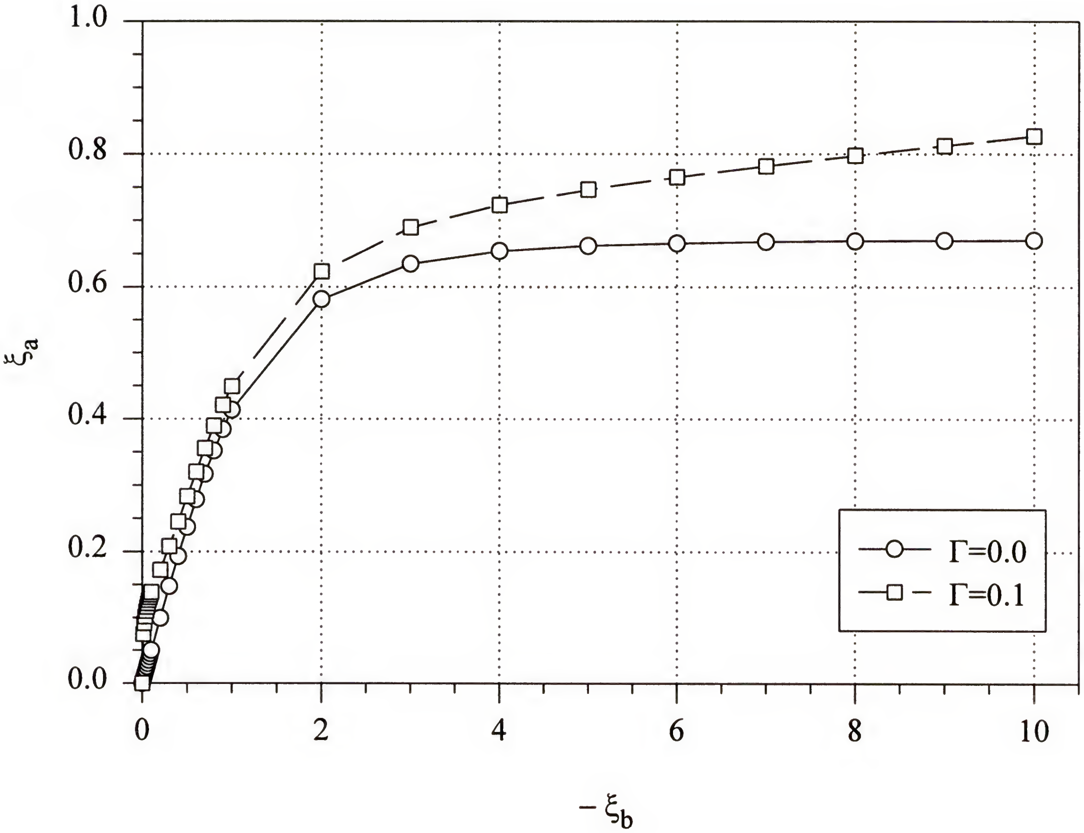

Figure 4.4 Relationship between inlet zone and outlet zone of the lubricant using Swift-Stiber (Reynolds) boundary condition

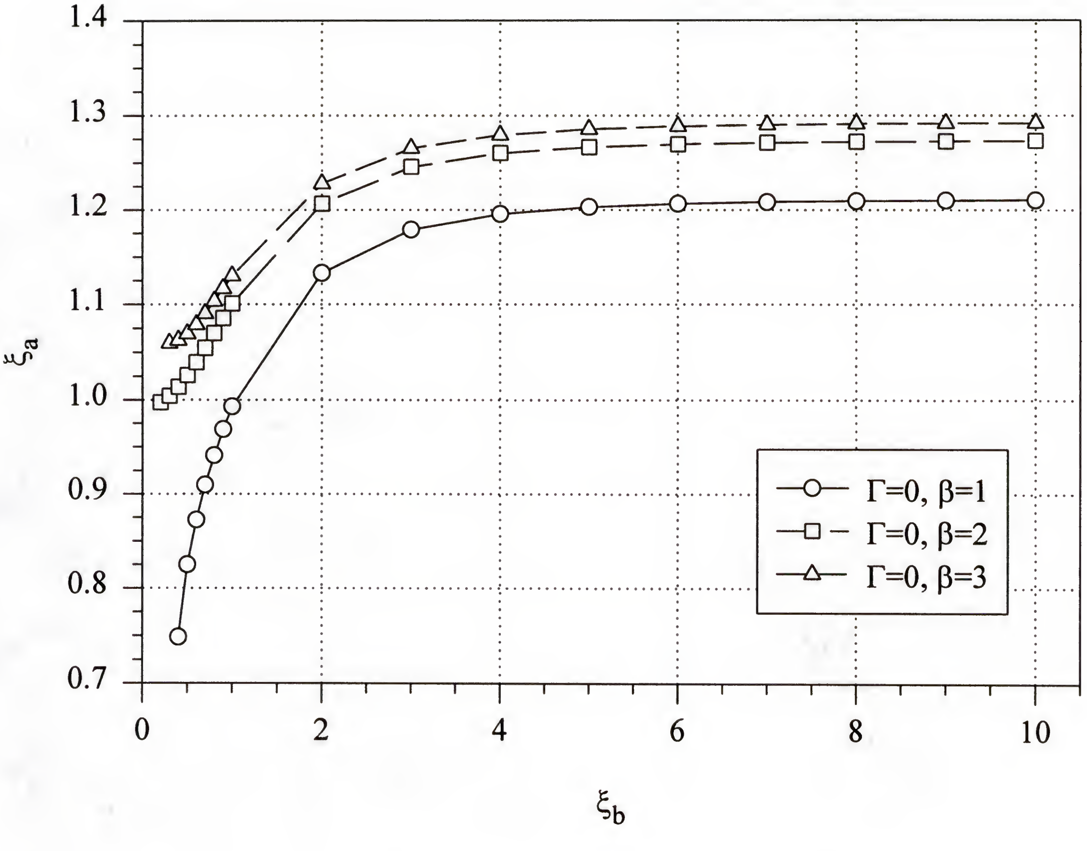

Figure 4.5 Relationship betwen inlet zone and outlet zone of the lubrication by using separation boundary condition, and Coyne - Elrod boundary condition

CHAPTER 5
THERMOHYDODYNAMIC ANALYSIS IN THE LUBRICATING REGION

5.1 Introduction

When there is oil present in the vicinity of two surfaces, a lubricating film manages to move between the surfaces and completely separate them. This allows the load exerted on the surfaces to be supported or transmitted with small friction forces. The lubrication of these surfaces can be achieved in different ways which can be specially shaped to ensure lubrication, as in the slider and cylinder-plane cases shown in Figure (1-1-b). This is called hydrodynamic lubrication (HDL). In this rolling or sliding element systems, the combined effect of pressure and temperature on the oil work together to produce a film. This type of lubrication is called thermohydrodynamic lubrication (THD).

THD exists in successfully lubricated non-contacts between heavily loaded rolling and sliding machine components that do not conform to each other. This type of lubrication is characterized by the ability to generate pressures and temperature that are of sufficient magnitude to increase the lubricant viscosity considerably. The combined physical effects which constitute the complete THD problem are as follows:

1. The hydrodynamic effect implies that the lubricant obeys the laws of viscous flow;
2. The thermal effects are significant when the shear heating is large enough to significantly alter the viscosity of lubricant due to the high temperature;

3. The variable viscosity effect is very important especially in heavily loaded cases where the pressure and temperature changes are substantial.

The analysis of THD problem has proven to be highly complex. One of the difficulties arises from the fact that the viscosity of the lubricant varies exponentially with temperature. Another difficulty is setting its boundary conditions resulting from cavitation effects. The resulting governing equations are highly nonlinear differential equations combining of the hydrodynamic, and energy equations. The numerical solution of these equations is very difficult since its convergence is extremely sensitive to the changes in the major parameters, especially the properties of the lubricant.

5.2 Literature Review

In the early 1880s Beauchamp Tower performed experimental investigation to study friction in journal bearings. Osborne Reynolds eventually introduced the concept of the hydrodynamic lubrication theory and derived the Reynolds equation describing the pressure distribution in hydrodynamic bearings [22]. The design of hydrodynamic bearings is generally based on the assumption of constant viscosity without heat effects. Early works considering such heat effects in fluid film system considered the change of the entire lubricant viscosity with temperature rise in systems such as bearings. Cope systematically derived the governing equations for viscous flow in bearing systems [29]. Based on the assumption that lubricant oil carries away the entire frictional heat, he derived a simplified energy equation in which he neglected the variation of viscosity across the film.

After Cope's work, which is known as adiabatic theory, some authors explained the effect of temperature in slider bearings [26, 27, 30, 32, 48]. They found that the pressure distribution based on the adiabatic theory is significantly lower than that predicted by the isothermal theory. Starting from this theory Zrenkiewicz included the temperature variation across the film in the energy equation and solved the governing equation of a simple two-dimensional parallel surface bearing [49]. For the variation of viscosity both along and across the fluid film, Dowson first proposed the generalized Reynolds equation which is a function of viscosity based on temperature [50]. A model which predicts bearing performance based on realistic thermal boundary conditions on the stationary and moving surfaces and variation of the film viscosity with temperature is finally introduced as the thermohydrodyanmic (THD). With the advent of high-speed digital computers, Dowson and Hudson presented THD solutions for a slider bearing in which the transfer to heat to the stationary solid was included [51-53]. Ezzat and Rohde also studied THD effects in a finite inclined-plane slider bearing [54-56]. They solved the Reynolds equation, a three-dimensional energy equation for the fluid and a two-dimensional heat conduction equation for the stationary solid along with a viscosity-temperature relation for the lubricant simultaneously.

Using a similar numerical solution procedure, Hueber proposed a study of the THD effects in sector trust bearings. His study contains a comparison of the THD results with isothermal and adiabatic boundary conditions [57, 58]. He concluded that bearing performance is strongly affected by the inlet temperature, speed, and film thickness. Most recently, Seireg and Wang presented a complete THD study of slider bearings and journal bearings in which a three-dimensional variation of lubricant viscosity and thermal expansion were considered [26, 27]. They explained the occurrence of high temperature at the central zone of system. Comparing their findings with experimental results, they found a considerable difference leading to the conclusion that THD solution by traditional shear zone may not be completely satisfactory.

5.3 Design Parameters

In the design of rotating systems such as bearings, the responsibility of an engineer is to provide customers with the system geometry, material specifications, and method of lubricant supply. For a given design condition, a number of parameters are engaged in determining the above specifications. To make the design process clear, the parameters can be classified into some parts according to their characteristics, as shown in Table 4.

Table 4: Design Parameters of Sliding Systems (Bearings, Disc)

	Parameter
Performance	Friction Load Lubricant Flow
Control	Maximum Temperature Maximum Pressure Minimum Film Thickness Speed
Geometry	Inclined Angle or eccentricity Width and Length, or Diameter
Auxiliary	Lubricant Supply Temperature Lubricant Type

Note: Newtonian case

Variables which influence the rotating system performance are as follows:

- Pressure: Lubricant pressure is developed due to a lubricant flow in the gap.

- Temperature: Lubricant temperature increases above the supply temperature due to viscous dissipation of the lubricant.
- Film thickness: The variation of the film thickness determines the pressure and temperature distributions.
- Viscosity of lubricants: Viscosity is highly dependent on temperature, and influences the load capacity significantly.
- Angle: slopes at which the pad is declined with respect to the runner

These variables are related with one other, as shown schematically in Figure (5.1).

5.4 Dependence of Viscosity on Temperature and pressure

This section presents the equation of state used to relate temperature and viscosity. Viscosity is the most important property of the oil or lubricant employed in THD, since it is a determining factor in pressure and film fluid dynamics between the rolling and sliding bodies.

Experiments have shown that viscosity is very sensitive to temperature and pressure changes[22. 36, 59]. Especially at high sliding speeds between the surfaces, both pressure and temperature within the lubricant film rise significantly as the lubricant passes through the lubricating zone. Accordingly, an approximate formula for the dependence of viscosity on temperature and pressure is necessary in order to solve the THD problem by numerical methods.

There are a number of empirical models available for the dependence of viscosity on temperature. These are all based upon the observation that the viscosity-temperature derivative depends primarily on the viscosity. The simplest but the least accurate model is by Reynolds [22].

$$\mu = \mu_0 e^{-\delta(T-T_0)} \tag{5.1}$$

where

$\delta = \dfrac{1}{T_B - T_A} ln\left(\dfrac{\mu_B}{\mu_A}\right)$ temperature/viscosity parameter

$\mu(T_A) = \mu_A$, $\mu(T_B) = \mu_B$

T_0, μ_0 are oil inlet temperature and viscosity, respectively.

This study employs this expression (5.1) because the effect of temperature is more sensitive to viscosity than that of pressure in the THD problem except for the elastohydrodynamic lubrication (EHD) problem. It is more convenient to use without severe error in this case. A more useful viscosity temperature relationship was reported in an reference [59]

$$\mu = k\, e^{\left(b/_{T+c}\right)} \tag{5.2}$$

where the three constants all have distinctive physical meanings.

The viscosity-pressure derivative is also primarily dependent on viscosity. Barus assumed a linear relationship and the following viscosity pressure dependence

$$\mu = \mu_0 e^{\alpha p} \tag{5.3}$$

where μ_0 is the viscosity at atmospheric pressure and α is a constant. This equation becomes inaccurate above 0.5 GPa, thus making it inappropriate for this analysis [36].

5.5 Simplified Reynolds Equation

The equation that governs the generation of pressure in the lubricant film is known as the Reynolds equation. It is the foundation for hydrodynamic lubrication analysis and was first derived by Reynolds in 1886 [22]. The Reynolds equation can be derived by applying the basic equations of motion and continuity to the lubricant. Its relevant form for thermal Newtonian flow is derived as follow. The generalized Reynolds equation [50] which combines the momentum and continuity equations also expresses the variation of density and viscosity across and along the lubrication film is as follows :

$$\frac{\partial}{\partial x}\left[(F_2+G_1)\frac{\partial p}{\partial x}\right]+\frac{\partial}{\partial y}\left[(F_2+G_1)\frac{\partial p}{\partial y}\right]$$

$$=h\left[\frac{\partial(\rho U)_2}{\partial x}+\frac{\partial(\rho V)_2}{\partial y}\right]-\frac{\partial}{\partial x}\left[\frac{(U_2-U_1)(F_3+G_2)}{F_0}+U_1G_3\right]$$

$$-\frac{\partial}{\partial y}\left[\frac{(V_2-V_1)(F_3+G_2)}{F_0}+V_1G_3\right]+\int_0^h\frac{\partial\rho}{\partial t}dz+(\rho w)_2-(\rho w)_1 \qquad (5.4)$$

where

$$F_0=\int_0^h\frac{1}{\mu}dz\ ;\ F_1=\int_0^h\frac{z}{\mu}dz\ ;\ F_2=\int_0^h\frac{\rho z}{\mu}\left(z-\frac{F_1}{F_0}\right)dz\ ;\ F_3=\int_0^h\frac{\rho z}{\mu}dz$$

$$G_1=\int_0^h\left[z\frac{\partial\rho}{\partial z}\left(\int_0^z\frac{z}{\mu}dz-\frac{F_1}{F_0}\int_0^z\frac{1}{\mu}dz\right)\right]dz\ ;\ G_2=\int_0^h\left[z\frac{\partial\rho}{\partial z}\left(\int_0^z\frac{1}{\mu}dz\right)\right]dz\ ;\ G_3=\int_0^h z\frac{\partial\rho}{\partial z}dz$$

Before deriving the much simplified equation, the following simplifying assumptions are made:

1. Body forces are negligible, due to the negligible mass of the film
2. Lubricant flow is laminar, since viscosity is high and Reynolds number is small and the lubricant is a Newtonian fluid.
3. Velocity gradients are only significant across the film thickness, because film thickness is much smaller than the dimensions of the lubricating zone.
4. Inertia and surface tension forces are negligible compared to viscous forces, since the lubricant's mass and acceleration are small.

5. There is no slip at the boundary surfaces and solid boundaries.
6. The lubrication of density is considered to be a function of temperature and pressure in cross film direction.

The generalized Reynolds equation (5.3.1) can be simplified as

$$\frac{\partial}{\partial x}\left[F_2\frac{\partial p}{\partial x}\right]+\frac{\partial}{\partial y}\left[F_2\frac{\partial p}{\partial y}\right]=\left(U_1-U_2\right)\frac{\partial}{\partial x}\left[\frac{F_3}{F_0}\right]+\int_0^h\frac{\partial \rho}{\partial t}dz \qquad (5.5)$$

where

$$F_0=\int_0^h\frac{1}{\mu}dz \;\; ; \;\; F_1=\int_0^h\frac{z}{\mu}dz \;\; ; \;\; F_2=\int_0^h\frac{\rho z}{\mu}\left(z-\frac{F_1}{F_0}\right)dz \;\; ; \;\; F_3=\int_0^h\frac{\rho z}{\mu}dz$$

The appropriate boundary conditions for Reynolds equation are

$p(x,0)=p(x,L)=p(0,y)=p(B,y)=0$ for slider bearings

The thermal expansion term of equation (5.5) in the z direction by using the equation of state of the fluid can be written as

$$\int_0^h\frac{\partial \rho}{\partial t}dz=\rho\int_0^h\left(-\alpha\frac{\partial T}{\partial t}+\frac{1}{\beta}\frac{\partial p}{\partial t}\right)dz=\frac{\rho}{\partial t}\left[\int_0^h\left\{-\alpha\partial T(x,y,z)+\frac{1}{\beta}\partial p(x,y)\right\}dz\right] \qquad (5.6)$$

where α, and β are the thermal expansion coefficient and bulk modulus of the lubricant respectively [26].

5.6 Energy Equation

This section presents the development of a parabolic energy equation for use in finding the temperature field in the lubricant film. The temperature distribution within the lubricant film can be determined from the solution of the conservation of energy equation subjected to appropriate boundary conditions. Considering only conduction and convection heat transfer, compression and shear work, and internal energy, the steady flow energy equation for a control volume of the lubricant can be written as

$$\dot{Q} + \dot{W}_{shear} = \dot{m}\left(H_{out} - H_{in}\right) \tag{5.7}$$

where $\dot{Q}$ is the rate of heat flow into the volume, $\dot{W}_{shear}$ is the rate of shear work done on the volume, $\dot{m}$ is the mass rate of flow through the volume, and H is the enthalpy of the fluid.

Before preceding further, the following simplifying assumptions are made:

1. Velocity gradients are significant only across the film thickness (as in the development of the generalized Reynolds equation)
2. The density of lubricant, ρ, within the THD film is constant.
3. The film is much shorter in the z-direction compared to x and y-directions so that the gradient of the velocity component in the z direction is ignored. However, temperature gradients are not ignored in those directions.
4. The thermal conductivity of the lubricant, k, within the THD film is constant.
5. Conductions in x, y and z-directions are not neglected compared to conduction to boundary surfaces.

Using the above assumptions, the energy equation for incompressible, thin film used in this study is

$$\begin{aligned} \rho c_p \frac{\partial T}{\partial t} = -\rho c_p \left[u \frac{\partial T}{\partial x} + v \frac{\partial T}{\partial y} + w \frac{\partial T}{\partial z} \right] + \beta T \left[u \frac{\partial p}{\partial x} + v \frac{\partial p}{\partial y} \right] \\ + k \left[\frac{\partial^2 T}{\partial x^2} + \frac{\partial^2 T}{\partial y^2} + \frac{\partial^2 T}{\partial z^2} \right] + \mu \left[\left(\frac{\partial u}{\partial z} \right)^2 + \left(\frac{\partial v}{\partial z} \right)^2 \right] \end{aligned} \tag{5.8}$$

The form of the energy equation (5.8) represents heat generated both due to shear and compression when a fluid elements is subjected to a velocity difference across its top and bottom surfaces. This heat is dissipated into the solid surfaces which the film contacts by conduction, and convection. The energy equation is subject to the initial condition as follows;

$$T(x,y,z;0) = T_{in} \tag{5.9}$$

and the appropriate boundary conditions for the energy equation are

$$T(0,y,z) = T_{in} \ ; \ \frac{\partial T(B,y,z)}{\partial x} = 0$$

$$\frac{\partial T(x,0,z)}{\partial y} = 0 \ ; \ \frac{\partial T(x,L,z)}{\partial y} = 0$$

$$\begin{cases} T(x,y,0) = T_{in} & T(x,y,h) = T_{in} : isothermal \\ \dfrac{\partial T(x,y,0)}{\partial z} = 0 \ ; & \dfrac{\partial T(x,y,h)}{\partial z} = 0 : adiabatic \\ T(x,y,0) = T_{in} & \dfrac{\partial T(x,y,h)}{\partial z} = 0 : THD \end{cases} \tag{5.10}$$

5.7 Dimensionless Analysis for the Governing Equations

There are many advantages to non-dimensionalizing the governing equations. One is that the results have generality and the problem of using different system of units is removed. Another big advantage is that the number of external variables is reduced, from those having dimensions to their various combinations in dimensionless group.

The following dimensionless variables are used to nondimensionalize the governing equations [26]:

$$p^* = \frac{p h_0^2}{\mu_0 U B} \ ; \ \mu^* = \frac{\mu}{\mu_0} \ ; \ h^* = \frac{h}{h_0}$$

$$u^* = \frac{u}{U} \ ; \ v^* = \frac{v}{U} \ ; \ w^* = \frac{w}{U}$$

$$x^* = \frac{x}{B} \ ; \ y^* = \frac{y}{B} \ ; \ z^* = \frac{z}{h} \tag{5.11}$$

$$T^* = \frac{T}{T_0} \;;\; t^* = \frac{t}{(B/U)} \;;\; Q^* = \frac{Q}{B^2 U\left(\frac{h_0}{B}\right)}$$

$$W^* = \frac{W}{\mu_0 U\left(\frac{B^3}{h_0^2}\right)} \;;\; F^* = \frac{F}{\mu_0 B U\left(\frac{B}{h_0}\right)}$$

Using the above variables the Reynolds equation can be written in dimensionless form as

$$\frac{\partial}{\partial x^*}\left[h^{*3} F_2^* \frac{\partial p}{\partial x^*}\right] + \frac{\partial}{\partial y^*}\left[h^{*3} F_2^* \frac{\partial p}{\partial y^*}\right]$$

$$= \frac{\partial}{\partial x^*}\left[h^* \frac{F_3^*}{F_0^*}\right] + \frac{\rho h_0 h^*}{\partial t^*}\left(\int_0^1 \left\{\left(-\alpha T_0 \partial T^*\right) + \frac{\mu_0 U B}{\beta h_0^2} \partial p^*\right\} dz^*\right) \tag{5.12}$$

where

$$F_0^* = \int_0^1 \frac{1}{\mu^*} dz^* \;;\; F_1^* = \int_0^1 \frac{z^*}{\mu^*} dz^* \;;\; F_2^* = \int_0^1 \frac{z^*}{\mu^*}\left(z^* - \frac{F_1^*}{F_0^*}\right) dz^* \;;\; F_3^* = \int_0^1 \frac{z^*}{\mu^*} dz^*$$

The dimensionless boundary conditions for Reynolds equation are

$$p^*(x^*, 0) = p^*\left(x^*, \frac{L}{B}\right) = p^*(0, y^*) = p(1, y^*) = 0 \text{ for bearings} \tag{5.13}$$

The dimensionless form of the energy equation is [26]

$$\frac{\partial T^*}{\partial t^*} = -u^* \frac{\partial T^*}{\partial x^*} - v^* \frac{\partial T^*}{\partial y^*} + \left[\frac{u^* z^*}{h^*}\left(\frac{\partial h^*}{\partial x^*}\right) - \frac{B w^*}{h_0 h^*}\right] \frac{\partial T^*}{\partial z^*} + \frac{k}{B U \rho c} \frac{\partial^2 T^*}{\partial x^{*2}} +$$

$$\frac{k}{B U \rho c} \frac{\partial^2 T^*}{\partial y^{*2}} + \left(\frac{Bk}{\rho c U} \frac{1}{h_0^2 h^{*2}}\right) \frac{\partial^2 T^*}{\partial z^{*2}} + \frac{\mu_0 U B}{h_0^2 \rho c T_0} \frac{\mu^*}{h^{*2}}\left[\left(\frac{\partial u^*}{\partial z^*}\right)^2 + \left(\frac{\partial v^*}{\partial z^*}\right)^2\right] +$$

$$\frac{B \alpha T^*}{\rho c_p} \frac{\mu_0 \mu^* U}{h_0^2 h^{*2}}\left[u^* \frac{\partial p^*}{\partial x^*} + v^* \frac{\partial p^*}{\partial y^*}\right] \tag{5.14}$$

where [54]

$$\frac{\partial^2 T^*}{\partial \bar{x}^{*2}} = \frac{\partial^2 T^*}{\partial x^{*2}} - \frac{\partial}{\partial x^*}\left[\frac{z^*}{h^*}\left(\frac{\partial h^*}{\partial x^*}\right)\frac{\partial T^*}{\partial z^*}\right] - \frac{z^*}{h^*}\left(\frac{\partial h^*}{\partial x^*}\right)\frac{\partial^2 T^*}{\partial x^* \partial z^*} + \frac{z^*}{h^*}\left(\frac{\partial h^*}{\partial x^*}\right)\frac{\partial}{\partial z^*}\left[\frac{z^*}{h^*}\left(\frac{\partial h^*}{\partial x^*}\right)\frac{\partial T^*}{\partial z^*}\right]$$

The dimensionless initial conditions for the energy equation is

$$T^*\left(x^*, y^*, z^*; 0\right) = 1 \tag{5.15}$$

and the appropriate non-dimensional THD boundary conditions for the energy equation are

$$T^*\left(0, y^*, z^*\right) = 1 \;\; ; \;\; \frac{\partial T^*\left(1, y^*, z^*\right)}{\partial x^*} = 0$$

$$\frac{\partial T^*\left(x^*, 0, z^*\right)}{\partial y^*} = 0 \;\; ; \;\; \frac{\partial T^*\left(x^*, {}^{L}\!/_{B}, z^*\right)}{\partial y^*} = 0$$

$$\begin{cases} T^*\left(x^*, y^*, 0\right) = 1 & T^*\left(x^*, y^*, 1\right) = 1 : \mathit{isothermal} \\ \dfrac{\partial T^*\left(x^*, y^*, 0\right)}{\partial z^*} = 0 \;\; ; & \dfrac{\partial T^*\left(x^*, y^*, 1\right)}{\partial z^*} = 0 : \mathit{adiabatic} \\ T^*\left(x^*, y^*, 0\right) = 1 & \dfrac{\partial T^*\left(x^*, y^*, 1\right)}{\partial z^*} = 0 : \mathit{THD} \end{cases} \tag{5.16}$$

The fluid film velocity profiles can be obtained from momentum equations and expressed as a function of pressure, and viscosity as follows:

$$\frac{\partial p}{\partial x} = \frac{\partial}{\partial z}\left(\mu \frac{\partial u}{\partial z}\right), \text{ and } \frac{\partial p}{\partial y} = \frac{\partial}{\partial z}\left(\mu \frac{\partial v}{\partial z}\right) \tag{5.17}$$

Boundary conditions for Equation (5.17) are

$$u = U, v = 0 \quad \text{at } z = 0$$

$$u = 0, v = 0 \quad \text{at } z = h \tag{5.18}$$

The velocity profile can be expressed as:

$$u = U\left(1 - \frac{\int_0^z \frac{1}{\mu} dz}{\int_0^h \frac{1}{\mu} dz}\right) + \left(\int_0^z \frac{z}{\mu} dz - \frac{\int_0^h \frac{z}{\mu} dz}{\int_0^h \frac{1}{\mu} dz} \int_0^z \frac{1}{\mu} dz\right)\frac{\partial p}{\partial x}$$

$$v = \left(\int_0^z \frac{z}{\mu} dz - \frac{\int_0^h \frac{z}{\mu} dz}{\int_0^h \frac{1}{\mu} dz} \int_0^z \frac{1}{\mu} dz \right) \frac{\partial p}{\partial y} \tag{5.19}$$

Using the transformation variables (5.11), the dimensionless velocity profiles are given by

$$u^* = \left(1 - \frac{\int_0^{z^*} \frac{z^*}{\mu^*} d z^*}{\int_0^{z^*} \frac{z^*}{\mu^*} d z^*} \right) + h^{*2} \left(\int_0^{z^*} \frac{z^*}{\mu^*} dz^* - \frac{\int_0^1 \frac{z^*}{\mu^*} dz^*}{\int_0^1 \frac{1}{\mu^*} dz^*} \int_0^{z^*} \frac{1}{\mu^*} dz^* \right) \frac{\partial p^*}{\partial x^*}$$

$$v^* = h^{*2} \left(\int_0^{z^*} \frac{z^*}{\mu^*} dz^* - \frac{\int_0^1 \frac{z^*}{\mu^*} dz^*}{\int_0^1 \frac{1}{\mu^*} dz^*} \int_0^{z^*} \frac{1}{\mu^*} dz^* \right) \frac{\partial p^*}{\partial y^*} \tag{5.20}$$

The cross film velocity w may be obtained from the continuity equation and integration with $w = 0$ at $z = 0$ and h as follows

$$\frac{\partial w}{\partial z} = -\left(\frac{\partial u}{\partial x} + \frac{\partial v}{\partial y} \right) \tag{5.21}$$

$$w^* = \left(\frac{h_0}{B} \right) \rangle - h^{*3} \left(\frac{\partial^2 p^*}{\partial x^{*2}} + \frac{\partial^2 p^*}{\partial x^{*2}} \right) \int_0^{z^*} \Omega \, dz^* - \left(\frac{\partial h^*}{\partial x^*} \right) \left(z^* \Xi - \int_0^{z^*} \Xi \, dz^* \right) + h^* \int_0^{z^*} \frac{\partial \Xi}{\partial x^*} dz^*$$

$$- \left[\frac{\partial p^*}{\partial x^*} \left\{ h^{*3} \int_0^{z^*} \frac{\partial \Omega}{\partial x^*} dz^* - h^{*2} \left(\frac{\partial h^*}{\partial x^*} \right) \left(z^* \Omega - 3 \int_0^{z^*} \Omega \, dz^* \right) \right\} \right] - h^{*3} \left(\frac{\partial p^*}{\partial y^*} \right) \int_0^{z^*} \frac{\partial \Omega}{\partial y^*} dz^* \Big\rangle \tag{5.22}$$

where

$$\Omega = \int_0^{z^*} \frac{z^*}{\mu^*} dz^* - \frac{\int_0^1 \frac{z^*}{\mu^*} dz^*}{\int_0^1 \frac{1}{\mu^*} dz^*} \int_0^{z^*} \frac{1}{\mu^*} dz^*, \text{ and } \Xi = \frac{\int_0^{z^*} \frac{1}{\mu^*} dz^*}{\int_0^1 \frac{1}{\mu^*} dz^*}$$

5.8 Performance Parameter of the Lubricating Systems

The following parameters play a major role on the hydrodynamic performance. The load carrying capacity for the slider moving system is;

$$W = \int_0^L \int_0^B p dx dy \tag{5.23}$$

The friction force can be computed from,

$$F = \int_0^L \int_0^B \tau_{zx}\big|_{z=0} dx dz \tag{5.24}$$

The inlet flow, outlet flow, and side leakage are,

$$Q_i = \int_0^L \int_0^B u\big|_{x=0} dy dz \tag{5.25}$$

$$Q_o = \int_0^L \int_0^B u\big|_{x=B} dy dz \tag{5.26}$$

$$Q_{side} = 2\int_0^B \int_0^h v\big|_{y=0} dx dz \tag{5.27}$$

There is no side leakage flow in the cavitation region $x \geq x_{cavitation}$ since the axial pressure gradient, $\frac{\partial p}{\partial z}$, is zero. Due to cavitation, the film is incomplete and the system is not covered with lubricant over the length.

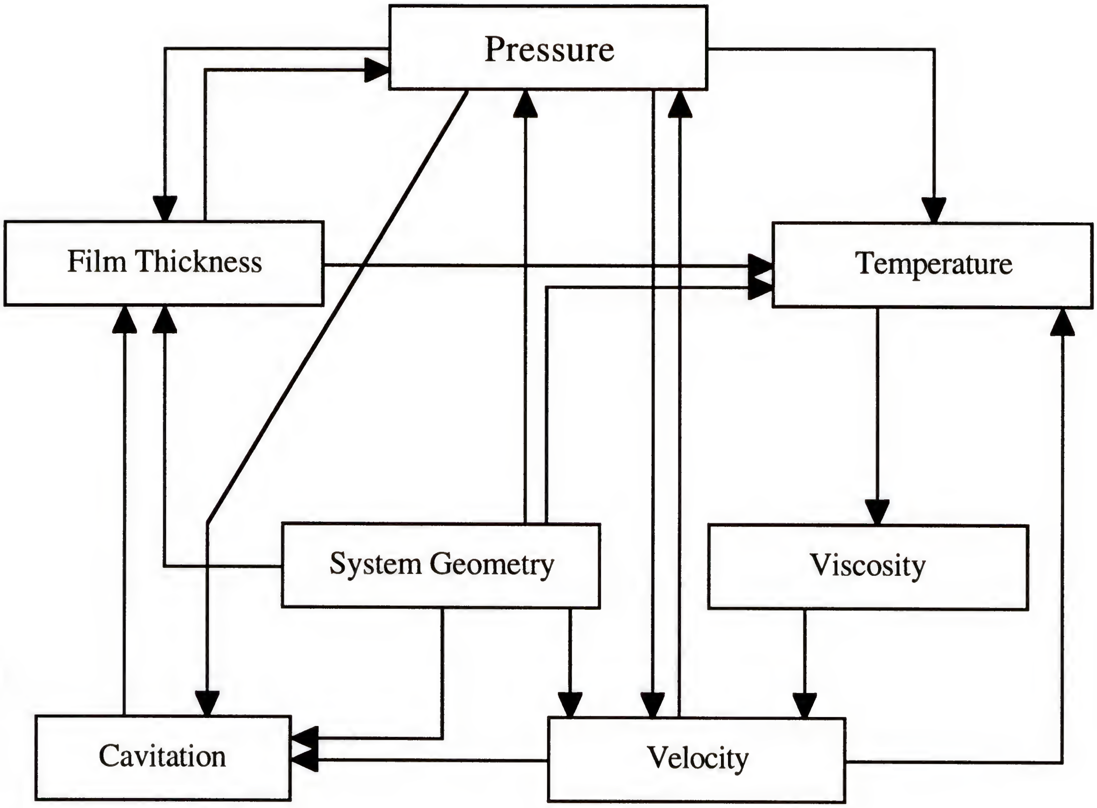

Figue 5.1 Relationship between variables in the lubrication problem of the sliding motion

CHAPTER 6
NUMERICAL TECHNIQUE

6.1 Introduction

Finite element methods (FEM) have been widely used in analysis of several research fields because irregular geometry shape can be easily accommodated at the element level without any difficulty for the setup of programming. Also, the size of the element can easily be varied over the region allowing the use of small elements whem necessary. This method has been gradually applied to deal with the problem of film thickness variation in lubrication analysis such as elastohydrodynamic (EHL) problem.

The FDM where the physical domain of a lubricant film can effectively be transformed to a rectangular computational domain is selected due to its suitability to THD problems without severe film thickness variation [26, 27, 60-62]. The equation of motion for a homogeneous fluid in the absence of a finite rate chemical reaction or mass diffusion is based on three physical conservation laws. Those are conservation of mass (continuity), conservation of linear momentum (Newton's second law), and conservation of energy (first law of thermodynamics). First, the Reynolds or energy equation is decoupled from the system of equations composed of the continuity and momentum equations. Therefore, the velocity and pressure fields are computed initially, and subsequently the energy equation may be solved for the temperature distribution. Second, due to the reduction of unknowns within the domain, the computer storage and memory requirements are reduced. The numerical solution of the THD problem requires the simultaneous solution of the Reynolds, film shape (especially important in the EHL problem), load, energy, and viscosity equations. The Reynolds and energy equations are formed to deal with constituent elements using the central finite difference method. These approximated equations are then solved by numerical methods. For this class of problems where the governing equations can be solved sequentially, it is advantageous to write a finite difference formulation suited for a staggered grid.

6.2 Finite Difference Form of the Reynolds Equation

For numerical computation, a finite difference form of the Reynolds equation is introduced. The dimensionless Reynolds equation is

$$\frac{\partial}{\partial x^*}\left[h^{*3} F_2^* \frac{\partial p}{\partial x^*}\right]+\frac{\partial}{\partial y^*}\left[h^{*3} F_2^* \frac{\partial p}{\partial y^*}\right]$$

$$=\frac{\partial}{\partial x^*}\left[h^* \frac{F_3^*}{F_0^*}\right]+\frac{\rho h_0 h^*}{\partial t^*}\left(\int_0^1\left\{\left(-\alpha T_0 \partial T^*\right)+\frac{\mu_0 UB}{\beta h_0^2}\partial p^*\right\}dz^*\right) \tag{6.1}$$

Using the following expressions (6.2), and the central differences approximations and substituting the Equation (6.1)

$$\frac{\partial}{\partial x^*}\left[h^{*3} F_2^* \frac{\partial p}{\partial x^*}\right]=3h^{*2} F_2^* \frac{\partial h^*}{\partial x^*}\left(\frac{\partial p^*}{\partial x^*}\right)+h^{*3}\frac{\partial F_2^*}{\partial x^*}\left(\frac{\partial p^*}{\partial x^*}\right)+h^{*3}F_2^*\left(\frac{\partial^2 p^*}{\partial x^{*2}}\right)$$

$$\frac{\partial}{\partial y^*}\left[h^{*3} F_2^* \frac{\partial p}{\partial y^*}\right]=3h^{*2} F_2^* \frac{\partial h^*}{\partial y^*}\left(\frac{\partial p^*}{\partial y^*}\right)+h^{*3}\frac{\partial F_2^*}{\partial y^*}\left(\frac{\partial p^*}{\partial y^*}\right)+h^{*3}F_2^*\left(\frac{\partial^2 p^*}{\partial y^{*2}}\right) \tag{6.2}$$

$$\frac{\partial}{\partial x^*}\left[h^* \frac{F_3^*}{F_0^*}\right]=\frac{F_3^*}{F_0^*}\frac{\partial h^*}{\partial x^*}+h^*\frac{\partial}{\partial x^*}\left(\frac{F_3^*}{F_0^*}\right)$$

Hence, equation (6.1) can now be written in finite difference form with the above substitutions as:

$$\Phi_1 p^*_{i+1,j}+\Phi_2 p^*_{i-1,j}+\Phi_3 p^*_{i,j+1}+\Phi_4 p^*_{i,j-1}+\Phi_5 p^*_{i,j}=\Phi_6 \tag{6.3}$$

where

$$\Phi_1 = \frac{3}{4} h^{*2}_{i,j} F2^{*}_{i,j} \left(h^{*}_{i+1,j} - h^{*}_{i-1,j} \right) + \frac{1}{4} h^{*3}_{i,j} \left(F2^{*}_{i+1,j} - F2^{*}_{i-1,j} \right)$$

$$\Phi_2 = -\frac{3}{4} h^{*2}_{i,j} F2^{*}_{i,j} \left(h^{*}_{i+1,j} - h^{*}_{i-1,j} \right) - \frac{1}{4} h^{*3}_{i,j} \left(F2^{*}_{i+1,j} - F2^{*}_{i-1,j} \right)$$

$$\Phi_3 = \frac{3}{4} h^{*2}_{i,j} F2^{*}_{i,j} \left(h^{*}_{i,j+1} - h^{*}_{i,j-1} \right) + \frac{1}{4} h^{*3}_{i,j} \left(F2^{*}_{i,j+1} - F2^{*}_{i,j-1} \right)$$

$$\Phi_4 = -\frac{3}{4} h^{*2}_{i,j} F2^{*}_{i,j} \left(h^{*}_{i,j+1} - h^{*}_{i,j-1} \right) - \frac{1}{4} h^{*3}_{i,j} \left(F2^{*}_{i,j+1} - F2^{*}_{i,j-1} \right)$$

$$\Phi_5 = -2 \left(h^{*3}_{i,j} F2^{*}_{i,j} \right) \left(\frac{\Delta x^{*2} + \Delta y^{*2}}{\Delta x^{*2} \Delta y^{*2}} \right)$$

$$\Phi_6 = \frac{1}{2} \left\{ \left(\frac{F3^{*}}{F0^{*}} \right)_{i,j} \left(h^{*}_{i+1,j-1} - h^{*}_{i-1,j-1} \right) + h^{*}_{i,j} \left[\left(\frac{F3^{*}}{F0^{*}} \right)_{i+1,j} - \left(\frac{F3^{*}}{F0^{*}} \right)_{i-1,j} \right] \right\}$$

In equation (6.3), Φ_1, Φ_2, Φ_3, and Φ_4 refer to the coefficients applied to the nodes around the central node, Φ_5, and Φ_6 is the source term.

The following two-step method is used. Equation (6.4) is solved iteratively using the point successive-over-relaxation (SOR) scheme with optimal relaxation factor, ω.

$$\begin{cases} \tilde{p}^{*k}_{i,j} = -\dfrac{1}{\Phi_5} \left(\Phi_1 p^{*k}_{i+1,j} + \Phi_2 p^{*k}_{i-1,j} + \Phi_3 p^{*k}_{i,j+1} + \Phi_4 p^{*k}_{i,j-1} - \Phi_6 \right) - p^{*k} \\ p^{*k+1}_{i,j} = p^{*k}_{i,j} + \omega \tilde{p}^{*k}_{i,j} \end{cases} \tag{6.4}$$

where $\tilde{p}$ is the intermediate calculated pressure value and k is the index for iteration. In order to stop the output loop iteration, the following convergence criterion is used [26]:

$$\left\| p^{*k} \right\| = \left(\Sigma \left| p_{i,j}^{*k} \right|^2 \Delta x^{*} \Delta y^{*} \right)^{1/2} \leq 10^{-5} \text{ or}$$

$$\sum^{i=0,NX,j=0,NY} \frac{\left| p_{i,j}^{*k+1} - p_{i,j}^{*k} \right|}{p_{i,j}^{*k+1}} \leq ERR \tag{6.5}$$

where ERR is varied between 0.02 and 0.03, depending on the required accuracy of the solution.

6.3 Finite difference form of the Energy Equation

The numerical scheme, called alternating direction implicit, is employed for solving this parabolic energy equation. The ADI belongs to a class of methods known as "Approximate Factorization." In these methods, the original multidimensional FDEs are replaced by a series of finite difference equations with can be represented by tridiagonal formulations. The advantage of the ADI scheme lies in its simplicity and efficiency. The tridiagonal matrix inversion is very efficient to carry out on any computer. The implicit scheme computation removes the stringent time step limit. The dimensionless energy equation (5.18) can be expressed as [26]

$$T_t^* = \Lambda_1 T^* + \Lambda_2 T^* + \Lambda_3 T^* + g + f\,T^* \qquad (6.6)$$

where

$$T_t^* = \frac{\partial T^*}{\partial t^*}$$

$$\Lambda_1 = \xi_1 \frac{\partial}{\partial x^*} + \psi_1 \frac{\partial^2}{\partial x^{*2}} \;\; ; \;\; \Lambda_2 = \xi_2 \frac{\partial}{\partial y^*} + \psi_2 \frac{\partial^2}{\partial y^{*2}} \;\; ; \;\; \Lambda_3 = \xi_3 \frac{\partial}{\partial z^*} + \psi_3 \frac{\partial^2}{\partial z^{*2}}$$

By center difference scheme and the Taylor series, equation (6.6) becomes as follows:

$$\frac{T^{*n+1} - T^{*n}}{\Delta t^*} = \frac{1}{2}\left(\Lambda_1 T^{*n+1} + \Lambda_1 T^{*n}\right) + \frac{1}{2}\left(\Lambda_2 T^{*n+1} + \Lambda_2 T^{*n}\right) +$$

$$\frac{1}{2}\left(\Lambda_3 T^{*n+1} + \Lambda_3 T^{*n}\right) + \frac{1}{2}\left(g^{n+1} + g^n\right) + \frac{1}{4}\left(f^{n+1} + f^n\right)\left(T^{*n+1} + T^{*n}\right) + O\left(\Delta t^{*2}\right) \qquad (6.7)$$

Rearranging equation (6.7),

$$\left(1 - \frac{\Delta t^*}{2}\Lambda_1 - \frac{\Delta t^*}{2}\Lambda_2 - \frac{\Delta t^*}{2}\Lambda_3\right) T^{*n+1} = \left(1 + \frac{\Delta t^*}{2}\Lambda_1 + \frac{\Delta t^*}{2}\Lambda_2 + \frac{\Delta t^*}{2}\Lambda_3\right) T^{*n} +$$

$$\frac{\Delta t^*}{2}\left(g^{n+1}+g^n\right)+\frac{\Delta t^*}{4}\left(f^{n+1}+f^n\right)\left(T^{*n+1}+T^{*n}\right)+O\left(\Delta t^{*3}\right) \qquad (6.8)$$

Adding $\left(\frac{\Delta t^{*2}}{4}\Lambda_1\Lambda_3+\frac{\Delta t^*}{2}\Lambda_2\right)T^{*n+1}$ to both sides of equation (6.8),

$$\left(1-\frac{\Delta t^*}{2}\Lambda_1-\frac{\Delta t^*}{2}\Lambda_3+\frac{\Delta t^{*2}}{4}\Lambda_1\Lambda_3\right)T^{*n+1}=\left(1+\frac{\Delta t^*}{2}\Lambda_1+\frac{\Delta t^*}{2}\Lambda_3+\frac{\Delta t^{*2}}{2}\Lambda_1\Lambda_3\right)T^{*n}+$$

$$\Delta t^*\Lambda_2 T^{*n}+\left(\frac{\Delta t^{*2}}{4}\Lambda_1\Lambda_3+\frac{\Delta t^*}{2}\Lambda_2\right)\left(T^{*n+1}-T^{*n}\right)+\frac{\Delta t^*}{2}\left(g^{n+1}+g^n\right)+$$

$$\frac{\Delta t^*}{4}\left(f^{n+1}+f^n\right)\left(T^{*n+1}+T^{*n}\right)+O\left(\Delta t^{*3}\right) \qquad (6.9)$$

Since $\left(\frac{\Delta t^{*2}}{4}\Lambda_1\Lambda_3+\frac{\Delta t^*}{2}\Lambda_2\right)\left(T^{*n+1}-T^{*n}\right)$ is accurate to $O\left(\Delta t^{*2}\right)$ equation (6.9) reduces as follows:

$$\left(1-\frac{\Delta t^*}{2}\Lambda_1\right)\left(1-\frac{\Delta t^*}{2}\Lambda_3\right)T^{*n+1}=\left(1+\frac{\Delta t^*}{2}\Lambda_1\right)\left(1+\frac{\Delta t^*}{2}\Lambda_3\right)T^{*n}+$$

$$\Delta t^*\Lambda_2 T^{*n}+\frac{\Delta t^*}{2}\left(g^{n+1}+g^n\right)+\frac{\Delta t^*}{4}\left(f^{n+1}+f^n\right)\left(T^{*n+1}+T^{*n}\right)+O\left(\Delta t^{*3}\right) \qquad (6.10)$$

Assuming $f=f^{n+1}=f^n$, ADI scheme is as follows:

$$\begin{cases}\left(1-\frac{\Delta t^*}{2}\Lambda_1\right)T^{*n+\frac{1}{2}}=\left(1+\frac{\Delta t^*}{2}\Lambda_2+\frac{\Delta t^*}{2}\Lambda_3+\frac{\Delta t^*}{2}f\right)T^{*n}+\frac{\Delta t^*}{2}g^n\\ \left(1-\frac{\Delta t^*}{2}\Lambda_3-\frac{\Delta t^*}{2}f\right)T^{*n+1}=\left(1+\frac{\Delta t^*}{2}\Lambda_1\right)T^{*n+\frac{1}{2}}+\frac{\Delta t^*}{2}\Lambda_2 T^{*n}+\frac{\Delta t^*}{2}g^{n+1}\end{cases} \qquad (6.11)$$

Applying the proper difference formula and making element equation (6.11), the resulting equations (6.12), (6.13) can be solved with Thomas algorithm.

$$\begin{aligned}
T_{i,j,k}^{*n+\frac{1}{2}} = {} & \frac{\Delta t^*}{2} g^n + \left(1 + \frac{\Delta t^*}{2} f\right) T_{i,j,k}^{*n} + \\
& \frac{\Delta t^*}{2}\left(\xi_1 \frac{T_{i+1,j,k}^{*n+\frac{1}{2}} - T_{i-1,j,k}^{*n+\frac{1}{2}}}{2\Delta x^*} + \psi_1 \frac{T_{i+1,j,k}^{*n+\frac{1}{2}} - 2T_{i,j,k}^{*n+\frac{1}{2}} + T_{i-1,j,k}^{*n+\frac{1}{2}}}{\Delta x^{*2}} \right) + \\
& \frac{\Delta t^*}{2}\left(\xi_2 \frac{T_{i,j+1,k}^{*n} - T_{i,j-1,k}^{*n}}{2\Delta y^*} + \psi_2 \frac{T_{i,j+1,k}^{*n} - 2T_{i,j,k}^{*n} + T_{i,j-1,k}^{*n}}{\Delta y^{*2}} \right) + \\
& \frac{\Delta t^*}{2}\left(\xi_3 \frac{T_{i,j,k+1}^{*n} - T_{i,j,k-1}^{*n}}{2\Delta z^*} + \psi_3 \frac{T_{i,j,k+1}^{*n} - 2T_{i,j,k}^{*n} + T_{i,j,k-1}^{*n}}{\Delta z^{*2}} \right)
\end{aligned} \tag{6.12}$$

$$\begin{aligned}
\left(1 - \frac{\Delta t^*}{2} f\right) T_{i,j,k}^{*n+1} = {} & \frac{\Delta t^*}{2} g^{n+1} + T_{i,j,k}^{*n+\frac{1}{2}} + \\
& \frac{\Delta t^*}{2}\left(\xi_1 \frac{T_{i+1,j,k}^{*n+\frac{1}{2}} - T_{i-1,j,k}^{*n+\frac{1}{2}}}{2\Delta x^*} + \psi_1 \frac{T_{i+1,j,k}^{*n+\frac{1}{2}} - 2T_{i,j,k}^{*n+\frac{1}{2}} + T_{i-1,j,k}^{*n+\frac{1}{2}}}{\Delta x^{*2}} \right) + \\
& \frac{\Delta t^*}{2}\left(\xi_2 \frac{T_{i,j+1,k}^{*n} - T_{i,j-1,k}^{*n}}{2\Delta y^*} + \psi_2 \frac{T_{i,j+1,k}^{*n} - 2T_{i,j,k}^{*n} + T_{i,j-1,k}^{*n}}{\Delta y^{*2}} \right) + \\
& \frac{\Delta t^*}{2}\left(\xi_3 \frac{T_{i,j,k+1}^{*n+1} - T_{i,j,k-1}^{*n+1}}{2\Delta z^*} + \psi_3 \frac{T_{i,j,k+1}^{*n+1} - 2T_{i,j,k}^{*n+1} + T_{i,j,k-1}^{*n+1}}{\Delta z^{*2}} \right)
\end{aligned} \tag{6.13}$$

where

$$g = \frac{B\mu_0 \mu^* U}{\rho c_p T_0 h_0^2 h^{*2}} \left[\left(\frac{\partial u^*}{\partial z^*} \right)^2 + \left(\frac{\partial v^*}{\partial z^*} \right)^2 \right]$$

$$f = \frac{B\alpha \mu_0 \mu^* U}{\rho c_p h_0^2 h^{*2}} \left(u^* \frac{\partial p^*}{\partial x^*} + v^* \frac{\partial p^*}{\partial y^*} \right)$$

In terms of the format to take advantage of the tridiagonal form of the coefficient matrix, Equations (6.12) and (6.13) can be rewritten as

$$b T_{N-1}^* + d T_N^* + a T_{N+1}^* = c \tag{6.14}$$

where a, b, and c are coefficients.

For boundary conditions, T_0^* is known at one boundary and T_N^* at the other. In the range of *1* to *N-1*, all known $T's$ are collected in to the c term. The system can be cast into the following form although the first and last equations in the array may result from the auxiliary relationship.

$$\begin{bmatrix} d_0 & a_0 & 0 & \cdot & \cdot & \cdot & \cdot & 0 \\ b_1 & d_1 & a_1 & 0 & \cdot & \cdot & \cdot & 0 \\ 0 & b_2 & d_2 & a_2 & 0 & \cdot & \cdot & \cdot \\ \cdot & \cdot & \cdot & \cdot & \cdot & \cdot & \cdot & \cdot \\ \cdot & \cdot & \cdot & \cdot & \cdot & \cdot & \cdot & \cdot \\ \cdot & \cdot & \cdot & \cdot & \cdot & \cdot & \cdot & 0 \\ 0 & \cdot & \cdot & \cdot & 0 & a_{N-1} & d_{N-1} & a_{N-1} \\ 0 & \cdot & \cdot & \cdot & \cdot & 0 & b_N & d_N \end{bmatrix} \begin{bmatrix} T_0^* \\ T_1^* \\ T_2^* \\ \cdot \\ \cdot \\ \cdot \\ T_{N-1}^* \\ T_N^* \end{bmatrix} = \begin{bmatrix} c_0 \\ c_1 \\ c_2 \\ \cdot \\ \cdot \\ \cdot \\ c_{N-1} \\ c_N \end{bmatrix} \tag{6.15}$$

Referring to the tridiagonal matrix of coefficients above, the system is put into an upper triangular form by computing

$$d_j = d_j - \frac{b_j}{d_{j-1}} a_{j-1} \text{ and } c_j = c_j - \frac{b_j}{d_{j-1}} c_{j-1} \qquad j = 1,2,\ldots,N$$

then computing the unknowns from back substitution and then

$$T_k^* = \frac{c_k - a_k T_{k+1}^*}{d_k} \qquad k = N-1,\ldots,0$$

6.4 Grid System

Figures (6.1) and (6.2) illustrate the finite moving system configuration and geometry. Diagrams of journal and slider bearings are sketched with nomenclature. A journal bearing consists in its simplest form of two rigid cylinders. The outer cylinder is usually held stationary, while the inner cylinder rotates at an angular velocity. A slider bearing consists of two inclined plane surfaces. Film thickness in the lubricating region can be established on the angular coordinate, *θ*, for a journal bearing and on the x coordinate for a slider bearing. By the dimensionless transformation, a mesh of rectangular cells with constant sizes for the full shear zone model and variable sizes for the partial shear zone model is established for the development of the finite difference approximation. The lubricating region consists of the inlet, and outlet as shown in Figure (6.1) for a journal bearing and Figure (6.2) for a slider bearing. This is shown in Figure (6.3). in which δx^*, δy^*, and δz^* express the element size for x^*, y^*, and z^* respectively. The number of grids could be fixed for different operating conditions. The dimensions across the film thickness and film flow length are divided into 60 grids. Film flow width is divided into 10 grids. The structure of the finite difference mesh is shown on Figure (6.4). The geometrical configuration of generalized lubricating zone illustrated in Figure (6.4) is expressed as two structures with thin shear zone and full shear zone. The computational domain of finite moving system is plotted in two ways, one having a full shear zone for the lubricating region, the other having three different shear zone for stationary, and moving regions and a central thin shear zone to be discussed in Chapter 7.

A variable mesh nodal structure like the one shown in Figure (6.3-b) is used to provide close spacing in and around the thin shear zone to be discussed in next chapter. In this figure, the inlet is to the left and the outlet is to the right. The variable mesh helps to minimize the errors that can occur because of the large gradients in the thin shear zone with high shear rate.

6.5 Consistency and Stability

As seen in Equation (6.11), the numerical scheme for each of the two fractional steps from the energy equation is relatively simple. However, it is necessary to show that the combination of these two steps is consistent with the original governing equation. This is very hard to prove theoretically because of the existence of the three dimensions and two additional heating source terms. This is a weak-point in applying the method of fractional steps to the problems of fluid dynamics in several variables. However, this weak-point does not appear to affect the accuracy of the numerical model. For numerical accuracy, it is desirable to keep the time step sufficiently small, (typically Δt =2.5x10^{-5} sec) such that Courant number ($|\nu| = |c\,\Delta t/\Delta x| \leq 1$), where c is coefficient) does not become much lager than 1.

6.6 Computational Procedure

The computational procedures are summarized as follows. The flow chart for the computer program is shown in Figures (6.5). At the start of the numerical simulation the pressure and temperature fields are set to the inlet lubricant pressure and temperature. The velocity distribution of the film is calculated at each time step with the continuity and Newtonian shear velocity gradient relationship as shown in Figure (6.5). However, when the shear zone ratio, h_s/h, is evaluated as a function of operating system characteristic number to be introduced in the next chapter, the program requires proper initial velocity values for each zone of this model as shown in Figure (6.3). Also, it structures all shear action takes place in the shear zone which is at the center of the film.

(1) Supply all the physical input data. The data are the rotating system geometry, oil type, reference oil temperature, operating speed, and properties of the lubricants. Values of the input data allow the determination of nondimensional parameters.

(2) Initialize pressure, velocity, and temperature.

(3) Generate uniform grids of x, y, z coordinates.

(4) Compute coefficients for the simplified generalized Reynolds equation and solve the simplified generalized Reynolds equation to obtain a new pressure field for the film.

(5) Check the pressure profile. If the convergence criterion is not satisfied, then the current pressure profile is adjusted by iterative computation until it is satisfied.

(6) Calculate the velocity profile in the full shear zone.

(7) Update viscosity and determine temperature profile using energy equation with its boundary conditions.

(8) Repeat loop (4) to (8) until the pressure and temperature distributions reach steady state.

(9) Compute the load from the pressure distribution, friction force, flow rate, and heat convection. Output the pressure, the temperature distribution, and the bearing performance data.

6.7 Numerical Calculation and Comparison

An extensive amount of the thermohydrodynamic results are presented for slider bearing systems. Slider bearing systems in typical hydrodynamic cases are chosen for analyzing thermohydrodynamic phenomenon. These solutions are obtained using the finite difference scheme described in the previous chapter. A computer code is written in Fortran language to obtain numerical solutions to the THD problem. This code is originally developed by Wang to determine the shear zone ratio which are compatible with the experimental data performed for journal bearings [62]. For the results presented in the present study, his algorithm is mainly applied to give a more realistic solution to the problem.

The program is capable of generating results for any bearing geometry, and lubricant properties. The important design parameter and test fluid for the test slider bearings are presented in Table 5 for which other numerical results are available. The solutions are validated by comparing them to published experimental data and numerical results. This chapter then proceeds to develop a generalized process for THD analysis.

First, the validity of the energy equation with compression heating source is examined by comparing the steady state distribution in temperature and pressure to those published in the literature. Based on the validated algorithm, a new method is developed to use a rheological concept model to the adiabatic shear band and the glass transition behavior for comparison with recent experimental results.

Table 5: Design Parameters for Test Slider Bearings [26, 27, 62]

Case #	Length, B (inch)	Width, L (inch)	h_{min} (inch)	h_{max} (inch)	Velocity (ft/sec)	SAE (oil #)	Temp (° F)
1 *	3	3	0.002	0.004	100	30	100
2 *	3	3	0.002	0.004	50	30	100
3 *	3	3	0.002	0.004	200	30	100
4 *	3	3	0.002	0.004	100	50	100
5 *	3	3	0.002	0.004	100	30	150
6 *	3	3	0.002	0.004	100	10	100

Note: *: Full shear zone model (Newtonian case)

Table 6: Lubricant viscosity-temperature data, $\mu^*(T^*) = e^{\delta T_0(T^*-1)}$ [26, 62]

SAE oil #	5	10	30	50
μ, $lb-\sec/ft^2$	3.24 x 10^{-4}	6.6384 x 10^{-4}	0.00221	0.00504
δ	-0.0142	-0.0172	-0.022	-0.025

Table 7: Common Input Parameters on Bearing [26, 62]

$k = 0.075\,Btu/\left(hr - ft - {}^{o}F\right)$: conductivity

$\rho = 54.6\,lb_m/ft^3$: density

$c_p = 0.48\,Btu/lb_m - {}^{o}F$: specific heat

$\alpha = 0.00036\,{}^{0}F^{-1}$: thermal expansion coefficient

$\beta = 31.68 \times 10^6\,lb_f/ft^2$: bulk modulus

6.8 Model with Full Film Shear Zone in the Lubrication Zone

Developments in lubrication technology have been widely dedicated to industrial areas. The journal bearing is still the most encountered in engineering applications. However, for simple checks at different speeds and wide range of lubricants, the slider bearing with different geometries is considered.

The survey of such geometries is given in the Table 5. One of the main consideration is that viscous dissipation in the lubricating film, separating two surfaces in relative motion can results in high rates of heat generation. The purpose of this comparison is to confirm the numerical methods in the Newtonian case by comparing them to the numerical results of Ezzat and Rohde [54]. The system used for analysis is the three dimensional slider bearing systems shown in Figure (6.2). The length to width ratio is 1.0. An isothermal and adiabatic analysis are considered for the stationary solid surface. Transition motion of the slider bearing is calculated and is compared with Ezzat and Rohde's results [55]. The pressure and temperature traces of the slider bearing center are plotted in Figure (6.6) throughout Figure (6.9). Based on the steady state solution after 500 time steps (0.01 sec), the pressure-time and temperature-time traces for a constant speed, 100 ft/sec, SAE 30 oil, and 100 °F initial temperature are shown in Figure

(6.6) as typical time history results. The fluid film pressure is shown to increase proportionally during the first few milliseconds of operation, almost reaching its steady-state value. This is the transient time to reach constant running speed from motionless situation. Next, the transient response of the fluid film under various operating conditions is investigated. Results are presented graphically in Figure (6.7) throughout Figure (6.9). Another pressure-time and temperature-time plots for a constant speed (100 ft/sec) is shown in Figure (6.7) for different lubricant oils. Both pressure and temperature values increase with time and are relatively high for higher number lubricant oil since the initial value of viscosity associated with viscous heat generation is higher under the conditions. The time scale is of the order of milliseconds. The effect indicates the higher the running speed, the shorter the time to reach steady state.

Figures (6.8) and (6.9) represent the results after applying isothermal condition to the stationary pad. The effects of the initial temperature is presented in Figure (6.8). The effects of running speed on the transient performance is also shown in Figure (6.9). As shown in Figure (6.11), the higher maximum temperature corresponding to the adiabatic boundary condition are responsible foe the decreased maximum pressure compared to the isothermal boundary condition. Pressure values in the hydrodynamic lubrication regime with the very thin high shear effects can be obtained by keeping the generated heat in the central thin lubricating zone. This will be discussed in the next section. The rheological results with central thin adiabatic heat band and high shear rate are also discussed. Both steady-state solutions of maximum pressure and maximum temperature in the transient performance are in close agreement with the numerical solution by Ezzat and Rohde [54, 55]. The main reason there for the trivial difference which exists between the two results is due to the three-dimensional analysis used and to the addition of the compression heating source in the energy equation in the present study.

The pressure distribution in the fluid film is probably the most important factor in the analysis of the performance of lubricating system. The basic characteristics of all the pressure profiles are a thermohydrodynamic pressure built up in the lubricating zone and a pressure drop to the atmospheric pressure in the inlet and outlet zones. Figure (6.10) shows a typical pressure distribution in the lubricating zone of 60 x 10 x 60 mesh grid with side leakage. The pressure profiles in the lubricating zone for various operating conditions (running speed) are shown in Figure (6.11). The pressure distribution is strongly influenced by the running speed and the thermal boundary condition in the fluid film. The location of maximum pressure is slightly changed when using different thermal boundary conditions.

Figures (6.12-b), (6.13), and (6.14) are the corresponding isotherm contours in the central plane (defined as the y=L/2 plane). The effect of the thermal boundary condition at the stationary pad is shown in Figure (6.12). These results show very similar trends as the results of Ezzat and Rohde. In the case of the adiabatic condition no heat is transmitted to the stationary pad and a relatively high temperature boundary layer is formed as shown in Figure (6.12-a). Using both surface temperatures of the bearing as the initial temperature has the effect of reducing the temperature in the fluid film as shown in Figure (6.12-b). Most of heat dissipated is conducted away to the stationary pad causing the maximum temperature. Maximum temperature is only 160°F in Figure (6.12-b). Otherwise, Figure (6.12-a) shows the temperature contours when the interface between stationary pad and adjacent lubricant is assumed to be adiabatic. From the contours, it can be seen that there is small temperature variations along the film lubrication except around inlet zone. This boundary condition is unrealistic. But, it does serve to emphasize the influence of the thermal boundary condition. It also indicates the probability of the existence of such high temperature adiabatic shear boundary layer in the central thin lubricated region. Figures (6.13) and (6.14) show the effect of running speed and lubricant oil type on the fluid film thermal transients. In all cases, the stationary pad is assumed to be isothermal.

Figure (6.15) shows the velocity profiles in a full shear zone in the direction of motion. In the velocity stream the effect of the thermal boundary and running speed is demonstrated by the different shear rates at the region where the maximum pressure is acting. This steady-state THD performance for inclined slider bearing under the assumption of a full shear zone in fluid film is performed without the effect of heat conduction to the stationary pad in fluid film.

6.9 Summary and Conclusion

This chapter presents a detailed numerical method that is employed for the prediction of THD performance of fluid film bearings. A two-dimensional Reynolds equation for the pressure distribution, three-dimensional full energy equation for the temperature distribution, and velocity equation are transformed. The governing equation which combines the three main equations is solved in two ways for full shear and central shear respectively. The regular grid system is used for the full shear zone model. Some of the results using this approach are used to validate the developed 3 dimensional analysis with the assumption of lubrication with full shear zone by comparing the obtained results with published numerical results.

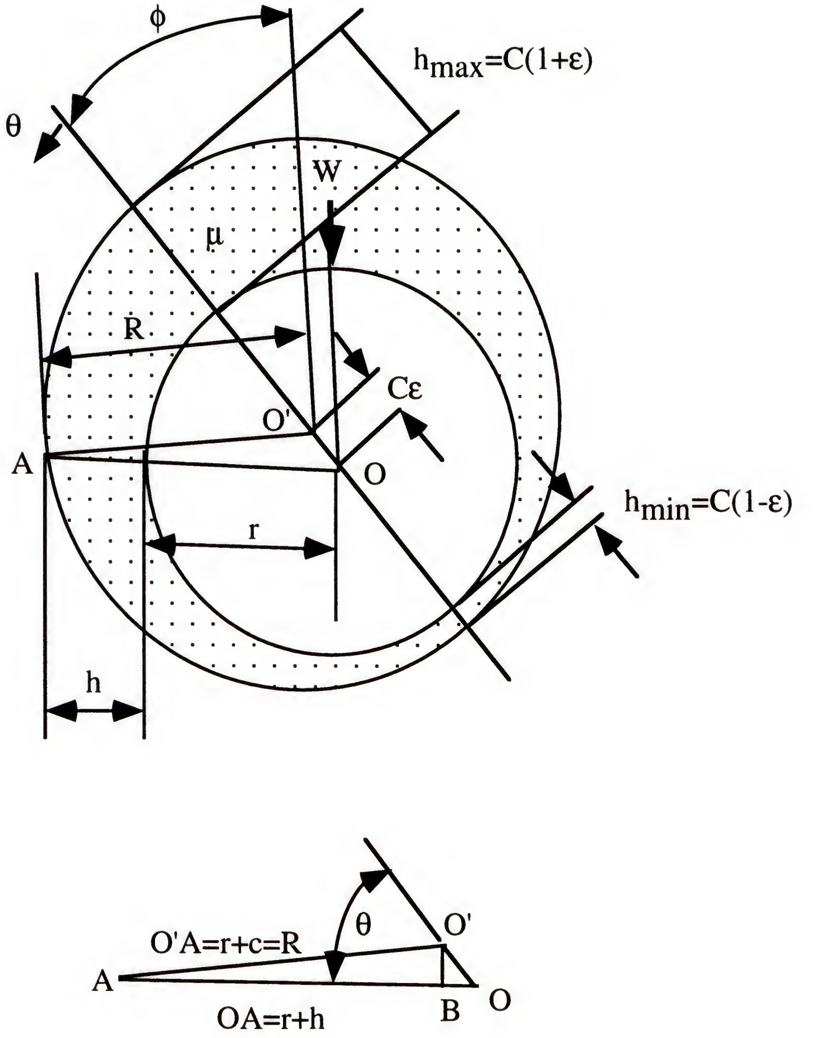

Figure 6.1 Diagram sketch of journal bearing

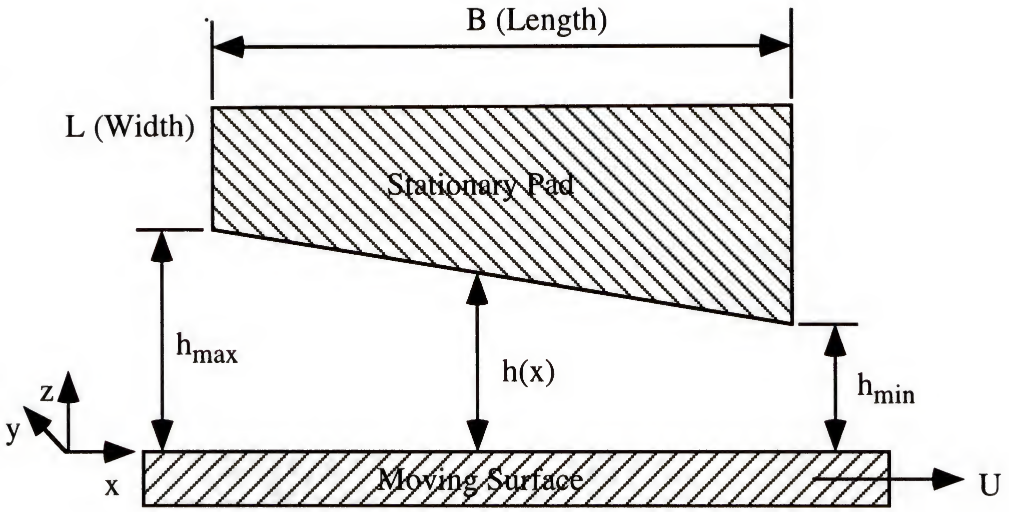

Figure 6.2 Diagram sketch of a slider bearing

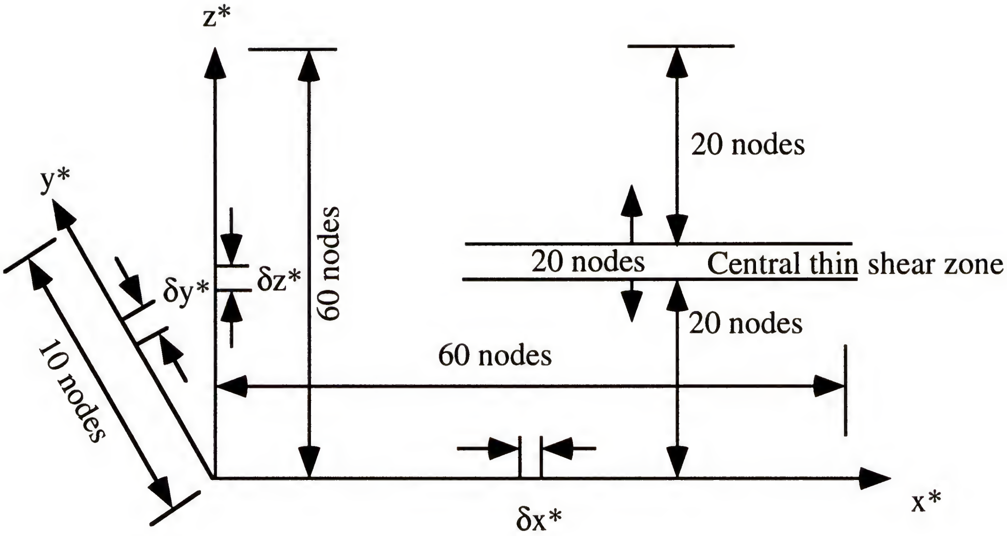

Figure 6.3 Nodal structure of computational domain of lubricating zone

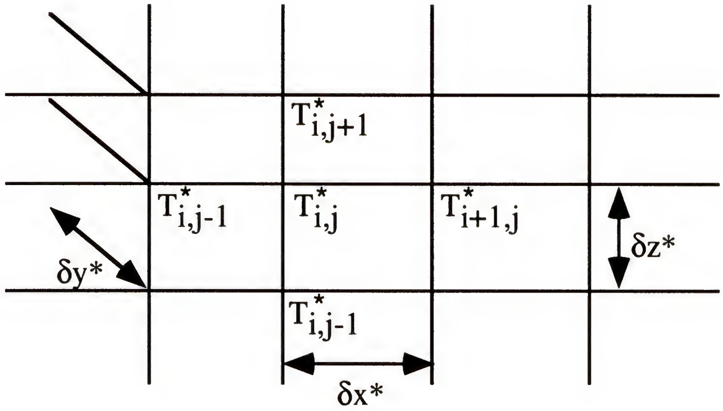

Figure 6.4 Finite difference mesh

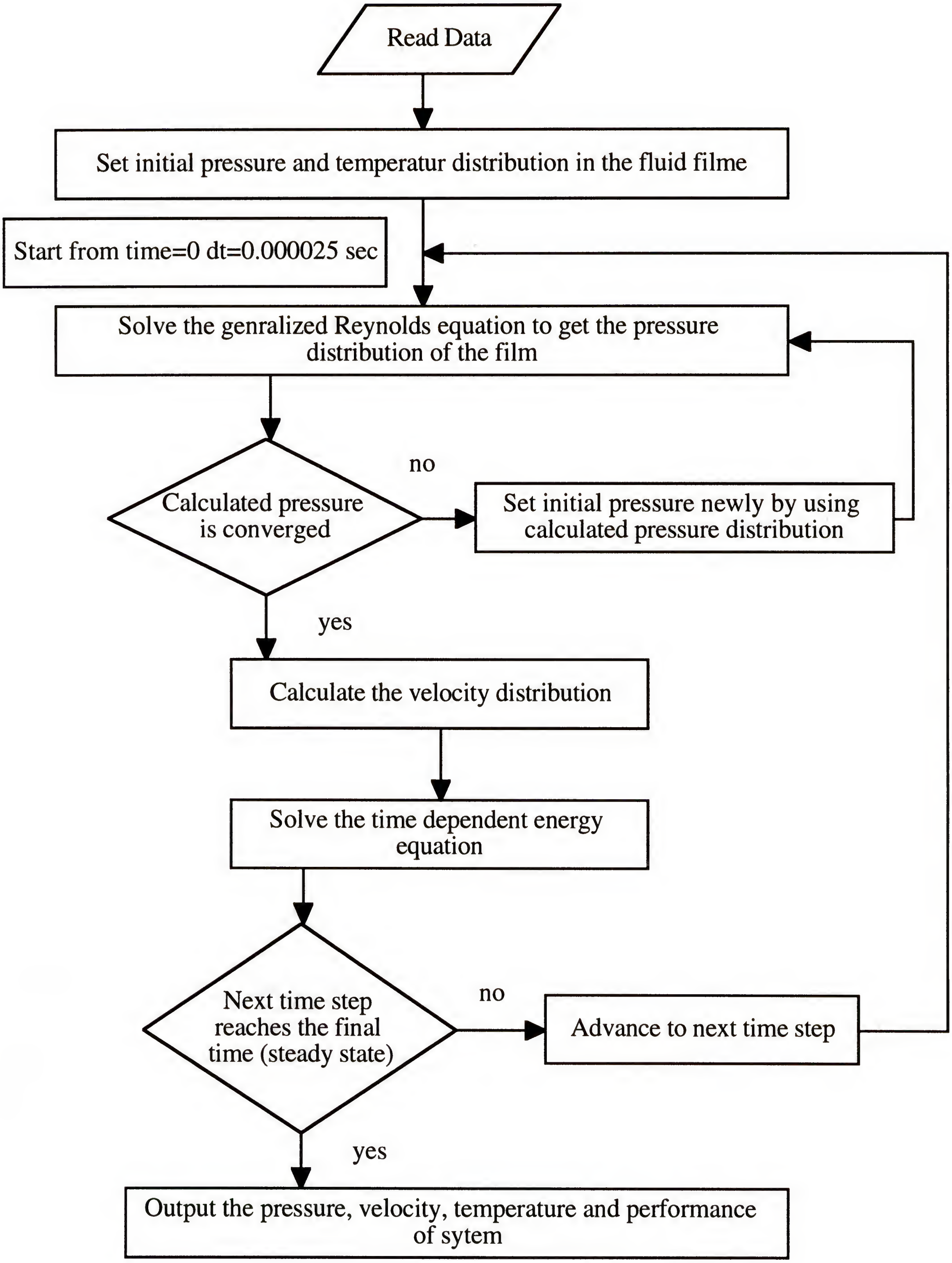
Read Data
Set initial pressure and temperatur distribution in the fluid filme
Start from time=0 dt=0.000025 sec
Solve the genralized Reynolds equation to get the pressure distribution of the film
Calculated pressure is converged
no
Set initial pressure newly by using calculated pressure distribution
yes
Calculate the velocity distribution
Solve the time dependent energy equation
Next time step reaches the final time (steady state)
no
Advance to next time step
yes
Output the pressure, velocity, temperature and performance of sytem

Figure 6.5 Program flow chart for THD analysis using the Newtonian behavior and full shear zone in lubricating region

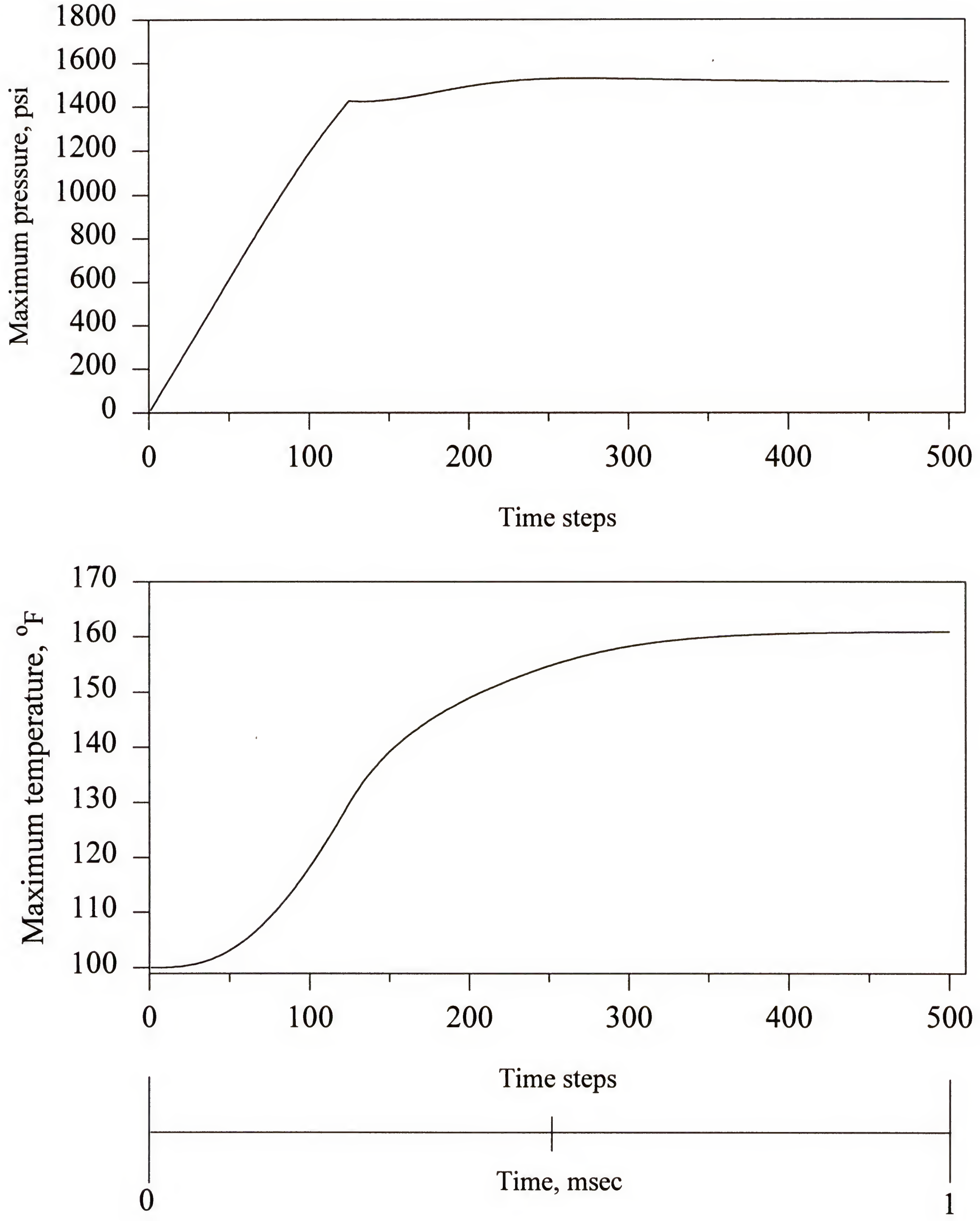

Figure 6.6. Slider bearing pressure and temperature history for full shear zone (SAE 30 oil, T_{in}=100 ^{o}F, U=100 ft/sec, B=L=3.0 inch, h_{min}=0.002 in, h_{max}=0.004 in)

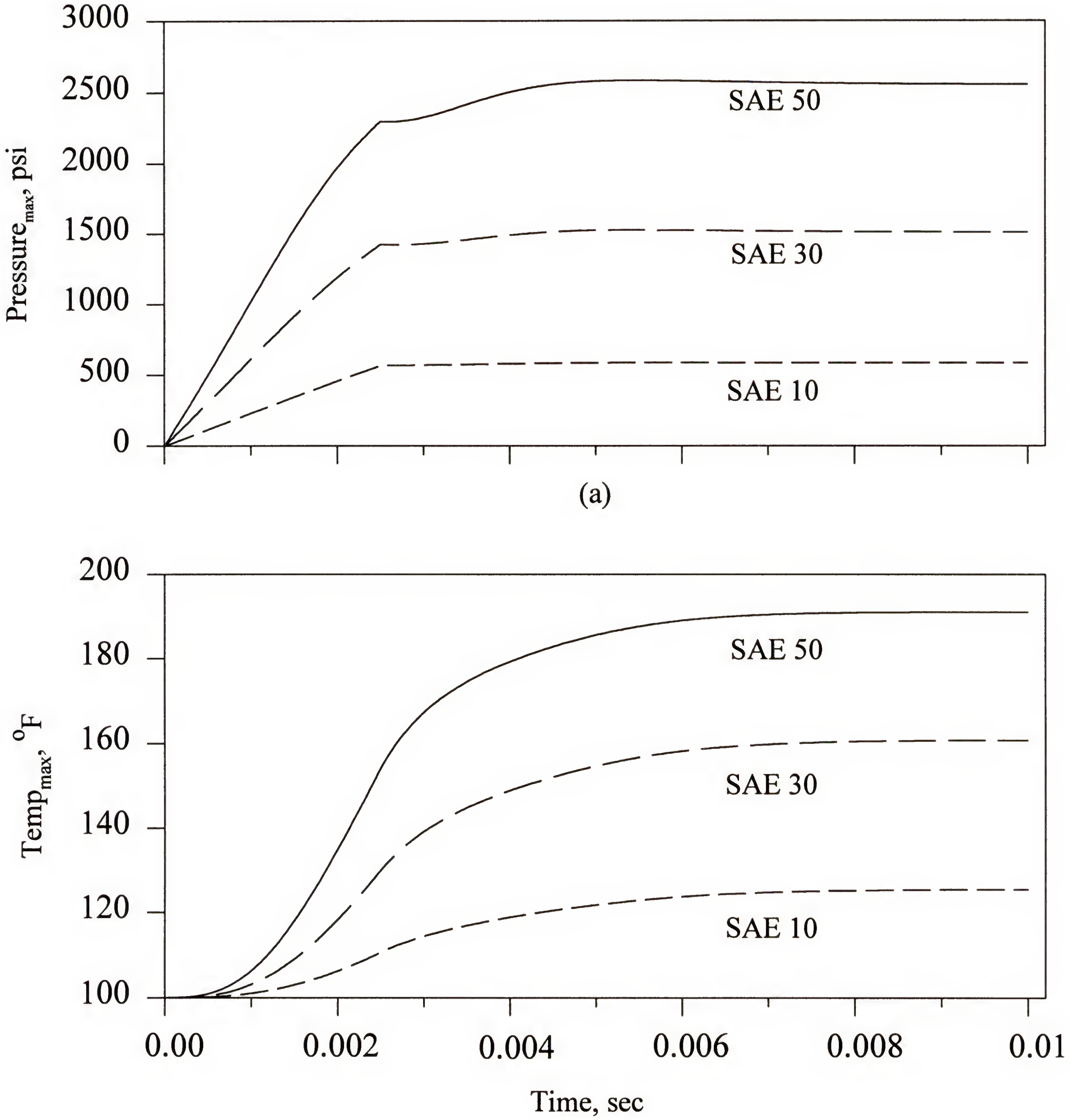

(a)

(b)

Figure 6.7 THD pressure (a), temperature (b) - time history
T_{in} = 100 ^{o}F, U=100 ft/sec, slider bearing, B=L=3.0 in,
h_{min}=0.002 in, h_{max}=0.004 in

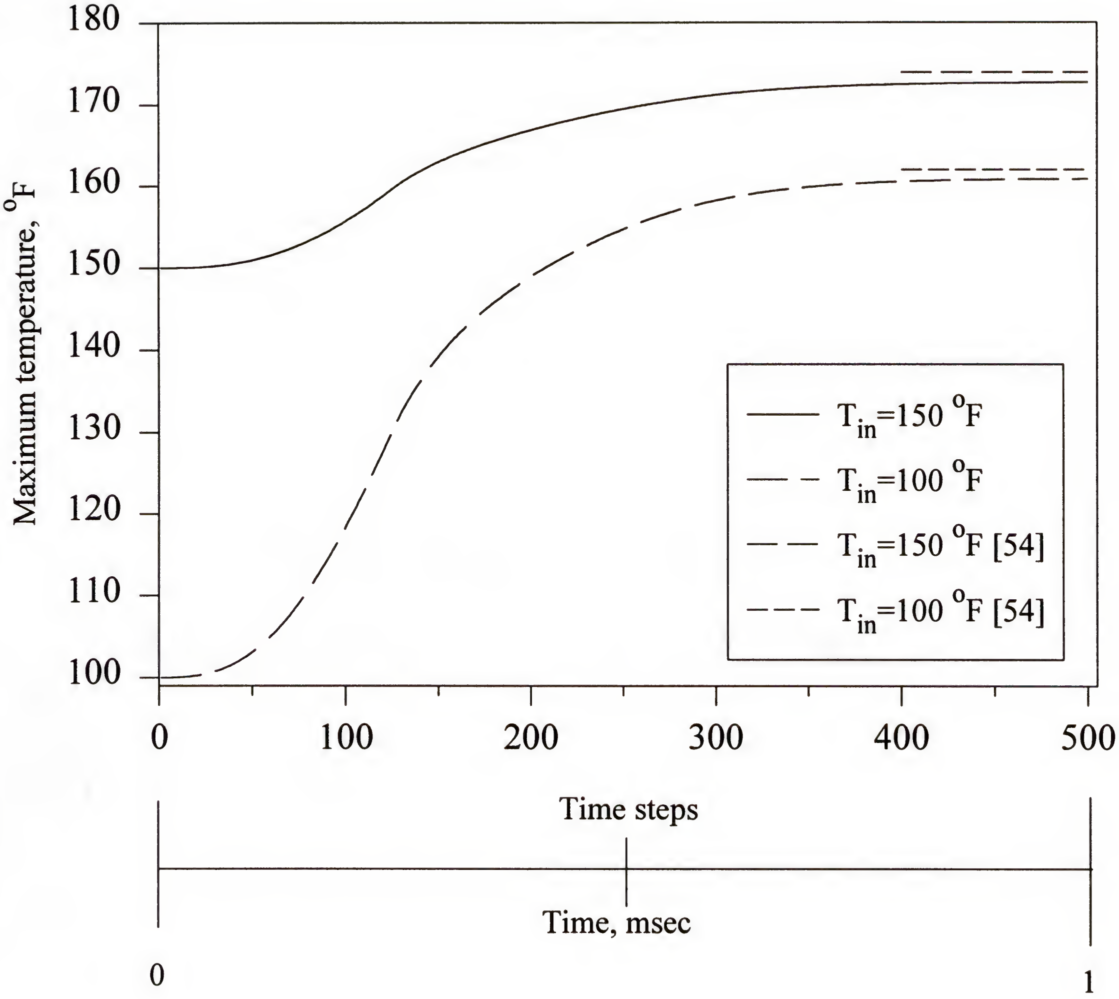

Figure 6.8 THD temperature -Time history
SAE 30 oil, U=100 ft/sec
Slider bearing (B=L=3.0 in, h_{min}=0.002 in, h_{max}=0.004 in)

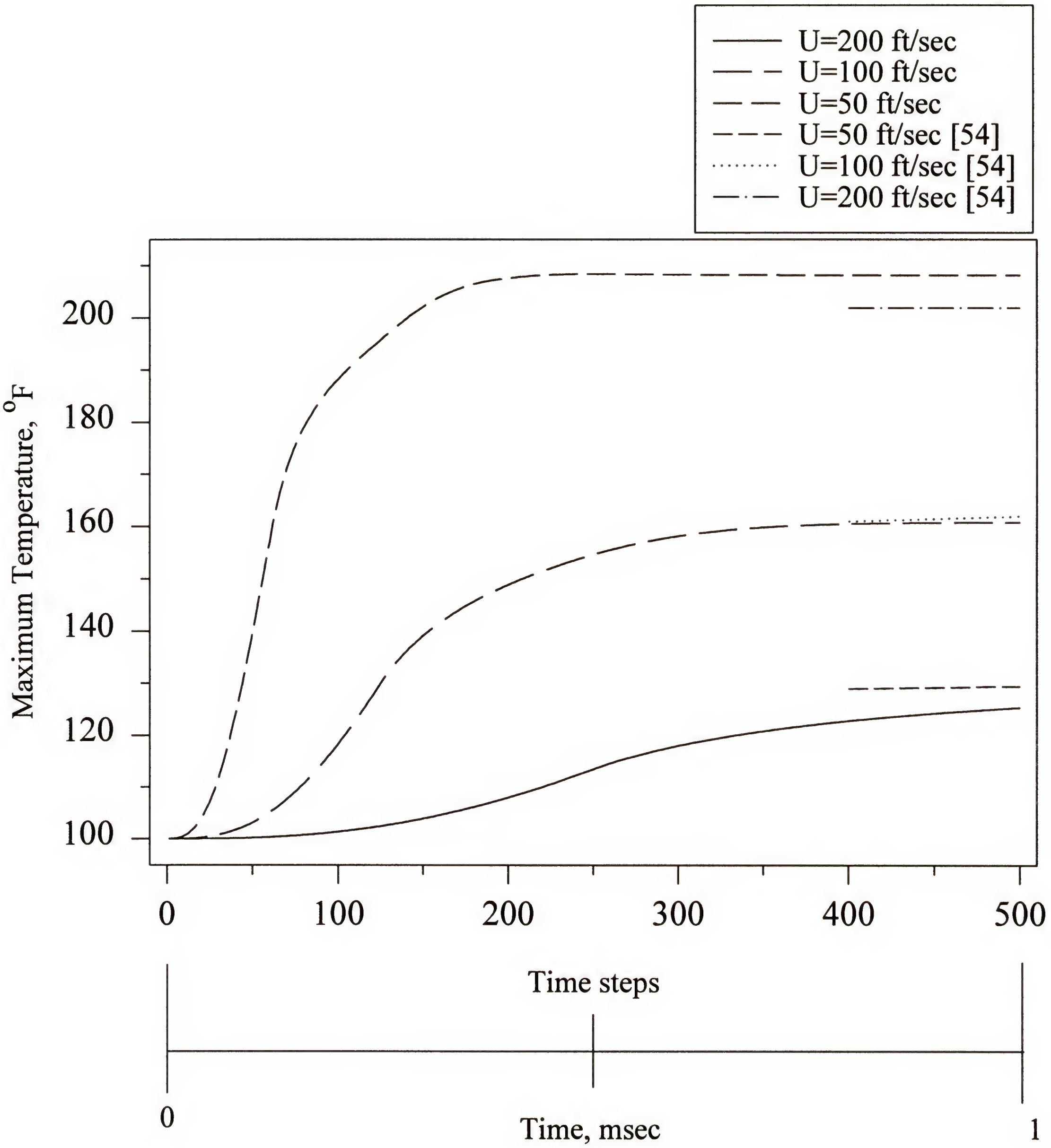

Figure 6.9 THD temperature-Time history
SAE 30 oil, T_{in}=100 °F
[Ezzat and Rohde] - steady state THD temperature solution

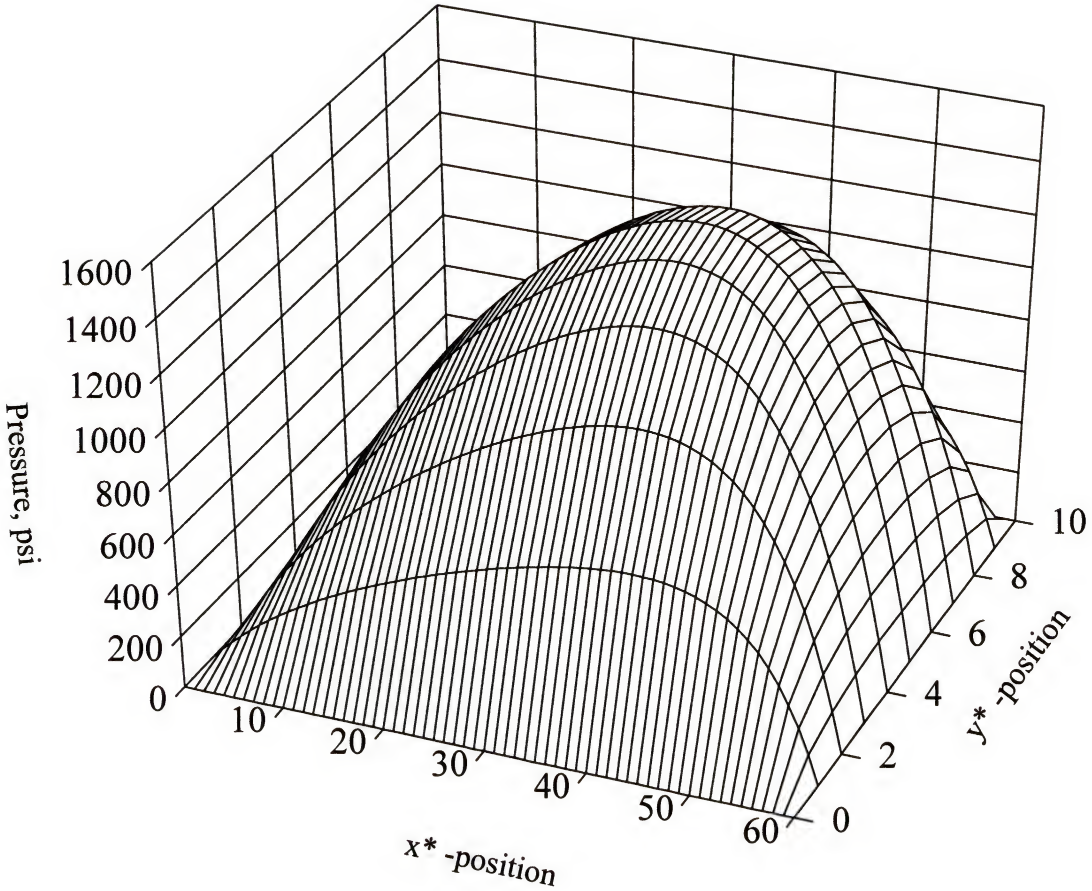

Figure 6.10. Pressure distribution
U=100 ft/sec, T_{in}=100 ^{o}F, SAE 30 oil, B=L=3.0 in,
h_{min}=0.002 in, h_{max}=0.004 in

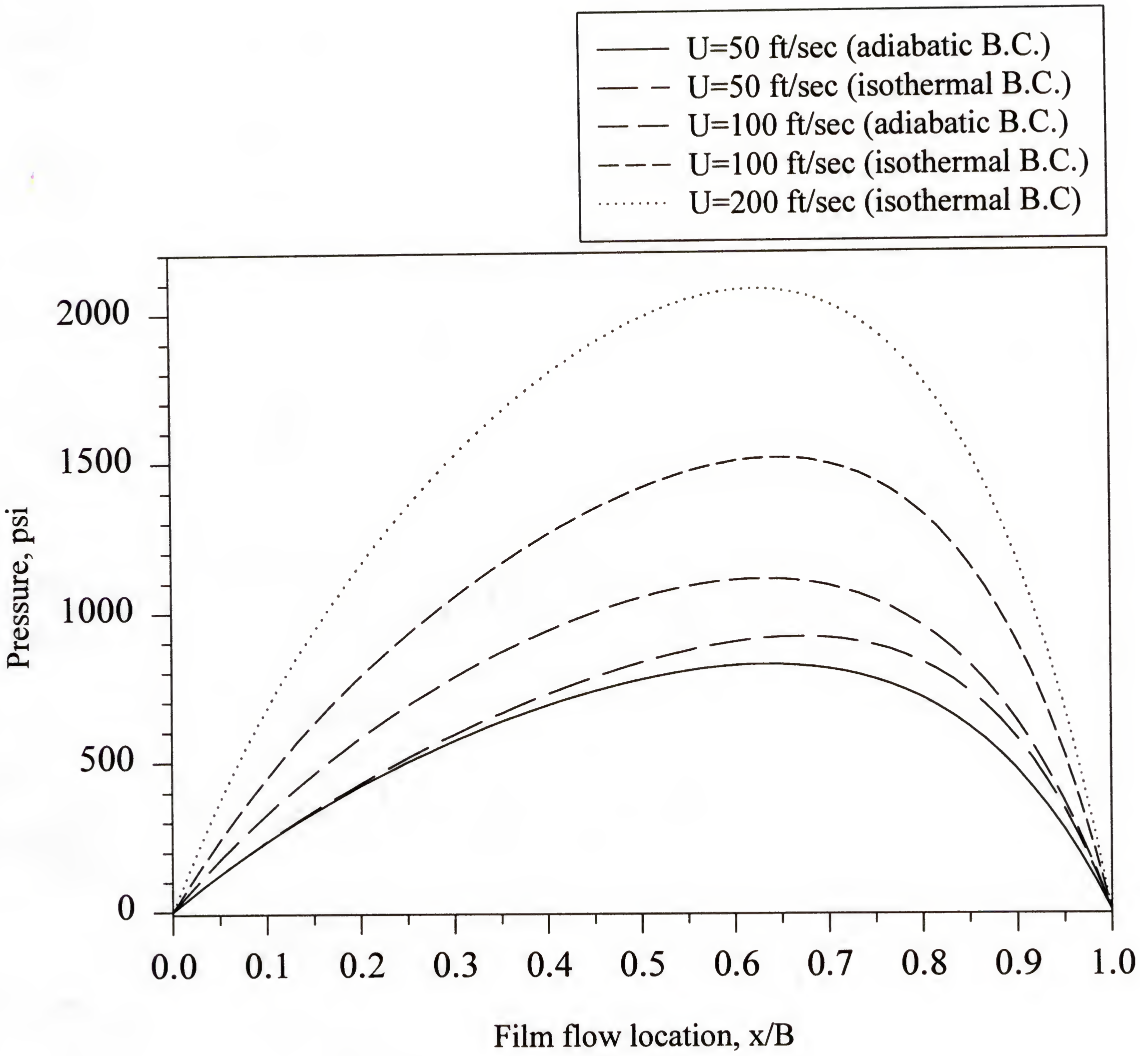

Figure 6.11 Pressure distribution along the middle plane of the slider bearing in the direction of motion (SAE 30 oil, $T_{in}=100\ ^{o}F$, B=L=3 in, $h_{min}=0.002$ in, $h_{max}=0.004$ in)

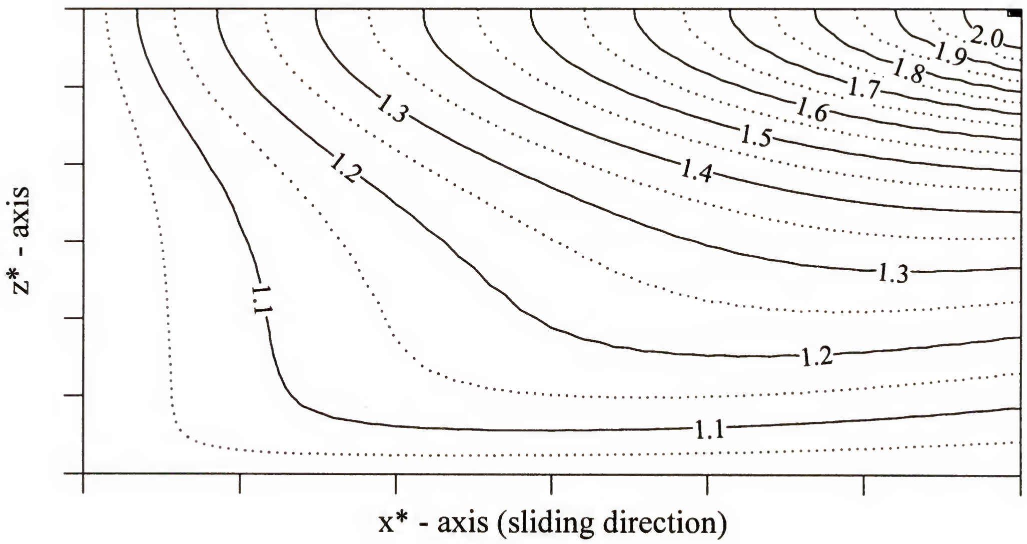

(a)

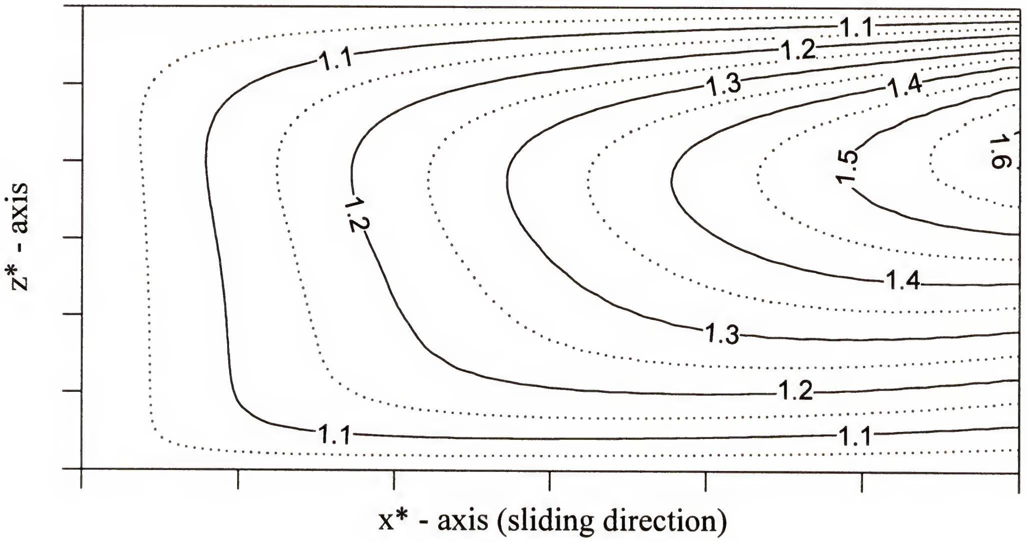

(b)

Figure 6.12 Mid-plane dimensionless film temperature distribution
U=100 ft/sec, $T_{in}=100^{O}F$,
B=L=3.0 in, SAE 30 oil, $h_{min}=0.002$ in, $h_{max}=0.004$ in)
(a) adiabatic boundaries for upper stationary pad
(b) boundaries with isothermal T_{in} for upper pad

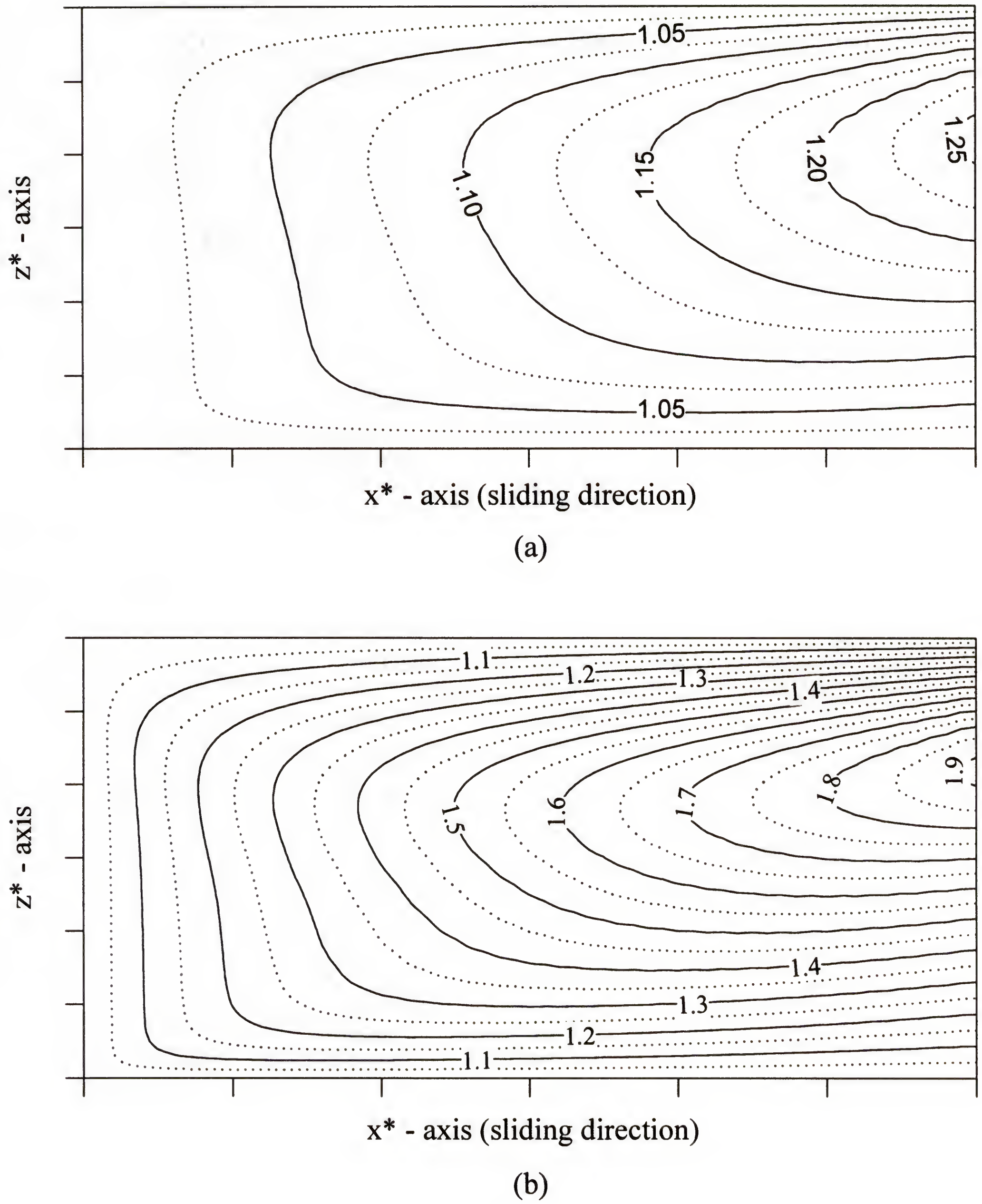

Figure 6.13. Dimensionless film temperature distribution of the bearing in the direction motion
(B=L=3.0 in slider bearing, h_{min}=0.002 in, h_{max}=0.004 in, Tin=100 ^{o}F, U=100 ft/sec,)

(a) SAE 10 oil
(b) SAE 50 oil

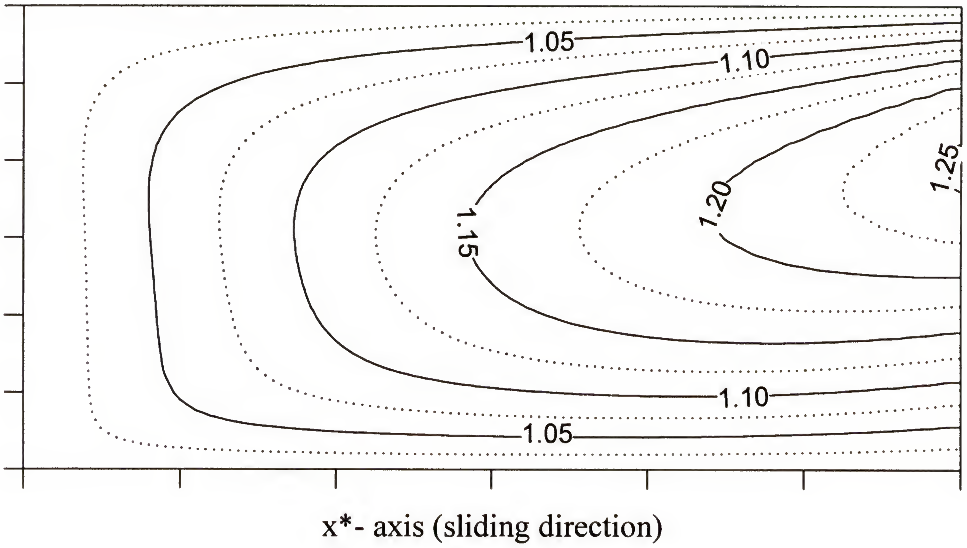

(a)

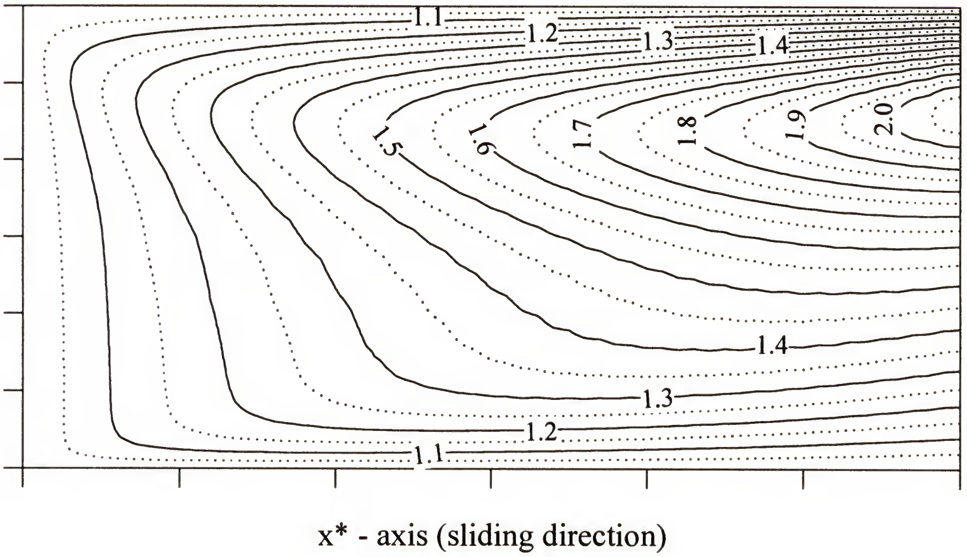

(b)

Figure 6.14 Dimensionless film temperature distribution of the slider bearing in the direction of motion
B=L=3.0 in, h_{min}=0.002 in, h_{max}=0.004 in, SAE 30 oil, T_{in}=100 °F, fixed temperature boundary condition for upper surface pad

(a) U=50 ft/sec
(b) U=200 ft/sec

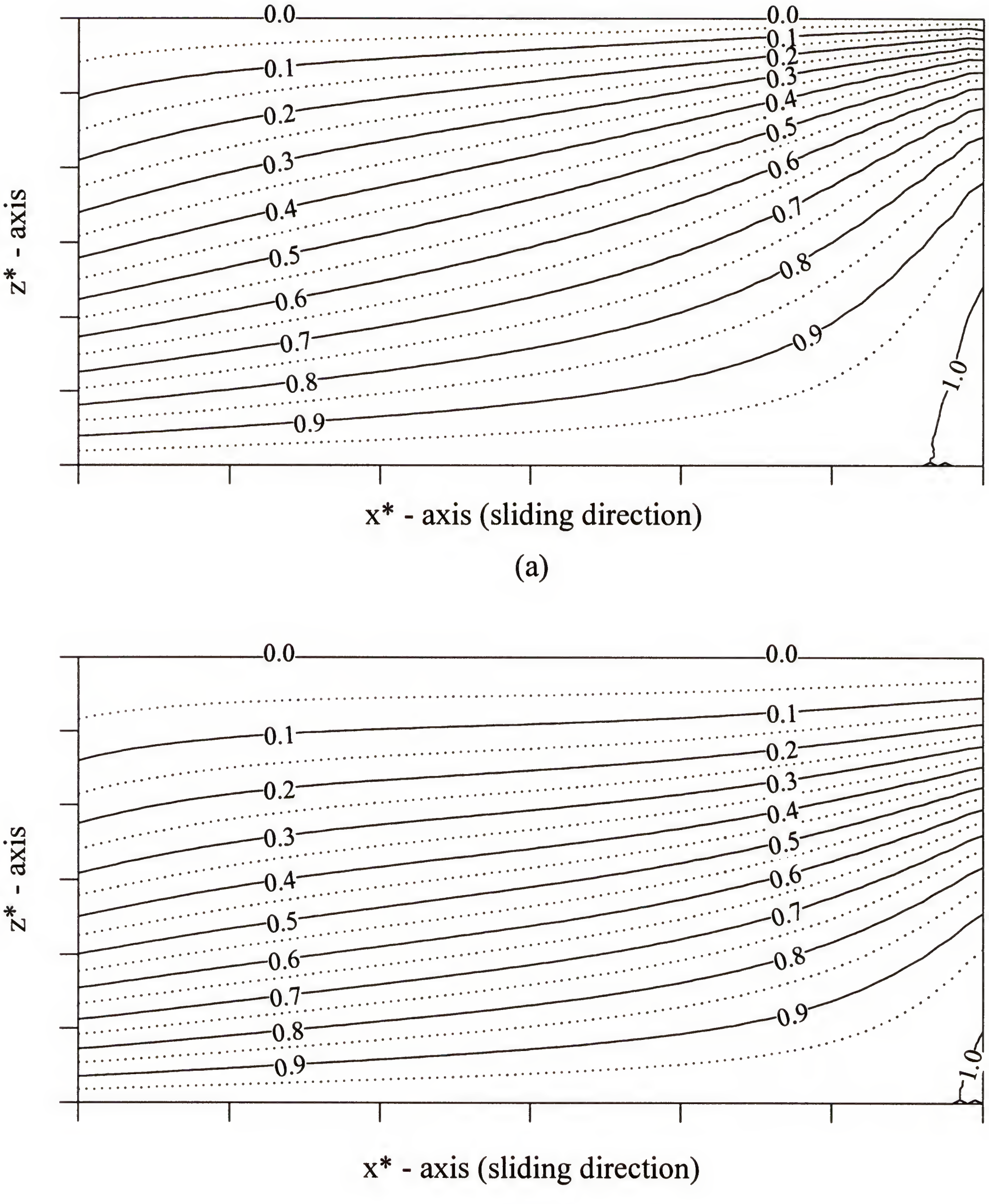

(a)

(b)

Figure 6.15 Mid-plane dimensionless film velocity distribution $U=100$ ft/sec, $T_{in}=100\ ^{o}F$, $B=L=3.0$ in slider bearing, SAE 30

(a) adiabatic boundaries

(b) boundaries with isothermal T_{in} for stationary pad

CHAPTER 7
THE RHEOLOGICAL MODEL

7.1 Introduction

The shear characterization of the thin high-pressure lubricant film has been the subject of investigation in recent years [26, 27, 63, 64]. The shear rheological behavior of the liquid under severe operating conditions displays several unique and interesting features that shear theory predicts and the liquid may undergo a glass transition. Starting with the work of Milne many works have been performed to evaluate the effect that non-Newtonian lubricants may have on the performance of bearings [65-71]. Some works listed on Table 8 show the diversity of lubricant models employed and the different effects produced by the various analytical approaches [72]. Such analytical approaches and experimental data can reduce the uncertainties prevailing in this area. Some studies in EHD condition have shown that the lubricant behavior cannot be described by a classical Newtonian model [64, 66, 67, 69-71, 73]. Also, some experiments support the unique rheological behavior which is observed in high pressure EHD lubrication conditions [64, 74]. Some models for describing the rheological behavior and thermal effects in lubricated EHD contacts have been proposed to fit the experimental finding [64, 70, 71]. Also, shear bands have been also observed in a high temperature flow visualization tests [64, 74].

In general, the development of rheological models considering the isothermal shear deformation in a homogeneous liquid is not likely to result in significant advances in the field. In lubricating systems with EHD contacts, relatively simple methods have been proposed based on experimental results [73]. Wang and Seireg have proposed a method to simulate the shear behavior of the film [27]. They simulated the rheological effects by classifying three different shear zones in Newtonian fluid films [26]. Their results showed the significant thermal effects in the central thin shear zone and indirectly verified the existence of the thin shear zone through correlations with experimental results. However, their model cannot describe all experiments and control some effects of the rheological trend because of using uniform shear zone ratio along the lubrication flow.

In this chapter the special model that is used in the thermohydrodynamic analysis of lubrication problem is introduced. It incorporates a modified velocity equation characterized by the inclusion of the non-Newtonian rheological model. It will also be based on the Bingham plastic model which is one of the rheological models describing the shear rheological response of the lubricant in the lubricating region. Theoretical studies of lubrication with Bingham model have explained the existence of liquid fluid (a possible rigid part) to be attached to one or the other surface by authors [75, 76]. A model of the behavior of Bingham fluids is presented by Tichy to exhibit a yield stress [77, 78]. He used a continuous mathematical function as the constitutive law and a generalized Reynolds equation to solve general lubrication problems and also indicated the influence of the stress parameter. This study will deal with viscous phenomena such as the case of a stationary layer and a uniform moving layer by introducing the concept of the yield stress. Furthermore, the goals of this study are (i) to present a continuous formulation which is applicable through the flow field to characterize the behavior (ii) to calculate the behavior in such lubrication conditions, and (iii) to compare these results with the predictions of the empirical theory (Square root relationship between pressure and velocity in a thin film) where applicable.

Table 8: Some Works on Non-Newtonian Lubricants [72]

Year	Author	Lubricant Model	Bearing to Application
1957	Milne	Viscoelastic	Slider
1967	Hsu	Pseudoplastic	Journal
1973	Tipei & Rohde	Directional Viscosity	Slider
1978	Harnoy	Viscoelastic	Journal
1983	Bourgin & Gray	Polymer Thickened	Journal
1984	Buckholz	Rheological	Journal
1991*	Tichy	Bingham Plastic	Journal
1992*	Tichy	Bingham Plastic	Slider

Note: * refer references [77, 78].

7.2 Non-Newtonian Behavior

A generalized form of Newton's law can be expressed as:

$$\tau = \eta\dot{\gamma} \tag{7.1}$$

where the viscosity η is any function of the scalar invariants of the shear rate $\dot{\gamma}$. If the non-Newtonian viscosity, η, is dependent on the components of the tensor $\dot{\gamma}$ then it also depends on combinations of the components of the scalar tensor.

The three independent combinations are

$$I_1 = \sum_i \dot{\gamma}_{ii},\ I_2 = \sum_i\sum_j \dot{\gamma}_{ij}\dot{\gamma}_{ji},\ \text{and}\ I_3 = \sum_i\sum_j\sum_k \dot{\gamma}_{ij}\dot{\gamma}_{jk}\dot{\gamma}_{ki} \tag{7.2}$$

The first invariant of the strain rate vanishes for an incompressible fluid, $I_1 = 2\left(\nabla \cdot \vec{V}\right) = 0$. For shearing flows, the third invariant of strain rate becomes zero. Hence, the viscosity, η, will be considered to depend only on I_2 [79-81]. For the lubrication geometry illustrated in Figure (2.1), $w << v$ and $\partial/\partial y << \partial/\partial z$, the shear rate magnitude, $\dot{\gamma}$, can be expressed as follows:

$$\dot{\gamma} = \sqrt{\frac{1}{2}\sum_i\sum_j \dot{\gamma}_{ij}\dot{\gamma}_{ji}} = \sqrt{\frac{1}{2}I_2} \tag{7.3}$$

$$\dot{\gamma} = \sqrt{\left(\frac{\partial u}{\partial z}\right)^2 + \left(\frac{\partial v}{\partial z}\right)^2} \tag{7.4}$$

where $\dot{\gamma}_{xz} = \frac{\partial u}{\partial z}$ and $\dot{\gamma}_{yz} = \frac{\partial v}{\partial z}$.

The components of the shear stress along the direction of film flow and film width flow are;

$$\tau_{xz} = \tau\frac{\dot{\gamma}_{xz}}{\dot{\gamma}} = \mu\frac{\partial u}{\partial z} + \frac{\left(\frac{\partial u}{\partial z}\right)}{\dot{\gamma}}\tau_0 \text{ and } \tau_{yz} = \tau\frac{\dot{\gamma}_{yz}}{\dot{\gamma}} = \mu\frac{\partial v}{\partial z} + \frac{\left(\frac{\partial v}{\partial z}\right)}{\dot{\gamma}}\tau_0 \tag{7.5}$$

Form Equation (7.5) the non-Newtonian viscosity for Bingham plastic model can be defined as;

$$\eta(\dot{\gamma}) = \mu + \frac{\tau_0}{\dot{\gamma}} \tag{7.6}$$

Therefore, the stress components can be expressed as follows;

$$\tau_{xz} = \eta(\dot{\gamma})\frac{\partial u}{\partial z} \text{ and } \tau_{yz} = \eta(\dot{\gamma})\frac{\partial v}{\partial z} \tag{7.7}$$

In most lubrication problems, $\frac{\partial u}{\partial z} >> \frac{\partial v}{\partial z}$. Hence Equation (7.7) becomes as follows

$$\tau_{xz} = \mu\frac{\partial u}{\partial z} + \tau_0 \text{ and } \tau_{yz} = \eta(\dot{\gamma})\frac{\partial v}{\partial z} \approx 0 \tag{7.8}$$

Figure (7.1) shows some examples of the shear rate and yield stress. In the first group the fluids are without yield stress, τ_0, curve (a) is for a Newtonian fluid for which the viscosity, η, is independent of the shear rate, $\dot{\gamma}$. Curve (b) describing the shear thinning fluid shows increasing shear stress less than in proportion to the shear rate, $\dot{\gamma}$. Curve (c) describing the shear thickening fluid shows increasing shear stress in proportion to the shear rate, $\dot{\gamma}$. In the second group of fluids with yield stress, τ_0, the fluid flows when the shear stress exceeds a yield stress. Otherwise, the fluid behaves as an elastic solid when the shear stress does not exceed the yield stress. Curve (d) describes Bingham plastic model. Curves (e) and (f) are for fluids behaving non-linearly with a yield stress. The Bingham plastic model of non-Newtonian fluid behavior has been used to describe the behavior of lubricants such as greases, the flow of melts and slurries. Theoretical studies of lubrication with the Bingham model will be based on the concept of rigid layers adhering to the surfaces at all locations along the fluid film.

7.3 Rheological Model Description

Some lubricants exhibit a critical shear behavior which can be modeled as a Bingham plastic under severe condition. The ideal Bingham plastic model is characterized by two parameters, a yield stress and a viscosity dependent on stress [78]. In this model, the fluid behaves as a rigid solid when the magnitude of the stress is less than the yield stress. Rigid layers can occur in the fluid film as three different types, stationary, uniform moving, and shear according the pressure gradient in the sliding direction.

In order to understand the non-Newtonian effect of lubricants by applying the concept of Bingham plastic model into the THD problem with constant film thickness it is necessary to develop an appropriate Reynolds type equation and modified elliptical type velocity equation which can handle the formation of layers in the fluid film. When stationary and uniform moving layers exist in the fluid film, Equation (2.19) representing the velocity is no longer valid. Therefore, a generalized Reynolds equation and an appropriate rheological model must be considered. Among the governing equations general descriptions for the velocity equation with rheological results are introduced. It is necessary to explain the reasons for employing the best elliptical shaped velocity profile of rheological behavior in the lubrication flow between two surfaces. Studies on non-Newtonian fluids have mainly depended on the models that is employed to decide on a proper choice the constitutive equation. This means totally different type governing equations for the problem under these conditions, specially velocity profile. As the differential and rate type have none of these conditions for the non-Newtonian phenomenon of lubrication problem, none of these models can adequately describe the experimental results that have been established.

The starting point in the flow characteristics of the non-Newtonian fluid under consideration from the flow of a Newtonian fluid is the existence of narrow layer around central lubrication region where the velocity gradients are exceedingly high. The existence of this thin layer is known to take place in certain non-Newtonian fluids [64]. This phenomenon can not be explained in terms of the classical method of the differential type from the Newtonian case. To avoid this difficulty the present model characterizes two different and antisymmetric profile shapes which velocity gradients are sharply changed in the central zone and the high pressure region to describe the rheological properties of non-Newtonian fluids. Conclusively, the main assumptions on which the velocity equation is based to explain the rheological properties at the high shear rates and shear stress at the interface between the two layers and the shear zone can be listed as follows:

1. Shear stress is proportional to the velocity gradient across the film.
2. The fluid can exhibit non-Newtonian behavior under certain extreme lubrication condition (thin films, high pressure etc).
3. The fluid will not slip at the interfaces between the two layers and the shear zone.
4. The pressure across the film is assumed to be constant.
5. The film thickness is very small and thus the flow is assumed to be laminar.

6. At the center location across fluid film the velocity gradient is assumed to change.
7. τ_A and τ_C in Figure (7.2) have low shear stress values along the fluid film in the full shear zone. And, τ_D and τ_E have the minimum shear stress values for the yield stress along the film flow.
8. Two oils of the same viscosity at a given test temperature and pressure are considered for the upper region and lower region in the shear zone.
9. It is assumed that velocity in the central region is a half of the uniform moving velocity.
10. The lubricant is assumed to be a Newtonian fluid.
11. For the lower region in the shear zone, the Newtonian velocity equation of the differential type is employed with the proper boundary condition including assumption (9). While, for the upper region in shear zone, velocity profile has the anti-symmetric shape of the lower region.

When the layers form within the lubricant film zone they are assumed to move at velocities, $u_{upper} = 0$, $u_{central} = f(\tau, \dot{\gamma})$, and $u_{lower} = U$ along the direction of motion. The velocity profiles and their corresponding shear stress in the xy plane can be illustrated as shown in Figure (7.2). Point A and C indicate a shear stress τ_A and $\tau_C < \tau_0$. The point on the centerline indicates a shear stress which is larger than a yield stress. Referring to Figures (7.2), and (7.3) the boundary conditions for the velocities can be written as:

$$u\big|_{z=0} = U \quad v\big|_{z=0} = 0,\ u\big|_{z=h} = 0,\ v\big|_{z=0} = 0$$

$$u\big|_{z=h_L} = U,\ u\big|_{z=h_u} = 0,\ u\big|_{z=h_c=h/2} = \frac{U}{2},\ v\big|_{z=h_L} = 0 \tag{7.9}$$

In the lower region of the central shear zone, $h_L \le z \le h_c$, the velocity distributions and their gradients are;

$$u=\frac{1}{2}U+\frac{1}{2}\frac{U}{F_0^a}F_0^c-\frac{1}{2}\frac{U}{F_0^a}\int_0^z\frac{1}{\eta}dz+\frac{dp}{dx}\left[\int_0^z\frac{z}{\eta}dz-\right.$$

$$\left.\left(\frac{F_1^a}{F_0^a}\right)\int_0^z\frac{1}{\eta}dz+\left(\frac{F_1^a}{F_0^a}\right)F_0^c-F_1^c\right] \qquad (7.10)$$

$$v=\frac{dp}{dy}\left[\int_0^z\frac{z}{\eta}dz-\left(\frac{F_1^a}{F_0^a}\right)\int_0^z\frac{1}{\eta}dz+\left(\frac{F_1^a}{F_0^a}\right)F_0^c-F_1^c\right] \qquad (7.11)$$

$$\frac{\partial u}{\partial z}=-\frac{1}{2}\frac{U}{\eta F_0^a}+\frac{1}{\eta}\frac{dp}{dx}\left[z-\frac{F_1^a}{F_0^a}\right] \qquad (7.12)$$

$$\frac{\partial v}{\partial z}=\frac{1}{\eta}\frac{dp}{dy}\left[z-\frac{F_1^a}{F_0^a}\right] \qquad (7.13)$$

where $F_0^a=\int_{h_L}^{h_c}\frac{1}{\eta}dz$, $F_1^a=\int_{h_L}^{h_c}\frac{z}{\eta}dz$, $F_0^c=\int_0^{h_c}\frac{1}{\eta}dz$, and $F_1^c=\int_0^{h_c}\frac{z}{\eta}dz$

The cross-film velocity w can be obtained by using the continuity Equation (2.14) and two differential forms with respect to x, and y, respectively, for the lower shear region.

$$w=-\left(\frac{\partial^2 p}{\partial x^2}+\frac{\partial^2 p}{\partial y^2}\right)\int_0^z\left[B^a+\left(\frac{F_1^a}{F_0^a}\right)F_0^c-F_1^c\right]dz+$$

$$\frac{1}{2}U\int_0^z\frac{\partial A^a}{\partial x}dz-\frac{\partial p}{\partial x}\int_0^z\frac{\partial B^a}{\partial x}dz-\frac{\partial p}{\partial y}\int_0^z\frac{\partial B^a}{\partial y}dz \qquad (7.14)$$

where $A^a=\frac{1}{F_0^a}\int_0^z\frac{1}{\eta}dz$, $B^a=\int_0^z\frac{z}{\eta}dz-\left(\frac{F_1^a}{F_0^a}\right)\int_0^z\frac{1}{\eta}dz$.

In the upper region of central shear zone, $h_c\le z\le h_u$, the velocity distributions and their gradients are;

$$u=\frac{1}{2}U+\frac{1}{2}\frac{U}{F_0^b}F_0^c-\frac{1}{2}\frac{U}{F_0^b}\int_0^z\frac{1}{\eta}dz-\frac{dp}{dx}\left[\int_0^z\frac{z}{\eta}dz-\right.$$

$$\left.\left(\frac{F_1^b}{F_0^b}\right)\int_0^z\frac{1}{\eta}dz+\left(\frac{F_1^b}{F_0^b}\right)F_0^c-F_1^c\right] \qquad (7.15)$$

$$v = -\frac{dp}{dy}\left[\int_0^z \frac{z}{\eta}dz - \left(\frac{F_1^b}{F_0^b}\right)\int_0^z \frac{1}{\eta}dz + \left(\frac{F_1^b}{F_0^b}\right)F_0^c - F_1^c\right] \tag{7.16}$$

$$\frac{\partial u}{\partial z} = -\frac{1}{2}\frac{U}{\eta F_0^b} - \frac{1}{\eta}\frac{dp}{dx}\left[z - \frac{F_1^b}{F_0^b}\right] \tag{7.17}$$

$$\frac{\partial v}{\partial z} = -\frac{1}{\eta}\frac{dp}{dy}\left[z - \frac{F_1^b}{F_0^b}\right] \tag{7.18}$$

where $F_0^b = \int_{h_c}^{h_u} \frac{1}{\eta}dz$, and $F_1^b = \int_{h_c}^{h_u} \frac{z}{\eta}dz$

$$w = -\left(\frac{\partial^2 p}{\partial x^2} + \frac{\partial^2 p}{\partial y^2}\right)\int_0^z \left[B^b + \left(\frac{F_1^b}{F_0^b}\right)F_0^c - F_1^c\right]dz +$$

$$\frac{1}{2}U\int_0^z \frac{\partial A^b}{\partial x}dz - \frac{\partial p}{\partial x}\int_0^z \frac{\partial B^b}{\partial x}dz - \frac{\partial p}{\partial y}\int_0^z \frac{\partial B^b}{\partial y}dz \tag{7.19}$$

where $A^b = \frac{1}{F_0^b}\int_0^z \frac{1}{\eta}dz$, $B^b = \int_0^z \frac{z}{\eta}dz - \left(\frac{F_1^b}{F_0^b}\right)\int_0^z \frac{1}{\eta}dz$.

The velocity distributions and their gradients in the rigid layer of $0 \le z \le h_L$ are,

$$u = U\,,\ v = \frac{\partial u}{\partial z} = \frac{\partial v}{\partial z} = 0\,, \tag{7.20}$$

and in the rigid layer region of $h_u \le z \le h$ are,

$$u = 0,\ v = \frac{\partial u}{\partial z} = \frac{\partial v}{\partial z} = 0\,, \tag{7.21}$$

A Reynolds equation for this type of fluid having layers (stationary layer and uniform moving layer) can be derived by using Equation (7.10) throughout Equation (7.21) into the continuity equation and integrating the resulting equation across the fluid film. The result is given in the similar form of Equation (5.5) obtained in Chapter 5. A generalized Reynolds equation that employs this model is given below.

$$\frac{\partial}{\partial x}\left[\left(F_2^a + F_2^b\right)\frac{\partial p}{\partial x}\right] + \frac{\partial}{\partial y}\left[\left(F_2^a + F_2^b\right)\frac{\partial p}{\partial y}\right] = \left(U_1 - U_2\right)\frac{\partial}{\partial x}\left[\left(\frac{F_3^a}{F_0^a} + \frac{F_3^b}{F_0^b}\right)\right] + \int_0^h \frac{\partial \rho}{\partial t}dz \tag{7.22}$$

where

$$F_2^a = \int_0^{h_c} \frac{\rho z}{\mu}\left(z - \frac{F_1^a}{F_0^a}\right)dz \ ; \ F_2^b = \int_{h_c}^{h} \frac{\rho z}{\mu}\left(z - \frac{F_1^b}{F_0^b}\right)dz\ , \ F_3^a = \int_0^{h_c} \frac{\rho z}{\mu}dz\ , \text{ and } F_3^b = \int_{h_c}^{h} \frac{\rho z}{\mu}dz$$

A similar set of equations as those of the previous Newtonian case are developed for the pressure behavior of the lubricant under severe operating condition with a Newtonian motor oil. In the case of no solid layer attached to upper stationary surface encountered in the Bingham model, the parameters F_2^b and $\frac{F_3^b}{F_0^b}$ disappear.

To account for the property variation with temperature, the energy equation must be considered. A form of energy equation for the non-Newtonian fluid can be written as follows,

$$\rho c_p \frac{DT}{Dt} = \nabla \cdot (k \nabla T) + \tau \nabla v \tag{7.23}$$

With proper formulation of the boundary conditions, a three-dimensional energy equation taking into account the temperature variation in the sliding direction, side direction, and across the lubricant film yields remarkably accurate results for THD problems.

In the adiabatic band having very high temperature due to high shear rate at the central zone, $0 \le z_s \le h_s$, the simplified energy equation and boundary conditions associated with the energy equation are;

$$\begin{aligned}\rho c_p \frac{\partial T_s}{\partial t} = -\rho c_p \left[u \frac{\partial T_s}{\partial x_s} + v \frac{\partial T_s}{\partial y_s} + w \frac{\partial T_s}{\partial z_s} \right] + \beta T_s \left[u \frac{\partial p}{\partial x_s} + v \frac{\partial p}{\partial y_s} \right] \\ + k \left[\frac{\partial^2 T_s}{\partial x_s^2} + \frac{\partial^2 T_s}{\partial y_s^2} + \frac{\partial^2 T_s}{\partial z_s^2} \right] + \eta \left[\left(\frac{\partial u}{\partial z_s} \right)^2 + \left(\frac{\partial v}{\partial z_s} \right)^2 \right]\end{aligned} \tag{7.24}$$

The boundary conditions associated with the energy equation for the shear zone are expected as;

$$T_s(0, y_s, z_s) = T_0$$

$$\left.\frac{\partial T_s}{\partial z_s}\right|_{z_s=0} = \left.\frac{\partial T_1}{\partial z_1}\right|_{z_1=h_1}, \quad \left.\frac{\partial T_s}{\partial z_s}\right|_{z_s=h_s} = \left.\frac{\partial T_2}{\partial z_2}\right|_{z_2=0}$$

$$\left.\frac{\partial T_s}{\partial x_s}\right|_{x_s=B} = \left.\frac{\partial T_s}{\partial y_s}\right|_{y_s=0} = \left.\frac{\partial T_s}{\partial y_s}\right|_{y_s=L} = 0 \tag{7.25}$$

In the uniform velocity moving layer, $0 \le z_1 \le h_1$, the energy equation becomes;

$$\rho c_p \frac{\partial T_1}{\partial t} = -\rho c_p U \frac{\partial T_1}{\partial x_1} + k\left[\frac{\partial^2 T_1}{\partial x_1^2} + \frac{\partial^2 T_1}{\partial y_1^2} + \frac{\partial^2 T_1}{\partial z_1^2}\right] + \beta T_1\left[U \frac{\partial p}{\partial x_1}\right], \tag{7.26}$$

and the boundary conditions for the above region are,

$$T_1(0, y_1, z_1) = T_1(x_1, y_1, 0) = T_0$$

$$\left.\frac{\partial T_1}{\partial z_1}\right|_{z_1=h_1} = \left.\frac{\partial T_s}{\partial z_s}\right|_{z_s=0}, \quad \left.\frac{\partial T_1}{\partial x_1}\right|_{x_1=B} = \left.\frac{\partial T_1}{\partial y_1}\right|_{y_1=0} = \left.\frac{\partial T_1}{\partial y_1}\right|_{y_1=L} = 0 \tag{7.27}$$

In the stationary layer zone, $0 \le z_2 \le h_2$, the energy equation and associated boundary conditions are,

$$\rho c_p \frac{\partial T_2}{\partial t} = k\left[\frac{\partial^2 T_2}{\partial x_2^2} + \frac{\partial^2 T_2}{\partial y_2^2} + \frac{\partial^2 T_2}{\partial z_2^2}\right] \tag{7.28}$$

$$T_2(0, y_2, z_2) = T_0$$

$$\left.\frac{\partial T_2}{\partial z_2}\right|_{z_2=0} = \left.\frac{\partial T_s}{\partial z_s}\right|_{z_s=h_u-h_L}, \quad \left.\frac{\partial T_2}{\partial x_2}\right|_{x_2=h} = \left.\frac{\partial T_2}{\partial x_2}\right|_{x_2=B} = \left.\frac{\partial T_2}{\partial y_2}\right|_{y_2=0} = \left.\frac{\partial T_2}{\partial y_2}\right|_{y_2=L} = 0 \tag{7.29}$$

7.4 Non-dimensionalization of the Governing Equations for Rheological Behavior

For the model, the governing equations and boundary conditions are non-dimensionalized using the following parameters in addition to the parameters used in the Newtonian case as follows;

$$\bar{\dot{\gamma}} = \frac{\dot{\gamma} h}{U}, \quad \bar{\tau}_0 = \frac{\tau_0 h_0}{\mu_0 U}, \quad \bar{\eta} = \frac{\eta}{\mu_0} \tag{7.30}$$

The non-dimensional viscosity for the present model as in the Bingham plastic model can be written as;

$$\bar{\eta}\left(\bar{\dot{\gamma}}\right) = \bar{\mu} + \frac{\bar{\tau}_0}{\bar{\dot{\gamma}}} \tag{7.31}$$

where $\bar{\dot{\gamma}} = \sqrt{\left(\frac{\partial \bar{u}}{\partial \bar{z}}\right)^2 + \left(\frac{\partial \bar{v}}{\partial \bar{z}}\right)^2}$.

The dimensionless form of Equation (7.7) which is valid at the central shear zone, $\left(0 \le \bar{z}_s \le \bar{h}_s\right)$, is;

$$\bar{\tau}_{\bar{x}_s \bar{z}_s} = \frac{1}{\bar{h}_s} \bar{\eta}\left(\bar{\dot{\gamma}}\right) \frac{\partial \bar{u}}{\partial \bar{z}_s} \quad \text{and} \quad \bar{\tau}_{\bar{y}_s \bar{z}_s} = \frac{1}{\bar{h}_s} \bar{\eta}\left(\bar{\dot{\gamma}}\right) \frac{\partial \bar{v}}{\partial \bar{z}_s} \tag{7.32}$$

otherwise,

$$\bar{\tau}_{\bar{x},\bar{z}} = \frac{1}{\bar{h}_s} \bar{\mu} \frac{\partial \bar{u}}{\partial \bar{z}_s} + \bar{\tau}_0 \tag{7.33}$$

Otherwise, at the other zones,

$$\bar{\tau}_{\bar{x}_1 \bar{z}_1} = \bar{\tau}_{\bar{y}_1 \bar{z}_1} = \bar{\tau}_{\bar{x}_2 \bar{z}_2} = \bar{\tau}_{\bar{y}_2 \bar{z}_2} = 0 \tag{7.34}$$

In the lower region $\left(0 \le \bar{z}_s \le {}^{h_s}\!/_{2}\right)$ of the flow in the shear zone, the non-dimensional velocity distribution and gradients are;

$$\bar{u} = \frac{1}{2} + \frac{1}{2} \frac{\bar{F}_0^c}{\bar{F}_0^a} - \frac{1}{2} \frac{1}{\bar{F}_0^a} \int_0^{\bar{z}_s} \frac{1}{\bar{\eta}} d\bar{z}_s + \bar{h}_s^{\,2} \frac{d\bar{p}}{d\bar{x}_s} \left[\int_0^{\bar{z}_s} \frac{\bar{z}_s}{\bar{\eta}} d\bar{z}_s - \left(\frac{\bar{F}_1^a}{\bar{F}_0^a} \right) \int_0^{\bar{z}_s} \frac{1}{\bar{\eta}} d\bar{z}_s + \left(\frac{\bar{F}_1^a}{\bar{F}_0^a} \right) \bar{F}_0^c - \bar{F}_1^c \right] \tag{7.35}$$

$$\bar{v} = \bar{h}_s^{\,2} \frac{d\bar{p}}{d\bar{y}_s} \left[\int_0^{\bar{z}_s} \frac{\bar{z}_s}{\bar{\eta}} d\bar{z}_s - \left(\frac{\bar{F}_1^a}{\bar{F}_0^a} \right) \int_0^{\bar{z}_s} \frac{1}{\bar{\eta}} d\bar{z}_s + \left(\frac{\bar{F}_1^a}{\bar{F}_0^a} \right) \bar{F}_0^c - \bar{F}_1^c \right] \tag{7.36}$$

$$\frac{\partial \bar{u}}{\partial \bar{z}_s} = -\frac{1}{2} \frac{1}{\bar{\eta}\, \bar{F}_0^a} + \frac{\bar{h}_s^{\,2}}{\bar{\eta}} \frac{d\bar{p}}{d\bar{x}_s} \left[\bar{z}_s - \frac{\bar{F}_1^a}{\bar{F}_0^a} \right] \tag{7.37}$$

$$\frac{\partial \bar{v}}{\partial \bar{z}_s} = \frac{\bar{h}_s^{\,2}}{\bar{\eta}} \frac{d\bar{p}}{d\bar{y}_s} \left[\bar{z}_s - \frac{\bar{F}_1^a}{\bar{F}_0^a} \right] \tag{7.38}$$

where $\bar{F}_0^a = \int_0^{\bar{h}_s/2} \frac{1}{\bar{\eta}} d\bar{z}_s$, and $\bar{F}_1^a = \int_0^{\bar{h}_s/2} \frac{\bar{z}_s}{\bar{\eta}} d\bar{z}_s$, $\left(\bar{F}_0^c = \int_0^{\bar{h}_s/2} \frac{1}{\bar{\eta}} d\bar{z}_s \text{, and } \bar{F}_1^c = \int_0^{\bar{h}_s/2} \frac{\bar{z}_s}{\bar{\eta}} d\bar{z}_s \right)$ for the computational domain of the shear zone.

$$\bar{w} = \left(\frac{h_0}{B} \right) \left\langle -\bar{h}_s^3 \left(\frac{\partial^2 \bar{p}}{\partial \bar{x}_s^{\,2}} + \frac{\partial^2 \bar{p}}{\partial \bar{y}_s^{\,2}} \right) \int_0^{\bar{z}_s} \left[\bar{B}^a + \left(\frac{\bar{F}_1^a}{\bar{F}_0^a} \right) \bar{F}_0^c - \bar{F}_1^c \right] d\bar{z}_s - \right.$$

$$\left(\frac{\partial \bar{h}_s}{\partial \bar{x}_s} \right) \left(\bar{z}_s \bar{B}^a - \int_0^{\bar{z}_s} \bar{B}^a \, d\bar{z}_s \right) + \bar{h}_s \int_0^{\bar{z}_s} \frac{\partial \bar{B}^a}{\partial \bar{x}_s} d\bar{z}_s - \left[\frac{\partial \bar{p}}{\partial \bar{x}_s} \left\{ \bar{h}_s^{\,3} \int_0^{\bar{z}_s} \frac{\partial \bar{A}^a}{\partial \bar{x}_s} d\bar{z}_s - \right. \right.$$

$$\left. \left. \left. \bar{h}_s^{\,2} \left(\frac{\partial \bar{h}_s}{\partial \bar{x}_s} \right) \left(\bar{z}_s \bar{A}^a - 3 \int_0^{\bar{z}_s} \bar{A}^a \, d\bar{z}_s \right) \right\} \right] - \bar{h}_s^{\,3} \left(\frac{\partial \bar{p}}{\partial \bar{y}_s} \right) \int_0^{\bar{z}_s} \frac{\partial \bar{A}^a}{\partial \bar{y}_s} d\bar{z}_s \right\rangle \tag{7.39}$$

where $\bar{A}^a = \frac{1}{\bar{F}_0^a} \int_0^{\bar{z}_s} \frac{1}{\bar{\eta}} d\bar{z}_s$, $\bar{B}^a = \int_0^{\bar{z}_s} \frac{\bar{z}_s}{\bar{\eta}} d\bar{z}_s - \left(\frac{\bar{F}_1^a}{\bar{F}_0^a} \right) \int_0^{\bar{z}_s} \frac{1}{\bar{\eta}} d\bar{z}_s$.

In the upper region $\left(\bar{h}_s/_2 \le \bar{z}_s \le \bar{h}_s \right)$ of the flow in the shear zone, the non-dimensional velocity distribution and gradients are

$$\bar{u} = \frac{1}{2} + \frac{1}{2} \frac{\bar{F}_0^c}{\bar{F}_0^b} - \frac{1}{2} \frac{1}{\bar{F}_0^b} \int_0^{\bar{z}_s} \frac{1}{\bar{\eta}} d\bar{z}_s - \bar{h}_s^{\,2} \frac{d\bar{p}}{d\bar{x}_s} \left[\int_0^{\bar{z}_s} \frac{\bar{z}_s}{\bar{\eta}} d\bar{z}_s - \right.$$

$$\left. \left(\frac{\bar{F}_1^b}{\bar{F}_0^b} \right) \int_0^{\bar{z}_s} \frac{1}{\bar{\eta}} d\bar{z}_s + \left(\frac{\bar{F}_1^b}{\bar{F}_0^b} \right) \bar{F}_0^c - \bar{F}_1^c \right] \tag{7.40}$$

$$\bar{v} = -\bar{h}_s^{\,2} \frac{d\bar{p}}{d\bar{y}_s} \left[\int_0^{\bar{z}_s} \frac{\bar{z}_s}{\bar{\eta}} d\bar{z}_s - \left(\frac{\bar{F}_1^b}{\bar{F}_0^b} \right) \int_0^{\bar{z}_s} \frac{1}{\bar{\eta}} d\bar{z}_s + \left(\frac{\bar{F}_1^b}{\bar{F}_0^b} \right) \bar{F}_0^c - \bar{F}_1^c \right] \tag{7.41}$$

$$\frac{\partial \bar{u}}{\partial \bar{z}_s} = -\frac{1}{2} \frac{1}{\bar{\eta} \bar{F}_0^b} - \frac{\bar{h}_s^{\,2}}{\bar{\eta}} \frac{d\bar{p}}{d\bar{x}_s} \left[\bar{z}_s - \frac{\bar{F}_1^b}{\bar{F}_0^b} \right] \tag{7.42}$$

$$\frac{\partial \bar{v}}{\partial \bar{z}_s} = -\frac{\bar{h}_s^{\,2}}{\bar{\eta}} \frac{d\bar{p}}{d\bar{y}_s} \left[\bar{z}_s - \frac{\bar{F}_1^b}{\bar{F}_0^b} \right] \tag{7.43}$$

where $\overline{F}_0^b = \int_{\bar{h}_s/2}^{\bar{h}_s} \frac{1}{\bar{\eta}} d\bar{z}_s$, and $\overline{F}_1^b = \int_{\bar{h}_s/2}^{\bar{h}_s} \frac{\bar{z}_s}{\bar{\eta}} d\bar{z}_s$

$$\overline{w} = \left(\frac{h_0}{B}\right)\left\langle + \bar{h}_s^3 \left(\frac{\partial^2 \bar{p}}{\partial \bar{x}_s{}^2} + \frac{\partial^2 \bar{p}}{\partial \bar{y}_s{}^2}\right) \int_0^{\bar{z}_s} \left[\overline{B}^b + \left(\frac{\overline{F}_1^b}{\overline{F}_0^b}\right) \overline{F}_0^c - \overline{F}_1^c\right] d\bar{z}_s - \right.$$

$$\left(\frac{\partial \bar{h}_s}{\partial \bar{x}_s}\right)\left(\bar{z}_s \overline{B}^b - \int_0^{\bar{z}_s} \overline{B}^b d\bar{z}_s\right) + \bar{h}_s \int_0^{\bar{z}_s} \frac{\partial \overline{B}^b}{\partial \bar{x}_s} d\bar{z}_s + \left[\frac{\partial \bar{p}}{\partial \bar{x}_s}\left\{\bar{h}_s{}^3 \int_0^{\bar{z}_s} \frac{\partial \overline{A}^b}{\partial \bar{x}_s} d\bar{z}_s - \right.\right.$$

$$\left.\left.\left.\bar{h}_s{}^2 \left(\frac{\partial \bar{h}_s}{\partial \bar{x}_s}\right)\left(\bar{z}_s \overline{A}^b - 3\int_0^{\bar{z}_s} \overline{A}^b d\bar{z}_s\right)\right\}\right] + \bar{h}_s{}^3 \left(\frac{\partial \bar{p}}{\partial \bar{y}_s}\right) \int_0^{\bar{z}_s} \frac{\partial \overline{A}^b}{\partial \bar{y}_s} d\bar{z}_s \right\rangle \tag{7.44}$$

where $\overline{A}^b = \frac{1}{\overline{F}_0^b} \int_0^{\bar{z}_s} \frac{1}{\bar{\eta}} d\bar{z}_s$, $\overline{B}^a = \int_0^{\bar{z}_s} \frac{\bar{z}_s}{\bar{\eta}} d\bar{z}_s - \left(\frac{\overline{F}_1^b}{\overline{F}_0^b}\right) \int_0^{\bar{z}_s} \frac{1}{\bar{\eta}} d\bar{z}_s$.

The non-dimensional velocity distributions and their gradients in the rigid layer region of $0 \le \bar{z}_1 \le \bar{h}_1$ are,

$$\bar{u} = 1,\ \bar{v} = \frac{\partial \bar{u}}{\partial \bar{z}_1} = \frac{\partial \bar{v}}{\partial \bar{z}_1} = 0, \tag{7.45}$$

and in the rigid layer region of $0 \le \bar{z}_2 \le \bar{h}_2$ are,

$$\bar{u} = 0,\ \bar{v} = \frac{\partial \bar{u}}{\partial \bar{z}_2} = \frac{\partial \bar{v}}{\partial \bar{z}_2} = 0, \tag{7.46}$$

A non-dimensional Reynolds equation for this type of layered fluid film (stationary layer, uniform moving layer, and shear zone) can be similarly applied to Equation (6.1) of Chapter 6 for the two dimensional case in the x-y plane.

$$\frac{\partial}{\partial \bar{x}}\left[\bar{h}^3\left(\overline{F}_2^a + \overline{F}_2^b\right)\frac{\partial \bar{p}}{\partial \bar{x}}\right] + \frac{\partial}{\partial \bar{y}}\left[\bar{h}^3\left(\overline{F}_2^a + \overline{F}_2^b\right)\frac{\partial \bar{p}}{\partial \bar{y}}\right] = \frac{\partial}{\partial \bar{x}}\left[\left(\bar{h}\frac{\overline{F}_3^a}{\overline{F}_0^a} + \bar{h}\frac{\overline{F}_3^b}{\overline{F}_0^b}\right)\right] +$$

$$\frac{\rho h_0 \bar{h}}{\Delta \bar{t}}\left(\int_0^1 \left\{\left(-\alpha T_0 \partial \overline{T}\right) + \frac{\mu_0 U B}{\beta h_0^2} \partial \bar{p}\right\} d\bar{z}\right) \tag{7.47}$$

where

$$\overline{F}_2^a = \int_0^{\overline{h}_c} \frac{\rho \bar{z}}{\overline{\mu}} \left(\bar{z} - \frac{\overline{F}_1^a}{\overline{F}_0^a} \right) d\bar{z}\,;\ \overline{F}_2^b = \int_{\overline{h}_c}^1 \frac{\rho \bar{z}}{\overline{\mu}} \left(\bar{z} - \frac{\overline{F}_1^b}{\overline{F}_0^b} \right) d\bar{z}\,,\ \overline{F}_3^a = \int_0^{\overline{h}_c} \frac{\rho \bar{z}}{\overline{\mu}} d\bar{z}\,, \text{ and } \overline{F}_3^b = \int_{\overline{h}_c}^1 \frac{\rho \bar{z}}{\overline{\mu}} d\bar{z}$$

In the adiabatic band having very high temperature due to the high shear rate at the central zone, $0 \le \bar{z}_s \le \overline{h}_s$, the simplified non-dimensional energy equation is;

$$\frac{\partial \overline{T}_s}{\partial \bar{t}} = -(u)\frac{\partial \overline{T}_s}{\partial \bar{x}_s} + (-v)\frac{\partial \overline{T}_s}{\partial \bar{y}_s} + \left[\frac{\bar{u}\,\bar{z}_s}{\overline{h}_s}\left(\frac{\partial \overline{h}_s}{\partial \bar{x}_s} \right) - \frac{B\overline{w}}{h_0 \overline{h}_s} \right] \frac{\partial \overline{T}_s}{\partial \bar{z}_s} +$$

$$\frac{k}{BU\rho c_p}\frac{\partial^2 \overline{T}_s}{\partial \bar{x}_s^{\#2}} + \frac{k}{BU\rho c_p}\frac{\partial^2 \overline{T}_s}{\partial \bar{y}_s^{2}} + \left(\frac{Bk}{\rho c_p U}\frac{1}{h_0^2 \overline{h}_s^2}\frac{\partial^2 \overline{T}_s}{\partial \bar{z}_s^2} \right) +$$

$$\frac{\mu_0 UB}{h_0^2 \rho c_p T_0}\frac{\overline{\eta}}{\overline{h}_s^2}\left[\left(\frac{\partial \bar{u}}{\partial \bar{z}_s} \right)^2 + \left(\frac{\partial \bar{v}}{\partial \bar{z}_s} \right)^2 \right] +$$

$$\frac{B\alpha \overline{T}_s U}{\rho c_p}\frac{\mu_0 \overline{\eta}}{h_0^2 \overline{h}_s^2}\left[\bar{u}\frac{\partial \bar{p}}{\partial \bar{x}_s} + \bar{v}\frac{\partial \bar{p}}{\partial \bar{y}_s} \right] \tag{7.48}$$

where

$$\frac{\partial^2 \overline{T}_s}{\partial \bar{x}_s^{\#2}} = \frac{\partial^2 \overline{T}_s}{\partial \bar{x}_s^{2}} - \frac{\partial}{\partial \bar{x}_s}\left[\frac{\bar{z}_s}{\overline{h}_s}\left(\frac{\partial \overline{h}_s}{\partial \bar{x}_s} \right)\frac{\partial \overline{T}_s}{\partial \bar{z}_s} \right] - \frac{\bar{z}_s}{\overline{h}_s}\left(\frac{\partial \overline{h}_s}{\partial \bar{x}_s} \right)\frac{\partial^2 \overline{T}_s}{\partial \bar{x}_s \partial \bar{z}_s} +$$

$$\frac{\bar{z}_s}{\overline{h}_s}\left(\frac{\partial \overline{h}_s}{\partial \bar{x}_s} \right)\frac{\partial}{\partial \bar{z}_s}\left[\frac{\bar{z}_s}{\overline{h}_s}\left(\frac{\partial \overline{h}_s}{\partial \bar{x}_s} \right)\frac{\partial \overline{T}_s}{\partial \bar{z}_s} \right]$$

The non-dimensional boundary conditions associated with the energy equation for the shear zone can be considered as;

$$\overline{T}_s(0, \bar{y}_s, \bar{z}_s) = 1$$

$$\left.\frac{\partial \overline{T}_s}{\partial \bar{z}_s}\right|_{\bar{z}_s=0} = \left.\frac{\partial \overline{T}_1}{\partial \bar{z}_1}\right|_{\bar{z}_1=1},\ \left.\frac{\partial \overline{T}_s}{\partial \bar{z}_s}\right|_{\bar{z}_s=1} = \left.\frac{\partial \overline{T}_2}{\partial \bar{z}_2}\right|_{\bar{z}_2=0}$$

$$\left.\frac{\partial \overline{T}_s}{\partial \bar{x}_s}\right|_{\bar{x}_s=1} = \left.\frac{\partial \overline{T}_s}{\partial \bar{y}_s}\right|_{\bar{y}_s=0} = \left.\frac{\partial \overline{T}_s}{\partial \bar{y}_s}\right|_{\bar{y}_s=L/B} = 0 \tag{7.49}$$

In the uniform moving velocity layer, $0 \le \bar{z}_1 \le \overline{h}_1$, the energy equation becomes;

$$\frac{\partial \bar{T}_1}{\partial \bar{t}} = (-U)\frac{\partial \bar{T}_1}{\partial \bar{x}_1} + \left[\frac{U\bar{z}_1}{\bar{h}_1}\left(\frac{\partial \bar{h}_1}{\partial \bar{x}_1}\right)\right]\frac{\partial \bar{T}_1}{\partial \bar{z}_1} + \frac{k}{BU\rho c_p}\frac{\partial^2 \bar{T}_1}{\partial \bar{x}_1^{\#2}} +$$

$$\frac{k}{BU\rho c_p}\frac{\partial^2 \bar{T}_1}{\partial \bar{y}_1^2} + \left(\frac{Bk}{\rho c_p U}\frac{1}{h_0^2 \bar{h}_1^2}\right)\frac{\partial^2 \bar{T}_1}{\partial \bar{z}_1^2} +$$

$$\frac{B\alpha \bar{T}_1 U}{\rho c_p}\frac{\mu_0 \bar{\eta}}{h_0^2 \bar{h}_1^2}\left[\frac{\partial \bar{p}}{\partial \bar{x}_1}\right] \qquad (7.50)$$

and the boundary conditions for the above region are,

$$\bar{T}_1(0,\bar{y}_1,\bar{z}_1) = \bar{T}_1(\bar{x}_1,\bar{y}_1,0) = 1$$

$$\left.\frac{\partial \bar{T}_1}{\partial \bar{z}_1}\right|_{\bar{z}_1=1} = \left.\frac{\partial \bar{T}_s}{\partial \bar{z}_s}\right|_{\bar{z}_s=0}, \quad \left.\frac{\partial \bar{T}_1}{\partial \bar{x}_1}\right|_{\bar{x}_1=1} = \left.\frac{\partial \bar{T}_1}{\partial \bar{y}_1}\right|_{\bar{y}_1=0} = \left.\frac{\partial \bar{T}_1}{\partial \bar{y}_1}\right|_{\bar{y}_1=L/B} = 0 \qquad (7.51)$$

In the stationary layer zone, $0 \le \bar{z}_2 \le \bar{h}_2$, the non-dimensional energy equation and associated boundary conditions are,

$$\frac{\partial \bar{T}_2}{\partial \bar{t}} = \frac{k}{BU\rho c_p}\frac{\partial^2 \bar{T}_2}{\partial \bar{x}_2^{\#2}} + \frac{k}{BU\rho c_p}\frac{\partial^2 \bar{T}_2}{\partial \bar{y}_2^2} + \left(\frac{Bk}{\rho c_p U}\frac{1}{h_0^2 \bar{h}_2^2}\right)\frac{\partial^2 \bar{T}_2}{\partial \bar{z}_2^2} \qquad (7.52)$$

and the boundary conditions for the stationary region are,

$$\bar{T}_2(0,\bar{y}_2,\bar{z}_2) = 1$$

$$\left.\frac{\partial \bar{T}_2}{\partial \bar{z}_2}\right|_{\bar{z}_2=0} = \left.\frac{\partial \bar{T}_s}{\partial \bar{z}_s}\right|_{\bar{z}_s=1}, \quad \left.\frac{\partial \bar{T}_2}{\partial \bar{z}_2}\right|_{\bar{z}_2=1} = \left.\frac{\partial \bar{T}_2}{\partial \bar{x}_2}\right|_{\bar{x}_2=1} = \left.\frac{\partial \bar{T}_2}{\partial \bar{y}_2}\right|_{\bar{y}_2=0} = \left.\frac{\partial \bar{T}_2}{\partial \bar{y}_2}\right|_{\bar{y}_2=L/B} = 0 \qquad (7.53)$$

7.5 Numerical Scheme

The dimensionless equations are discretized and solved by the finite difference method. A forward formula is used for $\frac{\partial T}{\partial t}$ while central difference approximation is used for all other derivatives. The Reynolds equation is an elliptic partial differential equation and is solved using the Successive Over Relaxation method and the energy equation is solved by a fully implicit scheme. The difference form of the Reynolds equation for the present model is already introduced in Chapter 6. The Successive Over Relaxation method of two steps can be used in the same manner because an improved estimate of the pressure values is computed by applying the formula of Equation (6.14) at every grid point without considering the effect of the non constant grid size in the across film direction.

In the shear zone, $0 \le \bar{z}_s \le \bar{h}_s$, the non-dimensional energy equation can be expressed as the following element equation;

$$\left\{ \begin{aligned} &\left(1-\frac{\Delta\bar{t}}{2}\Lambda_1\right)\bar{T}_s^{\,n+\frac{1}{2}} = \left(1+\frac{\Delta\bar{t}}{2}\Lambda_2+\frac{\Delta\bar{t}}{2}\Lambda_3+\frac{\Delta\bar{t}}{2}f_s\right)\bar{T}_s^{\,n}+\frac{\Delta\bar{t}}{2}g_s^{\,n} \\ &\left(1-\frac{\Delta\bar{t}}{2}\Lambda_3-\frac{\Delta\bar{t}}{2}f_s\right)\bar{T}_s^{\,n+1} = \left(1+\frac{\Delta\bar{t}}{2}\Lambda_1\right)\bar{T}_s^{\,n+\frac{1}{2}}+\frac{\Delta\bar{t}}{2}\Lambda_2\bar{T}_s^{\,n}+\frac{\Delta\bar{t}}{2}g_s^{\,n+1} \end{aligned} \right. \tag{7.54}$$

where

$$\Lambda_1=\xi_1\frac{\partial}{\partial\bar{x}}+\psi_1\frac{\partial^2}{\partial\bar{x}^2},\ \Lambda_2=\xi_2\frac{\partial}{\partial\bar{y}}+\psi_2\frac{\partial^2}{\partial\bar{y}^2},\ \text{and}\ \Lambda_3=\xi_3\frac{\partial}{\partial\bar{z}}+\psi_3\frac{\partial^2}{\partial\bar{z}^2}$$

In the uniform moving zone, $0 \le \bar{z}_1 \le \bar{h}_1$, the ADI scheme for the non-dimensional energy equation is as follows;

$$\left\{ \begin{aligned} &\left(1-\frac{\Delta\bar{t}}{2}\Lambda_1\right)\bar{T}_1^{\,n+\frac{1}{2}} = \left(1+\frac{\Delta\bar{t}}{2}\Lambda_2+\frac{\Delta\bar{t}}{2}\Lambda_3+\frac{\Delta\bar{t}}{2}f_1\right)\bar{T}_1^{\,n} \\ &\left(1-\frac{\Delta\bar{t}}{2}\Lambda_3-\frac{\Delta\bar{t}}{2}f_1\right)\bar{T}_1^{\,n+1} = \left(1+\frac{\Delta\bar{t}}{2}\Lambda_1\right)\bar{T}_1^{\,n+\frac{1}{2}}+\frac{\Delta\bar{t}}{2}\Lambda_2\bar{T}_1^{\,n} \end{aligned} \right. \tag{7.55}$$

In the uniform stationary zone, $0 \le \bar{z}_2 \le \bar{h}_2$, the ADI scheme for the non-dimensional energy equation is as follows;

$$\left\{ \begin{aligned} &\left(1-\frac{\Delta\bar{t}}{2}\Lambda_1\right)\bar{T}_2^{\,n+\frac{1}{2}} = \left(1+\frac{\Delta\bar{t}}{2}\Lambda_2+\frac{\Delta\bar{t}}{2}\Lambda_3\right)\bar{T}_2^{\,n} \\ &\left(1-\frac{\Delta\bar{t}}{2}\Lambda_3\right)\bar{T}_2^{\,n+1} = \left(1+\frac{\Delta\bar{t}}{2}\Lambda_1\right)\bar{T}_2^{\,n+\frac{1}{2}}+\frac{\Delta\bar{t}}{2}\Lambda_2\bar{T}_2^{\,n} \end{aligned} \right. \tag{7.56}$$

where

$$g_s = \frac{B\mu_0 \overline{\eta} U}{\rho c_p T_0 h_0^2 \overline{h}_s^2} \left[\left(\frac{\partial \overline{u}}{\partial \overline{z}_s} \right)^2 + \left(\frac{\partial \overline{v}}{\partial \overline{z}_s} \right)^2 \right],$$

$$f_s = \frac{B\alpha \mu_0 \overline{\eta} U}{\rho c_p h_0^2 \overline{h}_1^2} \left(\overline{u} \frac{\partial \overline{p}}{\partial \overline{x}_s} + \overline{v} \frac{\partial \overline{p}}{\partial \overline{y}_s} \right), \text{ and } f_1 = \frac{B\alpha \mu_0 \overline{\eta} U}{\rho c_p h_0^2 \overline{h}_1^2} \left(U \frac{\partial \overline{p}}{\partial \overline{x}_1} \right)$$

7.6 The Computational Procedure

The shear rheological behavior of the lubricant in THD lubrication has been the subject of considerable research. The lubricant under highly transient conditions is subjected to relatively severe operating conditions. High pressure and high temperature at the central zone can induce a complex rheological response of lubricant. In the liquid region the shear rheoregical behavior would be expected to be a classical viscous behavior with possible rheological behavior at high rates of change of stress. All the dimensionless governing equations and boundary conditions are discretized using the finite difference method. To predict the non-Newtonian behavior of the present model based on the Bingham plastic model, the most important step in addition to the previous Newtonian case is to determine the boundaries of the uniform moving layer, stationary layer, and shear layer in the lubricating zone. Figure (7.4) shows the program flow chart for THD calculation of the non-Newtonian fluid films.

An arbitrary velocity profile where the velocity gradient is changed at the central line of the film thickness is assumed in the entire shear zone as in the Newtonian case in Chapter 6 for the initial condition. The corresponding pressure and temperature profiles are also initiated properly. In this analysis, no rigid layer formation, $h_1 = 0$ in the uniform moving velocity zone and $h_2 = 0$ in the stationary velocity zone, is assumed for the first computational cycle. The corresponding magnitude of the shear rate is computed from the initial velocity, pressure, and temperature profiles. Next, the Reynolds equation is solved using the SOR method. Having computed the pressure distribution, the velocity is computed and then the energy equation for the fluid is solved. At every cycle, the pressure, temperature, velocity, and shear zone ratio are updated until the steady state is reached. Here, the boundaries of h_1 and h_2 in the film thickness are determined from computed shear stresses and the resultant shear stress at every cycle. These points along the lubrication film are determined to define the boundaries of the regions where the resultant shear stress is less than the yield stress. Calculated zones are updated by Newzone=Oldzone-Oldzone*1/(NX*5)*2 regions. For a typical lubricating system simulation, the number of mesh points in the axial direction is set to $N_y = 10$, $N_x = 60$ mesh points along the lubrication film, and $N_z = 60$ ($N_{z_s} = 20$, $N_{z_1} = 20$, and $N_{z_2} = 20$) mesh points across the film thickness.

The following steps are the procedure to determine the existence of zones having uniform moving and stationary layers in the lubricating zone.

1. Assume that there is full shear formation in the lubricating zone for the first computational cycle.
2. Compute the resultant shear stress with initial velocity distribution.
3. Solve the Reynolds equation in the full shear zone assumed in step 1.
4. Calculate the velocity distribution of the non-Newtonian behavior by using the model with the gradient changing at the central zone across the film thickness.
5. Compute the resultant shear stress and compare it with the yield stress at every nodal points ($N_x = 60$) across lubrication film thickness and centrally axial points. Determine the region where the resultant shear stress is less than the yield stress. Once, shear zone ratio is computed, the values are updated to proceed next step.

6. Having determined the new shear zone ratios, step 2 ~ step 5 is repeated until the computational cycle reaches the final cycle for the steady state.
7. Print out all performance characteristics of the film.

7.7 Empirical Evaluation of the Thin High Shear Zone and Experimental Data

The basic concept of shear zone model is that shearing is assumed to occur only in a small zone located centrally in the fluid film instead of making the assumption of shear in the entire film [26, 27]. Due to the high rate of heat generation in the shear zone, the film is thought to expand in the across film direction contributing to the pressure rise in the film. The key to this concept lies in the time scale of the fluid expansion relative to the time scale of the fluid flow through the bearing space. The basic idea is that the fluid expansion rate is much faster than the flow rate which results in pressure development [31].

A constant shear zone thickness ratio was assumed and the model was solved for a fixed bearing geometry and running conditions. This was repeated until the peak pressure determined by the model matched the experimental peak pressure for the UW-1 bearing for the same operating conditions. Upon checking the pressure distributions predicted by the model, both axially and circumferentially, it was found that the predictions were nearly exact. This appeared to confirm the original hypothesis of a shear zone. This process was repeated for several experimental conditions from which an empirical relationship predicting the ratio of the shear zone height the film height was determined. The ratio, h_s/h was found to be a function of the product Sommerfeld number S and the Peclet number, Pe, $\frac{h_s}{h} = f(S \cdot P_e)$ [27].

$$S \cdot P_e = 0 \rightarrow \left(\frac{2}{5\pi}10^6\right) \qquad \frac{h_s}{h} = \frac{1}{2\pi}\left(\frac{S \cdot P_e}{10^6}\right)^{\pi/2} \tag{7.57}$$

$$S \cdot P_e = \left(\frac{2}{5\pi}10^6\right) \rightarrow 0 \qquad \frac{h_s}{h} = \frac{1}{5\pi}\left\{1 - \exp\left(\left(\frac{S \cdot P_e}{10^6} - \frac{1}{5\pi}\right)\Big/\left(\frac{2}{\pi}\right)\right)\right\} \tag{7.58}$$

where Sommerfeld and Peclet numbers are defined as follows.

$$S = \frac{1}{2\pi^2}\left(\frac{B}{h_{ave}}\right)^2 \frac{\mu U}{pB} \text{ for slider bearing} \tag{7.59}$$

$$P_e = \left(\frac{\rho c}{k}\right) BU \tag{7.60}$$

$$S = \left(\frac{R}{C}\right)^2 \frac{\mu N}{p} \text{ for journal bearing} \tag{7.61}$$

$$P_e = \left(\frac{\rho c}{k}\right) \pi R U \tag{7.62}$$

where p is the average pressure at the film and N is the speed in the journal bearing.

The behavior of an isoviscous fluid film wedge can be characterized based on Newtonian fluid dynamics by Sommerfeld number. The transient behavior of heat transfer in the fluid wedge is characterized by the Peclet number. To develop the empirical shear zone relationship the UW-1 bearing was selected due to the extensive test data available for various conditions [62]. The test conditions for the present model was selected from experiments which cover speeds from 100 to 2400 rpm for journal bearings and from 10 to 40 ft/sec for slider bearings. The lubrication oil ranged from SAE 10 to 50, and the eccentricity ratio for journal bearing ranged from 0.6 to 0.9 with inlet temperatures from 100 to 160 ^{o}F. Using this empirical relationship for h_s/h the model was checked by available experimental data. In all cases the model predictions matched well with the experimental data. The results from the model predicted the maximum pressures and the pressure distribution in all cases. To sum up empirical evaluation of the shear zone, the test conditions used are given in Tables 9 and 10.

Table 9: Design Parameters for Investigated Journal Bearings (UW-1) [26, 27, 62]

Case #	Diameter, D (in)	Width, L (in)	C, (in)	ε	Speed (rpm)	SAE (oil #)	Temp (^{o} F)
A	3.154	2.0	0.0134	0.9	1050	10	128
B	3.154	2.0	0.0134	0.9	2100	10	128
C	3.154	2.0	0.0134	0.87	1200	50	160
D	3.154	2.0	0.0134	0.87	2400	50	160
E	3.154	2.0	0.0134	0.6	1000	30	107
F	3.154	2.0	0.0134	0.6	2000	30	107

Table 10: Design Parameters for Investigated Slider Bearings (UW-3) [26, 27, 62]

Case #	Length, B (in)	Width, L (in)	h_{min} (in)	h_{max} (in)	Velocity (ft/sec)	SAE (oil #)	Temp (^{o} F)
G	3	3	0.004	0.008	40	10	100
H	3	3	0.004	0.008	20	10	100
I	3	3	0.004	0.008	10	30	100
J	3	3	0.004	0.004	10	30	100
K	3	3	0.006	0.006	10	30	100
L	3	3	0.008	0.008	10	30	100

7.8 A Parametric Investigation of the Effect of the Rheological Properties

7.8.1 Journal Bearing

The results of all cases of journal bearing (UW-1) listed in Table 9 are shown in Figure (7.5) throughout Figure (7.18). Figure (7.5) and (7.6) show the change of maximum pressure with respect to the rotating speed of the UW-1 journal bearing. For a bearing speed at a specific operation condition, the shear yield stress parameter used was obtained from the comparison with experimental data at the high speed (N>2000 rpm). The results of these THD analysis with the thermal effects of the thermal expansion in the across film direction show the same trend with the observed empirical relationship between the operating speed and film pressure of the bearing. The pressure in a fixed geometry fluid film is found to be proportional to the square root of speed [30, 32]. It is interesting to note that the journal bearing pressure and speed characteristics of two different oil types show the effect of lubricant properties such as viscosity, inlet temperature and the lubricant film thickness as defined by the eccentricity ratio on journal bearing performance by comparing Figures (7.5) and (7.6).

Figures (7.7) and (7.8) show the pressure-time history. The results were used to iteratively evaluate the yield shear stress parameter in the steady state solution which best fits the experimental pressure. The computer code is designed to evaluate the shear zone across the film flow as determined by the shear yield stress parameter after a transient time for reaching the operating bearing speed. From such transient time, the results show that the maximum pressures in the lubricating region are greatly influenced by the shear yield stress parameters. This shear yield stress parameter is also an important factor in determining the shear zone ratio which leads to significant increase in temperature in the central narrow shear zone. In Figure (7.7), when the bearing speed is 2400 rpm, the transient time to reach this speed is 0.025 sec and the steady state pressure is reached approximately after 0.5 sec. The time step used in this numerical simulation is 0.001 sec for computational stability. The maximum pressure at the steady state was used to determine the value of shear yield stress parameter which corresponds to given experimental data. Also, for some given operating conditions, several shear yield stress values were attempted in same manner. The best shear yield stress parameter was applied to find the shear zone ratio, h_s/h, by checking the yield region of the resultant shear stress along the film flow. The varying shear zone ratios for the investigated case B are plotted in Figure (7.9). Figures (7.10), (7.11) and (7.12) show the trend of the shear zone ratio along the film flow for case B, D, and F of the UW-1 journal bearing. From the computed results in each case, the dimensionless shear zone along the film flow are found to be in the same order of magnitude as the empirical boundary shear layer obtained by Equation (7.58) based on the isoviscous theory. A value of the shear stress parameter, $\bar{\tau}_0$=2.8, is needed for reaching yield in the solid boundaries, A and B in Figure (7.2). This result with $\bar{\tau}_0$<2.8 is also the same as that obtained by the THD analysis with full shear zone in this case. The calculated shear zone ratio mainly depends on the resultant shear stress which is affected by the velocity gradient and viscosity by temperature. The value of $\bar{\tau}_0 = \tau_0 h_0/\mu_0 U$ is mainly dependent on the value τ_0 and U. Also because the objective of this problem is to determine the thin shear zone in the central region it can be assumed that the other regions have the characteristics of solids, were $\tau_0 = F/A$. As shown in Figure (7.9) increasing the value of shear yield stress parameter tends to cause the formation of a wide region in which the velocity is nearly constant, which would be non-shearing fluid in the narrow lubrication zone. Under anti-symmetric velocity behavior in the shear zone, the points along the film flow direction can be systematically obtained by checking where the resultant shear stress at the solid boundary is less than the shear yield stress parameter.

The velocity profile of lubricant film at various locations along film flow direction are shown in Figure (7.13) for different operating conditions with SAE 50, T_{in} =160 °F, and eccentricity 0.9. In the beginning zone of lubrication region the velocity profile is almost linear. As the gap narrows in the converging region the lubricant gets squeezed in the thin shear zone and is forced to change its velocity so that the velocity profiles become concave in each half region of shear zone. The results came from the considered velocity equation which is assumed to cause large shear stress at the central region in the shear zone due to the high shear rate generated by the velocity gradient.

In Figures (7.14) and (7.15), the pressure distribution in the fluid film show some of the most important bearing performance characteristics such as the load carrying capacity, and the frictional force. The pressure distribution is strongly influenced by thermal effects in the fluid film. The thermal effects also depend on the central thin shear zone which leads to significant temperature rise. Figure (7.14) shows that the thin adiabatic shear zone resulting from the large shear yield stress parameter significantly reduces the pressure in the lubricating film. Figure (7.15) also shows that the pressure distribution along the center line of journal bearing is significantly influenced by bearing speed. As shown in Figures (7.14) and (7.15), the speed and the shear yield stress parameter are the main factors in determining the pressure distribution.

The temperature distribution is displayed in the central shear zone and at stationary and moving layers under the yield zone with the assumed rheological velocity field. In the thin shear zone, the zone is considered as an adiabatic shear band causing high temperature in the lubricating region Both boundaries of the shear zone are adiabatic. For the stationary layer, the interface with the stationary solid is assumed to be insulated. For the moving layer, the temperature at the interface with the moving solid is assumed to have the same value as the lubricant inlet temperature and the solid-like fluid is also assumed to be insulated. Figures (7.16), (7.17) and (7.18) show temperature distribution in the fluid film at the mid-plane of the journal bearing. The shear zones shown in the above Figures are magnified to have the same dimension as the other two layers for detailed temperature profile in illustration of the actual thin thickness. Figure (7.16) shows the results at the conditions of SAE 10 oil and high eccentricity ratio, $\varepsilon=0.9$. It should be note that most of the heat generation occurs in the central shear zone with high shear rate. Around 20° and 180°, temperature profile show relatively high temperature compared to any other circumferential location in the journal bearing. It is considered to be due to the low values of the shear zone ratio. Especially, the smallest value of shear zone ratio around 180° in the circumferential location shows the maximum temperature as can be seen in Figure (7.12). In the fluid film, of the bearing systems, the moving layer has low temperature but high gradient across film flow. There is some heat convection to the moving layer zone because lubricant in the moving layer is quickly replaced by the fresh lubricant attached to the moving surface.

7.8.2 Slider Bearings (Tapered and Parallel Bearings)

The results of the G, H, I cases for the tapered slider bearing (UW-3) listed in Table 10 are shown in Figure (7.19) throughout Figure (7.33). Also, the results of the J, K, L cases for the parallel slider are plotted in Figures (7.34) to (7.39). Figure (7.19) shows that the slider bearing pressure versus speed characteristics also has same trend as the pressure in a fixed geometry fluid film which is proportional to the square root of speed. Figures (7.20), (7.21) and (7.34) show the film pressure and temperature history of slider bearings. From the results, it can be seen that the speed of bearing is the main key to influence the pressure and temperature generated in the lubricating region of the slider bearing of a fixed geometry. As shown in Figure (7.34), the film thickness becomes also another important factor in a parallel slider bearing. The average film thickness of the tapered slider bearing ($h_{min}=0.004$ inch, $h_{max}=0.008$ inch) is set to be equal to the film thickness of the parallel surface slider bearing which is h=0.006 inch. Both sliders have a square stationary surface 3.0 inch in length and running speed at 10 ft/sec. The lubricant is SAE 30 and the inlet temperature is 100 °F. As shown in Figure (7.36), the results of the pressure distribution along the film flow direction shows significant difference between cases I and K. It is considered as the effect of thermal edge in the converging area which influences the build up of much higher pressure. The effect of the thermal expansion is very insignificant in building pressure in the lubricating region after reaching the operating speed of bearing as shown in the pressure history of Figure (7.21). The yield parameters which determine shear zone ratio along film flow direction has considerable influence on the pressure distribution, as shown in Figures (7.22), (7.23), and (7.35). The effect of various yield parameters in the cases of G, H, and K is illustrated by the trend of shear zone ratio in Figures (7.24), (7.25), (7.27), (7.29), and (7.37). Figures (7.25) and (7.27) show the trend of yield parameters and shear zones in the process of seeking the best agreement in the maximum pressure with experimental data and other THD analysis. Figures (7.26), (7.28) and (7.30) show the thickness of the dimensionless shear zone existing at central region across film flow against the dimensionless film thickness. The shear zone ratio for various positions along the film flow are plotted along with the empirical shear zone ratio by Equation (7.58). At the value shear stress parameter determined for the best correlation with the experimental data the computed shear zone ratios are within the boundaries of empirical shear zone ratio. Figures (7.31) and (7.38) show the velocity profiles within the shear zone in the sliding direction for slider bearings. It is expected that the pressure gradient in the exit region would be large due to the small dimensions of the shear zone ratio. Figures (7.32), (7.33), and (7.39) show the film temperature distribution for the slider bearing. Unlike the results for the journal bearing they show some convection effect in both layers. The high temperature lines around exit zone in the shear zone is due to the thin shear zone in that region. Heat generation takes place in the shear zone which is located in the center layer of the film and heat is carried away by convection as well as conduction (not considered here as the main cause of the temperature reduction on the solid surface).

A parametric investigation of the effect of film thickness on the shear zone was undertaken for the case of a parallel slider with B=L=3.0 inch using SAE 10 oil at 100 ^{o}F inlet temperature and speed U=10 ft/sec. Film thickness values from 0.002 to 0.1 inch were considered. The shear yield stress parameter used in oil cases was assumed to be $\bar{\tau}_0 = 15.0$. The maximum pressure, the average pressure and h$_s$/h at the inlet, center and exit region are given in Table 11. The Sommerfelt number ($S = \dfrac{1}{2\pi^2}\left(\dfrac{B}{h_{ave}}\right)^2 \dfrac{\mu U}{pB}$) and Peclet number ($P_e = \left(\dfrac{\rho c}{k}\right)BU$) are calculated for each case and the empirical h_s/h was also obtained from Equation (7.58). It can be seen from the table that the shear zone thickness from the proposed analysis reaches can asymptotic value of 0.065942 which is close to the value 0.063662 calculated from the empirical equation. It can also be seen that the proposed method shows that h_s/h at the center and exit region increases with increasing h which is consistent with the results of the empirical equation. Figure (7.40) shows a plot the shear zone for the considered case as obtained from the proposed approach.

7.9 Summary and Conclusion

The concept of the shear zone as determined by the shear yield stress parameter is introduced to explain the effect of the rheological properties of the lubricant on thin film behavior in tribology. The shear zone is hypothesized to be composed of two layers where anti-symmetric velocity behavior occurs in the central region of the lubricating film. Interfacial boundaries between the shearing fluid and the adjacent solid like fluid are determined from the points where the resultant shear stress is less than yield value. This approach produces thin shear zone at the central region of the film where the lubricant undergoes Newtonian behavior at two layers with mirror image dimensions about the central plane with anti-symmetric velocity behavior. The parametric investigation performed using different rheological properties can be applied to any thin film lubrication analysis in the laminar regime but does not appear to b applicable to conditions of very slow running speed (N<1000 rpm).

Table 11: A Parametric Investigation of the Effect of Film Thickness on the Shear Zone and Summarized Results Based on the Empirical Formula (7.58) for Evaluating the Shear Zone Thickness.

h (in)	$(h_s/h)_{cal}$			p_{max}(psi)	p_{ave}(psi)	S	Pe (10^6)	$(h_s/h)_{emp}$
	Inlet	Center	Exit					
0.002	0.110924	0.053987	0.002581	279.8932	123.4971	0.170199	3.14496	0.033312
0.004	0.083831	0.056191	0.032094	33.1293	13.8187	0.380265	3.14496	0.052911
0.006	0.074351	0.058484	0.046004	6.69668	2.7692	0.843368	3.14496	0.062571
0.01	0.068634	0.060871	0.056191	0.66574	0.2759	3.047348	3.14496	0.063662
0.02	0.065942	0.063356	0.063356	0.02341	0.009989	21.04223	3.14496	0.063662
0.1	0.065942	0.065942	0.065942	0.00001	4.464 e-6	1883.641	3.14496	0.063662

Note: B=L=3.0 inch, SAE 10, U=10 ft/sec, Time=0.1 sec, $\bar{\tau}_0 = 15.0$

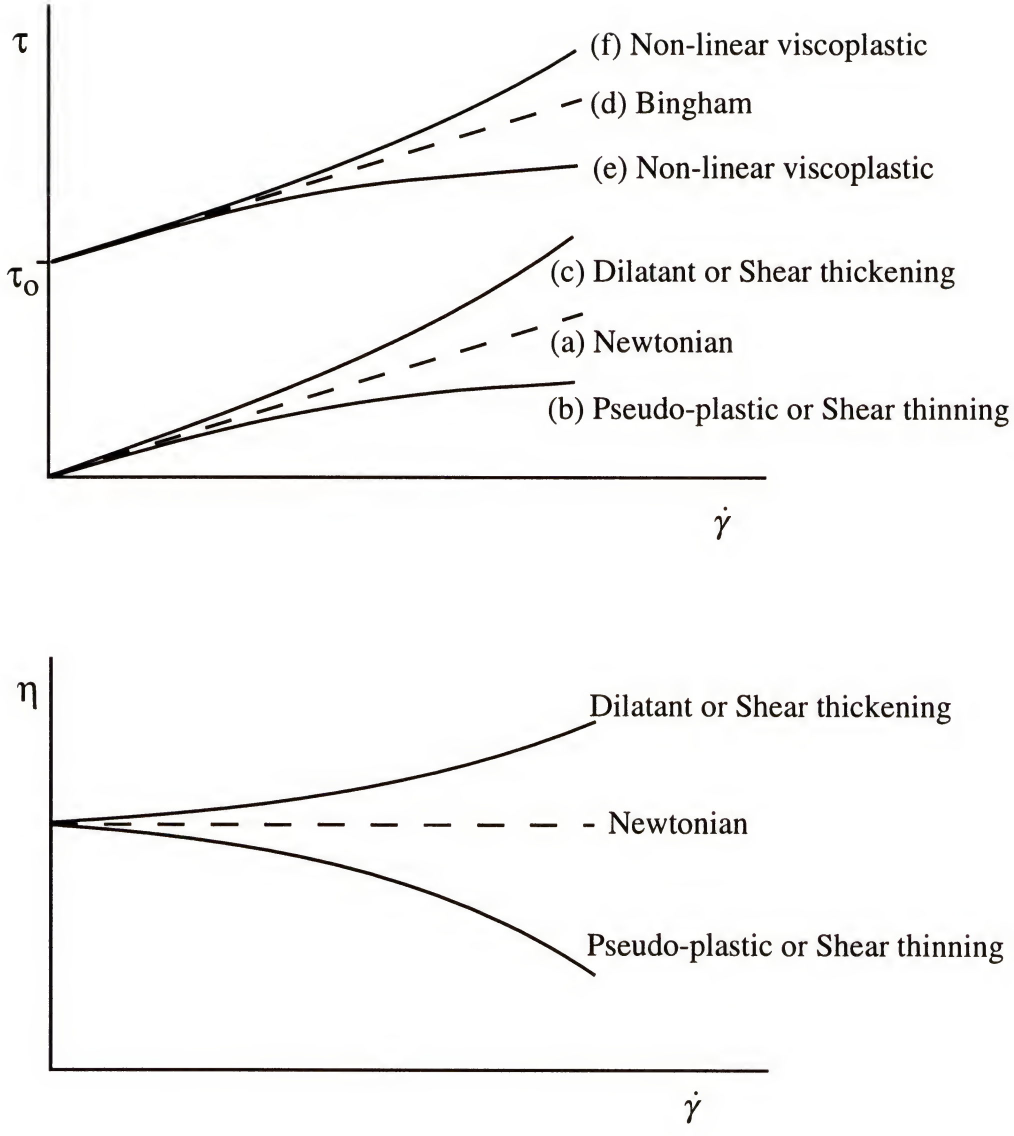

Figure 7.1 Shear stress vs. Shearing rate for Bingham body; τ_0 is the yield stress, Pseudo-plastic or shear-thinning, and Dilatant or shear-thickening. Dashed lines show Newtonian behavior [79].

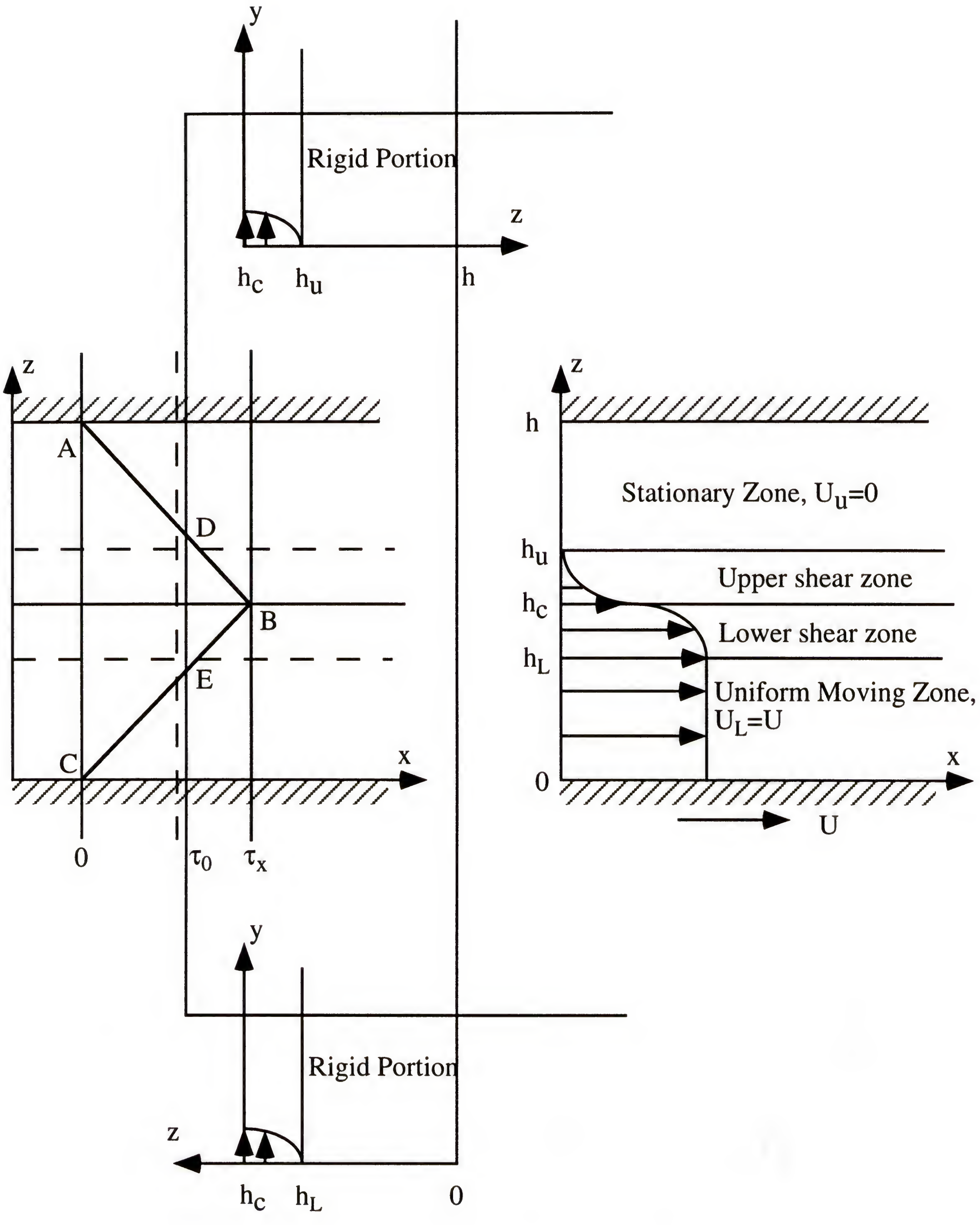

Figure 7.2 Rigid layers attached to upper and lower surfaces for explaining the Non-Newtonian behavior in fluid film

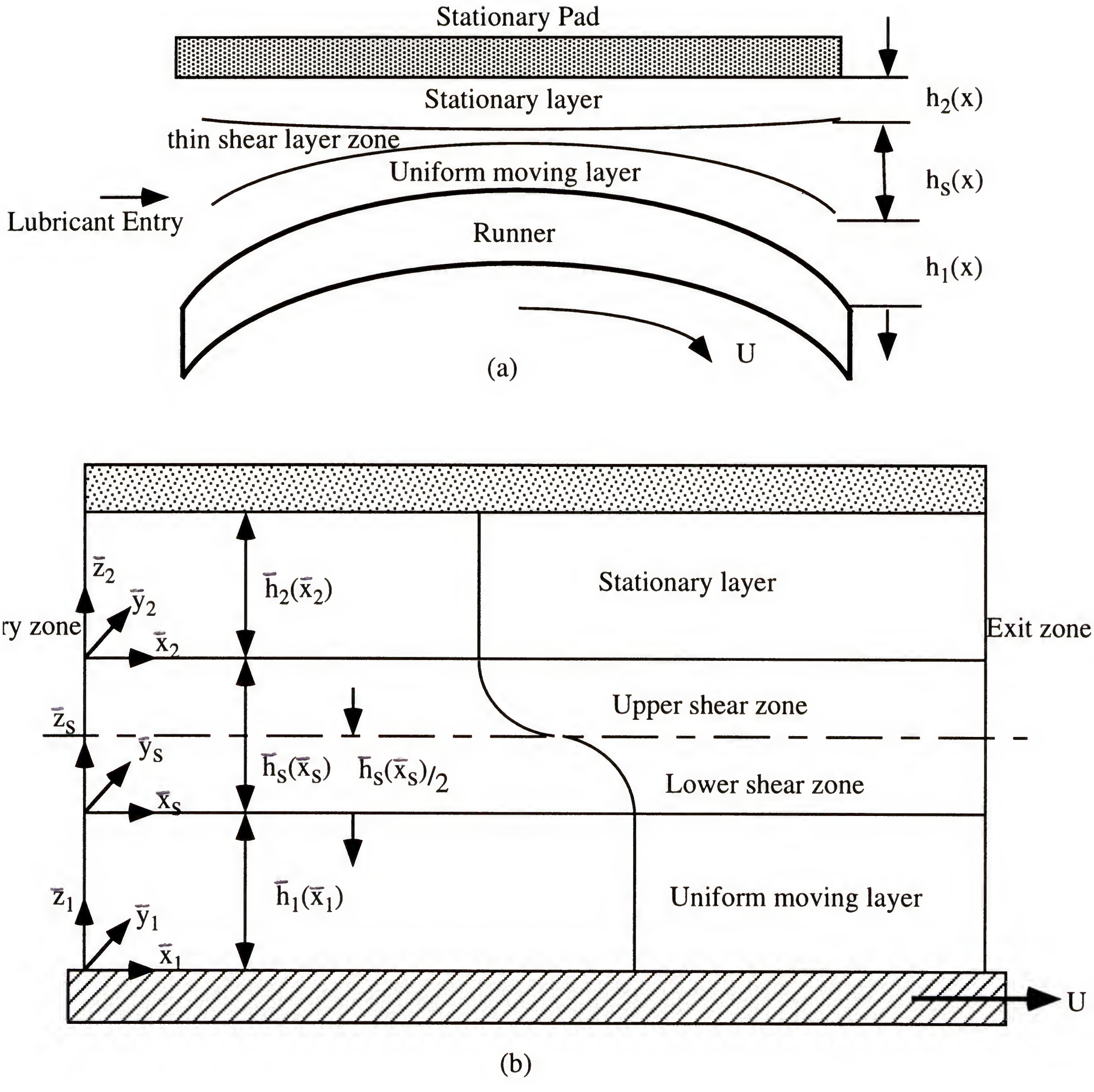

Figure 7.3 (a) Finite lubrication system configuration and geometry
(b) The computational domain

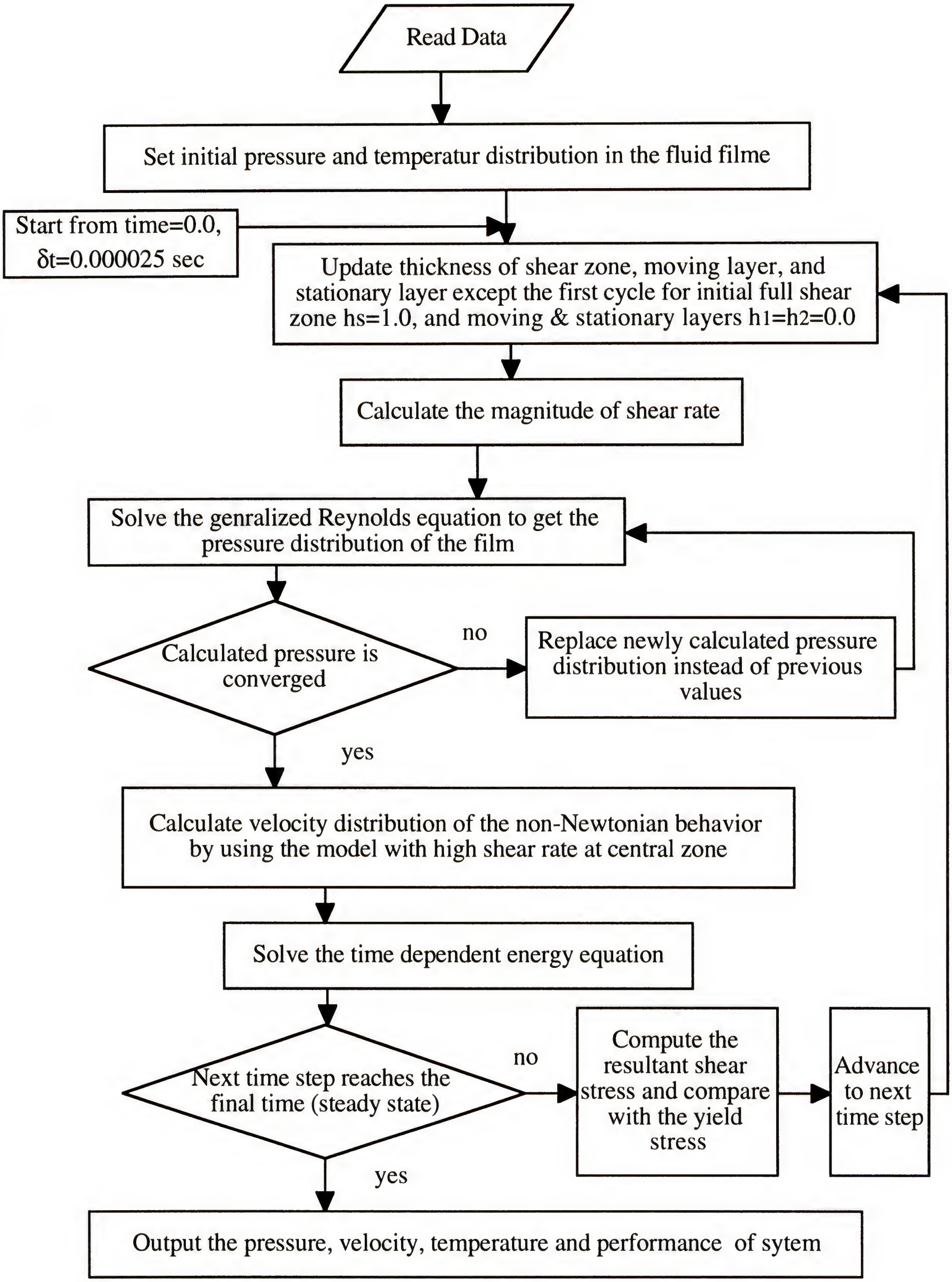
Read Data
Set initial pressure and temperatur distribution in the fluid filme
Start from time=0.0, δt=0.000025 sec
Update thickness of shear zone, moving layer, and stationary layer except the first cycle for initial full shear zone hs=1.0, and moving & stationary layers h1=h2=0.0
Calculate the magnitude of shear rate
Solve the genralized Reynolds equation to get the pressure distribution of the film
Calculated pressure is converged
no
Replace newly calculated pressure distribution instead of previous values
yes
Calculate velocity distribution of the non-Newtonian behavior by using the model with high shear rate at central zone
Solve the time dependent energy equation
Next time step reaches the final time (steady state)
no
Compute the resultant shear stress and compare with the yield stress
Advance to next time step
yes
Output the pressure, velocity, temperature and performance of sytem

Figue 7.4 Program flow chart of THD analysis using the Non-Newtonian velocity expression of the Rhelogical behaviors

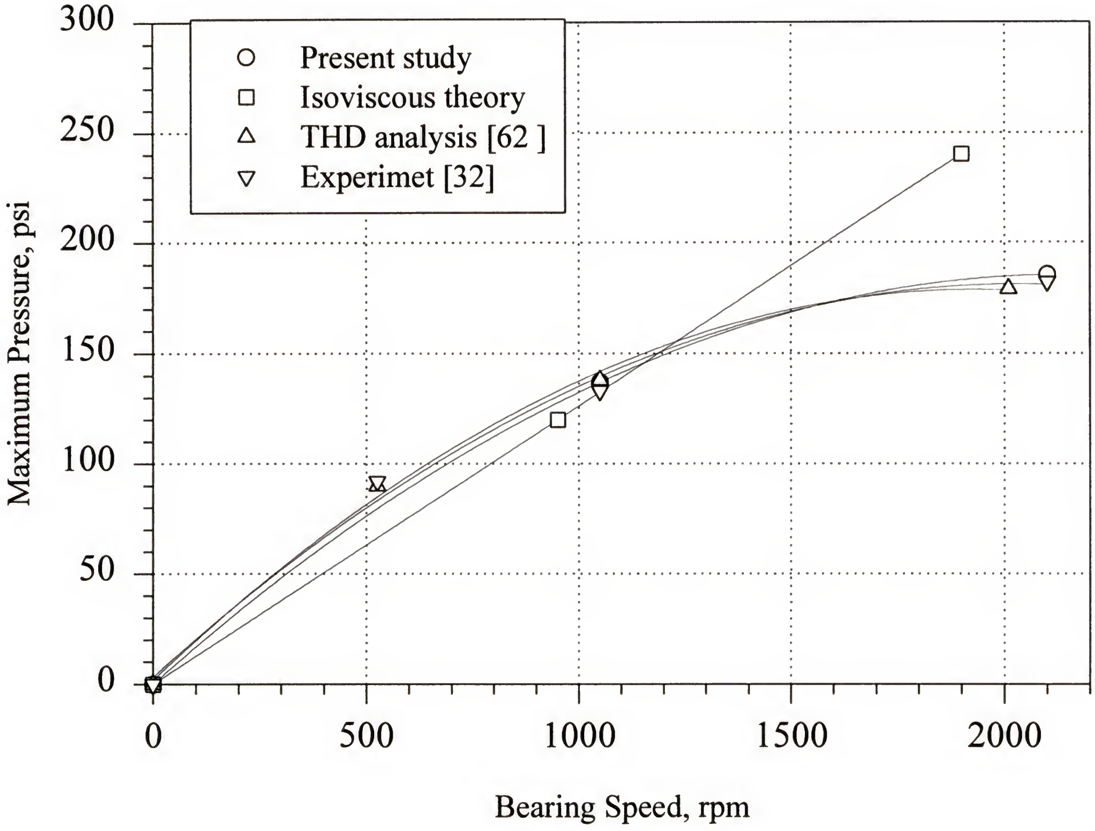

Figure 7.5 Journal bearing pressure-moving speed characteristics
D=3.154 in, L=2 in, C=0.0134 in, SAE 10, T_{in}=128 ^{o}F, ε=0.9

N=1050 rpm : Transient time 0.3 sec, $\bar{\tau}_0$=15
N=2100 rpm : Transient time 0.5 sec, $\bar{\tau}_0$=15

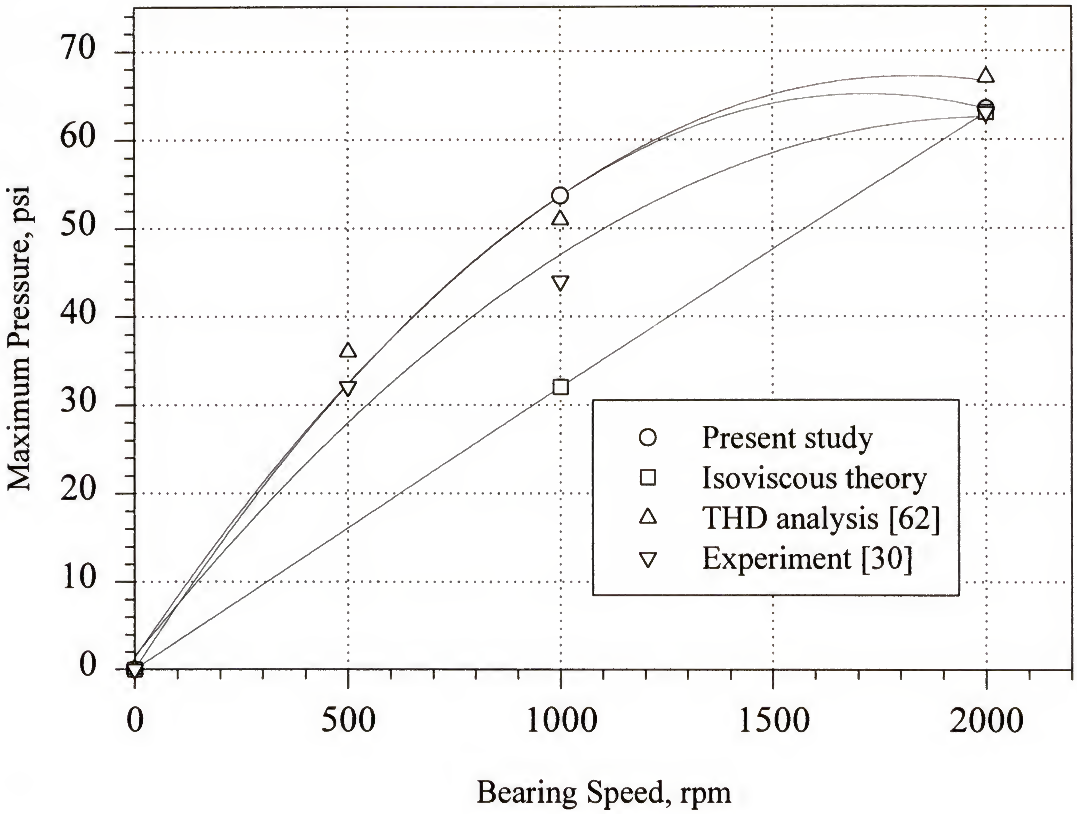

Figure 7.6 Journal bearing pressure-moving speed characteristics
D=3.154 in, L=2 in, C=0.0134 in, SAE 30, T_{in}=107 °F, ε=0.6

N=1000 rpm : Transient time 0.1 sec, $\bar{\tau}_0$=8
N=2000 rpm : Transient time 0.05 sec, $\bar{\tau}_0$=8

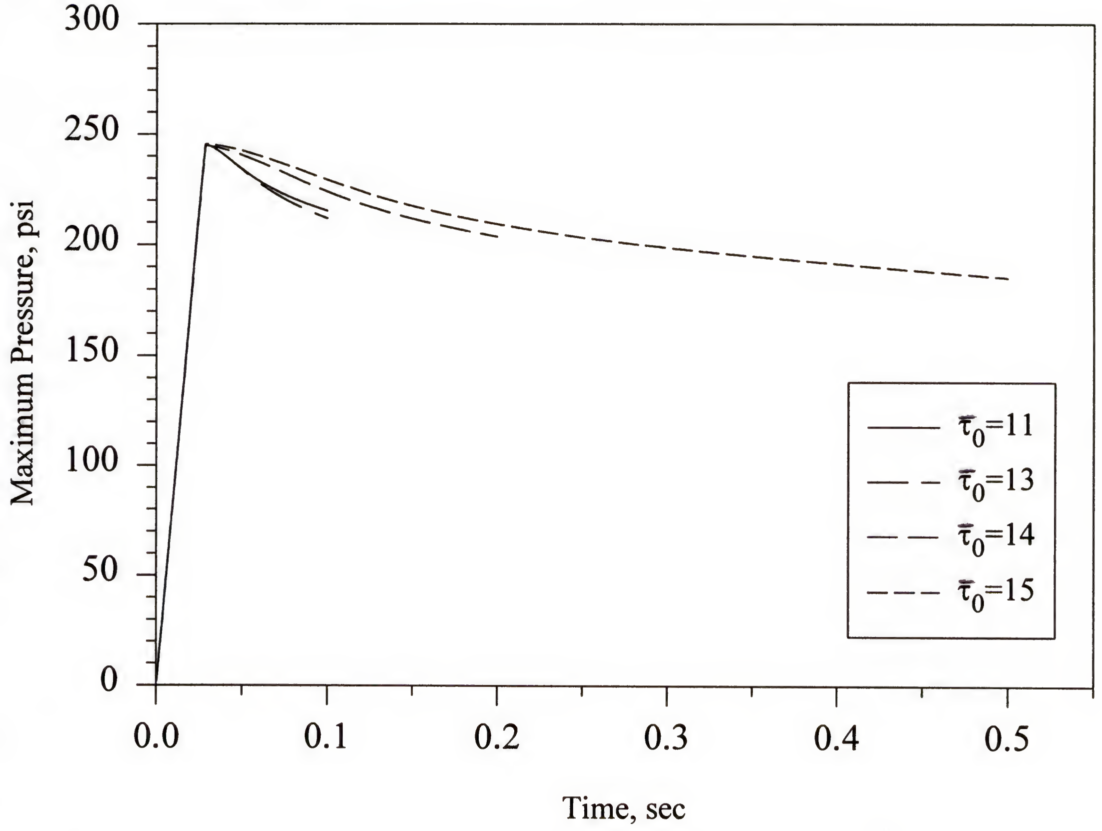

Figure 7.7 Journal bearing pressure history for various yield shear stress parameter
D=3.154 in, L=2.0 in, C=0.0134 in, SAE 10, T_{in}=128 ^{o}F, N=2100 rpm, ε=0.9

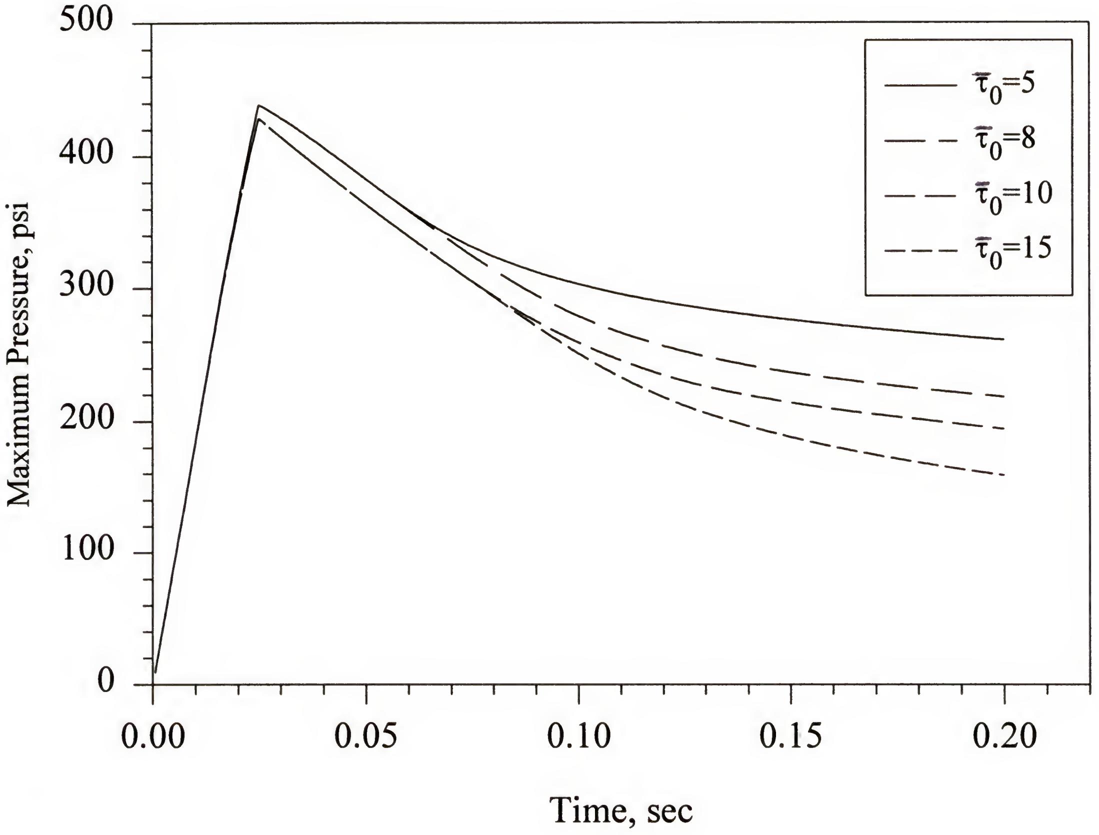

Figure 7.8 Journal Bearing pressure history for various shear yield stress parameters

D=3.154 in, L=2.0 in, C=0.0134 in, SAE 50, T_{in}=160 ^{o}F, N=2400 rpm, ε=0.87

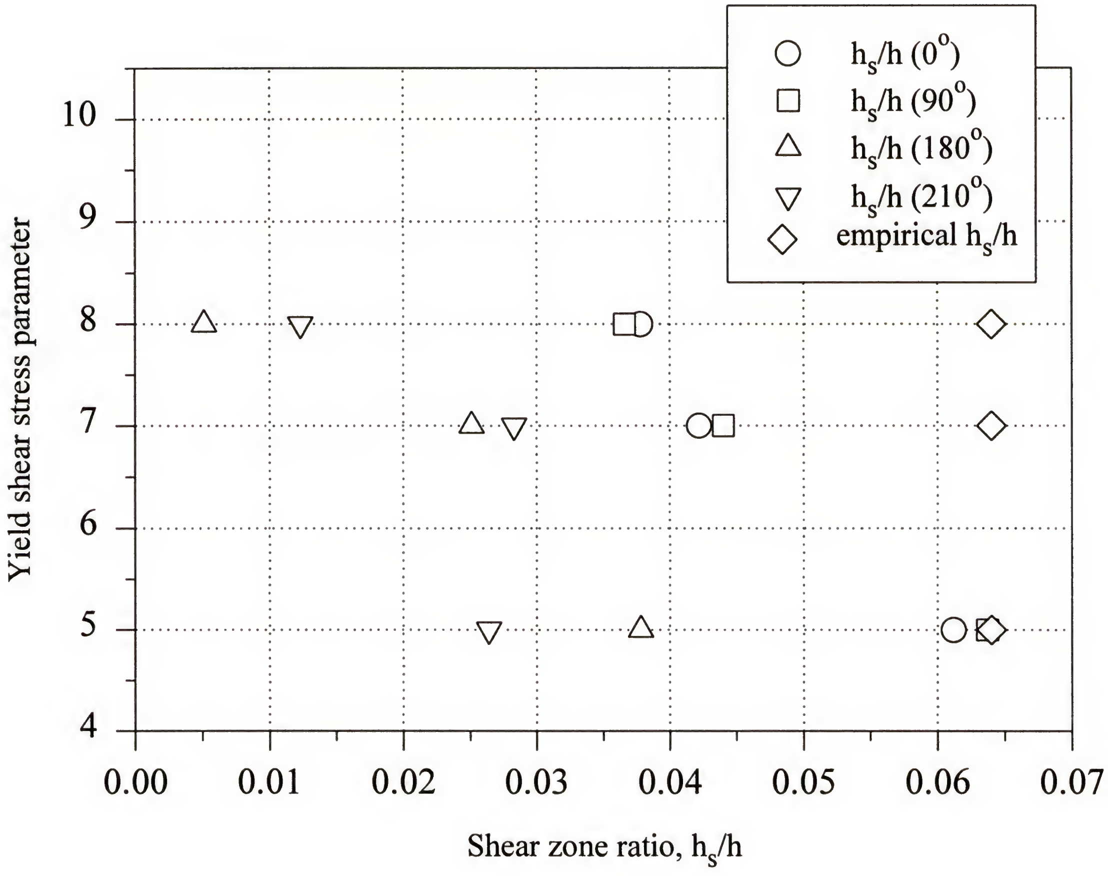

Figure 7.9 Shear zone ratio (h_s/h), based on the THD analysis with various shear yield stress parameters, D=3.154 in, L=2.0 in, C=0.0134 in, ε=0.6, T_{in}=107 ^{o}F, SAE 30, N=2000 rpm

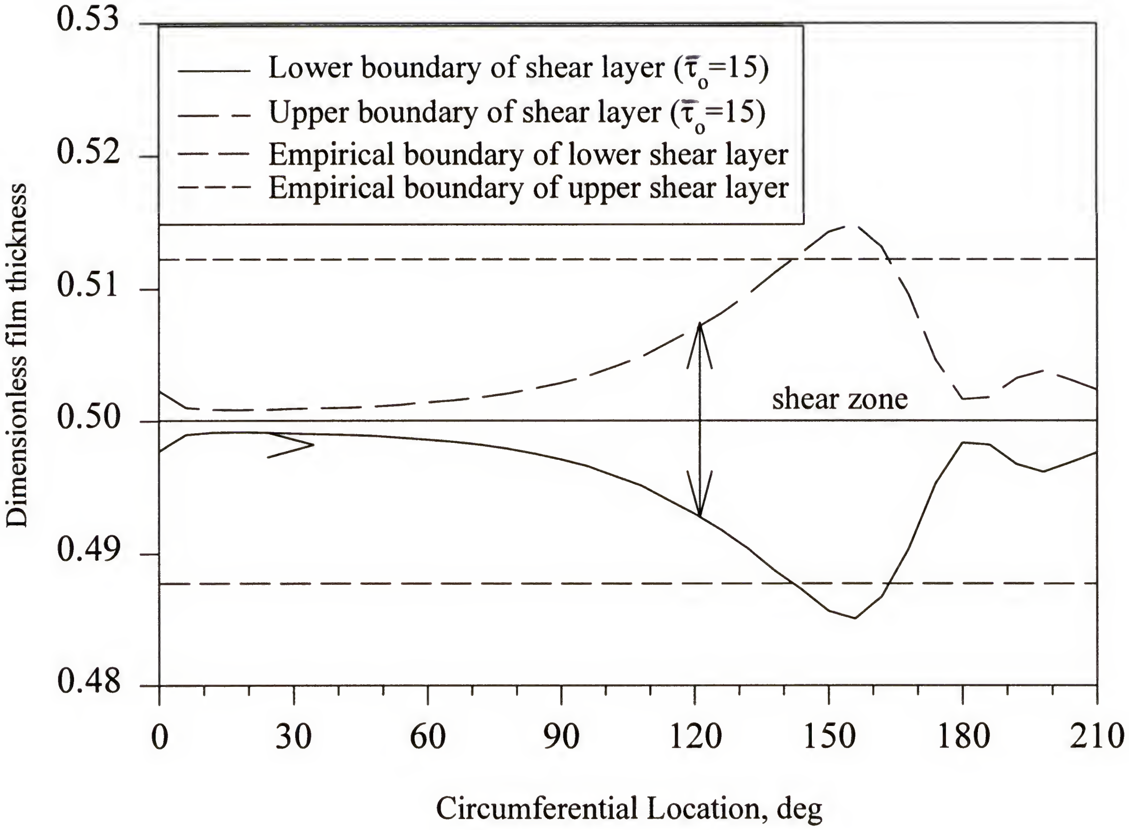

Figure 7.10 Shear zone ratio along film flow direction
D=3.154 in, L=2.0 in, C=0.0134 in, ε=0.9, T_{in}=128 °F,
SAE 10, Time=0.5 sec, N=2100 rpm

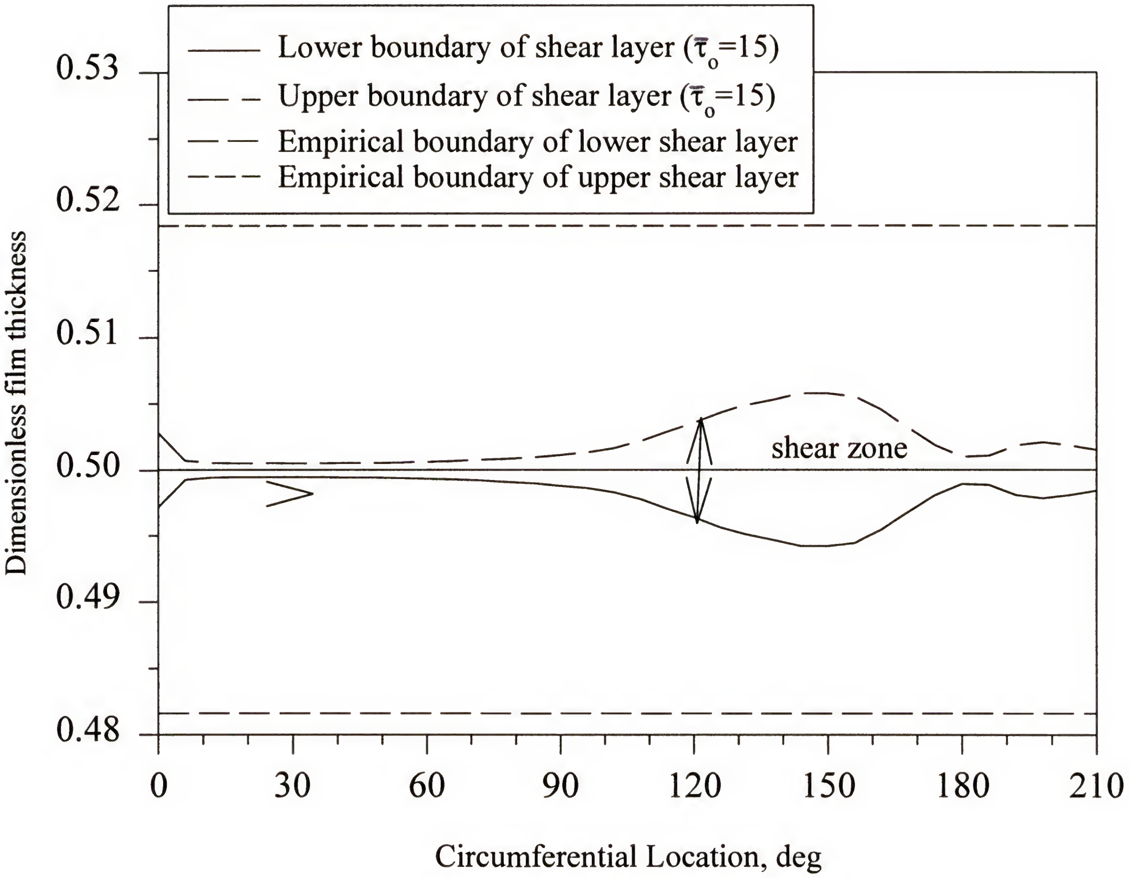

Figure 7.11 Shear zone ratio along film flow direction
D=3.154 in, L=2.0 in, C=0.0134 in, ε=0.87, T_{in}=160 ^oF,
SAE 50, Time=0.2 sec, N=2400 rpm

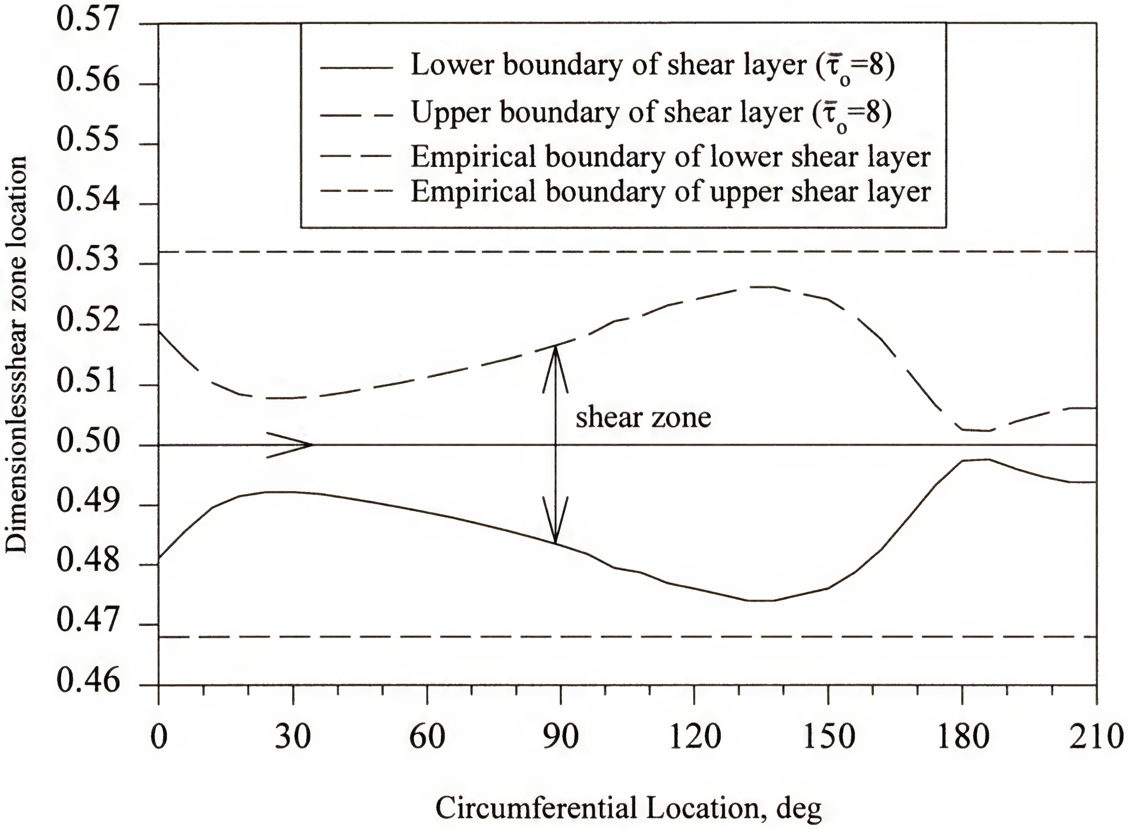

Figure 7.12 Shear zone ratio along film flow direction
D=3.154 in, L=2.0 in, C=0.0134 in, ε=0.6, T_{in}=107 °F,
Time=0.1 sec, N=2000 rpm, SAE 30

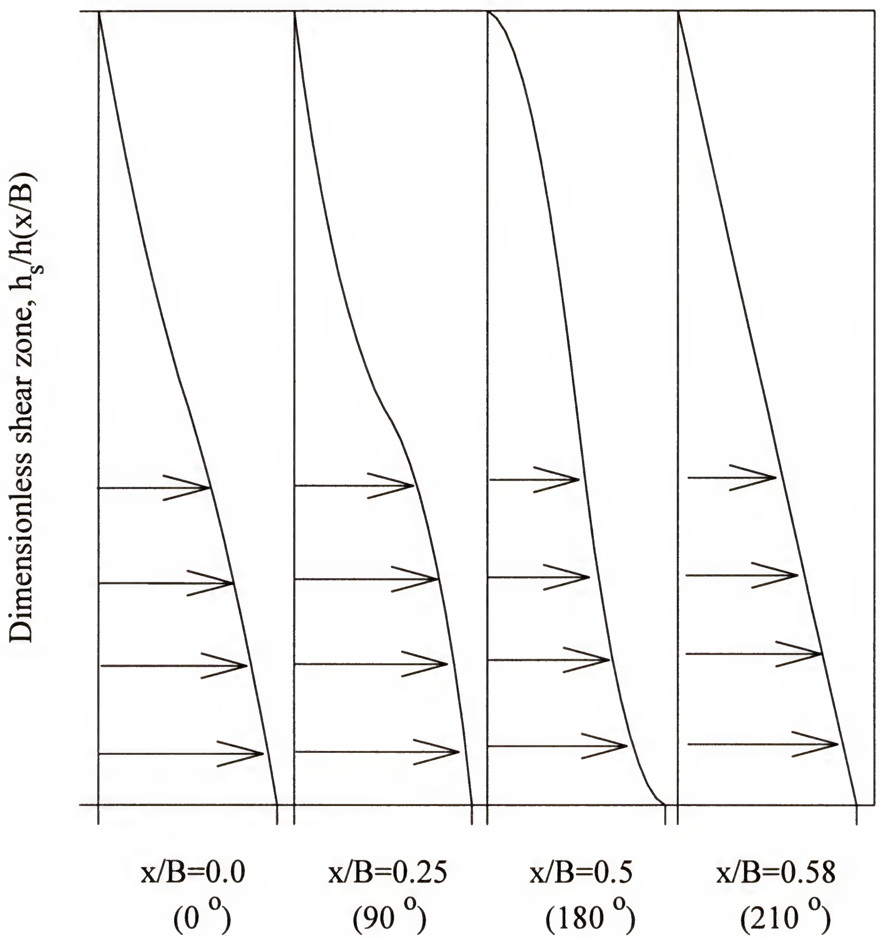

Figure 7.13 Velocity profile in the shear zone along the mid plane of the journal bearing in the direction of motion D=3.154 in, L=2.0 in, C=0.0134 in, ε=0.87, SAE 50, T_{in}=160 °F, N=2400 rpm, Transient time=0.2 sec, $\bar{\tau}_0$=15

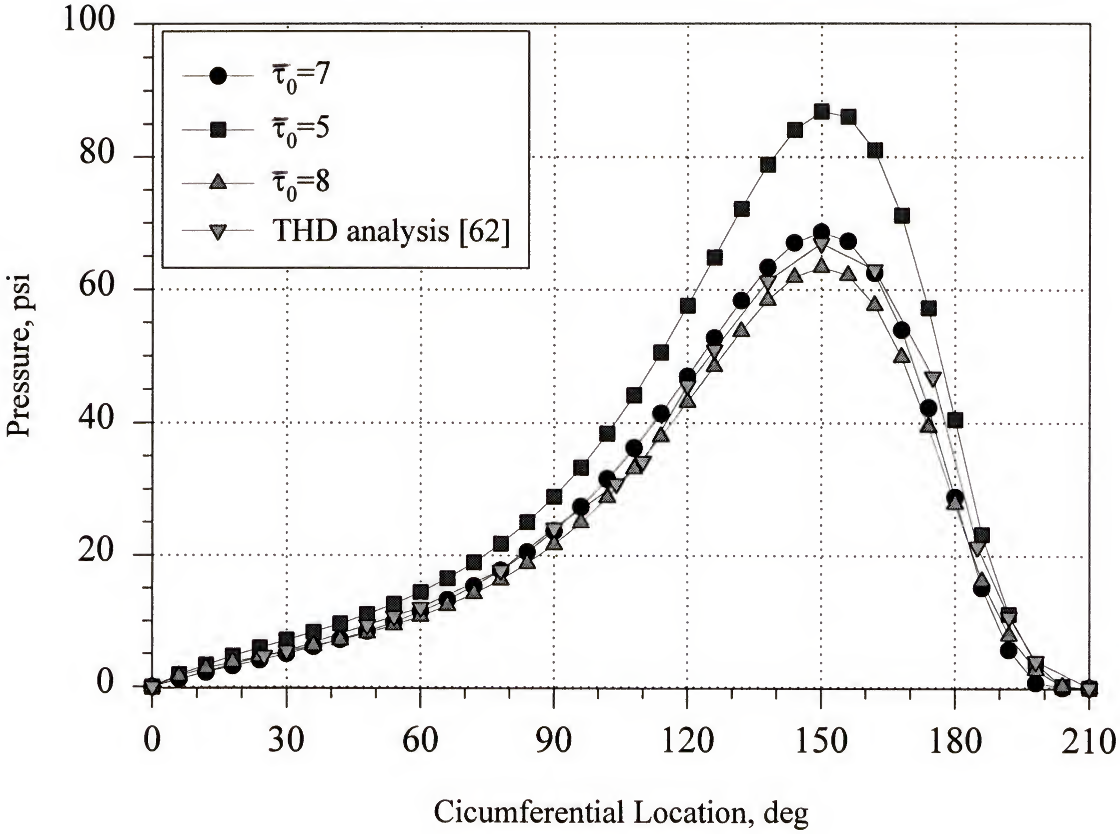

Figure 7.14 Pressure distribution for various shear yield parameters along the center-line of the journal bearing in the direction of sliding motion, D=3.154 in, L=2.0 in, C=0.0134 in, ε=0.6, N=2000 rpm, SAE 30, T_{in}=107 ^{o}F, time=0.1 sec

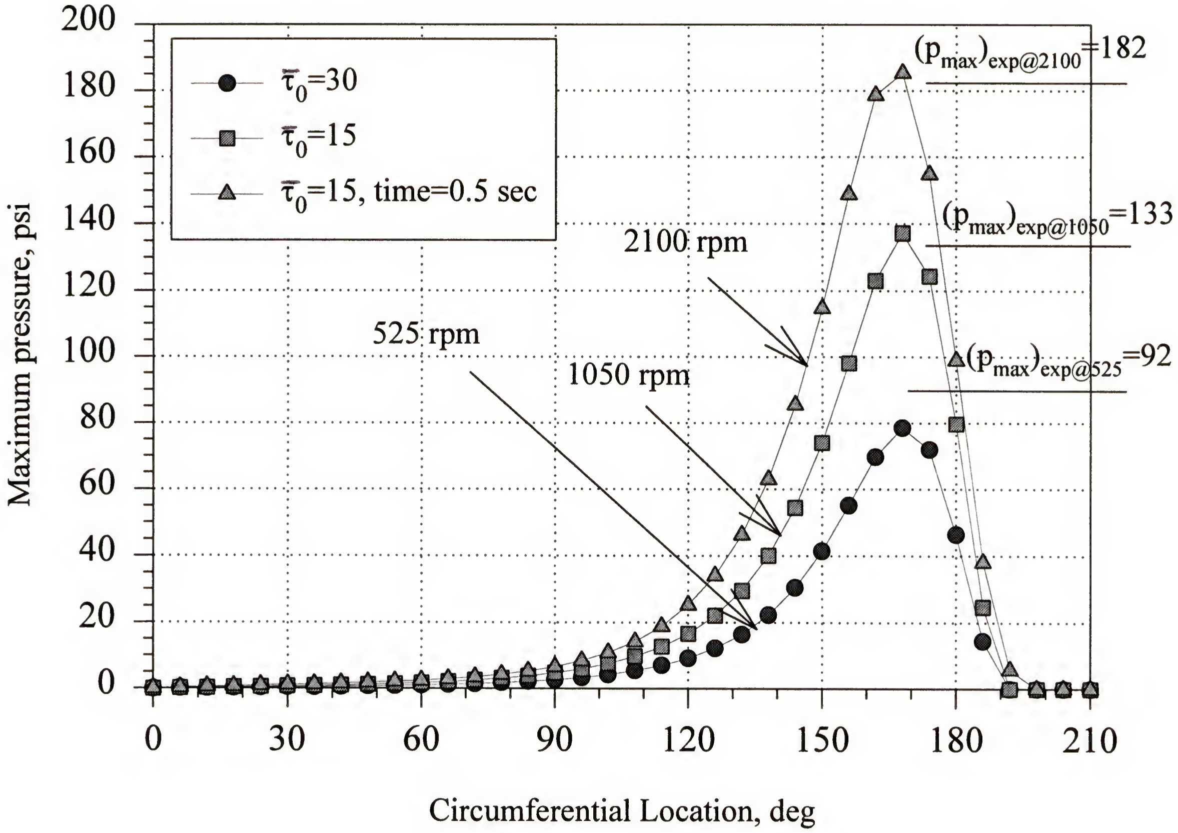

Figure 7.15 Pressure distribution for various bearing running speed along the center line of the journal bearing in the direction of sliding motion D=3.154 in, L=2.0 in, C=0.0134 in, ε=0.9, SAE 10, T_{in}=128 ^{o}F

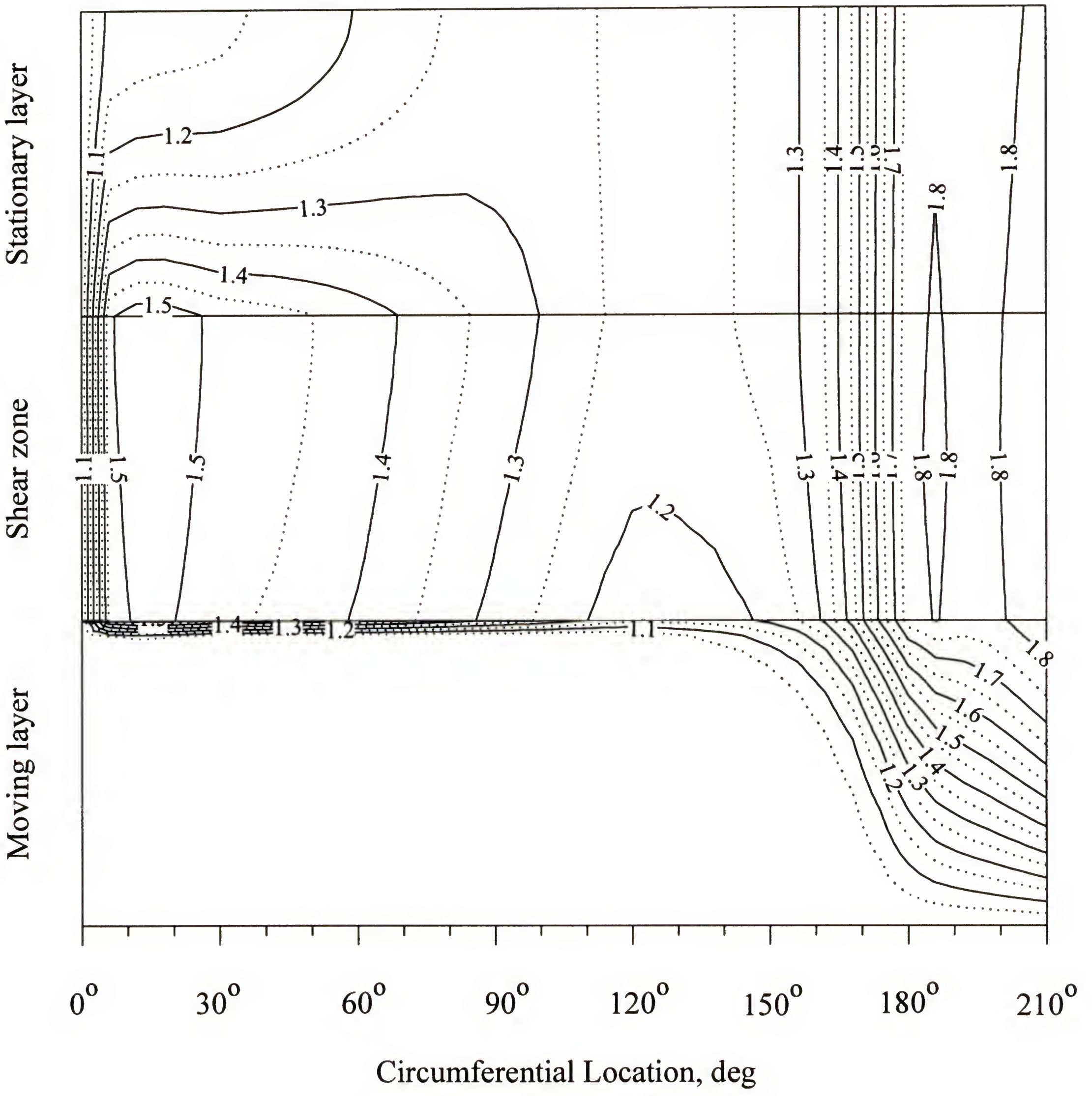

Figure 7.16 Dimensionless film temperature distribution at the journal bearing mid plane in the sliding direction
D=3.154 in, L=2.0 in, C=0.0134 in, ε=0.9, SAE 10
T_{in}=128 °F, Time=0.5 sec, $\bar{\tau}_0$=15, N=2100 rpm

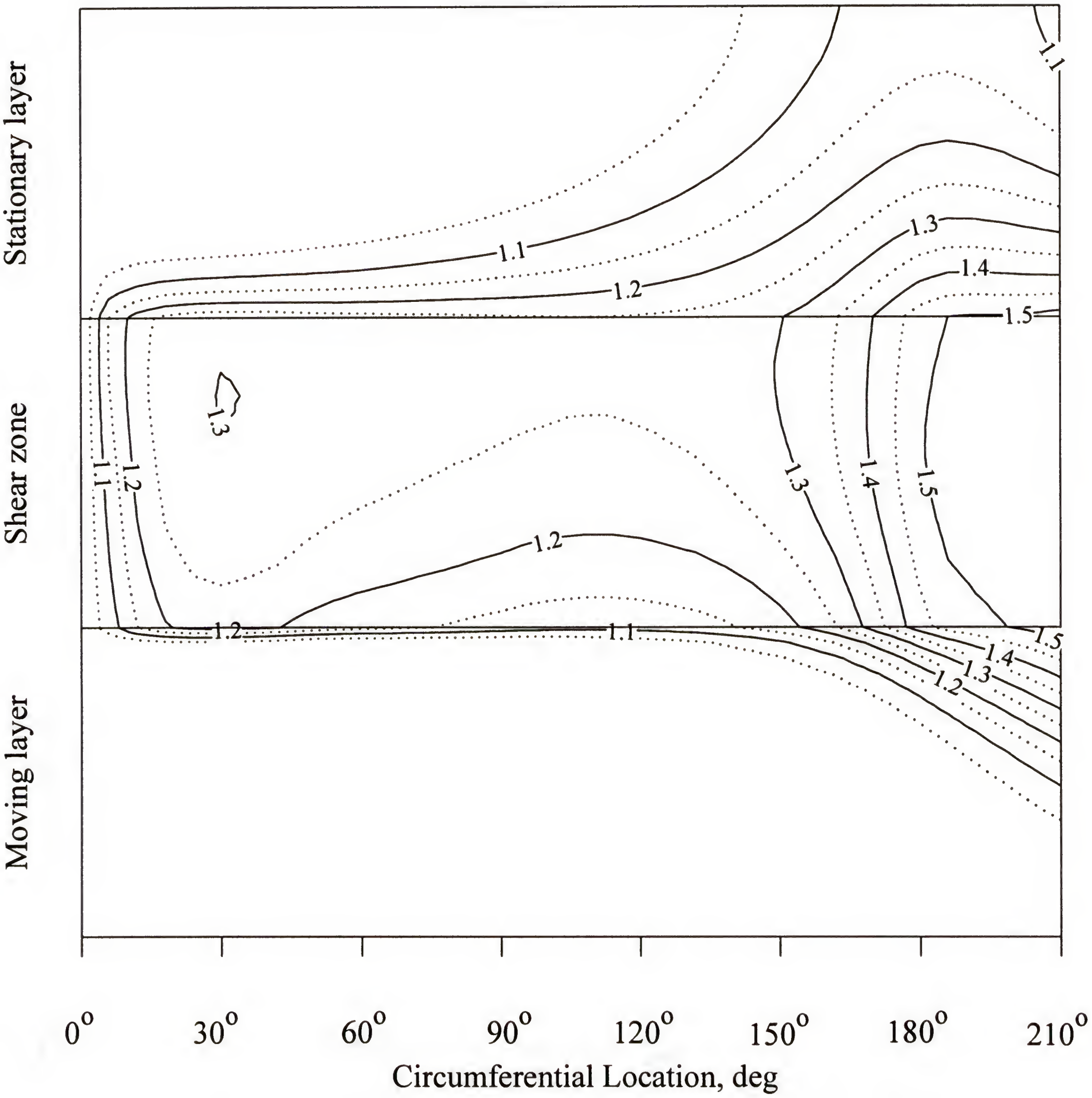

Figure 7.17 Dimensionless film temperature distribution at the journal bearing mid plane in the sliding direction

D=3.154 in, L=2.0 in, C=0.0134 in, ε=0.6, SAE 30, T_{in}=107°F, Time=0.05 sec, $\bar{\tau}_0$=7, N=2000 rpm

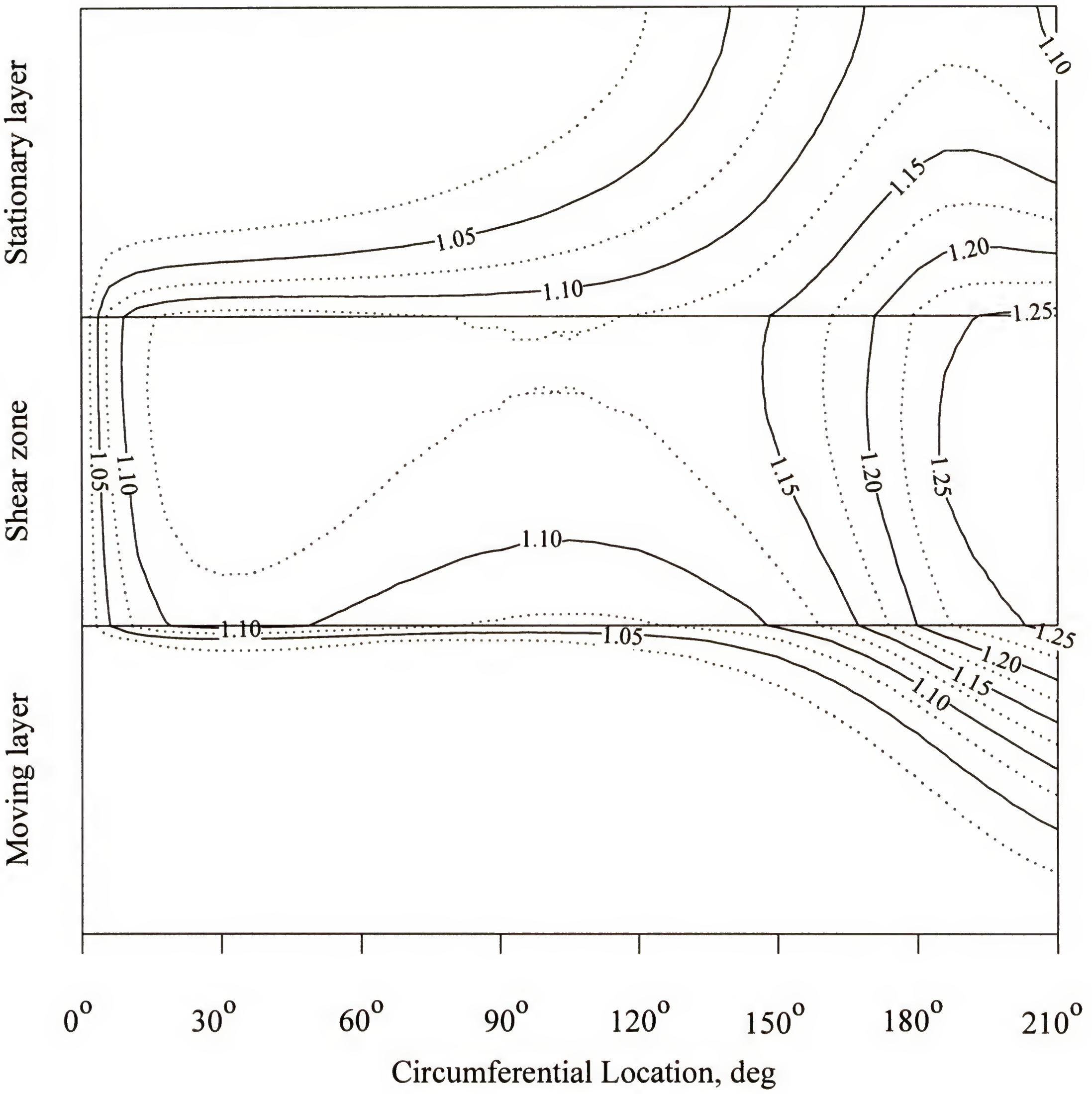

Figure 7.18 Dimensionless film temperature distribution at the journal bearing mid plane in the sliding direction
D=3.154 in, L=2.0 in, C=0.0134 in, e=0.6, SAE 30, T_{in}=107 °F, Time=0.1 sec, $\bar{\tau}_0$=8, N=1000 rpm

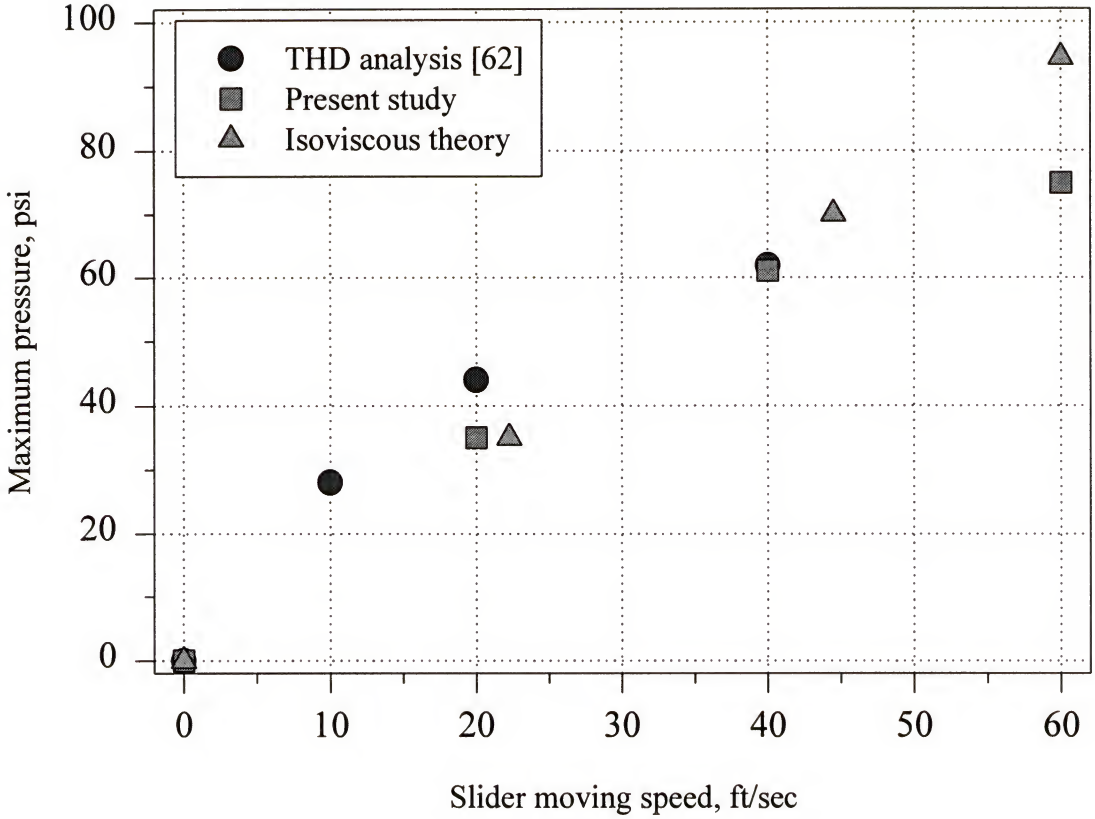

Figure 7.19 Slider bearing pressure-moving speed characteristics B=L=3.0 in, h_{min}=0.004 inch, h_{max}=0.008 inch, SAE 10, T_{in}=100 ^{o}F, time=0.02 sec, $\bar{\tau}_0$=10.0

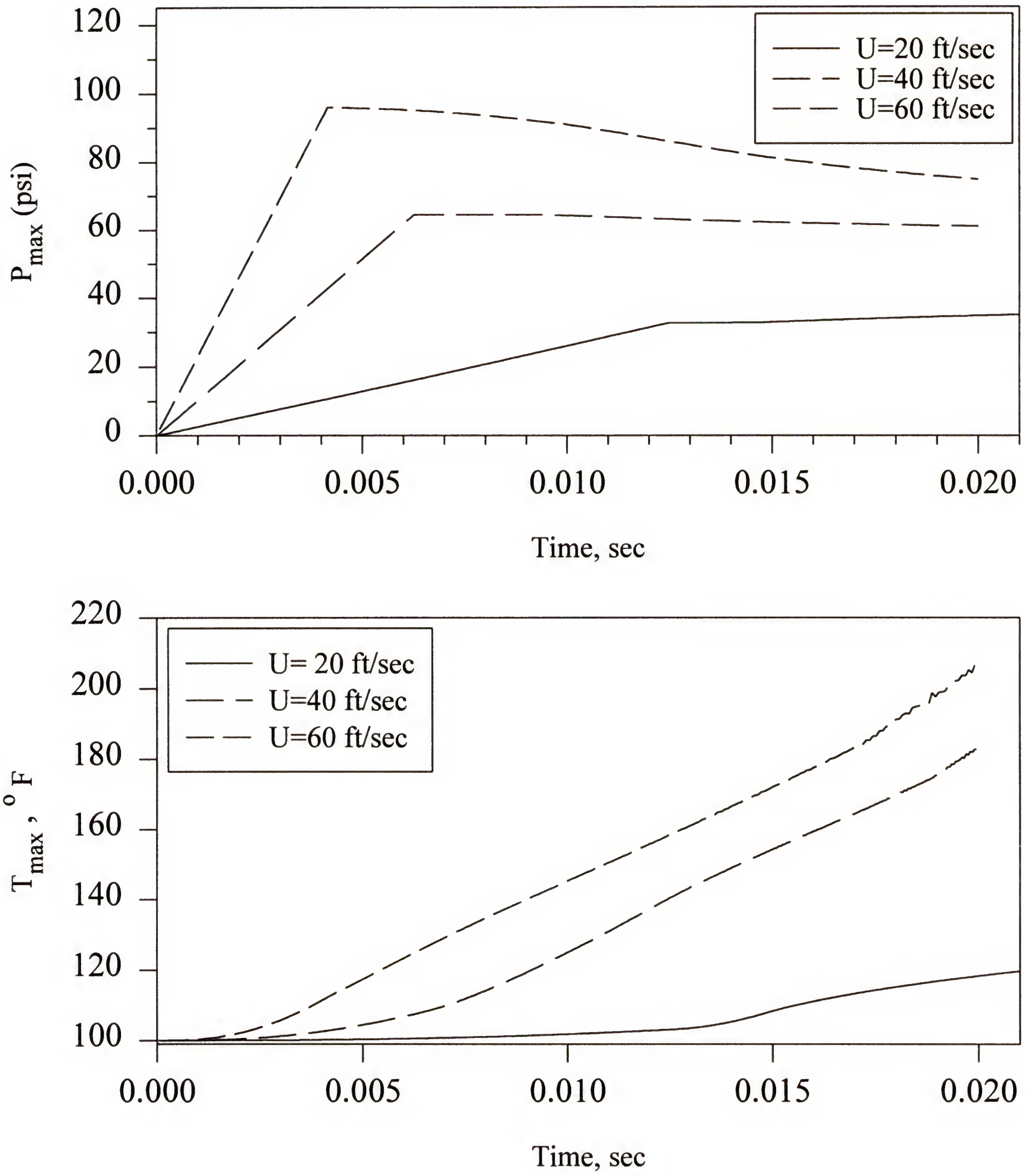

Figure 7.20 Maximum pressure and temperature history for various runnung speeds, B=L=3.0 in, h_{min}=0.004 in, h_{max}=0.008 in, $\bar{\tau}_0$=10.0, SAE 10, T_{in}=100 ^oF

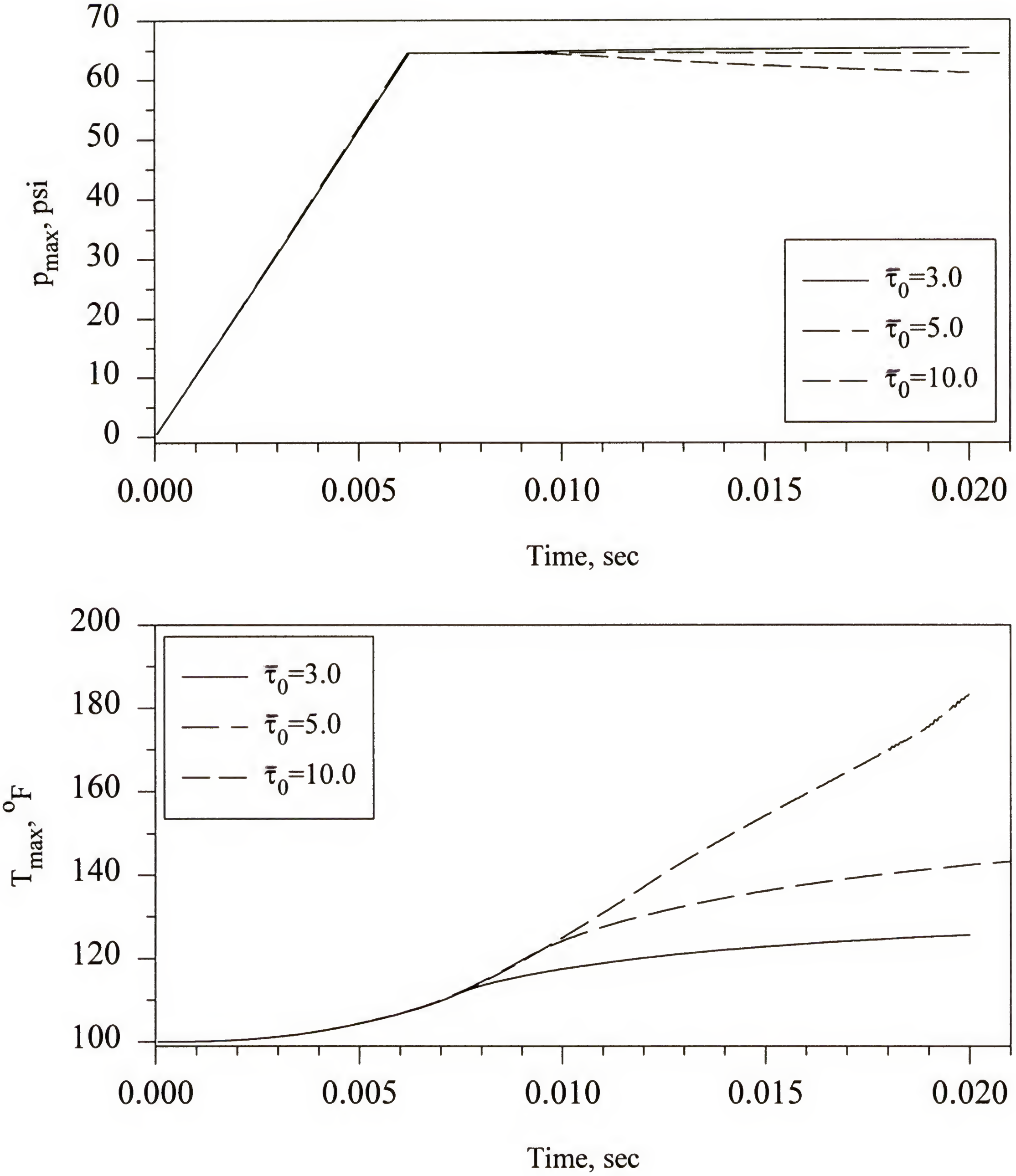

Figure 7.21 Slider bearing maximim pressure and temperature history for various shear yield stress parameters, B=L=3.0 in, h_{min}=0.004 in, h_{max}=0.008 in, U=40 ft/sec, SAE 10, T_{in}=100 ^{o}F, Time=0.2 sec

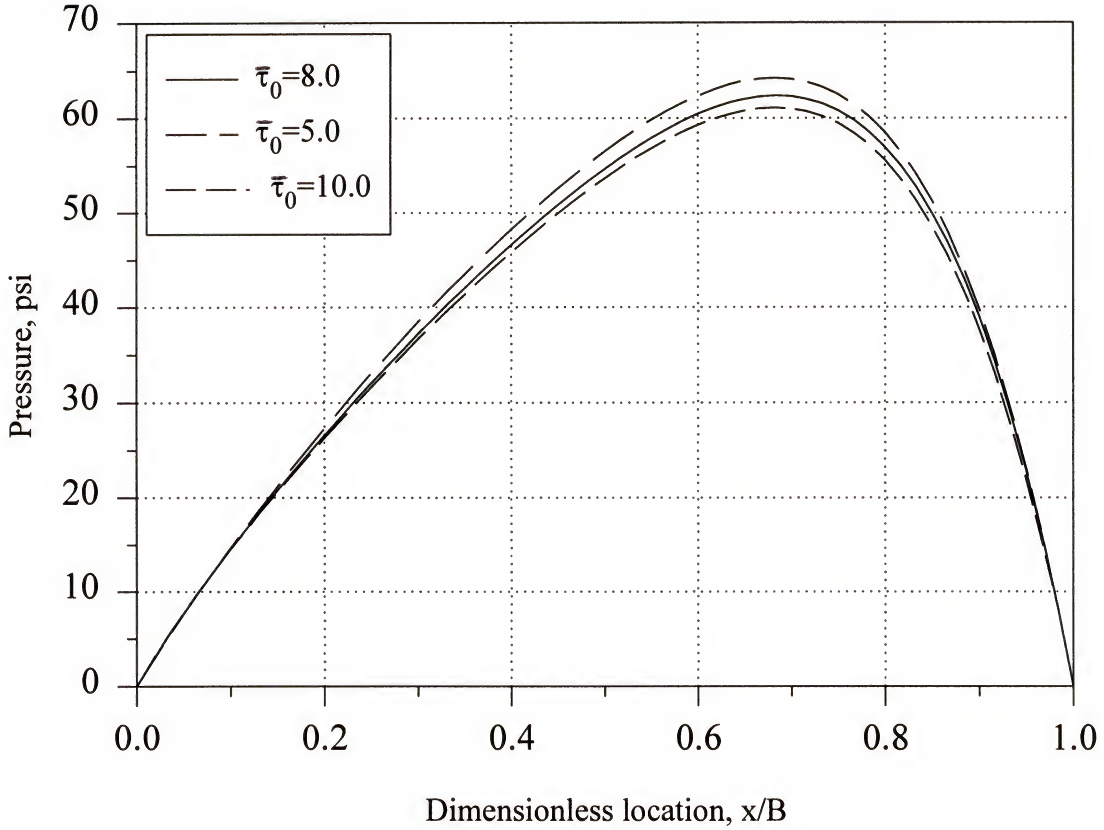

Figure 7.22 Pressure distribution along the center line of the slider bearing in the directionof sliding,
SAE 10, h_{min}=0.004 in, h_{max}=0.008 in, T_{in}=100 ^oF, Time=0.02 sec, U=40 ft/sec, B=L=3.0 in

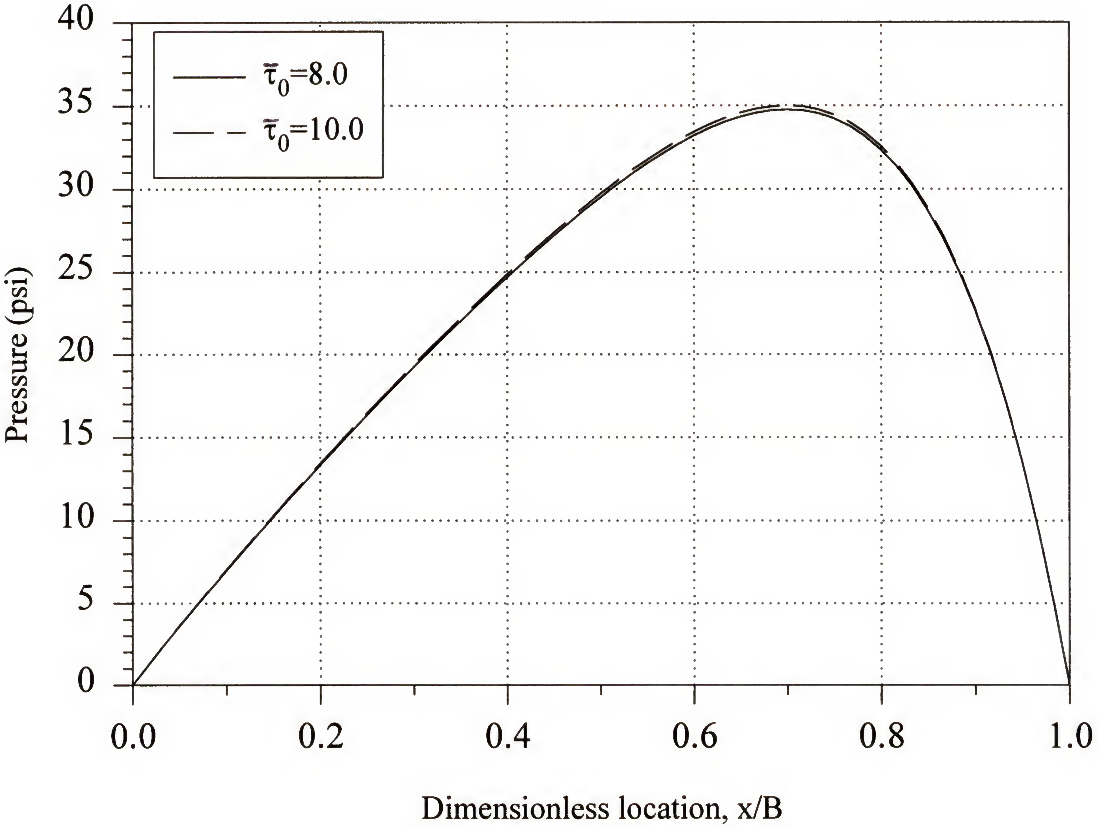

Figure 7.23 Pressure distribution along the center line of the slider system in the direction of sliding,
SAE 10, h_{min}=0.004 in, h_{max}=0.008 in, T_{in}=100 ^oF,
U=20 ft/sec, B=L=3.0 in,

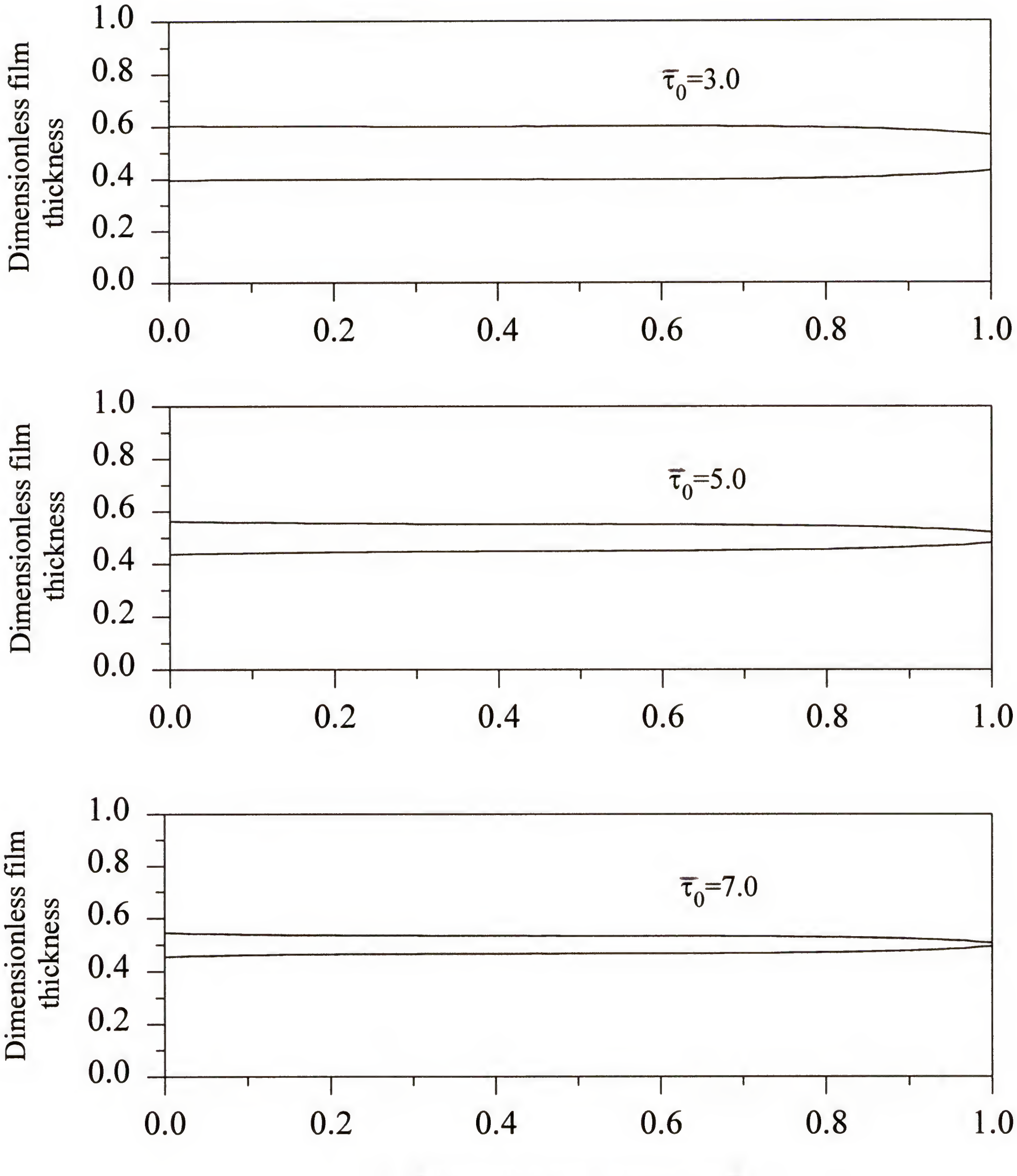

Figure 7.24 Shear zone ratio with two other layers for various shear yield stress parameters, B=L=3.0 in, h_{min}=0.004 in, h_{max}=0.008 in, Tin=100 ^oF, U=40 ft/sec, and SAE 10

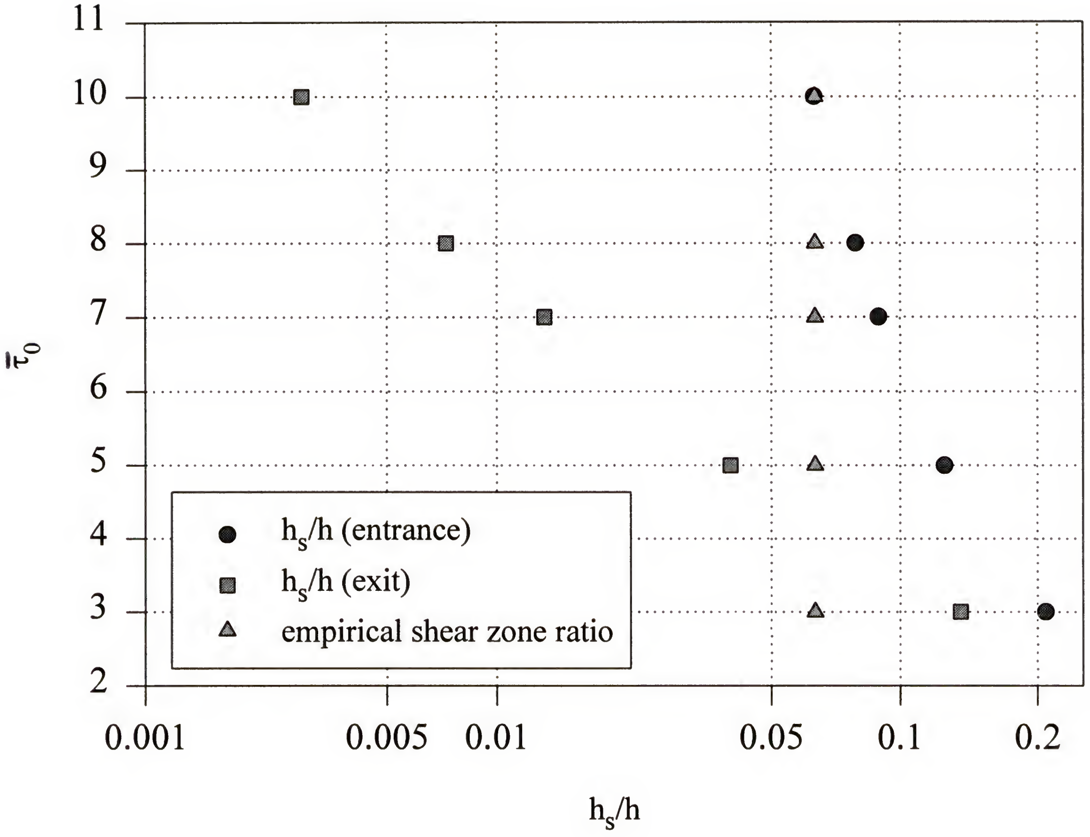

Figure 7.25 Shear zone ratio (h_s/h), based on thermohydrodynamic analysis with various shear yield stress parameters
h_{min}=0.004 in, h_{max}=0.008 in, B=L=3.0 in,
T_{in}=100 ^oF, U=40 ft/sec, SAE 10

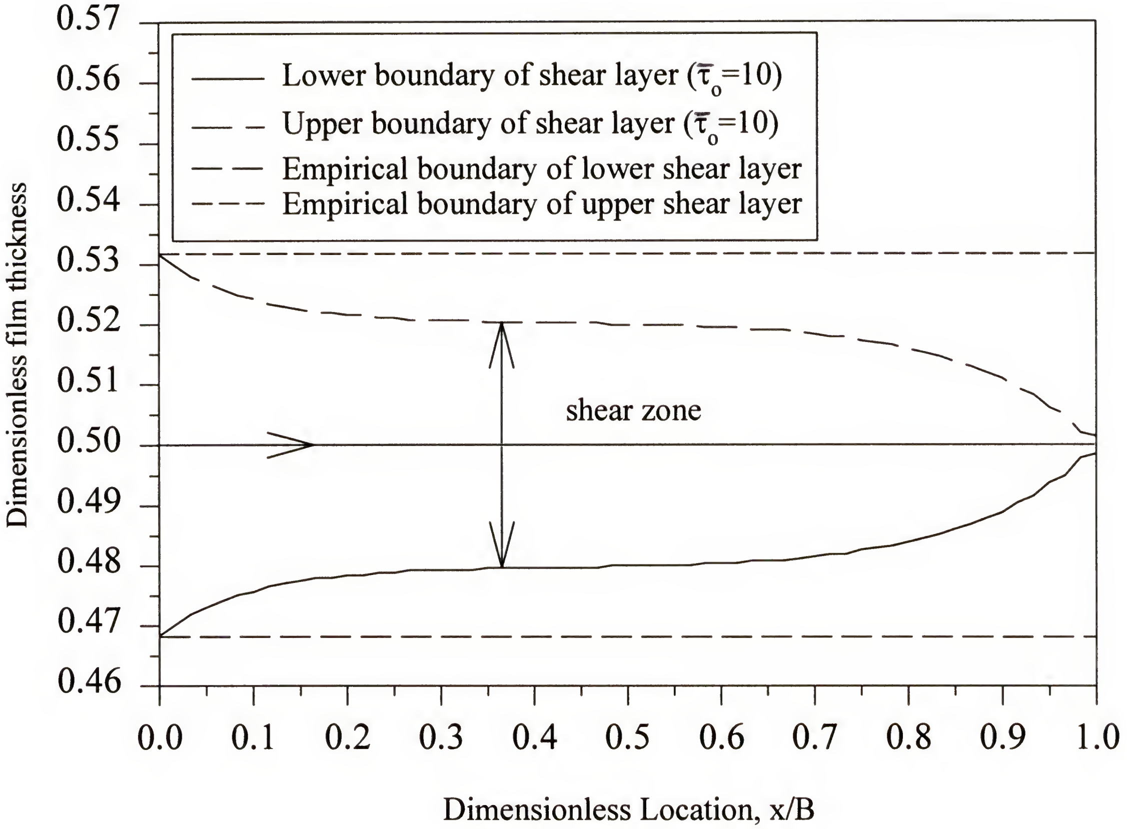

Figure 7.26 Shear zone ratio along the film flow direction
B=L=3.0 in, h_{min}=0.004 in,. h_{max}=0.008 in, T_{in}=100 ^{o}F,
Time=0.2 sec, U=40 ft/sec, SAE 10, $\bar{\tau}_0$=10

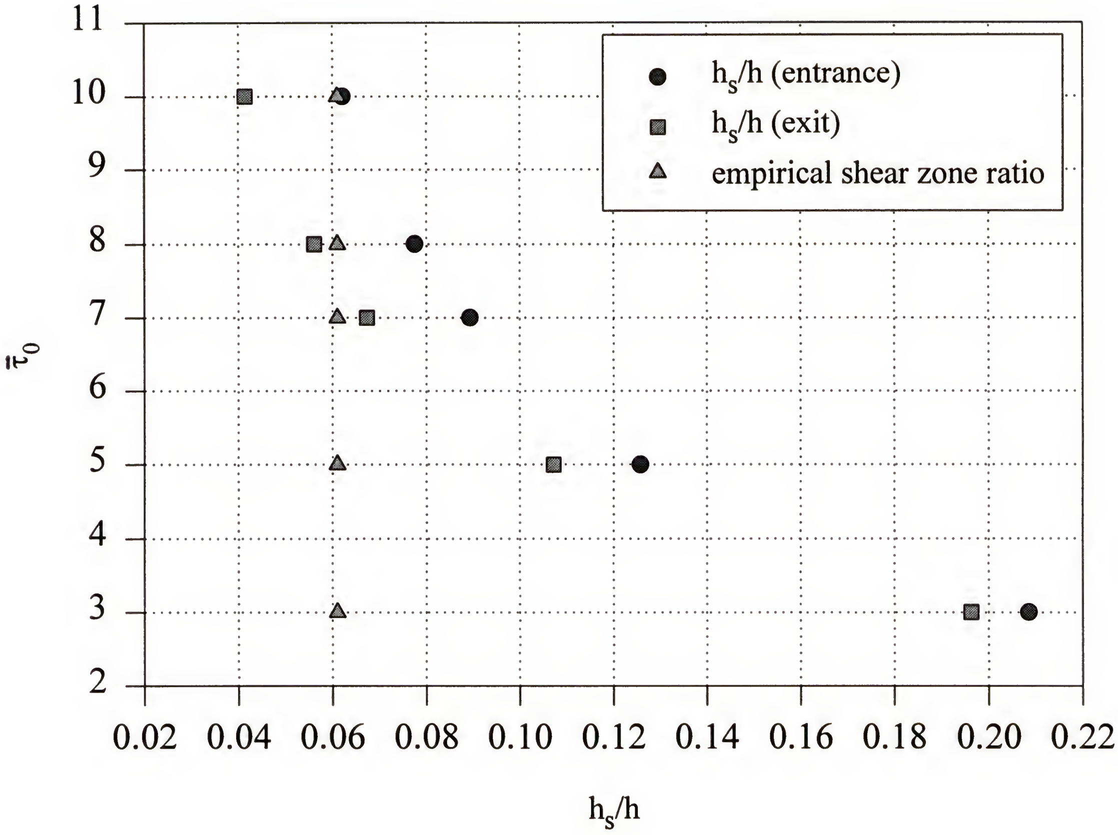

Figure 7.27 Shear zone ratio (h_s/h), based on thermohydrodynamic analysis with various shear yield stress parameters
h_{min}=0.004 in, h_{max}=0.004 in, B=L=3.0 in,
T_{in}=100 °F, U=20 ft/sec, SAE 10

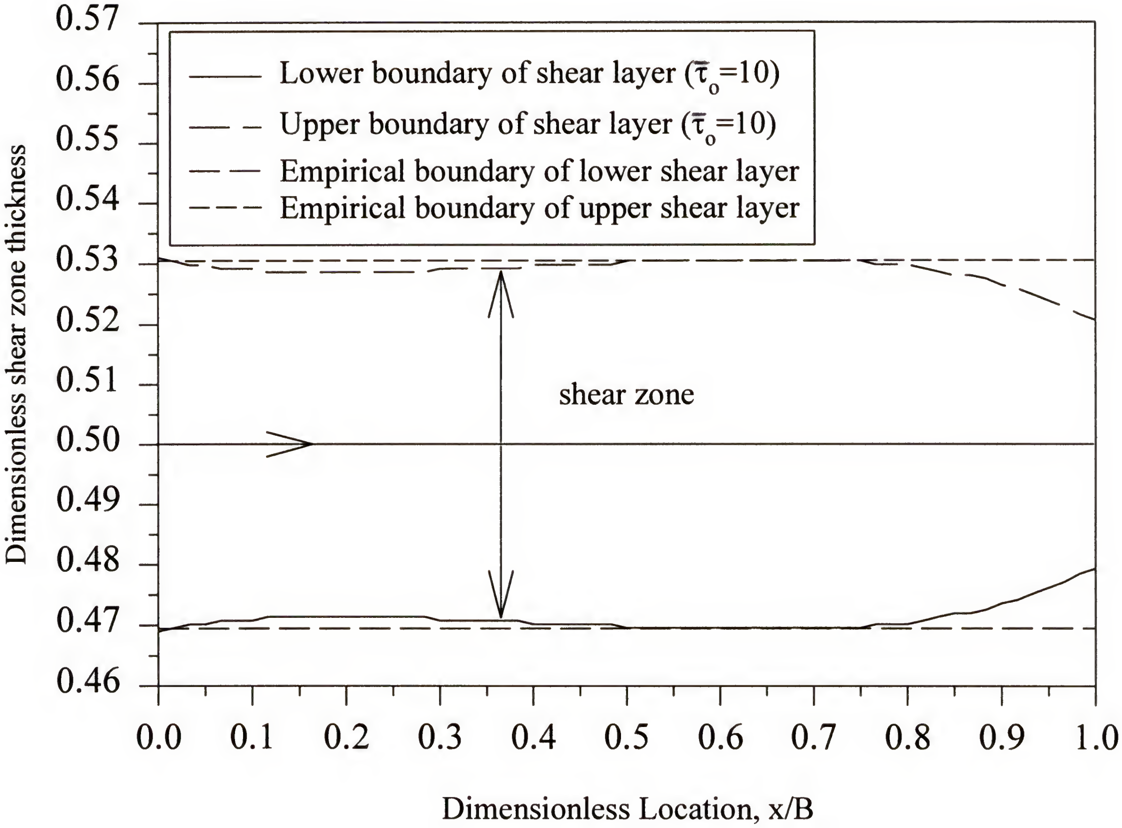

Figure 7.28 Shear zone ratio along film flow direction
B=L=3.0 in, h_{min}=0.004 in,. h_{max}=0.008 in, T_{in}=100 ^{o}F,
Time=0.2 sec, U=20 ft/sec, SAE 10, $\bar{\tau}_0$=10

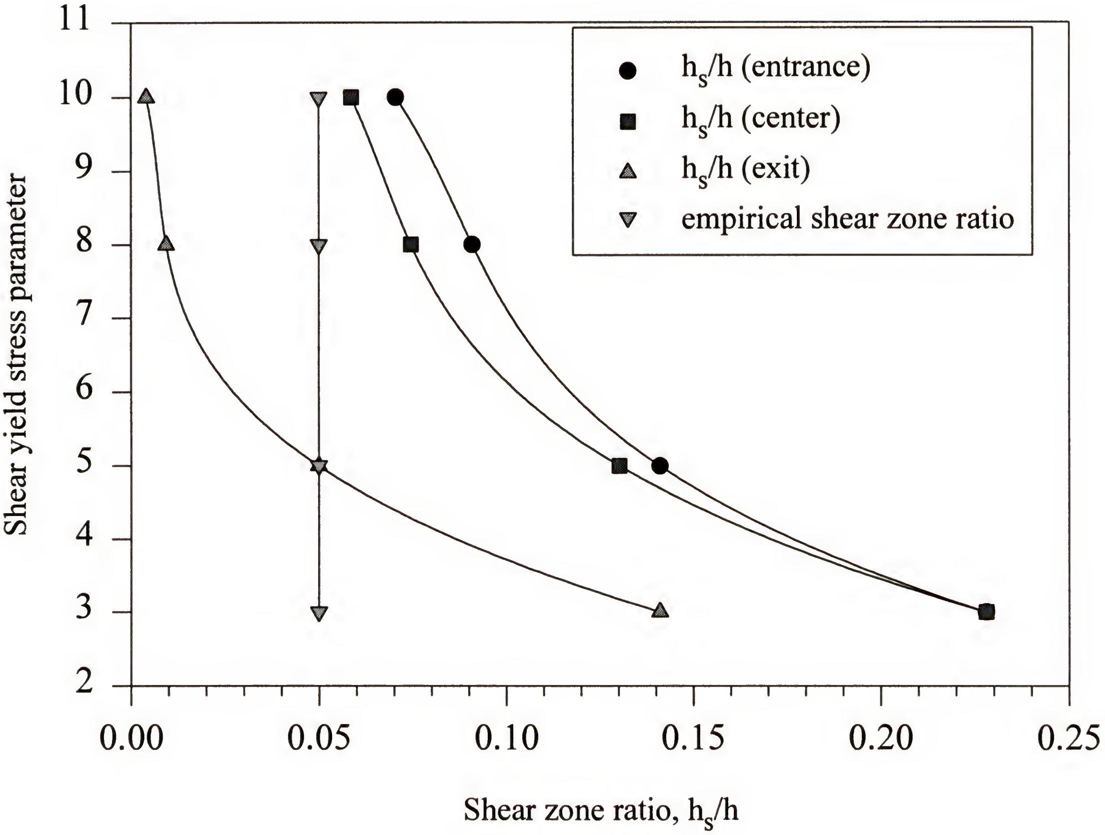

Figure 7.29 Shear zone ratio (h_s/h), based on thermohydrodynamic anaysis for various shear yield stress parameters
h_{min}=0.004 in, h_{max}=0.008 in, B=L=3.0 in,
T_{in}=100 °F, U=10 ft/sec, Time=0.1 sec, SAE 30

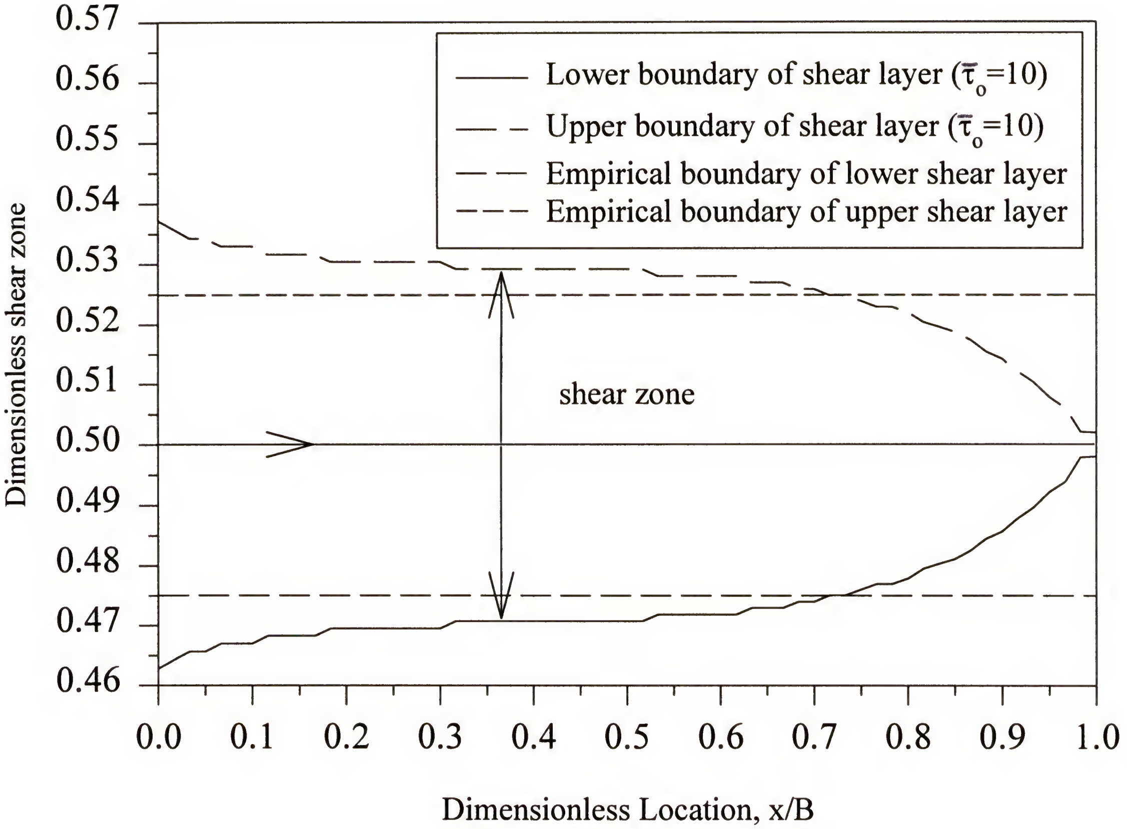

Figure 7.30 Shear zone ratio along the film flow direction
B=L=3.0 in, h_{min}=0.004 in,. h_{max}=0.008 in, T_{in}=100 ^oF,
Time=0.1 sec, U=10 ft/sec, SAE 30, $\bar{\tau}_0$=10

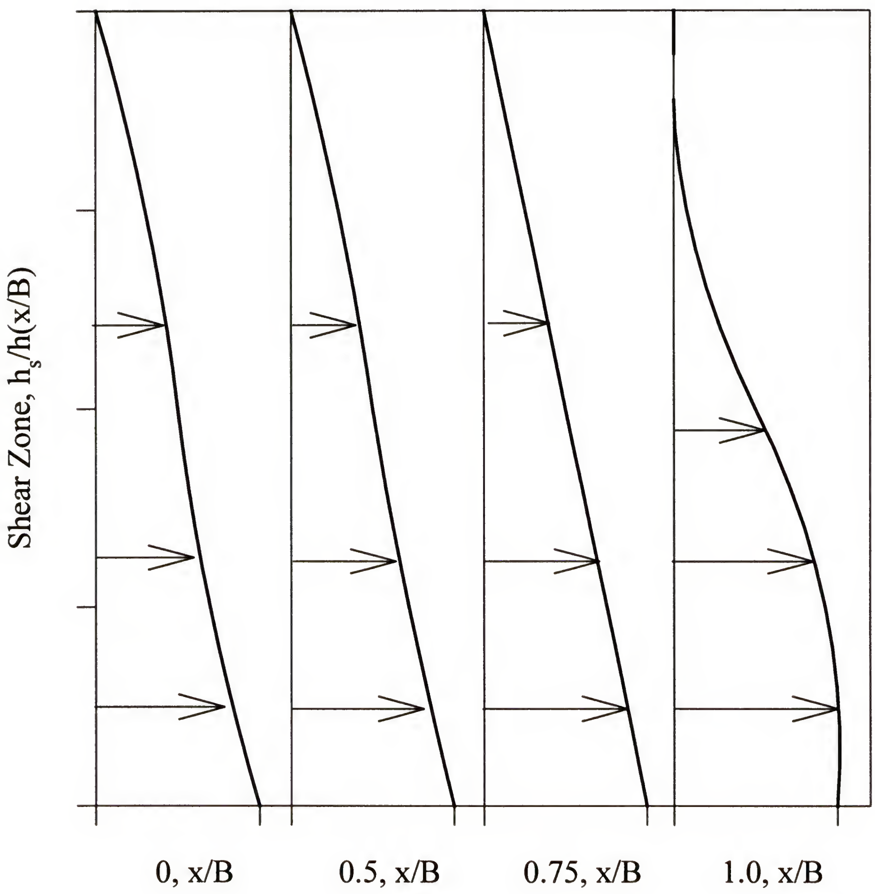

Figure 7.31 Velocity profile in the shear zone, h_s, along the mid-plane of the slider bearing in the direction of motion B=L=3.0 in, h_{min}=0.004 in, h_{max}=0.008 in,U=40 ft/sec, SAE 10, $\bar{\tau}_0$=10.0, T_{in}=100 °F, time=0.02 sec

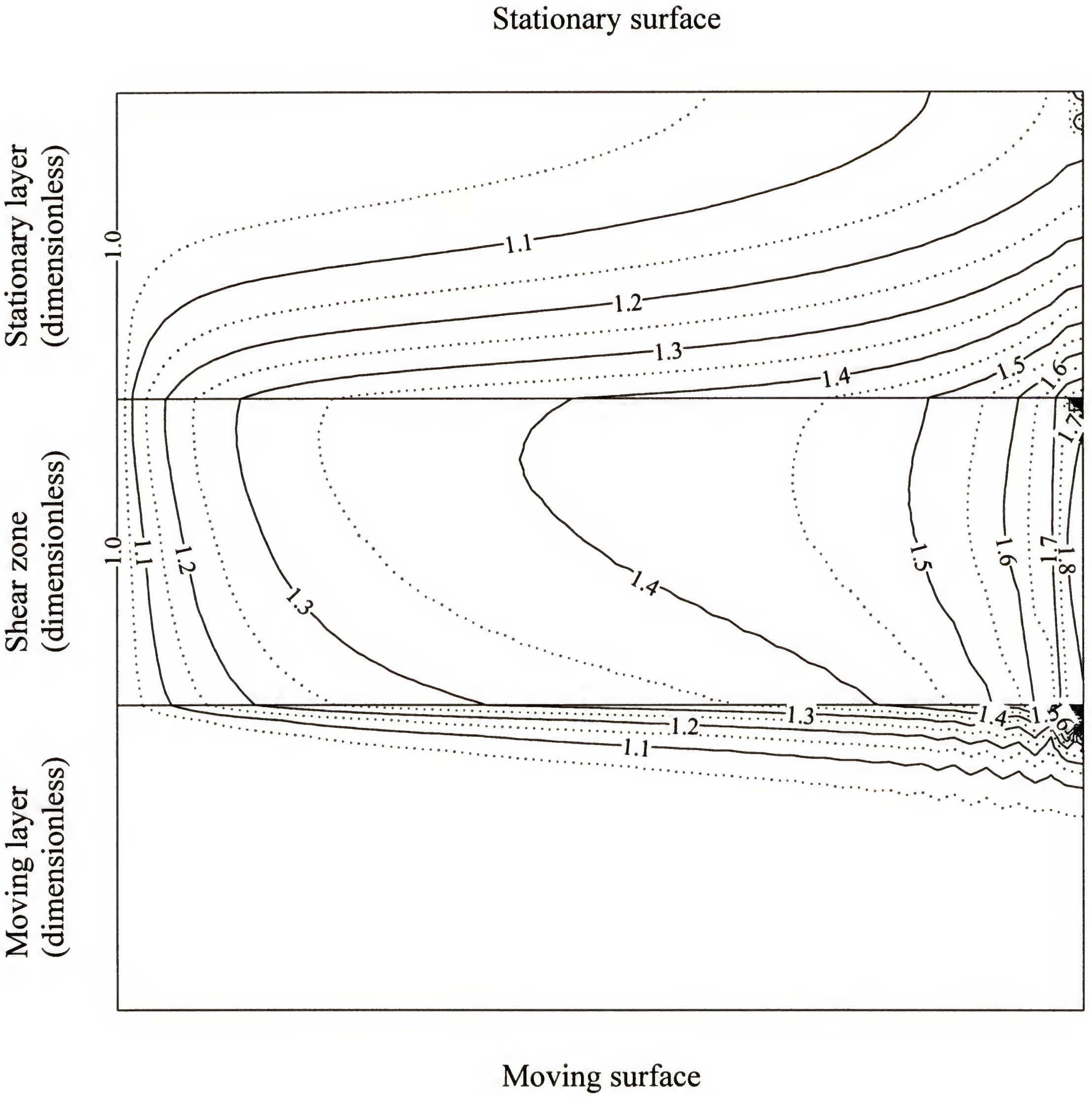

Figure 7.32 Dimensionless film temperature distribution along the central line of the slider bearing in the direction of film moving, B=L=3.0 in, h_{min}=0.004 in, h_{max}=0.008 in, SAE 10, T_{in}=100 ^{o}F, $\bar{\tau}_o$=10.0, U=40 ft/sec, time=0.02 sec

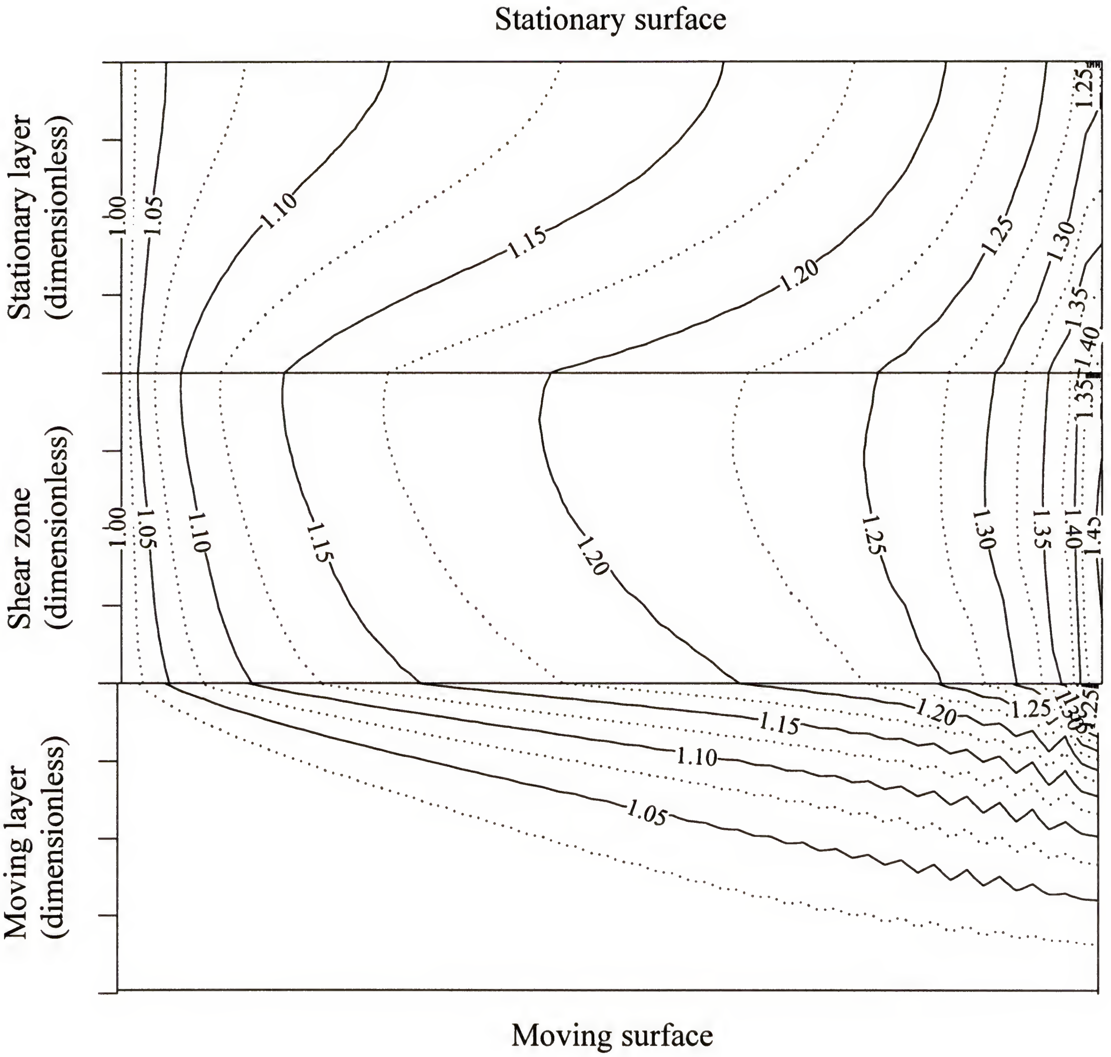

Figure 7.33 Dimensionless film temperature distribution along the central line of the slider bearing in the direction of film moving, B=L=3.0 in, h_{min}=0.004 in, h_{max}=0.008 in, SAE 30, T_{in}=100 °F, $\bar{\tau}_0$=10.0, U=10 ft/sec, Time=0.1 sec

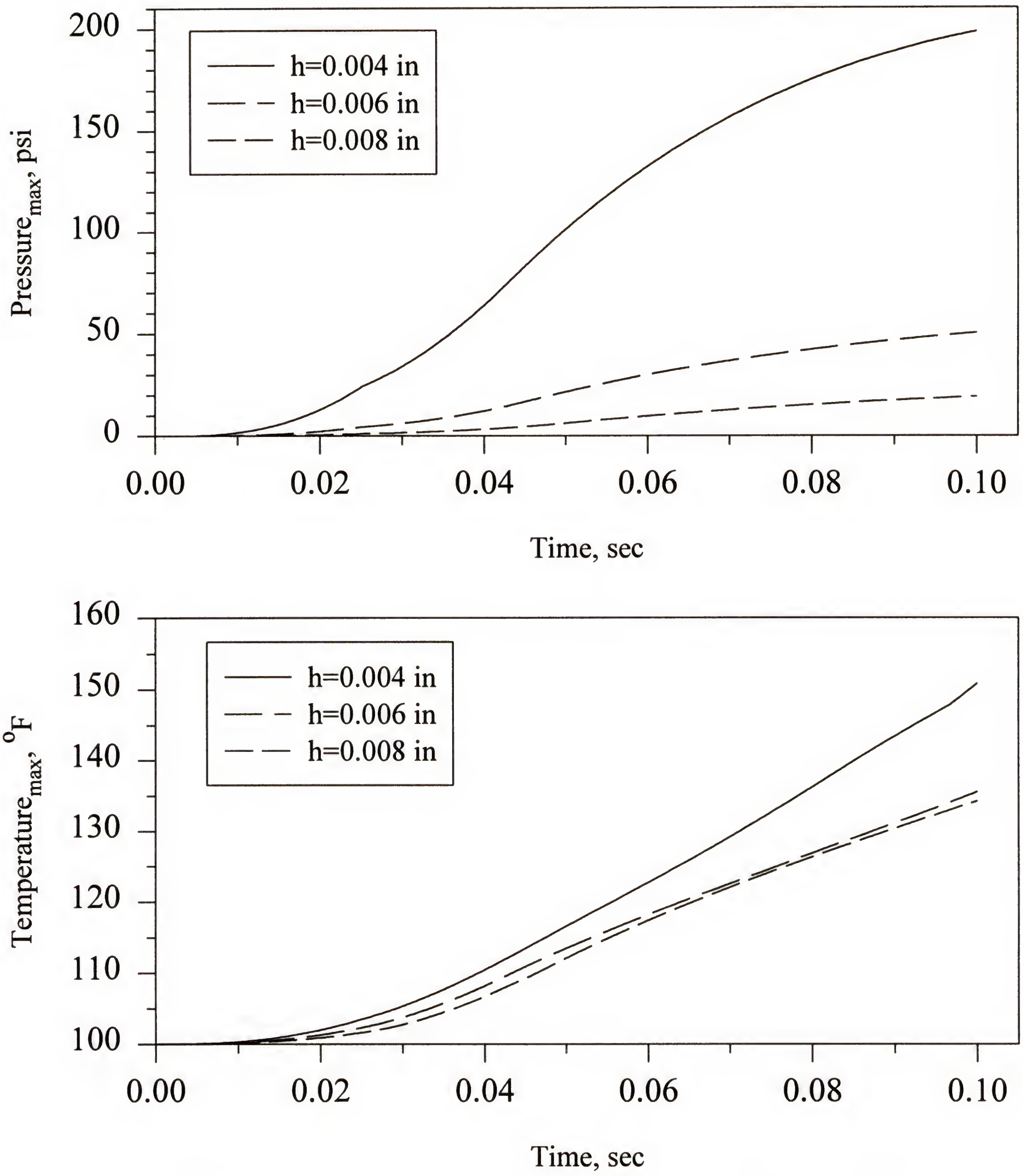

Figure 7-34 Parallel slider bearing maximum pressure and temperature history for various parallel clearances B=L=3.0 in, h=0.004 in ($\bar{\tau}_0$=13), 0.006 in ($\bar{\tau}_0$=15), and 0.008 in, ($\bar{\tau}_0$=27), U=10 ft/sec, SAE 30, T_{in}=100 ^{o}F, Time=0.1 sec

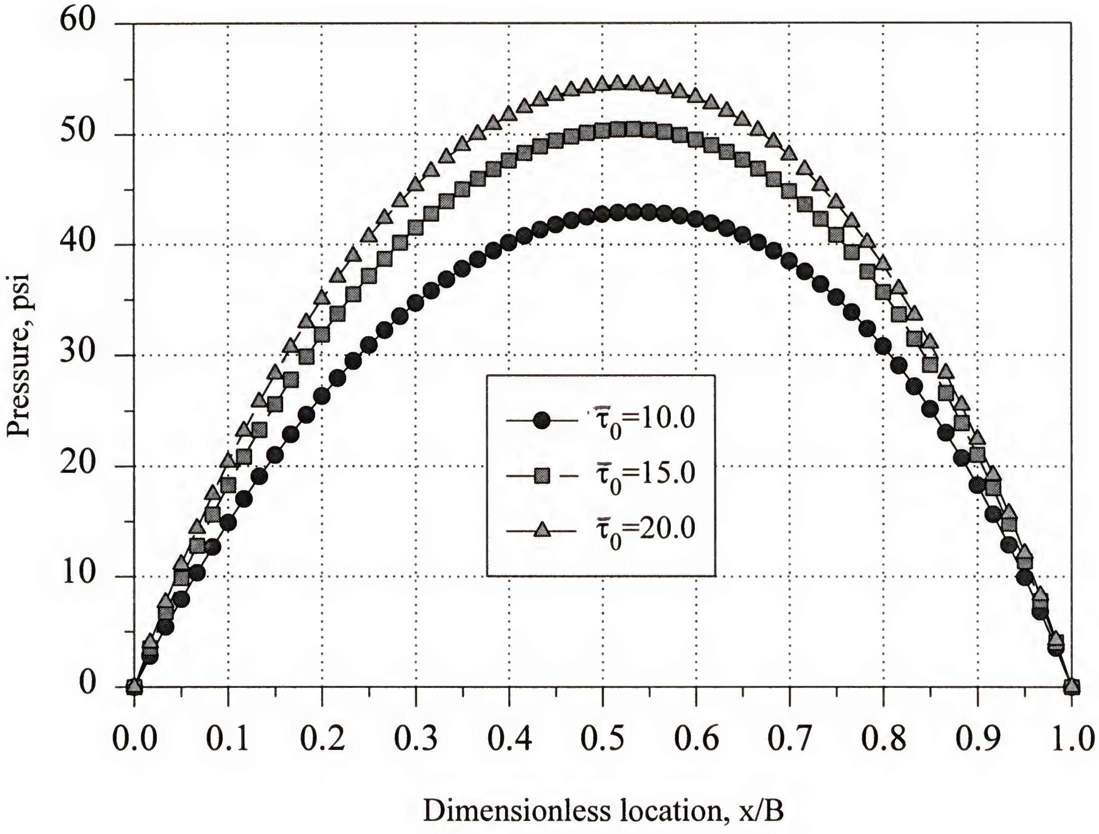

Figure 7.35 Pressure distribution along the central line of the parallel surface bearing in the direction motion,
B=L=3.0 in, SAE 30, T_{in}=100 ^{o}F, U=10 ft/sec, h=0.006 in,
Time=0.1 sec

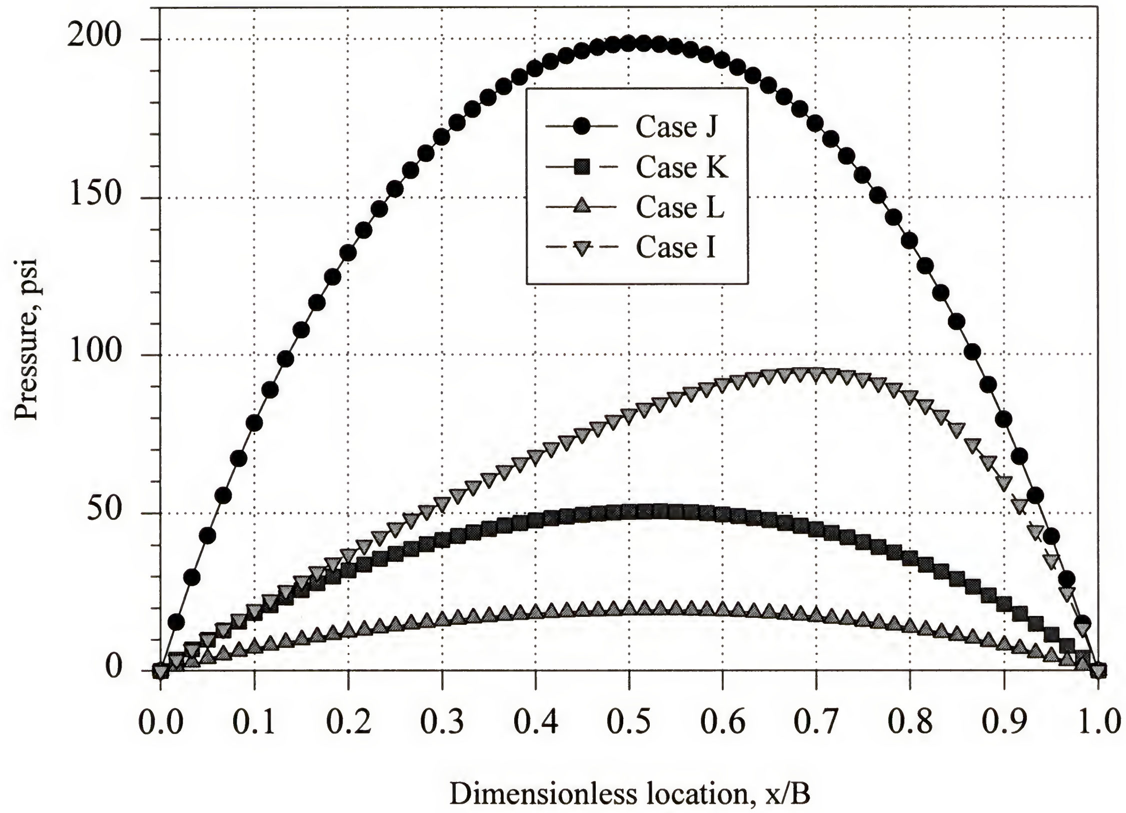

Figure 7.36 Pressure distribution along the central line of the slider bearings in the direction of motion, B=L=3.0 in, SAE 30, T_{in}=100 °F, U=10 ft/sec, Transient time=0.1 sec

Case J - Parallel slider, h=0.004 in, $\bar{\tau}_0$=13
Case K - Parallel slider, h=0.006 in, $\bar{\tau}_0$=15
Case L - Parallel slider, h=0.008 in, $\bar{\tau}_0$=27
Case I - Tapered slider, h_{min}=0.004 in, h_{max}=0.008 in, $\bar{\tau}_0$=10

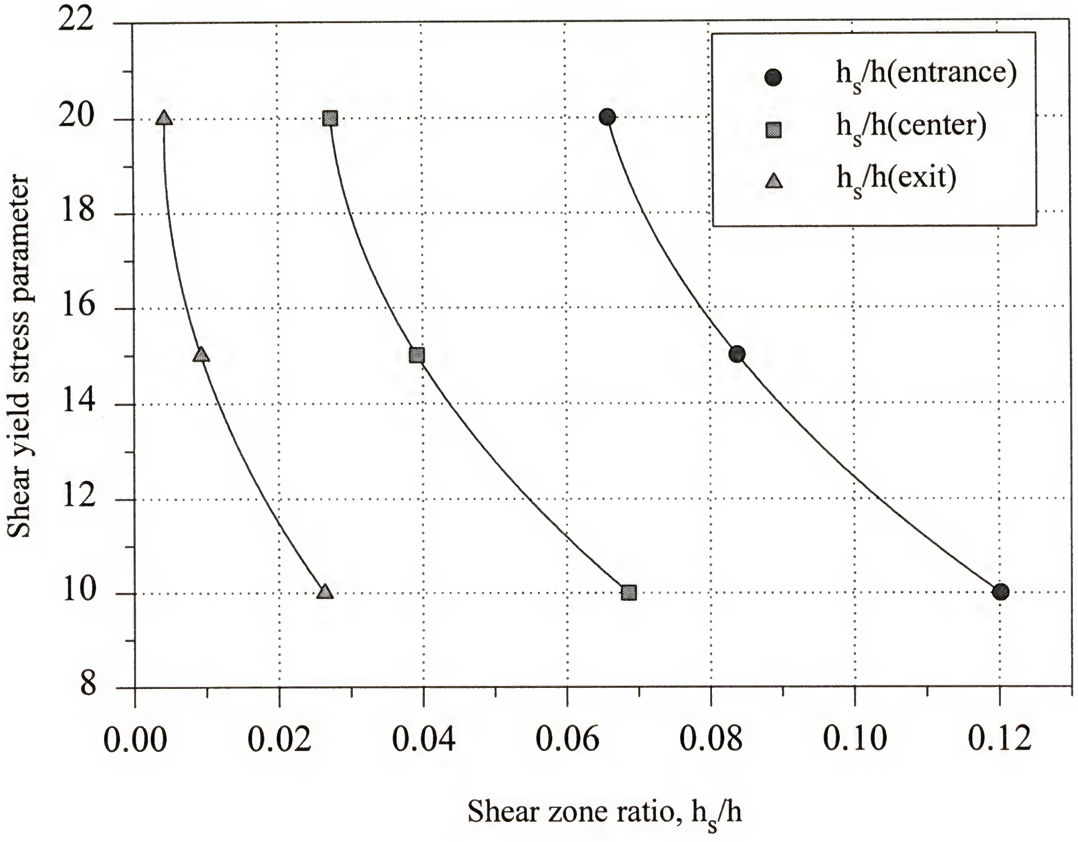

Figure 7.37 Shear zone ratio (h_s/h), based on thermohydrodynamic analysis for various shear yield stress parameters, $\{=\tau_o h_o/(\mu_o U)\}$, B=L=3.0 in, SAE 30, T_{in}=100 °F, U=10 ft/sec, h=0.006 in, Time=0.1 sec

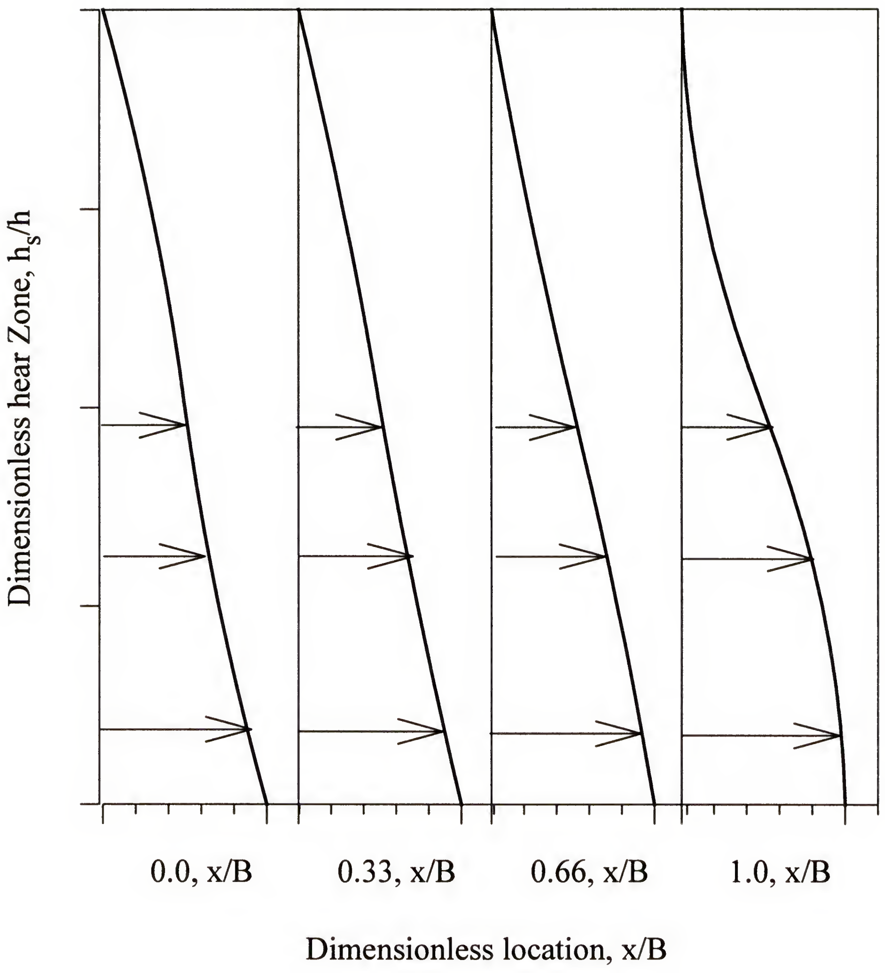

Figure 7.38 Velocity profile in the shear zone, h_s/h, along the mid-plane of the parallel slider bearing in the direction of motion B=L=3.0 inch, h_{min}=0.006 inch, U=10 ft/sec, SAE 30, $\bar{\tau}_0$=15.0, T_{in}=100 °F, time=0.1 sec

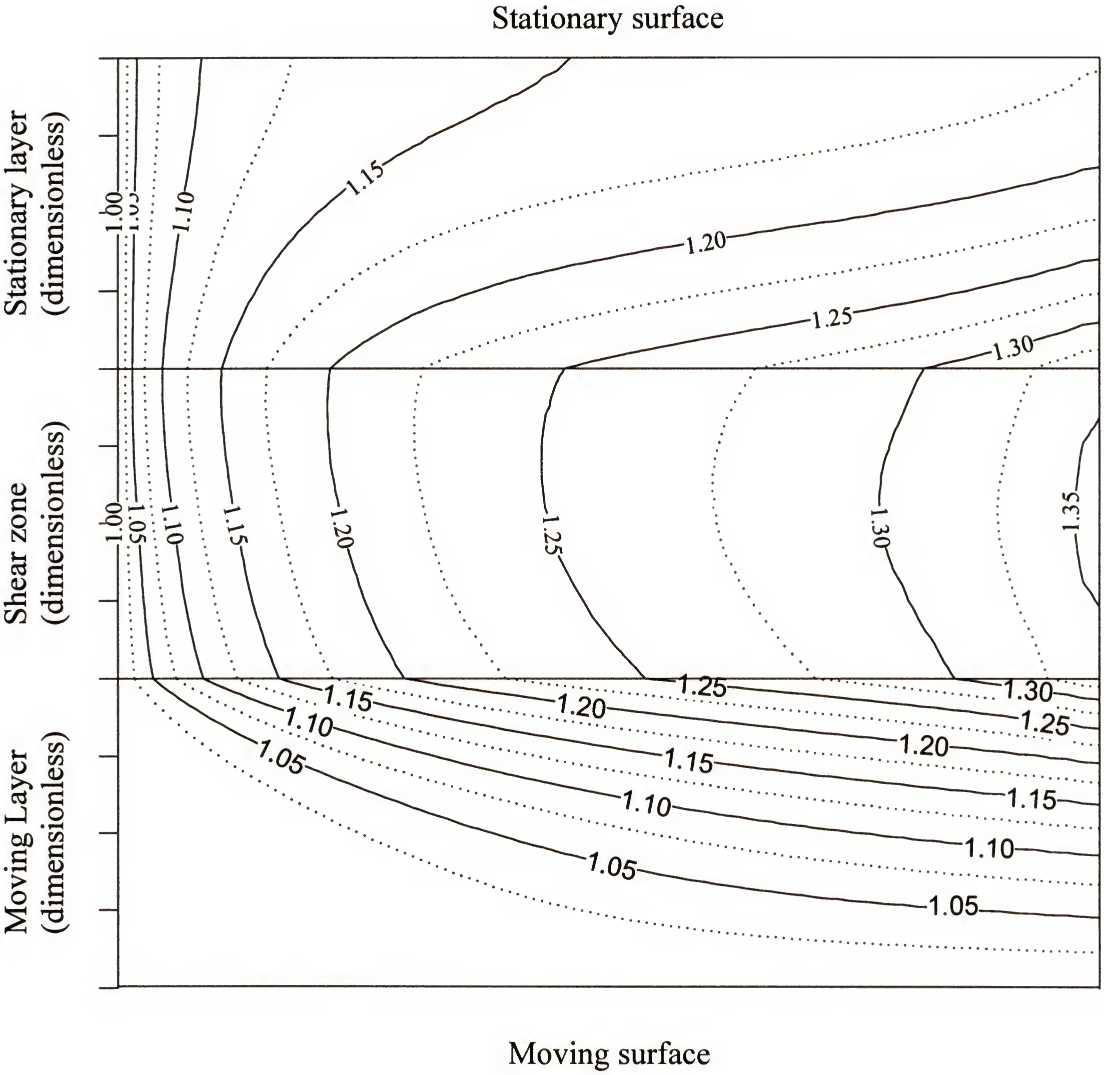

Figure 7.39 Dimensionless film temperature distribution along the central line of the parallel slider bearing in the direction of film moving
B=L=3.0 in, h=0.006 in, SAE 30, T_{in}=100 ^{o}F, $\bar{\tau}_0$=15.0,
U=10 ft/sec, Time=0.1 sec

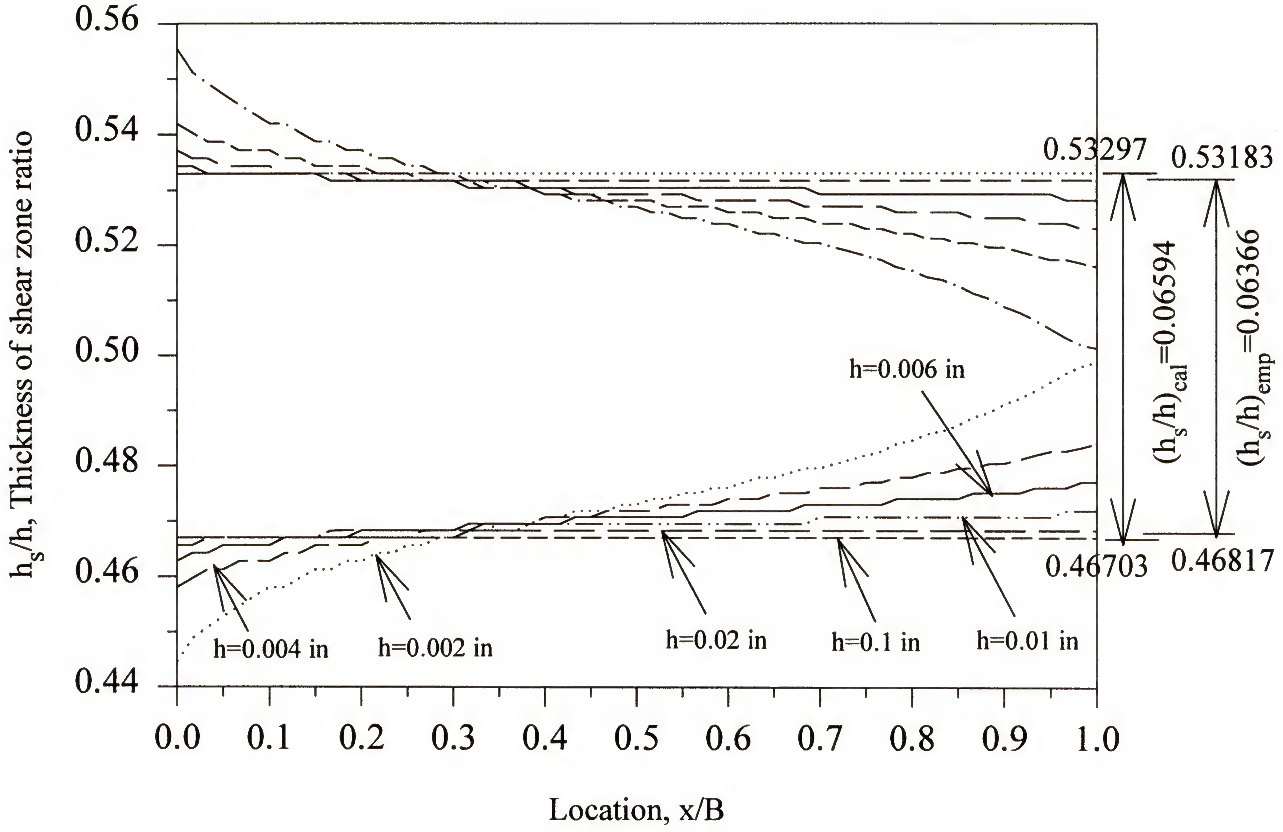

Figure 7.40 The trend of the shear zone ratio with various film thickness along the film flow direction in the parallel slider
B=L=3.0 in, T_{in}=100 ^oF, Time=0.1 sec, U=10 ft/sec,
SAE 10, $\bar{\tau}_0$=15

CHAPTER 8
SUMMARY, CONCLUSIONS AND RECOMMENDATIONS

8.1 Summary and Conclusions

The main goal of the thesis is to develop a mathematical procedure for more accurate prediction of the film thickness as well as the velocity, shear and pressure distribution in fixed geometry tribological systems. In response to this goal numerical solutions are presented for flow condition on a free surface, free surface with constraint and thermohydrodynamic lubrication between two surfaces. The effect of surface tension, speed, system geometry, and lubricant rheological properties on the velocity, temperature and pressure distribution in the film are investigated. The following summarizes the findings of the reported study:

Some general analysis for the free surface generated by the withdrawal process is presented as an extension of the Landau-Levich theory. The film thickness of the meniscus is found to affected primarily by Capillary number, (Ca), at low speeds and also by Reynolds number, (Re), at high speeds. In the domain of, $Ca < 10$, the results for Newtonian liquids on inclined plates are obtained. Beyond $Ca = 10$, it is important to consider the effect of the inertia force in the analysis of the free surface by the withdrawal process. The analytical solution was obtained as an extension of the flat plate case by applying geometric analogy to a rotating disk. The depth of the submerged portion of the disk in the oil container was found to have significant effect on the film thickness generated by surface tension. The numerical solutions for predicting the withdrawal film thickness on the rotating disk has been shown to be stable for Ca <10 and in good agreement with experiments using a 6 inch diameter disc rotating at speeds below 180 rpm. The film thickness and mass flow rate on the rotating disk can consequentially be used to determine the boundary conditions in the lubrication problem.

A general theoretical treatment of steady, two-dimensional, Newtonian film splitting flows between a rotating disc and a stationary surface has been presented. The simple mathematical formulation based on the lubrication model can predict the dimensionless film thickness to be formed after the outlet zone. It is found to be a function of the two boundary points and the gravity number. To determine the two boundary points, one of the models used considers the Swift-Stieber (Reynolds) boundary condition at the exit region where the lubrication flow splits. The other model considers the continuity boundary condition governed by the geometrical parameter H_0/R (minimum gap/disc radius), rotating speed, and Ca using the mathematical techniques developed by Coyne and Elrod. The splitting film thickness is expressed by the dimensionless flow rate and the splitting position. This position is determined from the entrance position which is based on the previous results of the withdrawal process. The major point is that the Swift-Stieber (Reynolds) boundary condition is not suitable for dealing with the existence of a negative pressure before the separation and the effect of surface tension which is significant at low speeds. At a critical speed, there exists an interaction between the pressure distribution before the meniscus region and the interfacial pressure controlled by surface tension. Beyond that speed the phenomenon can be simply modeled by Swift-Stieber (Reynolds) boundary condition which is used in the analysis of slider and journal bearing systems.

A numerical method is developed for the THD lubrication of slider and journal bearings considering both the full shear zone and the partial shear zone taking into consideration the thermal effect. The computational technique requires the simultaneous solution of the Newtonian hydrodynamic, the viscosity variation and the energy equations. The results include the lubricant pressure profile, film thickness, and temperature distribution within the lubrication zone. The analysis leads to the following main conclusions:

1. The results of the Newtonian behavior in the full shear zone show that the temperature rise in the lubrication zone is proportional to the sliding speed, but the thermal effects are not significant enough to reduce the pressure in the lubrication region.
2. The major component of heat generation under sliding conditions is by shear and for cooling is by conduction.
3. The relationship between the operating speed and film pressure in a fixed geometry bearing as obtained from both the Newtonian and Rheological models is found to follow the square root dependency of pressure on speed as proposed by Seireg.
4. The use of the Bingham model in fluid film lubrication is introduced. The non-Newtonian fluid under consideration differs from the Newtonian fluids in the existence of a narrow central layer in the lubrication zone where the velocity gradients are exceedingly high. From this consideration an anti-symmetric velocity model for the Newtonian fluids was presented.
5. The Bingham model with anti-symmetric velocity profiles in the shear zone was incorporated with the Reynolds equation and the energy equation for THD lubrication analysis.
6. The shear zone was determined from the condition where the shear stress exceeds the shear yield stress parameter which defines the interfacial boundary between the solid and fluid behavior. The computational method was used to evaluate the shear yield stress

parameter, $\bar{\tau}_0$, which gives values for the film the maximum pressure corresponding to the experimental data.

7. The results, show that the present model can be applied for lubrication conditions with running speeds, $U > 10$ ft/sec in the slider bearings and in the journal bearings corresponds to $N > 1000$ rpm. It is shown that the shear yield stress parameter as determined for a journal bearing or slider bearing is applicable for the same geometric parameters at different running speed.

8. Except very low speeds ($U < 10$ ft/sec or $N < 1000$ rpm) and very small clearance $h_{min} < 0.001$ inch) the range for dimensionless shear yield stress parameter in investigated bearings is 7 ~ 15.

9. The calculated thickness of the shear zone along the lubrication flow direction was compared with the empirical relationship [28] for calculating shear zone dimensions as a function of the product of Sommerfeld number (S) and Peclet number (Pe). The calculated shear zone dimensions by the shear yield stress parameter are of the same order of magnitude as those calculated from the empirical relationship.

10. The results of the parametric study for the effect of the film thickness in the shear zone in the parallel slider bearing show the same trend and approximately the same asymptotic value for h_s/h as predicted by the empirical equation.

8.2 Recommendations

1. Needless to say further and more detailed studies need to be performed for full understanding of the withdrawal problems including their applications in lubrication. More attention should be focused on the effect of surface tension on the film thickness in the free surface and on the film flow behavior in the clearance between the rotating disc and stationary surface. The effect of surface tension acting in the entrance region where

lubrication begins which is known to be influenced by the rheological behavior of lubricants and the modified Bingham model in the lubrication region should be extended by considering the effect of the surface tension.

2. The present research has provided further insight for better understanding of THD lubrication under the considered conditions. There are many opportunities to continue research in each of the problem areas investigated. The derived simple form of flow under THD lubrication can be readily extended to incorporate more Non-Newtonian effects.

3. Broader experimental confirmation for the theoretical models is also necessary. The results obtained from two experimental slider bearing and two journal bearing cases should be checked for a wider range of bearing geometries and speeds.

4. A number of problems of thermohydrodynamic lubrication under special conditions have been studied. These include cases where the thermal effect is important. The Reynolds equation, energy equation, and a semi-empirical equation have been coupled to solve the THD problem. However, in addition to the rhelogical phenomenon with an adiabatic high shear rate band in the lubrication region, heat conduction and cavitation effects must be also considered in further studies.

5. The shear yield stress is shown in this study to have a major influence on the shear zone and the corresponding behavior of the lubricating film. Developing reliable data on its magnitude for different oils at different temperatures, pressure and shear rates would be necessary for the prediction of film behavior.

6. When reliable shear yield stress data are available, it would be interesting to study the effect of film thickness and speed on the maximum pressure using both the full film shear and partial shear zone assumptions.

REFERENCES

1 Van Rossum, J., "Viscous Lifting and Drainage of Liquids," *J. Appl. Sci., Res.* A7, p121 (1958)

2 Gutfinger, C., and Tallmadge, J. A., "Entrainment of Liquid Films," *Ind. Eng. Chem.*, 59, p18 (1967)

3 Landau, L., and Levich, B., "Dragging of a Liquid by a Moving Plate," *Acta Physicochimica, U.R.R.S.*, 17, p41 (1942)

4 Ludviksson, V., and Lightfoot, E. N., "Deformation of Advancing Menisci," *A.I.Ch.E. J.*, 14, p674 (1968)

5 White, D. A., "Theory of Drag Out of Liquids on Flat Plates," *Chem. Eng. Sci.*, 20, p33 (1965)

6 Jeffreys, H., "The Draining of a Vertical Plate," *Proc. Comb. phil. Soc.*, 26, p204 (1930)

7 Deryagin, B. V., and Levi, S. M., *Film Coating Theory*, Focal Press, New York (1962)

8 Tallmadge, J. A., "Theory of Entrainment for Angular Withdrawal of Flat Supports," *A.I.Ch.E. J.*, 17, p243 (1971)

9 Tharmalingam, S., and Wilkinson, W. L., "The Coating of Newtonian Liquids onto A Rotating Roll," *Chem. Eng. Sci.*, 33, p1481 (1978)

10 Tharmalingam, S., and Wilkinson, W. L., "The Coating of Newtonian onto A Rotating at Low Speeds," *Poly. Eng. Sci.*, 18, p1155 (1978)

11 Spiers, R. P., Subbaraman, C. V., and Wikinson, W. L., "Free Coating of a Newtonian Liquid onto a Vertical Surface," *Chem. Eng. Sci.*, 29, p389 (1974)

12 Spiers, R. P., Subbaraman, C. V., and Wikinson, W. L., "Free Coating of a Non-Newtonian Liquid onto a Vertical Surface," *Chem. Eng. Sci.*, 30, p379 (1975)

13 Groenveld, P., and Van Dortmund R. A., "The Shape of the Air Adhering During the Formation of Viscous Liquid Films by Withdrawal," *Chem. Eng. Sci.*, 25, p1571 (1970)

14 Groenveld, P., "High Capillary Number Withdrawal from Viscous Newtonian Liquids by Flat Plates," *Chem. Eng. Sci.*, 25, p33 (1970)

15 Groenveld, P., "Low Capillary Number Withdrawal," *Chem. Eng. Sci.*, 25, p1259 (1970)

16 Savage, M. D., "Cavitation in Lubrication. Part 1. On Boundary Conditions and Cavity-Fluid Interfaces," *J. Fluid Mech.*, 80, p743 (1977)

17 Savage, M. D., "Cavitation in Lubrication. Part 2. Analysis of Wavy Interfaces," *J. Fluid Mech.*, 80, p757 (1977)

18 Pearson, J. R. A., "The Instability of Uniform Viscous Flow under Rollers and Spreaders," *J. Fluid Mech.*, 7, p481 (1960)

19 Floberg, L., "Lubrication of Two Rotating Cylinders at Variable Lubricant Supply with Reference to the Tensile Strength of the Liquid Lubricant," *J. Lubr. Tech.*, p155 (1973)

20 Williamson, A. S., "The Tearing of an Adhesive Layer between Flexible Tapes Pulled Apart," *J. Fluid Mech.*, 52, p639 (1972)

21 Greener, J., and Middleman, S., "Theoretical and Experimental Studies of the Fluid Dynamics of a Two-Roll Coater," *Ind. Eng. Chem. Fundam.*, 18, p35 (1979)

22 Reynolds, O., "On the Theory of Lubrication and Its Application to Mr. Beauchamp Tower's Experiments, Including an Experimental Determination of the Viscosity of Olive Oil," *Phil. Trans. Roy. Soc.* London A177, p157 (1886)

23 Walowit, J. A., and Anno, J. N., *Modern Developments in Lubrication Mechanics*, John Wiley & Sons, New York (1975)

24 Rashid, M., and Seireg, A. A., "Heat Partition and Transient Temperature Distribution in Layered Concentrated Contacts Part I. Theoretical Model," *J. Trib.*, 109, p487 (1987)

25 Rashid, M., and Seireg, A. A., "Heat Partition and Transient Temperature Distribution in Layered Concentrated Contacts Part II. Dimensionless Relationships and Results," *J. Trib.*, 109, p496 (1987)

26 Wang, N. Z., and Seireg, A. A., "Thermohydrodynamic Lubrication Analysis Incorporating Thermal Expansion Across the Film," *J. Trib*, 116, p681 (1994)

27 Wang, N. Z., and Seireg, A. A., "Empirical Prediction of the Shear Layer Thickness in Lubricating Films," *J. Trib*, 117, p444, (1995)

28 Fogg, A., "Fluid Film Lubrication of Parallel Thrust Surfaces," *Proceedings of Institute of Mechanical Engineering*, 155, p49 (1946)

29 Cope, W. F., "The Thermohydrodynamic Theory of Film Lubrication," *Proc. Roy. Soc.* A197, p201 (1949)

30 Seireg, A., and Dandage, S., "Empirical Design Procedure for the Thermohydrodyanmic Behavior of Journal Bearings," *J. Lubr. Tech.*, p135 (1982)

31 Lacey, J. J., "Use of Dimensional Analysis to Predict the Thermohydrodynamic Behavior of Fluid Films," Ph.D. Dissertation Topic Proposal, University of Wisconsin-Madison (1996)

32 Seireg, A., and Ezzat, H., "Thermohydrodynamic Phenomena in Fluid Film Lubrication," *J. Lubr. Tech.*, 95, p187 (1973)

33 Schlichting, H., *Boundary Layer Theory*, McGraw-Hill, New York (1985)

34 Cameron, A., *Basic Lubrication Theory*, Longman Group Ltd., New York, p103 (1970)

35 Hamrock, B. J., and Dowson, D., *Ball Bearing Lubrication: The Elastohydrodynamics of Elliptical Contacts*, John Wiley & Sons, New York (1981)

36 Gohar, R., *Elastohydrodynamics*, John Wiley & Sons, New York (1988)

37 Barwell, F. T., *Bearing Systems*, Oxford University Press, Oxford (1979)

38 Soroka, A. J., and Tallmadge, J. A., "A Test of the Inertial Theory for Plate Withdrawal," *A.I.Ch.E. J.*, 17, p505 (1971)

39 Levich, V. G., *Physicochemical Hydrodynamics,* Prentice Hall, New York (1962)

40 Pitts, E., and Greiller, J., "The Flow of Thin Liquid Films Between Rollers," *J. Fluid Mech.*, 11, p33 (1961)

41 Savage, M. D., "Mathematical Models for Coating Process," *J. Fluid Mech.*, 117, p443 (1982)

42 Coyle, D. J., Macosko, C. W., and Scriven, L. E., "Film-Splitting Flows in Forward Roll Coating," *J. Fluid Mech.*, 171, p183 (1986)

43 Taylor, C. M., "Separation Cavitation in Lightly Loaded Fluid Film Bearings with Both Surfaces in Motion," *J. Mech. Eng. Sci.*, 16, p147 (1974)

44 Taylor, C. M., "Film Rupture for a lubricated Cylinder Lightly Loaded against a Plane," *J. Mech. Eng. Sci.*, 16, p225 (1974)

45 Ruschak, K. J., "Boundary Conditions as a Liquid/Air Interface in Lubrication Flows," *J. Fluid Mech.*, 119, p107 (1982)

46 Coyne, J. C., and Elrod, H. G., "Conditions for Rupture of a Lubricating Film, Part I – Theoretical Model," *J. Lubr. Tech.*, p451 (1970)

47 Swift, H. W., "The Stability of Lubricating films in Journal Bearings," *J. Instn. Civ. Engrs.,* 233 (Pt 1), p267 (1931)

48 Wang, N. Z., "Experimental Investigation in the Performance of the Thermohydrodynamic Lubrication of Reciprocating Slider Bearing," M.S. Thesis, University of Wisconsin-Madison (1984)

49 Zienkiewicz, O., "Temperature Distribution Within Lubricating Film Between Parallel Bearing Surfaces and its Effect on the Pressure Developed," *Proc. Conf. Lub. Wear Inst. Engrs.*, 28, p135 (1958)

50 Dowson, D., "A Generalized Reynolds Equation for Fluid Film Lubrication," *Int. J. Mech. Sci.*, Pergamon Press Ltd, 4, p159 (1962)

51 Dowson, D., and Hudson, J. D., "Thermohydrodynamic Analysis of the Infinite Slider Bearing: Part I, the Plane Inclined Slider Bearing," *Proc. Inst. Mech. Engr.*, p34 (1963)

52 Dowson, D., and Hudson, J. D., "Thermohydrodynamic Analysis of the Infinite Slider Bearing: Part II, the Parallel Surface Bearing," *Proc. Inst. Mech. Engr.*, p45 (1963)

53 Dowson, D., Hudson, J., Hunter, B., and March, C., "An Experimental Investigation of the Thermal Equilibrium of Steadily Loaded Journal Bearings," *Proc. Inst. Mech. Engr.*, 101, 3B (1966)

54 Ezzat, H. A., and Rohde, S. M., " A Study of the Thermohydrodynamic Peformance of Finite Slider Bearings," *ASME J. Lubr. Tech.*, 95, p298 (1973)

55 Ezzat, H. A., and Rohde, S. M., "Thermal Transients in Finite Slider Bearings," *ASME J. Lubr. Tech.*, 95, p298 (1973)

56 Rohde, S. M., and Oh, K. P., "A Thermoelastohydrodynamic Analysis of a Finite Slider Bearing," *J. Lubr. Tech.*, p450 (1975)

57 Huebner, K. H., "A Three Dimensional Thermohydrodynamic Analysis of Sector Thrust Bearings," *ASLE Trans.*, 17, p62 (1973)

58 Huebner, K. H., "Application of Finite Element Methods to Thermohydrodynamic Lubrication," *Int. J. Numerical Methods in Engineering*, 8, p139 (1974)

59 Crouch, R. F., and Cameron, A., "A Viscosity-Temperature Equations for Lubricants," *J. Inst. Petroleum*, 47, p307 (1961)

60 Khonsari, M. M., and Beaman, J. J., "Thermohydrodynamic Analysis of Laminar Incompressible Journal Bearings," *ASLE Trans.*, p141 (1986)

61 Khonsari, M. M., and Wang, S. H., "Notes on Transient THD Effects in a Lubricating Film," *Trib. Trans.*, 35, p177 (1992)

62 Wang, N. Z., "Thermohydrodynamic Lubrication Analysis Incorporating Thermal Expansion Across Film," Ph.D. Dissertation, University of Wisconsin-Madison (1993)

63 Szeri, A. Z., *Tribology: Friction, Lubrication, and Wear*, Hemisphere Publishing co., New York (1980)

64 Bair, S., Qureshi, F., and Khonsari, M., "Adiabatic Shear Localization in Liquid Lubrication Under Pressure," *ASME J. Trib*, 116, p705 (1994)

65 Milne, A. A., "A Theory of Grease Lubrication of a Slider Bearing," *Proc. Second Intn. Cong. of Rheology*, p427 (1958)

66 Huang, X. B., and Wilson, W. R. D., "Theory of Viscoplastic Lubrication: Part I-Basic Relationships," *J. Trib*, 114, p469 (1992)

67 Streator, J. L., Gerhardstein, J. P., and McCollum, C. B., "The Low-Pressure Rheology of Ultra-Thin Lubricant Films and Its Influence on Sliding Contact," *J. Trib.*, 116, p119 (1994)

68 Sinha, P., and Singh, C., "Lubrication of a Cylinder on a Plane With a Non-Newtonian Fluid Considering Cavitation," *J. Trib.*, 104, p168 (1982)

69 Feng, R., and Rames,. K. T., "The Rheology of Lubricants at High Shear Rates," *J. Trib.*, 115, p640 (1993)

70 Bair, S., and Winer, W. O., "The High Pressure, High Shear Stress Rheology of Liquid Lubricants," *ASME J. Trib.*, 114, p1 (1992)

71 Bair, S., and Winer, W. O., "The High Shear Stress Rheology of Liquid Lubricants at Pressure of 2 to 200Mpa," *J. Trib.*, 112, p246 (1990)

72 Pinkus, O., "The Reynolds Centenial: A Brief History of the Theory of Hydrodynamic Lubrication," *ASME J. Trib.*, 109, p2 (1987)

73 Houpert, L., Flamand, L., and Berthe D., "Rheological and Thermal Effects in Lubricated E.H.D. Contacts," *J. Lubr. Tech.*, 103, p526 (1981)

74 Bai, Y., and Dodd, B., *Adiabatic Shear Localization*, Pergamon Press, Oxford (1992)

75 Wada, S., Hayashi, H., and Haga, K., "Behavior of a Bingham Solid in Hydrodynamic Lubrication: Part I, General Theory," *Bull. JSME*, 16, P422 (1973)

76 Wada, S., Hayashi, H., and Haga, K., "Behavior of a Bingham Solid in Hydrodynamic Lubrication: Part II, Application to Step Bearing," *Bull. JSME*, 16, P432 (1973)

77 Tichy, J. A., "Hydrodynamic Lubrication Theory for the Bingham Plastic Model," *J.Rheol.*, 35, p477 (1991)

78 Dorier, C., and Tichy, J. A., "Behavior of a Bingham-like Viscous Fluid in Lubrication Flows," *J. Non-Newtonian Fluid Mech.*, 45, p291 (1992)

79 Tanner, R. I., *Engineering Rheology*, Clarendon Press, Oxford (1985)

80 Feguson, J., and Kemblowski, *Applied Fluid Rheology*, Elsevier Applied Science, London and New York (1991)

81 Bird, R. B., Armstrong, R. C., and Hassager, O., *Dynamics of Polymeric Liquids, Volume 1 Fluid Mechanics*, John Wiley and Sons, Inc., New York (1987)

BIOGRAPHICAL SKETCH

Joon Hyun Kim was born on the 24th of August, 1961, at Kyungsan, Kyungbook, in the Rebulic of Korea.

He graduated from Sung Kyun Kwan University with a Bachelor of Science in Mechanical Engineering in 1980. After graduation he served the mandatory military duty as first lieutenant in the Korean Army for three years. He had worked in KIA Motors as an engineer & technical planner before he came to the United States in 1990. His Master of Science degree in mechanical and aerospace engineering was obtained at the University of Missouri-Columbia in August, 1993. He continued his studies of mechanical engineering at the University of Florida in 1993. Under the full direction of Ebaugh Professor Ali A. Seireg he received a Doctor of Philosophy degree in mechanical engineering in May, 1998. He plans to continue conducting his research in both areas of tribology and fluid mechanics.

I certify that I have read this study and that in my opinion it confirms to acceptable standards of scholarly presentation and is fully adequate, in scope and quality, as a dissertation for the degree of Doctor of Philosophy.

Ali A. Seireg

Ali A. Seireg, Chairman
Ebaugh Professor of Mechanical
Engineering

I certify that I have read this study and that in my opinion it confirms to acceptable standards of scholarly presentation and is fully adequate, in scope and quality, as a dissertation for the degree of Doctor of Philosophy.

James F. Klausner

James F. Klausner
Associate Professor of Mechanical
Engineering

I certify that I have read this study and that in my opinion it confirms to acceptable standards of scholarly presentation and is fully adequate, in scope and quality, as a dissertation for the degree of Doctor of Philosophy.

William E. L

William E. Lear
Assistant Professor of Mechanical
Engineering

I certify that I have read this study and that in my opinion it confirms to acceptable standards of scholarly presentation and is fully adequate, in scope and quality, as a dissertation for the degree of Doctor of Philosophy.

Jill E. Peterson

Jill E. Peterson
Associate Professor of Mechanical
Engineering

I certify that I have read this study and that in my opinion it confirms to acceptable standards of scholarly presentation and is fully adequate, in scope and quality, as a dissertation for the degree of Doctor of Philosophy.

Li C. Shen
Associate Professor of Mathematics

This dissertation was submitted to the Graduate Faculty of the College of Engineering and to the Graduate School and was accepted as partial fulfillment of the requirements for the degree of Doctor of Philosophy.

May 1998

Winfred M. Phillips
Dean, College of Engineering

Karen A. Holbrook
Dean, Graduate School